UNIVERSITÄT BAYREUTH

Biochemische Evaluation und strukturelle Optimierung von Naphtopyran-Derivaten mit Mikrotubuli-destabilisierenden, antiangiogenen und *c*-MYB-inhibierenden Eigenschaften

DISSERTATION

zur Erlangung des akademischen Grades eines
Doktors der Naturwissenschaften (Dr. rer. nat.)
an der Fakultät für Biologie, Chemie und Geowissenschaften
der Universität Bayreuth

vorgelegt von

Leonhard Hans Friedrich Köhler
aus Nürnberg

Bayreuth, 2023

Die vorliegende Arbeit wurde in der Zeit von März 2020 bis Februar 2023 in Bayreuth am Lehrstuhl Organische Chemie I unter Betreuung von Herrn Prof. Dr. Rainer Schobert angefertigt.

Vollständiger Abdruck der von der Fakultät für Biologie, Chemie und Geowissenschaften der Universität Bayreuth genehmigten Dissertation zur Erlangung des akademischen Grades eines Doktors der Naturwissenschaften (Dr. rer. nat.)

Dissertation eingereicht am: 22.02.2023

Zulassung durch die Promotionskommission: 08.03.2023

Wissenschaftliches Kolloquium: 28.09.2023

Amtierender Dekan: Prof. Dr. Benedikt Westermann

Prüfungsausschuss:

Prof. Dr. Rainer Schobert	(Gutachter)
Prof. Dr. Carlo Unverzagt	(Gutachter)
Prof. Dr. M. Ullmann	(Vorsitz)
Prof. Dr. K. Ersfeld	

"Mystery creates wonder and wonder is the basis of man's desire to understand"
- Neil Armstrong -

Für meine wundervollen Eltern

Inhaltsverzeichnis

Abkürzungsverzeichnis

ADME	*Absorption distribution metabolism and excretion*
ALK	*Anaplastic lymphoma kinase*
All	Allyl
ALT	*Alternative lengthening of telomerases*
Ang	Angiopoetin
APAF1	*Apoptotic protease activating factor 1*
AR	Androgenrezeptor
Bad	*BCL-2-antagonist of cell death protein*
BAK	*BCL-2 homologous killer*
BAX	*BCL-2 associated X protein*
Bcl-2	*B-cell lymphoma 2 protein*
Bcl-xl	*B-cell lymphoma-extra-large protein*
BCR-ABL	Hybrides Onkoprotein des BCR-ABL-Gens
BER	*Base excision repair*
BID	*BH3 interacting-domain death agonist*
Bim	*Bcl-2 Interacting Mediator of cell death*
Bmf	*Bcl-2-modifying factor*
BODIPY	*4,4-difluor-4-bor-3a,4a-diaza-s-indacen*
Bu	Butyl
CA4	*Combretastatin A4*
CAF	*Cancer-associated fibroblasts*
cAMP	*Cyclic adenosine monophosphate*
CAR	*Chimeric antigen receptor*
CBP	*CREB-binding protein*
$CD4^+/CD8^+$	*Cluster of differentiation 4/8 of immune cells*
CDK1	*Cyclin-dependent kinase 1*
c-MYB	*MYB proto-oncogene like protein*
CREB	*cAMP response element-binding protein*
CSC	*Cancer stem cells*
CTC	*Circulating cancer cells*
Cys	Cystein
DBD	DNA-bindende Domäne

DISC	*Death-inducing signaling complex*
DKC1	*Dyskerin*
DNA	*Desoxyribonucleic acid*
EB	*End-binding protein*
ECM	*Extracellular matrix*
EET	*Epithelial-endothelial transition*
EGFR	*Epidermal growth factor receptor*
EMT	*Endothelial-mesenchymal transition*
ERBB2	*Receptor tyrosine-protein kinase erbB-2*
Et	Etyl
FACS	*Fluorescence-activated cell sorting*
FADD	*Fas-associated death domain protein*
FANCM	*Fanconi anemia complementation group M*
FASL	*FAS ligand*
FASR	*FAS receptor*
Fc-Fragment	*crystallizable fragment*
FGF	*Fibroblast growth factor*
FLASH	*FLICE-associated huge protein*
FLICE	Caspase 8
GDP	Guanosindiphosphat
GTP	Guanosintriphosphat
Hpg	Homopropargylglycin
IGF1R	*Insulin-like growth factor receptor*
IC_{50}	Halbmaximale inhibitorische Konzentration
IL	Interleukin
IM	Interphase-Mikrotubuli
*i*Pr	Isopropyl
MAP	*Microtubule-associated protein*
Mcl-1	*Induced myeloid leukemia cell differentiation protein*
MDA	*Microtubule-destabilizing agent*
MET	*Mesenchymal-endothelial transition*
MMP	*Matrix metalloproteinase*
MOMP	*Mitochondrial outer membrane permeabilization*
MTA	*Microtubule-targeting agent*

MTOC	*Microtubule-organizing center*
mTOR	*Mechanistic target of rapamycin*
MTT	*3-(4,5-Dimethylthiazol-2-yl)-2,5-diphenyltetrazoliumbromid*
MYB	MYB-Gen
MYBMIM	*Peptidomimetic inhibitor of c-MYB*
MYB-NFIB	Hybrides Onkoprotein des MYB-NFIB-Gens
MYC	*MYC proto-oncogene*
N-CoR	*Nuclear receptor co-expressor 1*
NF-κB	*Nuclear factor κ-light-chain-enhancer*
NK-Zelle	Natürliche Killerzelle
Noxa	*Phorbol-12-myristate-13-acetate-induced protein*
NRD	Negative regulierende Domäne
p16	*CDK inhibitor 2A*
p21	*CDK-interacting protein 1*
p300	*Histone acetyltransferase p300*
p53	Tumorsuppressorprotein p53
PDGF	*Platelet derived growth factor*
Pi	Anorganisches Phosphat
PML	*Promyelocytic leukemia protein*
Pr	Propyl
Puma	*P53 upregulated modulator of apoptosis*
Ras	*Rat sarcoma proto-oncogene*
RB	*Retinoblastoma protein*
Rho	*Ras homologue GTPases*
ROS1	*Receptor tyrosine kinase ROS1*
RTK	*Receptor tyrosine kinase*
SAC	*Spindle-associated checkpoint*
SAR	Struktur-Wirkungs-Beziehungen
SASP	*Senescence-associated secretory phenotype*
SIV	Subintestinale Vene
TAD	Transaktivierungsdomäne
TERC	*Telomerase RNA component*
TERT	*Telomerase reverse transcriptase*
TGF-β	*Transforming growth factor β*

Tif1β	*Transcriptional intermediary factor 1β*
TIP60	*Histone acetyltransferase KAT5*
TMP	3,4,5-Trimethoxyphenyl
TNF	*Tumor necrosis factor*
TNFR	*Tumor necrosis factor receptor*
TP53	p53-Gen
TRAIL	*TNF-related apoptosis-inducing ligand*
TRAILR	*TNF-related apoptosis-inducing receptor*
TRK	*Tropomyosin receptor kinase*
T-Zelle	T-Lymphozyte
Ub	Ubiquitin
VE-Cadherin	*Vascular endothelial cadherin*
VEGF	*Vascular endothelial growth factor*
VEGFR	*Vascular endothelial growth factor receptor*
Wnt	*Secreted lipid-modified signaling glycoproteins*
γ-TuRC	*γ-tubulin ring complex*

Zusammenfassung

Seit mehr als einem Jahrhundert arbeitet die internationale Forschungsgemeinschaft an der Entwicklung neuer Therapien für maligne Neoplasien. Trotz immenser Investitionen ist die Entdeckung eines Heilmittels nicht absehbar und stellt auch die modernsten Behandlungsstrategien immer wieder vor neue Herausforderungen. Da Krebs in sehr unterschiedlichen Zelltypen entsteht, führen die spezifischen Eigenschaften des Ursprungsgewebes zu einem sehr komplexen Krankheitsbild. Das macht eine universelle Therapie unmöglich und in den meisten Fällen den Einsatz von Kombinationstherapien erforderlich. Genetische Instabilität und stressbedingte Selektion der Krebszellen begünstigen die Weitergabe von Onkogenen und verursachen unbeständige Krankheitsverläufe. Aus diesem Grund müssen hochdosierte Zytostatika mit schwerwiegenden Nebenwirkungen eingesetzt werden, um die Resistenzentwicklung und Differenzierung der Krebszellen zu unterdrücken und so Tumorrezidiven vorzubeugen. Mit der gezielten Kombination verschiedenartiger, Target-spezifischer Pharmakophore zu multifunktionalen Wirkstoffen können jedoch therapieassoziierte Begleiterscheinungen, antagonistische Wechselwirkungen oder Resistenzen verringert wurden.

Die im Rahmen dieser Arbeit durchgeführten präklinischen Studien umfassen drei Substanzserien potenzieller Wirkstoffkandidaten, die hinsichtlich ihrer biochemischen Eigenschaften charakterisiert und optimiert wurden. Strukturell leiten sich die Testsubstanzen von den antiproliferativen sowie Tubulin-destabilisierenden Wirkstoffen LY290181 und Combretastatin A4 ab, wobei durch die gezielte Modifikation des 2-Amino-4-phenyl-4*H*-chromen-3-carbonitril-Grundgerüsts verschiedene biologische Targets adressiert werden.

An humanen Krebszelllinien konnten die entitätenspezifische Selektivität des antiproliferativen Potentials (MTT-Assay), intrazelluläre Lokalisation (Alkin-Azid-Click Chemie) sowie substanzinduzierte Effekte auf Zellzyklus (FACS-Analyse), Zytoskelett (Konfokalmikroskopie) und Zellmotilität (2D Tube-Formation-Assay) evaluiert werden. Weitere molekulare Wirkmechanismen wie Interferenz mit Mikrotubulidynamik, Caspaseinduktion, CDK1-Aktivität oder metabolischer Stabilität wurden mittels *in-vitro*-Enzym-Assays untersucht. Außerdem ermöglichte ein neuartiger Luciferase-Reporter-Assay das Screening potenzieller Inhibitoren der *c*-MYB-vermittelten Transkription. Im

Zebrafisch-Modell konnten sowohl die antiangiogenen Effekte als auch die Toxizität *in vivo* evaluiert werden, was darüber hinaus Hinweise auf die therapeutische Breite bei Vertebraten gibt. Ergänzend wurden pharmakokinetische ADME-Simulationen (*Absorption distribution metabolism and excretion)* und Docking-Studien (Tubulin) durchgeführt.

Im ersten Teilprojekt konnten für drei von fünfzehn 4*H*,5*H*-Pyran[3,2-*c*]chromen-5-on-Derivate neben spezifischer Zytotoxizität gegenüber malignen Zellen auch moderate Tubulin-bindende und Mikrotubuli-destabilisierende Effekte nachgewiesen werden. In diesem Zusammenhang sind vor allem die Substanzen mit ein- oder zweifach halogenierten Methoxyphenyl-Gruppen hervorzuheben. Die Immunofluoreszenzfärbung des Zytoskeletts zeigte ein vermehrtes Auftreten von Spindelabberationen und einen deutlichen Anstieg an bi- und multipolaren Mitosespindeln. Der beobachtete G2/M-Zellzyklusarrest konnte mit einer reduzierten CDK1 Aktivität und der vermuteten Akkumulation im Zellkern in Zusammenhang gebracht werden. Obwohl signifikante antiangiogene Effekte im Zebrafischmodell beobachtet wurden, lagen die wirksamen Konzentrationen relativ nahe an der letalen Dosis, was auf eine hohe *in-vivo*-Toxizität hindeutet.

Die im zweiten Teilprojekt behandelten 4*H*-Benzo[*h*]chromene wurden auf der Basis des Mikrotubuli-destabilisierenden und *c*-MYB-inhibierenden Naphthopyran-Derivats Bcr-TMP synthetisiert und in einem ersten Substanzscreening bezüglich zytotoxischer und *c*-MYB-inhibitorischer Eigenschaften analysiert. Sieben strukturell verwandte Vertreter mit vielversprechenden Eigenschaften wurden weiterführend auf ihre Fähigkeit untersucht, Tubulin zu binden, das Zytoskelett zu zerstören und den Zellzyklus zu arretieren. Dabei zeigte sich eine Korrelation zwischen zunehmender Alkylkettenlänge der 4-Alkoxygruppe und einer Abnahme der Aktivität. Neben einem ausgeprägten G2/M Zellzyklusarrest nach bereits 6 h waren eine vollständige Dissoziation der Mikrotubuli und eine erhöhte Caspaseaktivität nach 24 h die Folge. Das Propargyloxyderivat, welches ursprünglich für die intrazelluläre Lokalisierung hergestellt wurde, konnte sich aufgrund verbesserter Target-Bindung in Dockingstudien mit überlegener *in-vitro*-Tubulinpolymerisationsinhibition behaupten. Zusätzlich wurde eine beachtliche Angiogenese-Inhibition im Zebrafisch-Modell sowie eine außergewöhnlich große therapeutische Breite nachgewiesen. Vielversprechende

pharmakologische Eigenschaften und metabolische Stabilität verdeutlichen zudem die Relevanz als potenzielle Leitstruktur für weitere Studien.

Der dritte Teil dieser Arbeit erörtert die Struktur-Wirkungs-Beziehungen (SAR) einer weiteren Serie strukturverwandter 7-Methoxy-4-aryl-4*H*-chromene. Im Vergleich zu Vertretern der bereits beschriebenen 4*H*,5*H*-Pyran[3,2-*c*]chromen-5-on-Derivate und 4*H*-Benzo[*h*]chromen-Analoga konnte eine leichte Steigerung der Aktivität hinsichtlich Zytotoxizität und die Inhibition des Transkriptionsfaktors *c*-MYB erreicht werden. Der Wirkstoff mit einem 3,5-Diiod-4-methoxyphenyl-Substituenten erwies sich als besonders wirksam für die Zellzyklusarretierung in der G2/M-Phase und die Destabilisierung des Mikrotubuli-Zytoskeletts. Eine Ausnahme bildet das Zebrafischmodell, bei dem im Gegensatz zum 3-Chlor-4,5-dimethoxy-Derivat keine signifikanten Auswirkungen auf die Angiogenese und eine erhöhte Toxizität *in vivo* beobachtet wurde. Die Angiogenesehemmung des Chlorderivats war nicht nur vergleichbar mit der des bereits klinisch eingesetzten Axitinib, sondern zeigte auch eine ausgezeichnete Selektivität gegenüber Krebszellen und eine Inhibition von *c*-MYB im nanomolaren Bereich.

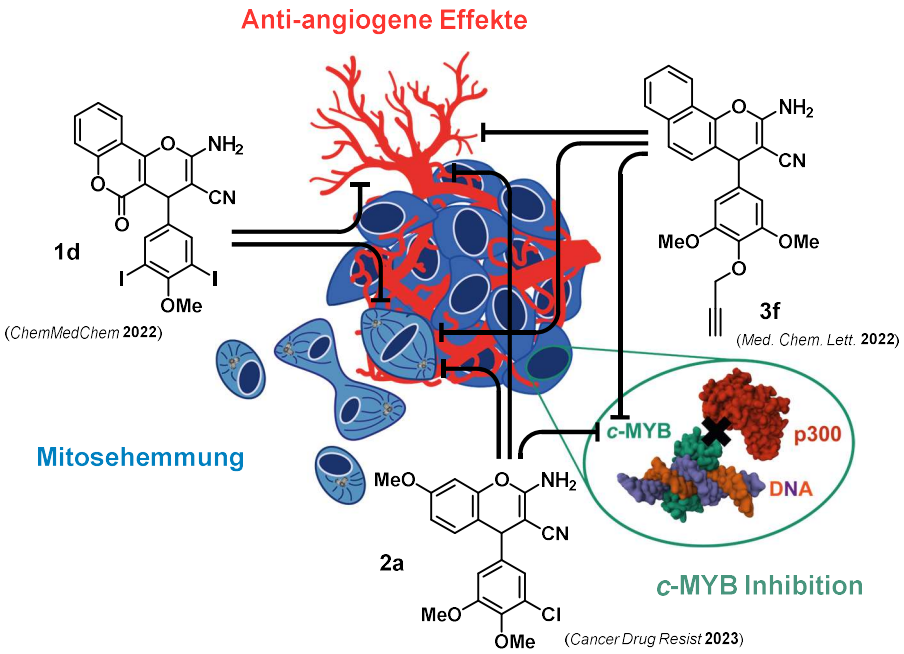

Summary

For more than a century, the international research community has been working to develop new therapies for malignant neoplasms. But despite huge investments, the discovery of a cure is not in sight and continues to pose new challenges to even the most advanced treatment strategies. Since cancer develops in many different cell types, the specific characteristics of each tissue lead to a very complex clinical picture, which makes it impossible to provide a universal therapy and requires the use of combination therapies in most cases. Genetic instability and stress-induced selection of cancer cells favor the propagation of oncogenes and lead to a volatile disease progression. For this reason, high-dose cytostatic drugs with severe side effects must be used to suppress the development of resistance and differentiation of cancer cells and thus prevent tumor recurrence. However, combining different target-specific pharmacophores into multifunctional agents can reduce therapy-related side effects, antagonistic interactions or resistances.

The preclinical studies performed in this work include three series of potential drug candidates characterized and optimized concerning their biochemical properties. The compounds are structurally derived from the antiproliferative and tubulin-destabilizing agents LY290181 and combretastatin A4, with the 2-amino-4-phenyl-4*H*-chromene-3-carbonitrile backbone modified to address multiple biological targets.

In human cancer cell lines, compound-specific selectivity of antiproliferative potential (MTT assay), intracellular localization (alkyne-azide click chemistry), as well as compound-induced effects on the cell cycle (FACS analysis), cytoskeleton (confocal microscopy) and cell motility (2D tube formation assay) could be evaluated. Further molecular mechanisms of action such as microtubule dynamics, caspase induction, CDK1 activity or metabolic stability were investigated using *in vitro* enzyme assays. In addition, a novel luciferase reporter assay was used to screen potential inhibitors of *c*-MYB-mediated transcription. The zebrafish model was used to assess both antiangiogenic effects and toxicity *in vivo*, providing insight into the therapeutic index in vertebrates. In addition, pharmacokinetic ADME simulations and docking studies (tubulin) were performed.

The first part of the project showed that three of the fifteen 4*H*,5*H*-pyran[3,2-*c*]chromen-5-one derivatives had moderate tubulin binding and microtubule destabilizing activities

and were specifically cytotoxic against malignant cells. Here, the compounds with one or two halogenated trimethoxyphenyl groups are of particular interest. Immunofluorescence staining of the cytoskeleton indicated an increase of spindle aberrations as well as bi- and multipolar mitotic spindles. G2/M cell cycle arrest was associated with reduced CDK1 activity and presumed nuclear accumulation. Although significant antiangiogenic effects were observed in the zebrafish model, the effective concentrations were relatively close to the lethal dose, indicating a high level of toxicity *in vivo*.

The 4*H*-benzo[*h*]chromenes investigated in the second subproject were synthesized based on the recently published microtubule-destabilizing and *c*-MYB-inhibiting naphthopyran derivative Bcr-TMP and screened for cytotoxic and *c*-MYB-inhibitory properties. Seven structurally related compounds with promising properties were further tested for their ability to bind tubulin, disrupt the cytoskeleton and arrest the cell cycle. This revealed a correlation between increasing alkyl chain length of the 4-alkoxy group accompanied by a decrease in activity. In addition to a pronounced G2/M cell cycle arrest after 6 hours, complete microtubule dissociation and increased caspase activity were observed after 24 hours. The alkynyl derivative, initinally designed for intracellular localization, also performed well in docking studies due to improved target binding and superior *in vitro* tubulin polymerization inhibition. In addition, the zebrafish model has demonstrated remarkable inhibition of angiogenesis and a broad therapeutic spectrum. Its relevance as a potential lead structure for further studies is demonstrated by its promising pharmacological properties and metabolic stability.

The third part of this work deals with the structure-activity relationships of another series of structurally related 7-methoxy-4-aryl-4*H*-chromenes. Compared to the reported 4*H*,5*H*-pyran[3,2-*c*]chromen-5-one derivatives and 4H-benzo[*h*]chromen analogues, a slight increase in activity was achieved concerning cytotoxicity and inhibition of the transcription factor *c*-MYB. In particular, the 3,5-diiodo-4-methoxyphenyl substituent has been shown to be particularly effective in arresting the cell cycle at G2/M and destabilizing the microtubule cytoskeleton. An exception is the zebrafish model, where in contrast to the 3-chloro-4,5-dimethoxy derivative, no significant effect on angiogenesis and increased toxicity were observed *in vivo*. The antiangiogenic activity of the chloro-derivative was comparable to that of the clinically

used axitinib, but also showed excellent selectivity towards cancer cells and inhibited *c*-MYB in the nanomolar range.

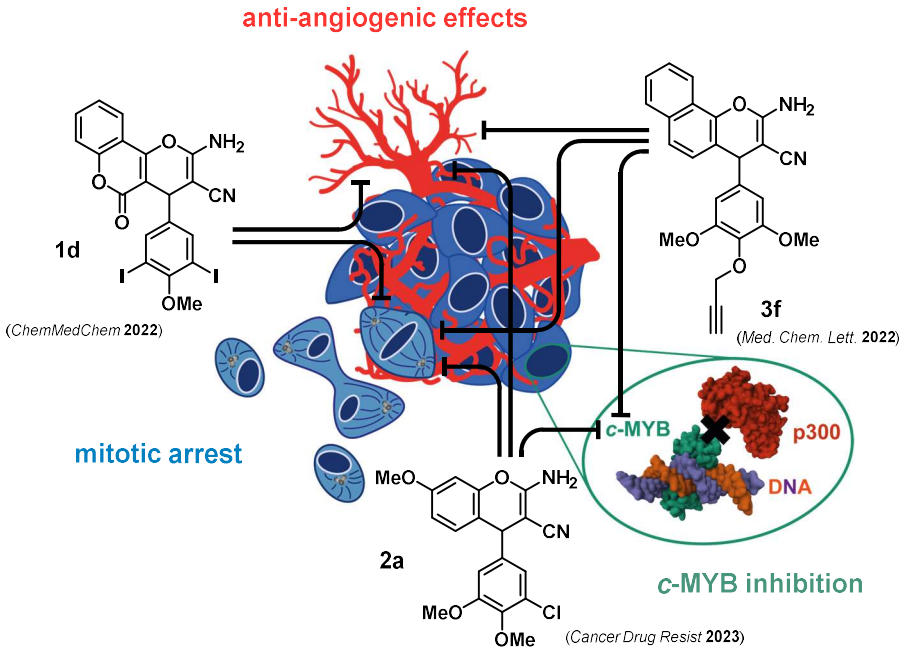

1. Einleitung

1.1 Krebs-assoziierte Eigenschaften: „Hallmarks of Cancer“

Trotz bahnbrechender Fortschritte bei der klinischen Behandlung von Krebs, sind viele Mechanismen, die zur Entstehung, dem Wachstum oder der Resistenzbildung gegenüber Chemotherapeutika beitragen, noch nicht vollständig geklärt. Da ein Tumor vielmehr einem eigenständigen Organismus mit differenzierten Zelltypen ähnelt und nicht, wie lange angenommen, nur eine Ansammlung von homogenen Krebszellen darstellt, wird die Erforschung sowie die Behandlung immer wieder vor neue Herausforderungen gestellt. Grundlage für ein umfassendes Verständnis der Krebsentstehung ist eine Kategorisierung der biochemischen Mechanismen, die einer neoplastischen Erkrankung zugrunde liegen. Die als „*Hallmarks of Cancer*“ von HANAHAN und WEINBERG postulierten Eigenschaften, stellen vereinfacht die Merkmale dar, in denen sich ein Tumor von gesundem Gewebe unterscheidet.[1]

Dies umfasst Proliferation-induzierende Stimuli, Umgehung von Wachstumssuppressoren, proliferative Immortalität, Resistenz gegenüber natürlichem und induziertem Zelltod, Irreführung des Immunsystems, die Verbreitung durch Invasion und Metastasierung, Aufhebung von stoffwechselregulierenden Mechanismen sowie Induktion von Angiogenese. Zusätzlich wird dies durch eine erhöhte Mutationsrate sowie Tumorgenese-fördernde Entzündungsreaktionen begünstigt.[2] Die jüngst erweiterte Darstellung der Tumor-assoziierten Merkmale umfasst außerdem das Tumor-Mikrobiom ebenso wie die epigenetische Neuprogrammierung als potentielle Einflussfaktoren und eine phänotypische Variationsbreite sowie zelluläre Seneszenz als zentralen Bestandteil der sogenannten *Hallmarks* (Abb. 1).[3] Diese stark vereinfachte Darstellung wird der Komplexität einer Krebserkrankung zwar nicht annähernd gerecht, bietet aber ein Organisationsprinzip, das die Ausgangsposition für die Identifikation neuer krebsspezifischer Targets liefert. Ein zentrales Ziel ist dabei die zugrundeliegenden Veränderungen im Erbgut (Onkogene) zu lokalisieren, da möglicherweise mehr als 1% des gesamten humanen Erbguts durch Mutation zur Entstehung von Krebs beitragen können.[4] Potenzielle Onkogene sind insbesondere solche, die Proteine mit wichtigen Zellzykluskontrollfunktionen, Apoptose, Wachstumsstimulation, Transkription oder Signaltransduktion kodieren.[5] Obwohl die Veränderungen des Genoms für verschiedene Tumorarten sehr spezifisch sind und stark variieren können, besteht

gemeinhin eine Korrelation zwischen der Mutationsrate und der Malignität eines Tumors.[6,7] Vor allem die Instabilität des Tumorzellgenoms spielt eine wichtige Rolle in der Entwicklung einer malignen Krebserkrankung.[8]

Abbildung 1: Die von HANAHAN *et al.* definierten charakteristischen Eigenschaften von Krebszellen (*Hallmarks of cancer*). [Eigene Darstellung nach HANAHAN *et al. 2022*][3]

1.1.1 Genetische Instabilität

Die erhöhte Neigung bei der Zellteilung eine Veränderung des Erbguts zu erfahren, wird als Genomische Instabilität bezeichnet und im Kontext eines Mutator-Phänotyps diskutiert.[9] Dieser beschreibt die Akkumulation von Mutationen, die eine weitere Mutagenese begünstigen und zu einer starken genetischen und phänotypischen Heterogenität innerhalb des sich entwickelnden Tumors beitragen.[10] Dieses Phänomen ist hauptsächlich bei hereditären-Krebsarten die treibende Kraft für eine erhöhte Mutationsrate, wohingegen bei zufällig entstehenden Neoplasien als Hauptursache Onkogen-induzierter Stress bei der DNA-Replikation vermutet wird.[11] Sogenannte Driver-Mutationen verleihen einer Subpopulation bei gleichem Mikromilieu einen Wachstumsvorteil, was zu einer Verbreitung dieser Eigenschaften innerhalb eines Tumors führt (Abb. 2).[12] Selektionsprozesse können dabei hypoxische Bedingungen, Reaktionen des Immunsystems oder auch eine Therapie darstellen, die über einen langen Zeitraum zu einer Anpassung der malignen Zellen führt und in vielen Fällen die Resistenzbildung sowie das Auftreten von Tumorrezidiven bedingt. [13–16] DNA-Reparaturmechanismen wie die *base exicion repair* (BER) sind essenziell für die Aufrechterhaltung der genetischen Integrität, da jede menschliche Zelle täglich

schätzungsweise 70000 DNA-Schäden (Punktmutationen, Einzel- oder Doppelstrangbrüche) ausgesetzt ist, die im Fall von Doppelstrangbrüchen auch Chromosomenaberrationen zur Folge haben können.[17]

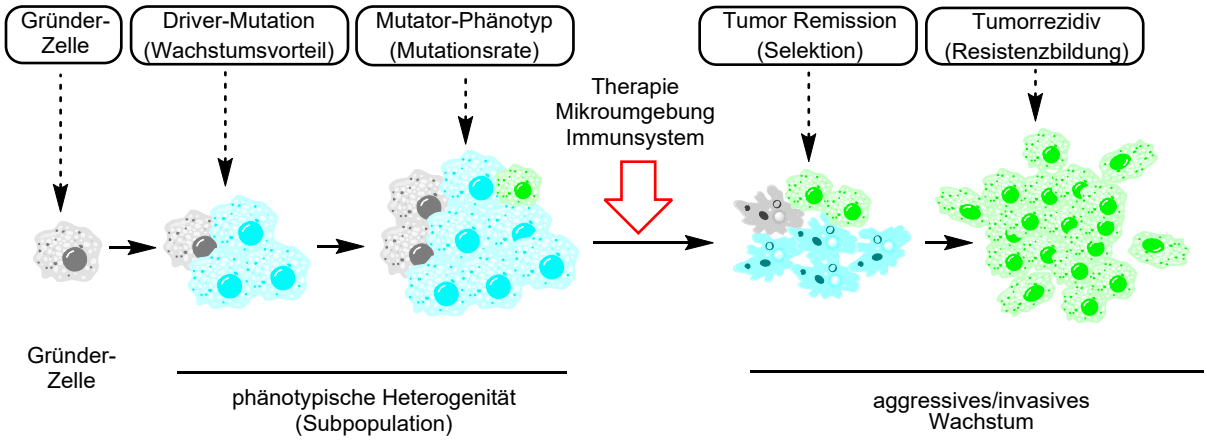

Abbildung 2: Auswirkungen phänotypischer Heterogenität auf die Tumorentwicklung und den Selektionsprozesses von Tumorzell-Subpopulationen. [Eigene Interpretation nach NIIDA *et al.* 2018][18]

Es wird dabei zwischen strukturellen (Deletion, Amplifikation, Inversion, Insertion und Translokation) oder numerischen (Aneuploidie) Abnormalitäten unterschieden.[19] Mutationen in Genen, die für DNA-Reparaturproteine kodieren, oder fehlerhafte Kontrollmechanismen, die zu deren Herunterregulierung führen, sind häufig die Ursache genetischer Instabilität.[20] Darüber hinaus besteht eine enge Verknüpfung mit dem apoptotischen Zelltod, der bei irreparablen DNA-Doppelstrangbrüchen, Telomerdysfunktionen oder einem aneuploiden Zustand, die Weitergabe von Mutationen verhindern soll.[21]

1.1.2 Zelltodresistenz

Der programmierte Zelltod (Apoptose) ist eine wichtige Barriere gegenüber unkontrollierter Zellproliferation und der Entstehung genetischer Instabilität. Apoptose kann extern, etwa durch Immunzellen (extrinsischer Mechanismus, Granzym/Perforin initiiert), oder intrazellulär durch beispielsweise DNA-Schäden (intrinsischer Mechanismus) induziert werden (Abb. 3).[22] Die Granzym/Perforin-vermittelte Apoptose wird durch T-Lymphozyten oder natürliche Killerzellen (NK-Zellen) ausgelöst und ist ein wesentlicher Abwehrmechanismus des Immunsystems gegen Virus-infizierte oder entartete Zellen.[23] Sekretierte Perforine bilden durchlässige Transmembrankanäle in der Zellmembran der Zielzellen und machen diese für verschiedene Granzym-Serinproteasen durchlässig. Diese induzieren die Apoptose

sowohl durch *interacting-domain death agonist* (BID) -vermittelte Freisetzung von Cytochrom C als auch durch direkte Aktivierung von Caspasen.[24] Die intrinsische Apoptose-Kaskade wird durch oxidativen Stress oder als Antwort auf DNA-Schäden durch den Tumorsuppressor p53 über die Aktivierung von pro-apoptotischen Signalproteinen der Bcl-2-Familie initiiert. Vertreter wie das *BCL-2 associated X protein* (BAX) oder *BCL-2 homologous killer* (BAK) bewirken eine Permeabilisierung der äußeren Mitochondrienmembran (MOMP) was die Freisetzung von Cytochrom C nach sich zieht.[25] Dort bildet es mit dem *apoptotic protease activating factor 1* (APAF1) das Apoptosom und setzt durch die Spaltung von Procaspase-9 die Caspasekaskade in Gang, welche schlussendlich die Apoptose zur Folge hat.[26] Der extrinsische Weg kann durch T-Lymphozyten initiiert werden, die durch sogenannte Todesliganden (FASL, TRAIL, TNF) die jeweiligen Todesrezeptoren (FASR, TRAILR, TNFR) aktivieren.[27–29] Adapterproteine wie das *Fas-associated death domain protein* (FADD) bilden mit den Initiator-Caspasen 8 und 10 den DISC (*death-inducing signalling complex*), welcher für die Einleitung der proteolytischen Kaskade verantwortlich ist und wie bei der intrinsischen Aktivierung die Effektor-Caspasen 3, 6 und 7 aktiviert .[30]

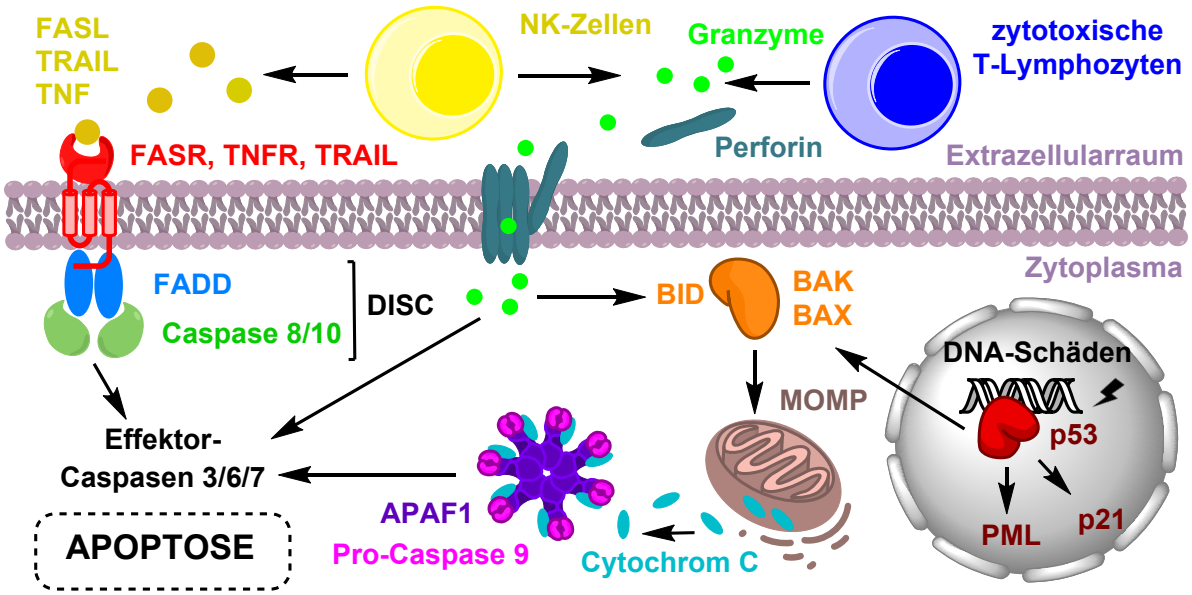

Abbildung 3: Vereinfachte Darstellung der Apoptose-Kaskade bestehend aus Granzym/Perforin-vermittelten, extrinsischen und intrinsischen Signalwegen. [Freie Interpretation nach CARNEIRO *et al.* 2020][30]

Diese hochkomplexen Mechanismen stehen unter der Kontrolle sogenannter Tumorsuppressorproteine, die das Überleben jeder Zelle bestimmen, indem sie pro- oder antiapoptotische Stimuli regulieren.[31,32] Der Transkriptionsfaktor p53 nimmt hierbei eine Schlüsselfunktion ein, da er bei DNA-Schäden zu einer verstärkten

Transkription von Zellzyklus-arretierenden (p21), Apoptose induzierenden (BAX) oder Seneszenz auslösenden Proteinen wie das *promyelocytic leukemia protein* (PML) beiträgt.[33–35] Eine Beeinträchtigung der p53-Funktion steht deshalb auch in einem kausalen Zusammenhang mit der Entstehung von vielen Malignomen, was in mindestens 50% aller Tumore Mutationen im *TP53*-Gen geschuldet ist.[36] Bei mehr als 75% handelt es sich um *missens*-Mutationen die entweder einen Funktionsverlust bewirken oder neomorphe Aktivitäten hervorbringen die Prozesse wie Invasion, Metastasierung oder Proliferation begünstigen können.[37,38] Neben der Apoptose ist die Autophagozytose eine zellphysiologische Reaktion auf Stresssituationen wie Nährstoffmangel. Dabei werden zelleigene Bestandteile in Autophagosomen eingeschlossen und mit Hilfe von Lysosomen verdaut, um in nährstoffarmer Umgebung, wie etwa im Zentrum eines Tumors, überleben zu können.[39] Im Zusammenhang mit einer Substanz- oder Strahlungsbehandlung, kann Autophagozytose in Krebszellen zu einer Überdauerung der Therapie und anschließender Regeneration beitragen.[40]

Die Seneszenz stellt einen weiteren Tumorsuppressor-Mechanismus dar, welcher die unbegrenzte Teilung von somatischen Zellen durch kürzer werdende Telomere reguliert und der Entstehung von Krebs entgegenwirkt.[41] Diese replikative Seneszenz arretiert den Zellzyklus irreversibel in seiner G1- oder G2/M-Zellzyklusphase wobei die Zelle weiterhin metabolisch aktiv bleibt.[42] Des Weiteren kann Seneszenz auch als Reaktion auf DNA-Schäden oder oxidativen Stress durch p53 und p16 (*CDK inhibitor 2A*) regulierte Signalwege ausgelöst werden.[43] Die Fähigkeit seneszenter Zellen, eine Vielzahl an extrazellulären Modulatoren, darunter Wachstumsfaktoren, Zytokine, Proteasen und Lipide zu sekretieren wird als Seneszenz-assoziierter, sekretorischer Phänotyp (SASP) definiert. Der SASP kann in diesem Kontext die Seneszenz verstärken und durch immunvermittelte Zerstörung von seneszenten Tumorzellen, Förderung der Geweberegeneration oder Eingrenzung von Fibrosen zur Tumorbekämpfung beitragen, aber andererseits auch chronische Entzündungsreaktionen verursachen, sowie das Wachstum und Überleben von Tumorzellen stimulieren.[44] Dieser oft durch Chemo- oder Strahlentherapie hervorgerufene SASP ist nicht immer Bestandteil einer irreversiblen Inaktivierung von Krebszellen, sondern kann in Form einer transitorischen Seneszenz auch eine Überlebensstrategie darstellen.[45] Eine SASP-induzierte Immunantwort kann bei der Beseitigung von seneszenten Zellen die Selektion von latenten

Stammzelleigenschaften begünstigen und einen Zellzyklus-Wiedereintritt zur Folge haben.[46] Die Invertierung der Zellzyklusblockade wird zudem mit einem erhöhten Wachstumspotential und vermehrtem Auftreten in Rezidivtumoren assoziiert.[47]

1.1.3 Proliferative Immortalität

Somatische Zellen sind bis auf wenige Ausnahmen an eine maximale Anzahl an Teilungszyklen gebunden, die sogenannte Hayflick-Grenze, welche sich aus der stetigen Verkürzung der Telomerenden von Chromosomen bei der Mitose ergibt.[48] Beim Erreichen einer kritischen Telomerlänge wird p53-abhängig entweder Seneszenz induziert oder Apoptose ausgelöst, um unkontrolliertem Wachstum oder der Akkumulation von Replikationsfehlern entgegenzuwirken.[49] Sich kontinuierlich teilende Zellen (Knochenmarkszellen, Keimzellen, Stammzellen und Immunzellen) sind in der Lage dieses Limit zu überschreiten, indem sie den Ribonukleoproteinkomplex, auch Telomerase genannt, exprimieren, der die Telomerenden stetig verlängert.[50] Der Enzymkomplex besteht aus der katalytischen *telomerase reverse transcriptase* (TERT), der Telomerase-RNA-Matrize (TERC) und Dyskerin (DKC1).[51] Die unbegrenzte Teilungsfähigkeit von Krebszellen setzt im Rückschluss eine permanente Verlängerung der Telomere voraus, was entweder durch die Überexpression von Telomerase (~90%) oder in einigen wenigen Fällen durch den Prozess des *alternative lengthening of telomerases* (ALT) ermöglicht wird.[52,53] In diesem Szenario wird durch homologe Rekombination von benachbarten Telomersequenzen die Verlängerung mittels *Fanconi anemia complementation group M* (FANCM) und DNA Polymerase δ realisiert.[54] Neben der Telomerverlängerung nimmt TERT Einfluss auf eine Reihe wichtiger Signalwege (Wnt/β-Catenin, NF-κB, MYC), die ebenfalls mit der Entstehung und Ausbreitung von Krebs in Verbindung gebracht werden.[55]

1.1.4 Veränderte Signaltransduktion

In somatischen Geweben wird die Zellproliferation über Signaltransduktionswege reguliert um ein Gleichgewicht (Homöostase) zwischen verschiedenen Zelltypen zu gewährleisten. Alle Zellen sind auf Stimulatoren (Wachstumsfaktoren, Mitogene) angewiesen, um in einen proliferierenden Zustand überzugehen oder können durch inhibierende Faktoren (Tumorsuppressoren) wieder in einen Ruhezustand versetzt werden.[56] Diese Signale werden über Transmembranrezeptoren in die Zelle übertragen, indem Signalmoleküle an der Zelloberfläche binden und intrazellulär eine

Signalkaskade auslösen.[57] Neben der Proliferation werden auch Prozesse wie Differenzierung, Motilität oder Viabilität der Zelle reguliert, die von HANAHAN *et al.* umgangssprachlich als zelluläre Schaltkreise benannt wurden (Abb. 4).[2]

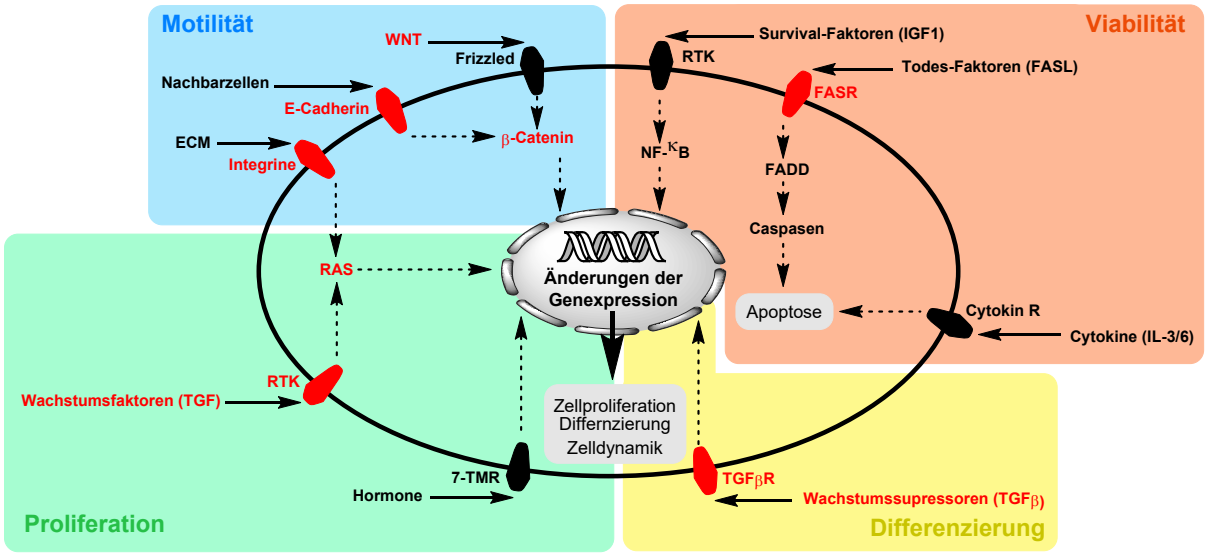

Abbildung 4: Vereinfachte Darstellung der interzellulären (durchgezogene Pfeile) und intrazellulären (gestrichelte Pfeile) Signaltransduktionswege, die Motilität, Viabilität, Proliferation und Differenzierung regulieren sowie wichtige Vertreter der Transmembranrezeptoren und Signalmolekülen, die in malignen Zellen teilweise mutiert sind (rot). [Freie Interpretation nach HANAHAN *et al.* 2011][2]

Die Charakterisierung der entarteten Signaltransduktion in Krebszellen wird dadurch erschwert, dass ein Teil der Zusammenhänge bis heute nicht verstanden ist und sich die meisten Signalwege in einem komplexen Netzwerk gegenseitig kontrollieren. Offensichtlich machen sich alle malignen Zellen auf die eine oder andere Weise von dieser Regulation unabhängig, um sich auch ohne Wachstumsstimulation unbegrenzt teilen zu können. Strategien, um von externen Wachstumsfaktoren unabhängig zu werden, können darin bestehen, die umgebenden Zellen zur Sekretion dieser Faktoren anzuregen (parakrine Sekretion) oder sie durch Veränderung der Genexpression selbst zu produzieren (autokrine Sekretion).[58,59] Überexprimierte oder durch Mutationen konstitutiv aktivierte Transmembranrezeptoren sowie die Unterbrechung von Regulationsmechanismen und Tumorsuppressoren können die Ursache einer verstärkten Signalaktivierung sein. Neben p53 ist das Retinoblastom-Protein (RB) ein zentraler Kontrollknotenpunkt bei der Regulation des Zellzyklus, und eine Inaktivierung ist in vielen Fällen für die Entstehung von Krebs verantwortlich.[60] Zell-Zell-Adhäsionsproteine (Cadherine) oder Matrix-Rezeptoren (Integrine) können zusätzlich Einfluss auf Zellkohärenz und Signaltransduktion nehmen indem sie Zellwachstum, Differenzierung oder Motilität unterdrücken.[61,62]

1.1.5 Angiogenese

Bei der Bildung von Blutgefäßen wird grundsätzlich zwischen der Neubildung aus endothelialen Vorläuferzellen (Vaskulogenese) und der Angiogenese aus bestehenden Gefäßen unterschieden.[63] Erstere baut während der Embryogenese das Herz und die grundlegende Gefäßstruktur aus sich differenzierenden Hämangioblasten auf, während die Angiogenese durch Spaltungsvorgänge oder lokale Sprossbildung mittels endothelialer Zellmigration für die Bildung von Blutgefäßkapillaren verantwortlich ist.[64–66] Mit Ausnahme der Wundheilung und reproduktiver Prozesse ist die Angiogenese praktisch inaktiv und wird nur durch pro-angiogene Wachstumsfaktoren angeregt. Zu den wichtigsten Aktivatoren zählen der *fibroblast growth factor* (FGF), der *vascular endothelial growth factor* (VEGF), Angiopoetin (Ang) und der *plated derived growth factor* (PDGF), die während der Angiogenese verschiedene Prozesse regulieren.[67] Außerdem spielt die Reorganisation der *extracellular matrix* (ECM) durch sogenannte Matrix-Metalloproteasen (MMP), Urokinasen und Integrine eine wichtige Rolle.[68–70]

Im frühen Stadium eines Tumors wird das Wachstum auf eine begrenzte Verfügbarkeit von Sauerstoff und Nährstoffen durch Diffusion beschränkt. Daraus resultiert ein konzentrisches Mikromilieu bestehend aus einer stark proliferierenden äußeren Zellschicht, einem hypoxischen Bereich im Inneren und einem nekrotischen Kern.[71,72] Die Entstehung von makroskopischen Tumoren setzen deshalb eine gewisse Vaskularisierung des Tumorgewebes voraus was auch als *angiogenic switch* bezeichnet wird.[73] Dies ist das Ergebnis einer Gleichgewichtsverschiebung durch Herunterregulierung von Angiogeneseinhibitoren (Thrombospondine, Interferone) bei gleichzeitiger Steigerung der Expression von Wachstumsfaktoren (VEGF) durch Transkriptionsfaktoren wie den *hypoxia inducible factor* (HIF-1α).[74–77] Außerdem können immobilisierte pro-angiogene Faktoren auch durch den proteolytischen Abbau der ECM freigesetzt werden.[78] Die durch chronisch-aktivierte Angiogenese entstandenen Tumorendothelzellen sind oft morphologisch entartet und bilden chaotische und unregelmäßig-verzweigte Blutgefäße.[79] Fehlende Zell-Zell-Verknüpfungen (*tight junktions*), geringe Stabilisierung durch Pericyten und eine ungleichmäßige Basalmembran lassen Lücken in den Gefäßwänden auftreten was unstetigen Blutfluss und Ausblutungen zur Folge hat (Abb. 5).[80] Es wurde beobachtet, dass Bereiche der Gefäßwand mit Tumorzellen ohne endothelspezifische Oberflächenantigene ausgekleidet sind (Mosaikgefäße), die direkten Kontakt mit dem

Blutstrom ermöglichen und möglicherweise einen starken Einfluss auf die Ausbreitung von Tumorzellen im Organismus (Metastasierung) haben.[81,82]

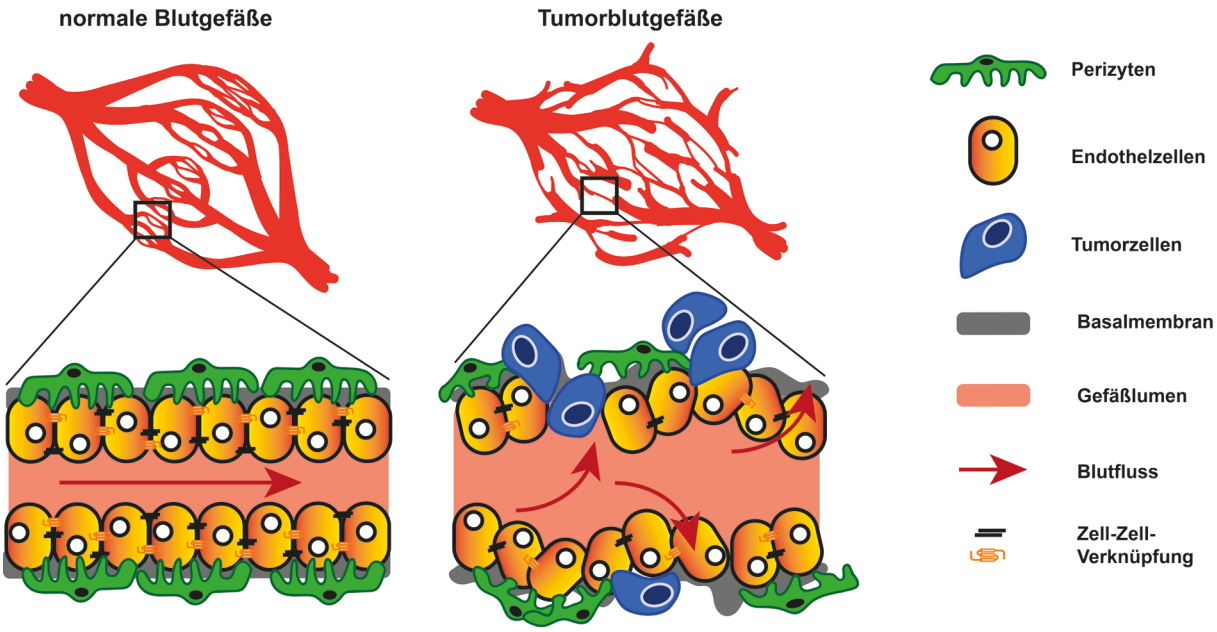

Abbildung 5: Vergleichende Darstellung von gesunden Blutgefäßen und Tumorblutgefäßen anhand der Struktur und dem zellulären Aufbau. [Eigene Darstellung nach LUGANO *et al.* 2020][83]

Wenn es zu einer vollständigen Substitution von Endothelzellen durch gefäßimitierende Tumorzellen kommt, die ein Angiogenese-unabhängiges Gefäßsystem aufbauen, wird auch von vaskulärer Mimikry gesprochen.[84] Durch hypoxische Bedingungen innerhalb des Tumors wird das Differenzierungspotential von *cancer stem cells* (CSCs) verstärkt, die im Laufe einer *epithelial-endothelial transition* (EET) endotheliale Eigenschaften erwerben und so beispielsweise VE-Cadherin zur Zelladhäsion oder Fibronektin für eine Verankerung in der ECM exprimieren.[85,86]

1.1.6 Invasion und Metastasierung

Unter Metastasierung wird eine Verbreitung von Tumorzellen an anatomisch entfernte Orte versanden, die ausgehend vom Primärtumor verschiedene Stadien der morphologischen Veränderung und Anpassung durchlaufen.[87] Die schrittweise erfolgende Metastasierung beginnt mit der EMT-vermittelten Abspaltung einzelner Zellen vom Primärtumor und der Migration in umliegendes Gewebe (Invasion), gefolgt von dem Eindringen in Blut- oder Lymphgefäße (Intravasation), der Verteilung im Organismus (Zirkulation), dem erneuten Austreten durch die Gefäßwand

(Extravasation) und einer erfolgreichen Ansiedlung des Sekundärtumors (Kolonisierung) in einem neuen Micromilieu (Abb. 6).[88]

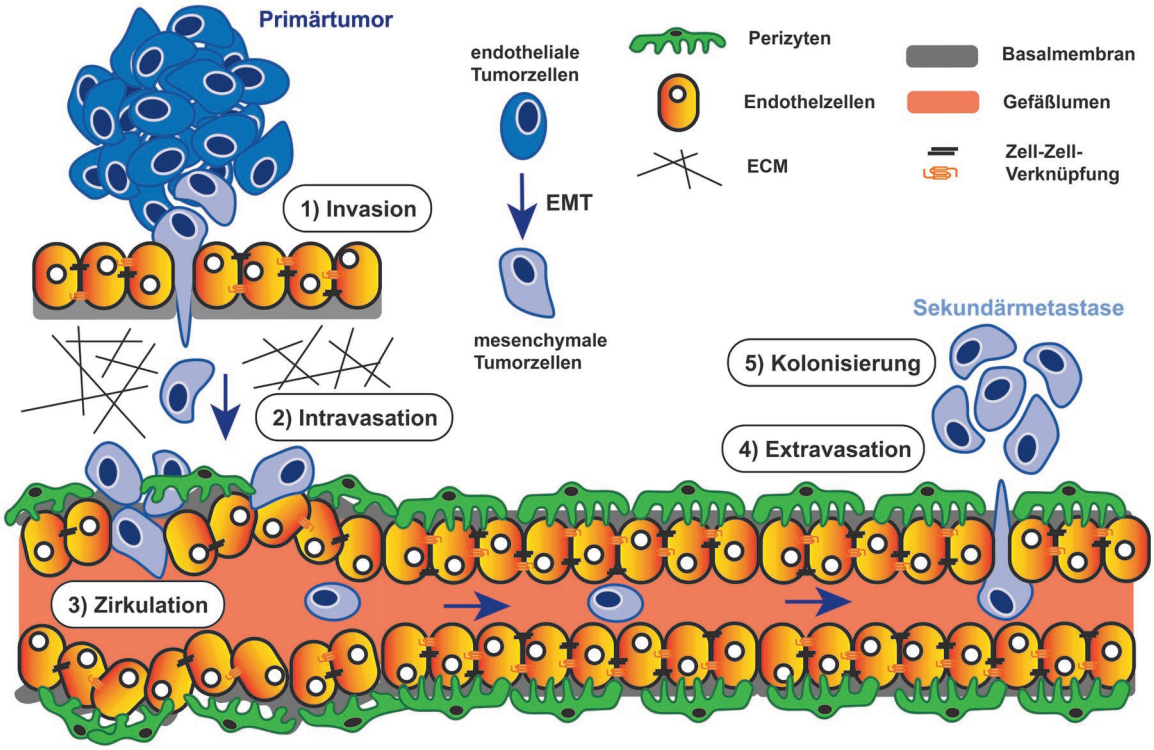

Abbildung 6: Schematische Darstellung des Metastasierungsprozesses mit EMT-vermittelter Invasion (1), Intravasation (2), Zirkulation (3), Extravasation (4) und Kolonisierung (5). [Eigene Darstellung nach MAIJDPOOR *et al.* 2021][88]

Epithelzellen zeichnen sich normalerweise durch eine starke Verknüpfung mit ihren Nachbarzellen (*tight junctions*, *gap junctions* oder *adherent junctions*), apikal-basale Polarität und eine Verankerung in der Basallamina aus, während Mesenchymzellen eine spindelförmige Morphologie und migratorische Eigenschaften zeigen.[89] Der Übergang von epithelialer Morphologie zu einem mesenchymalen Erscheinungsbild wird allgemein als *epithelial-mesenchymal transition* (EMT) bezeichnet und ist ein sukzessive-verlaufender Prozess der verschiedene Zwischenstadien einschließt.[90] Initiiert wird die phänotypische Veränderung oft durch eine Transkriptionsfaktor-vermittelte Verringerung der E-Cadherin Expression, die einerseits das Ablösen von benachbarten Endothelzellen begünstigt und andererseits β-Catenin in das Cytoplasma freisetzt, das weitere EMT-Signalkaskaden in Gang setzt.[91] Als Resultat werden für Mesenchymzellen charakteristische Proteine wie N-Cadherin und Vimetin exprimiert, umliegende *cancer-associated fibroblasts* (CAFs) zur Produktion von EMT-induzierendem *transforming growth factor β* (TGF-β) angeregt und ECM-abbauende MMPs freigesetzt.[92,93] Diese Eigenschaften ermöglichen eine gerichtete Migration von

Einzelzellen oder Zellkolonien durch die ECM und fördern zudem die Intravasation der Zellen in Lymph- oder Blutgefäße. Anhand von Aktin-vermittelter Protrusion werden Filopodien und Lamellipodien gebildet, die sich mittels focaler Adhäsion in der Umgebung verankern können und die Zelle durch Aktin-Myosin Kontraktion in eine Richtung bewegen.[94] Die transendotheliale Migration ist noch nicht vollständig verstanden, erfolgt aber unter dem Einfluss verschiedener Faktoren wie zelluläre Eigenschaften (Genexpression, mesenchymaler Phänotyp), zelluläres Microenvironment (CAFs, Neutrophile) oder mechanische Einflüsse (interstitieller Druck, endotheliale Stabilität).[95] Die Ausbreitung von *circulating tumor cells* (CTCs) in Blut oder Lymphe erfordert zelluläre Anpassungen an die exponierte Umgebung, um außerhalb des Zellverbandes vor Anoikis und Immunreaktionen geschützt zu sein.[88] Anoikis ist eine Form der Apoptose, die in Endothelzellen nach Ablösung von der ECM auftritt und in CTCs durch TGF-β oder HIF-1α inhibiert wird.[96,97] Eine Umgehung des Immunsystems wird hauptsächlich durch die Interaktion mit CAFs, Neutrophilen oder Thrombozyten erreicht indem die CTC-Oberfläche durch Clusterbildung maskiert und vor beispielsweise natürlichen Killerzellen geschützt wird.[98] Thrombozyten spielen auch bei der TGF-β und NF-κB vermittelten transendothelialen Extravasation in umliegendes Gewebe und bei der erneuten Ausprägung invasiver Eigenschaften eine wichtige Rolle.[99] Nach vollständigem Eindringen in das Gewebe verweilen die Tumorzellen oft lange Zeit in einem Ruhezustand, um Immunreaktionen zu umgehen und sich an das fremde Milieu anzupassen.[100] Für das erneute Eintreten in ein proliferatives Stadium müssen die bei der EMT durchlaufenen phänotypischen Veränderungen umgekehrt und eine *mesenchymal endothelial transition* (MET) vollzogen werden.[101] Schließlich kommt es zur Bildung von Tochtergeschwülsten (Metastasen) in lebenswichtigen Organen, was die Hauptursache hoher Sterblichkeitsraten darstellt.[102] Aus diesem Grund ist ein biochemisches Verständnis aller krebsspezifischen Merkmale von grundlegender Bedeutung für die Entwicklung neuer Wirkstoffe und zielgerichteter Therapieansätze. Nachfolgend werden die Fortschritte der letzten Jahrzehnte näher erörtert und im Kontext aktueller Wirkstoffforschung diskutiert.

1.2 Antitumorale Wirkstoffe

Mit der Entdeckung der Röntgenstrahlen Ende des 19. Jahrhunderts und der Etablierung der ersten Strahlentherapie nahm die medizinische Behandlung von Tumorerkrankungen ihren Anfang. Die Wirksamkeit des ersten chemotherapeutischen Präparats wurde 1942 von GOODMAN und GILMAN anhand des DNA-alkylierenden Stickstofflostes bewiesen und setzte damit den Grundstein für die moderne Chemotherapie.[103,104] Nicht viel später entdeckte FABER den Antimetaboliten der Folsäure (Aminopterin **1**), welcher eine Remission bei leukämiekranken Kindern bewirkte und den Vorläufer des heutzutage immer noch eingesetzten Methotrexats **2** darstellt.[105] In den darauffolgenden Jahren kamen weitere Antimetabolite wie 5-Fluoruracil **3** (1962), Topoisomeraseinhibitoren wie Doxorubicin **4** (1974), DNA-Alkylanzien wie Cisplatin **5** (1978) oder Mitosehemmer wie Paclitaxel **6** (1992) auf den Markt und sollten die Krebstherapie bis heute stark beeinflussen (Abb. 7).[106–108]

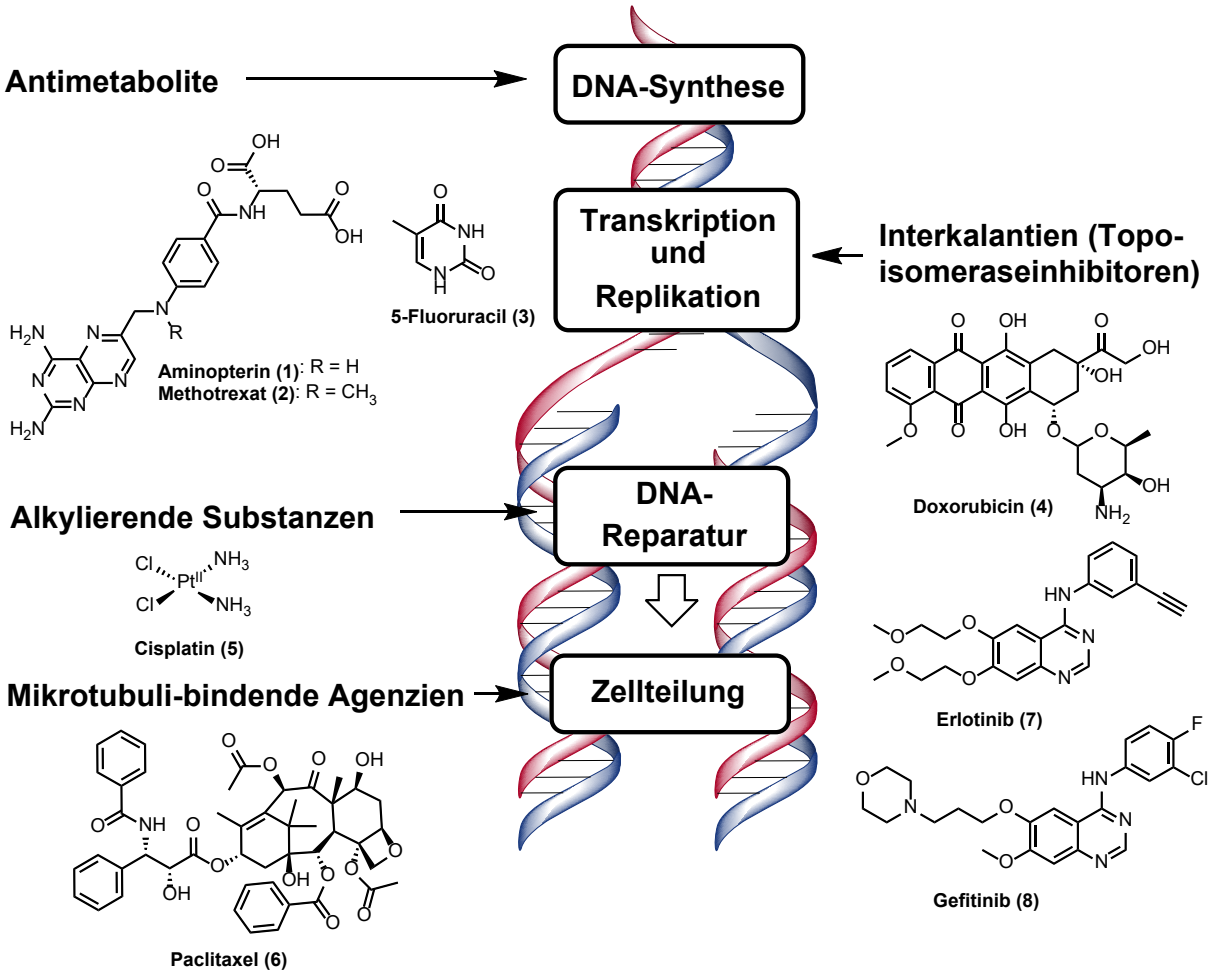

Abbildung 7: Strukturen und molekulare Targets klinisch angewendeter Krebstherapeutika. DNA-Synthese (Aminopterin **1**, Methotrexat **2**, 5-Fluoruracil **3**), Transkription und Replikation (Doxorubicin **4**, Erlotinib **7**, Gefitinib **8**), DNA-Reparatur (Cisplatin **5**) und Zellteilung (Paclitaxel **6**).

Neben vielen weiteren zugelassenen Zytostatika veränderten sich auch die Therapiestrategien von einzelnen Wirkstoffen hin zu Kombinationstherapien aus unterschiedlichen Wirkstoffklassen, Strahlentherapie und onkologischer Chirurgie. Obwohl die Überlebenschancen von Krebspatienten nachhaltig verbessert werden konnten, brachte die klassische Chemotherapie schwerwiegende Nebenwirkungen durch die Schädigung gesunder Zellen, sowie die Entstehung von Resistenzen mit sich.[109,110] Mit einem immer umfassenderen Verständnis der molekularen Mechanismen von Krebserkrankungen konnten zielgerichtete Strategien gegenüber spezifischen Targets wie Zellzyklusregulatoren, Wachstumsfaktoren, Apoptoseinhibitoren oder Angiogenese-kontrollierenden Proteinen entwickelt werden, was die Ära der *targeted therapy* einläutete.[108] Dazu gehören hauptsächlich *small molecule inhibitors*, die gezielt Proteine wachstumsfördernder Signalkaskaden wie Tyrosinkinasen inhibieren (Gefitinib **7**, Erlotinib **8**).[111] Daneben werden auch zunehmend monoklonale Antikörper eingesetzt, um tumorspezifische Antigene für das Immunsystem zu markieren (Ipilimumab), Wachstumsfaktoren im Blut zu immobilisieren (Bevacizumab) oder als Konjugate gezielt Wirkstoffe im Tumor anzureichern (Inotuzumab-Ozogamicin **13**).[112–114] In den letzten Jahren wurden mit der Zulassung moderner Behandlungsstrategien wie Tumorvakzinen (Sipuleucel-T), Gentherapien (CAR-T-Zelltherapie), dem Einsatz onkolytischer Viren (Talimogen laherparepvec) und Stammzelltherapien (hämatopoetische Stammzelltransplantation) viele vielversprechende Therapieansätze weiterentwickelt.[115–118]

1.2.1 Multifunktionalität

Die erste Kombinations- oder Polychemotherapie wurde mit der Verabreichung von Methotrexat und 6-Mercaptopurin Ende der 1950er Jahre erprobt und bis heute durch etliche neue Kombinationspräparate und Therapieregime erweitert.[119] Die Kombination verschiedener Wirkstoffe hat jedoch nicht nur die Wirksamkeit verbessert und die Resistenzbildung vermindert, sondern ist oft mit stärkeren Nebenwirkungen verbunden und kann stellenweise zu antagonistischen Wechselwirkungen führen.[120] Neben Prodrug-Strategien ist die kovalente Verknüpfung pharmakologisch aktiver Strukturelemente, um neue bioaktive Moleküle zu erzeugen, eine weitere Alternative zur gebräuchlichen Kombinationstherapie.[121] Eine hybrides Arzneimitteldesign kann die Wirksamkeit verbessern, Resistenzen überwinden oder eine Visualisierung

ermöglichen ohne zusätzliche Neben- oder Wechselwirkungen zu erzeugen (Abb. 8).[122]

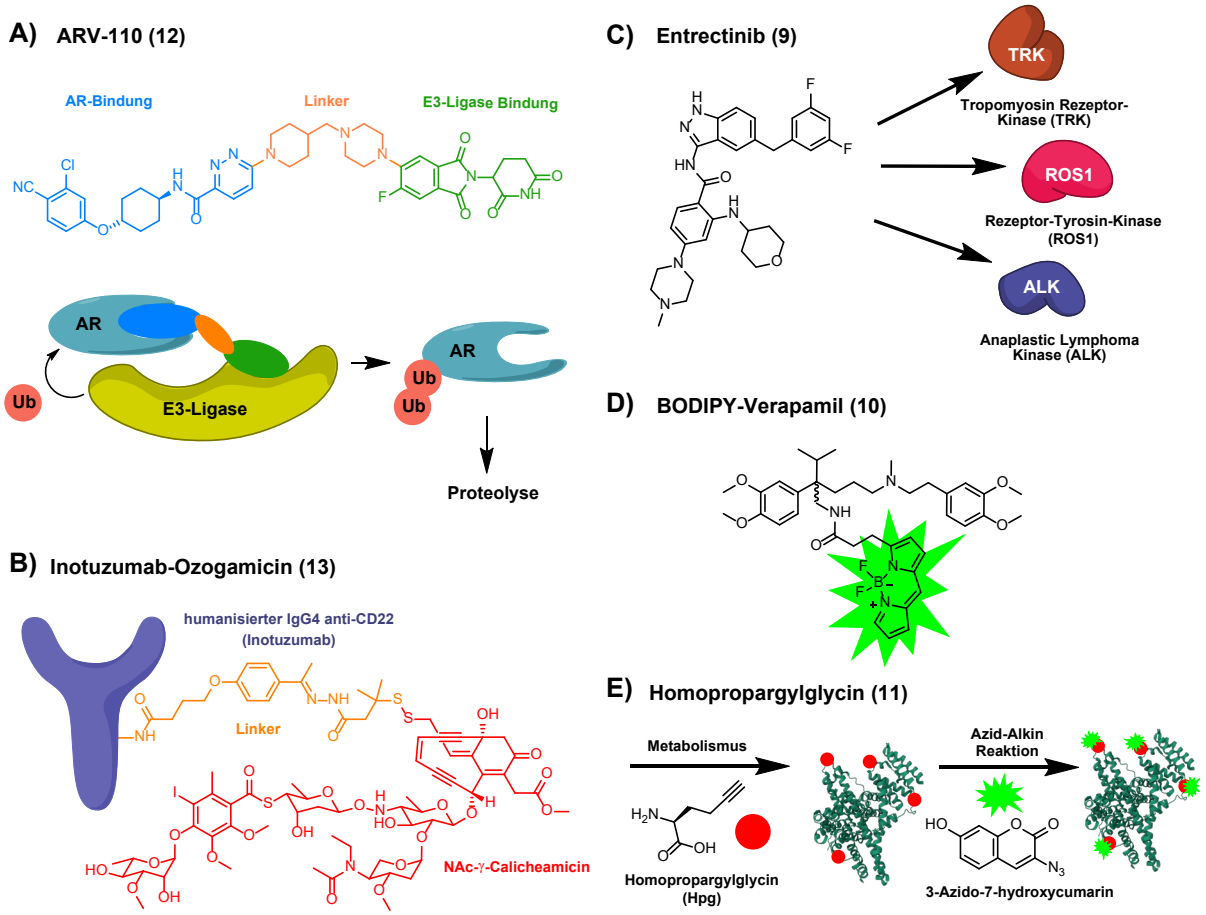

Abbildung 8: Darstellung unterschiedlicher Anwendungsstrategien multifunktionaler Wirkstoffe: (A) Proteolyse-Targeting-Chimären (ARV-110)[123], (B) Antikörper-Konjugate (Inotuzumab-Ozogamicin)[114], (C) Multi-Target-Inhibitoren (Entrectinib)[124], (D) Fluoreszenzmarkierte Wirkstoffe (BODIPY-Verapamil)[125] und (E) bioorthogonal markierbare Metabolite (Homopropargylglycin).[126]

Proteolyse-Targeting-Chimären (PROTACs) wie ARV-110 **12** bringen durch die Bindung zweier Targets den Androgenrezeptor (AR) in die Nähe der E3-Ligase, die durch Ubiquitinierung (Ub) für den proteolytischen Abbau sorgt. Im Vergleich zu konventionellen Inhibitoren bietet die PROTAC-Strategie Vorteile wie die Reduktion von Off-Target-Effekten, die Spezialisierung auf schwer adressierbare Targets und eine geringere Therapieresistenz, da nicht das aktive Zentrum des Zielproteins gebunden wird.[123] Zu den pleiotropen Wirkmechanismen gehören auch Wirkstoff-Antikörper-Konjugate (Inotuzumab-Ozogamicin **13**), die durch Anreicherung des Wirkstoffs in der unmittelbaren Umgebung des Tumors lokal zu deutlich höheren Wirkstoffkonzentrationen bei gleichzeitig geringer Schädigung des gesunden Gewebes führen.[114] Der Multi-Target-Inhibitore Entrectinib **9** besitzt aufgrund seiner pleiotropen Struktur synergistische antiproliferative Effekte indem sowohl TRK

(*tropomyosin receptor kinase*) als auch ROS1 (*receptor tyrosine kinase*) und ALK (*anaplastic lymphoma kinase*) inhibiert werden.[124] Fluorophor-gekoppelte Verbindungen (BODIPY-Verapamil **10**) oder bioorthogonal markierbare Reste (Homopropargylglycin **11**) ermöglichen die Visualisierung von molekularen Mechanismen innerhalb von Zellen und sind daher für die Forschung von größerer Bedeutung.[125,126]

1.2.2 Tubulin als Target in der Krebstherapie

Um zu verstehen, wie *microtubule targeting agents* (MTAs) wirken, müssen zunächst die molekularen Mechanismen des Tubulin-Zytoskeletts verstanden werden. Mikrotubuli sind aus αβ-Tubulin-Heterodimeren aufgebaute Biopolymere, die einem dynamischen Gleichgewicht aus Auf- und Abbau unterliegen. Ausgangspunkt der Polymerisation können das *microtubule-organizing center* (MTOC), der Golgi-Apparat oder frei im Zytoplasma vorliegende γ-Tubulin-Ring-Komplexe (γ-TuRC) sein, an denen sich die zuvor gebildeten Protofilamente (Ketten aus αβ-Tubulin) mit dem α-Ende anlagern (Abb. 9).[127]

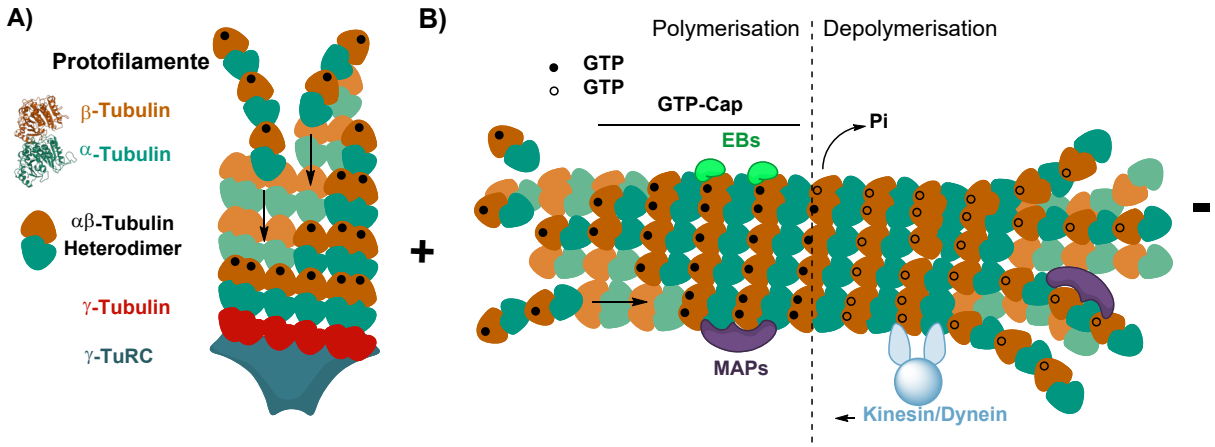

Abbildung 9: (A) Initiationsprozess der Mikrotubulipolymerisation am γ-TuRC. (B) Dynamisches Gleichgewicht der Mikrotubuli mit beteiligten MAPs (EBs, Kinesin und Dynein). [Eigene Interpretation nach WU *et al.* 2017 und AKHANOVA *et al.* 2015][127,128]

Der γ-TuRC bildet normalerweise eine Röhrenstruktur aus 13 Protofilamenten, die ausgehend vom negativ geladenen α-Ende zum positiven β-Ende verlängert wird.[129] Eine leichte Versetzung der longitudinalen Tubulin-Kontakte bildet eine helikale Struktur und induziert eine stabilisierende Konformationsänderung des β-Tubulins durch GTP-Hydrolyse.[128] Zusätzlich wird das wachsende Plusende durch *end-binding proteins* (EBs) und die sogenannte GTP-Cap stabilisiert, um die weitere Polymerisation zu begünstigen.[130] Ihre Asymmetrie macht den gerichteten Transport

durch Motorproteine zum Minus- (Dyneine) oder Pluspol (Kinesine) möglich.[131] Der gesamte Prozess des Auf- und Abbaus wird durch Mikrotubuli-assoziierte Proteine (MAPs) oder posttranslationale Modifikationen der Tubulin-Monomere reguliert und ist maßgeblich an der intrazellulären Organisation, der Stabilität, dem Organellentransport und der Mitose beteiligt.[132,133] Da sich insbesondere Krebszellen durch eine erhöhte Zellteilungsrate auszeichnen, sind der für die Mitose essentielle Spindelapparat und die daran beteiligten Mikrotubuli wichtige therapeutische Zielstrukturen.

Die grundlegende Strategie von MTAs besteht darin, das dynamische Gleichgewicht zu verschieben, indem sie entweder die Mikrotubuli stabilisieren oder die Depolymerisation zu αβ-Tubulin-Heterodimeren begünstigen. Je nach Wirkstoffklasse binden diese an unterschiedliche Bereiche der αβ-Untereinheit und beeinflussen so die Wechselwirkungen der Tubulin-Monomere untereinander (Abb. 10).[134]

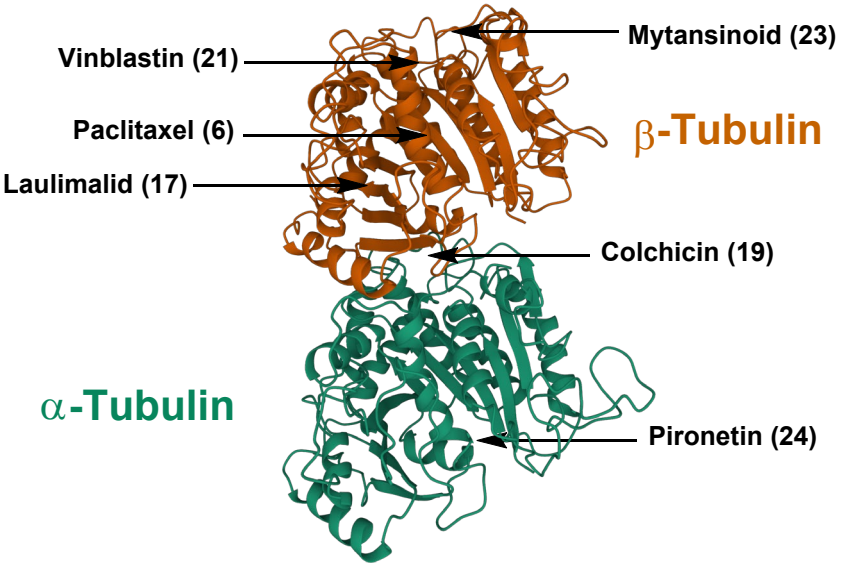

Abbildung 10: Heterodimer aus α- (grün) und β-Tubulin (orange) mit potenziellen MTA-Bindestellen (Mytansinoid, Vinblastin, Paclitaxel, Laulimalid, Colchicin, Pironetin). PDB: 1TUB. [Freie Interpretation nach STEINMETZ *et al.* 2018][134]

Die Taxan-Bindestelle befindet sich auf der Innenseite des β-Tubulins und wird von Paclitaxel **6**, Epothilon A **14**, Epothilon B **15** oder Discodermolid **16** durch hydrophobe und polare Wechselwirkungen durch eine Arretierung der αβ-Konformation stabilisiert (Abb. 11).[135] Auch die Bindung von Laulimalid **17** und Pelorusid A **18** führt zu einer Mikrotubuli-Stabilisierung, diese erfolgt jedoch an der äußeren Oberfläche des β-Tubulins in der Nähe der lateralen Kontaktstelle zwischen den Protofilamenten.[136] Der Bereich zwischen den α- und β-Untereinheiten des Heterodimers stellt die Colchicin-

Bindungstasche dar, die von Colchicin **19** oder Combretastatin A4 (CA4) **20** gebunden werden kann und eine Konformationsänderung innerhalb des Heterodimers hervorruft und damit die Bildung der Mikrotubuli verhindert.[137,138]

Taxan-Bindestelle

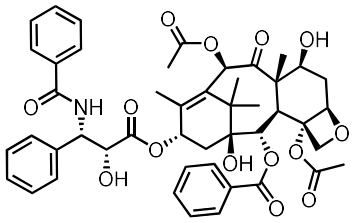

Paclitaxel (6)

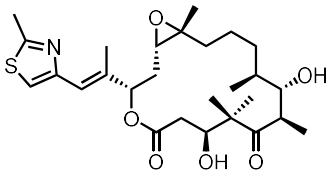

Epothilon A (14): R = H
Epothilon B (15): R = CH_3

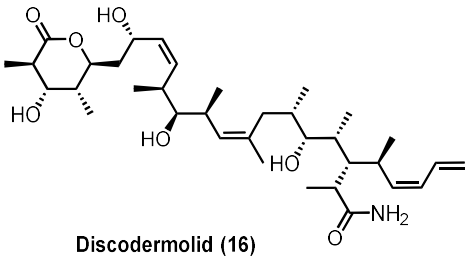

Discodermolid (16)

Laulimalid-Bindestelle

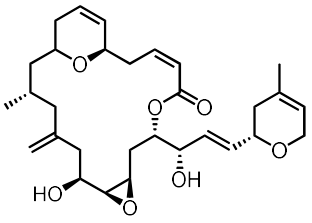

Laulimalid (17)

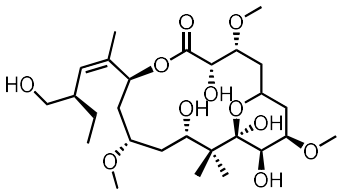

Perlorusid A (18)

Colchicin-Bindestelle

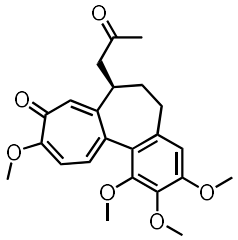

(S)-**Colchicin (19)**

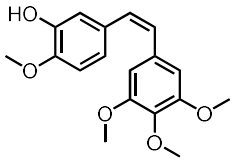

Combretastatin A4 (20)

Vinca-Bindestelle

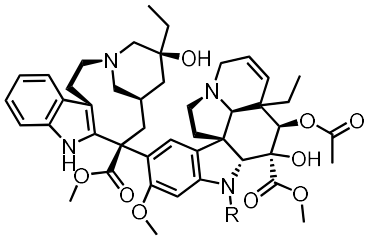

Vinblastin (21): R = CH_3
Vincristin (22): R = CHO

Mytansinoid-Bindestelle

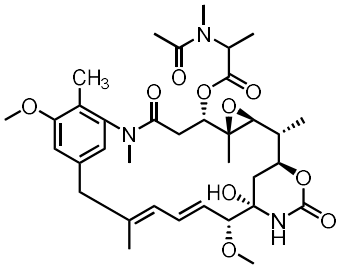

Maytansinoid (23)

Pironetin-Bindestelle

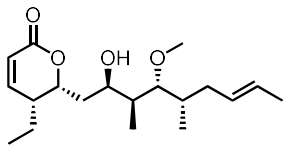

Pironetin (24)

Abbildung 11: Strukturformeln verschiedener Tubulin-bindender Wirkstoffe mit entsprechenden Bindestellen (BS). Taxan-BS (Paclitaxel, Epothilon A/B und Discodermolid), Laulimalid-BS (Laulimalid und Perlorusid A), Colchicin-BS (Colchicin und CA4), Vinca-BS (Vinblastin und Vincristin), Mytansinoid-BS und Pironetin-BS.

Eine weiter bekannte Stoffklasse der Mikrotubuli-destabilisierenden Agentien (MDAs) ist die der Vinca-Alkaloide (Vinblastin **21**, Vincristin **22**), welche zwischen zwei αβ-Dimeren die Protofilamente aufspalten oder durch ringförmige Oligomerisierung eine korrekte Bildung der Protofilamente verhindern.[139,140] Auch Derivate des Maytansinoid **23** können sich zwischen den αβ-Dimeren anlagern, besitzen jedoch eine andere Bindestelle und führen am Plus-Ende der Mikrotubuli zu einer Stagnation der Elongation.[135] Neben diesen nicht kovalent-bindenden Wirkstoffgruppen existiert ein weiterer Mechanismus bei dem Pironetin **24** kovalent an Cys316 der α-Untereinheit bindet, die Polymerisation am Minus-Ende blockiert und inaktive Pironetin-Tubulin-Heterodimere bildet.[141] Trotz unterschiedlicher Bindungsstellen haben die meisten MTAs bei geringer Dosierung jedoch eine ähnliche Wirkung, da die normalerweise dynamisch verlaufenden Prozesse stark verlangsamt ablaufen.[142]

MTAs finden heute breite Anwendung in der klinischen Krebstherapie, da sie Zellen unabhängig von ihrem Zellzyklusstadium adressieren können und sowohl Interphase-Mikrotubuli (IM) als auch die mitotische Spindel während der Zellteilung angreifen. Da eine Reihe von onkogenen Proteinen entlang der Mikrotubuli transportiert werden, führt eine Hemmung der dynamischen Abläufe zu einer Unterbrechung nachgeschalteter zellulärer Stoffwechselwege und verändert dadurch Signaltransduktion, Endozytose oder Sekretionsmechanismen.[143] Während der Mitose wird durch die Beeinträchtigung der Tubulin-Dynamik die Ausbildung des Spindelapparats gestört und durch den *spindle assembly checkpoint* (SAC) ein G_2/M-Zellzyklusarrest ausgelöst. Die Aktivierung von SAC und die Verzögerung der Mitose führt normalerweise zu einer mitotischen Katastrophe, die als Schutzmechanismus die fehlerhafte Zellteilung verhindert und entweder zum Zelltod oder zur Seneszenz führt.[144,145] Tumorzellen können jedoch durch sogenanntes *mitotic slippage* den Zellzyklusarrest verlassen, was einerseits zum Zelltod während des *DNA-damage checkpoint* des nächsten Zellzyklus führen kann, andererseits bei mehrfachem Auftreten auch Aneuploidie und Resistenz gegenüber MTAs zur Folge hat.[146] Da Aneuploidie normalerweise mit einer Zentrosomen-Amplifikation und multipolarer Zellteilung einhergeht, machen sich Krebszellen den Mechanismus des *centrosome clustering* zu Nutze um weiterhin eine bipolare Mitose vollziehen zu können.[147] Dies stellt ein vielversprechendes therapeutisches Target dar indem spezifisch aneuploide Zellen adressiert werden, wie am Beispiel von Griseofulvin gezeigt werden konnte.[148,149] Abgesehen von direkten Folgen eines zerstörten Tubulin-Zytoskeletts,

können weitere Zellzyklus-unabhängige Mechanismen Apoptose in Tumorzellen auslösen. So können MDAs die Transkription pro-apoptotischer Faktoren der Bcl-2-Familie (BAD, Puma, Noxa, BAX, BAK) erhöhen, an Dynein gebundene Apoptose-induzierende Proteine wie Bim und Bmf freisetzen oder antiapoptotische Stimuli (Bcl-2, Bcl-xl, Mcl-1) inhibieren.[150] Des Weiteren können akute Vaskular-disruptive Effekte auftreten die meistens mit Mirotubuli-destabilisierenden Substanzen assoziiert werden und sich aufgrund gestörter VE-Cadherin/β-Catenin/Akt-Signaltransduktion und Rho-vermittelter Aktin-Reorganisation direkt auf Morphologie und Zell-Zell-Kontakte von Endothelzellen auswirken.[151]

1.2.3 Inhibition der Angiogenese

Die Angiogenese ist ein essenzieller Bestandteil für die Entstehung solider Tumore und trägt maßgeblich zur Metastasierung bei. Im Allgemeinen können antiangiogene Strategien in drei Ansätze unterteilt werden: Reduktion der Tumorvaskularisation, Normalisierung der Gefäßmorphologie und Rekrutierung des Immunsystems.[152] Die direkte Hemmung der Angiogenese ist jedoch in der therapeutischen Anwendung mit einigen Schwierigkeiten verbunden, da es aufgrund der verminderten Durchblutung des Tumors zu einer Hypoxie-induzierten Steigerung der Aggressivität der Krebszellen und zu einer verminderten Verteilung von Chemotherapeutika kommt.[153] Außerdem reicht die alleinige Behandlung mit hohen Inhibitor-Konzentrationen häufig nicht aus, um eine Tumorregression zu induzieren, und muss mit anderen Chemotherapeutika kombiniert werden.[154] Im Gegensatz dazu wird die Hypothese diskutiert, dass eine spezifische Dosierung in geringer Konzentration zur Normalisierung der Gefäße beiträgt und sich positiv auf die Wirksamkeit konventioneller Strahlen-, Chemo- und Immuntherapie auswirkt.[155]

Auf molekularer Ebene gibt es verschiedene Targets die durch antiangiogene Wirkstoffe adressiert werden können (Abb. 12). Den größten Anteil zugelassener Wirkstoffe stellen Tyrosinkinaseinhibitoren (Imatinib **25**, Neratinib **26**, Axitinib **27**), die hauptsächlich die Signaltransduktion pro-angiogener Induktoren (BCR-ABL, EGFR, ERBB2) hemmen.[156] Darüber hinaus werden monoklonale Antikörper eingesetzt, um endogene Wachstumsfaktoren wie VEGF zu immobilisieren (Bevacizumab) oder deren Rezeptoren (VEGFR) zu inaktivieren (Ramucirumab) und damit das unkontrollierte Gefäßwachstum in soliden Tumoren einzuschränken.[113,157]

Tyrosinkinaseinhibitoren

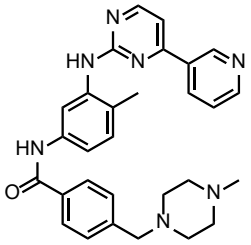

Imatinib (25)

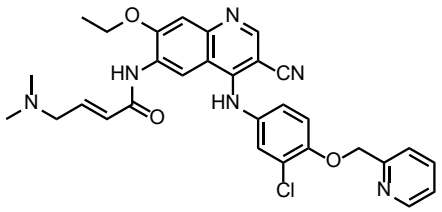

Neratinib (26)

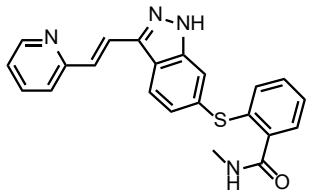

Axitinib (27)

Immunomodulatoren

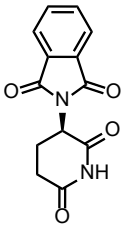

(R)-Thalidomid (29)

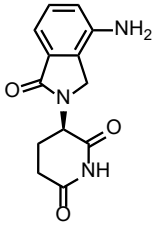

(R)-Lenalidomid (30)

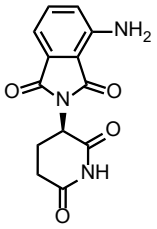

(R)-Pomalidomid (31)

mTOR-Inhibitoren

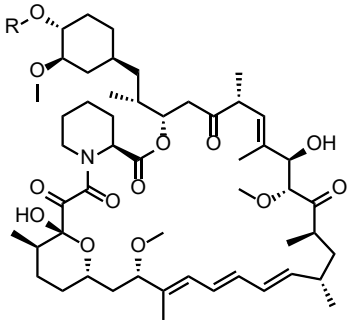

Everolimus (32): R = CH_2CH_2OH
Sirolimus (33): R = H

Abbildung 12: Strukturformeln antiangiogener Tyrosinkinaseinhibitoren (Imatinib, Neratinib und Axitinib), Immunomodulatoren (Thalidomid, Lenalidomid und Pomalidomid) sowie mTOR-Inhibitoren (Evolimus und Sirolimus).

Aflibercept ist das bisher einzige therapeutisch zugelassene rekombinante Fusionsprotein aus VEGFR-1 Domäne 3, VEGFR-2 Domäne 3 und dem crystallizable fragment (Fc-Fragment) von Immunglobulin G1.[158] Das maßgeblich durch den „Contergan-Skandal“ bekannt gewordene Thalidomid **29** zählt neben Lenalidomid **30** und Pomalidomid **31** zu den immunomodulatorischen Wirkstoffen.[159] Das extrem breite Wirkungsspektrum beinhaltet für die Krebstherapie relevante Effekte wie Apoptoseinduktion durch verminderte Bcl-2-Expression, Verstärkung diverser Immunrektionen mittels T-Zell-Aktivierung ($CD4^+/CD8^+$), sowie Angiogeneseinhibition durch die Herunterregulation von VEGF.[160] Außerdem konnte eine Reduktion der Angiogenese auch für mTOR-inhibierende Makrolide wie Everolimus **32** und Sirolimus **33** gezeigt werden.[161]

1.2.4 *c*-MYB-Inhibitoren

Aus der Familie der MYB-Transkriptionsfaktoren sind drei homologe Vertreter bekannt (*c*-MYB, A-MYB und B-MYB), die aufgrund von Amplifizierung oder erhöhter Transaktivierung der MYB-Gene an der Entstehung diverser Krebsarten beteiligt sind,

wobei im Folgenden nur *c*-MYB ausführlicher beschrieben wird.[162] Aufgrund zahlreicher regulatorischer Funktionen (Zellzyklusprogression, Differenzierung und Apoptose) in hämatopoetischen Zellen wird *c*-MYB hauptsächlich mit der Entstehung von akuter myeloischer Leukämie assoziiert, trägt jedoch auch in vielen soliden Tumorarten zur Malignität bei.[163] *C*-MYB besteht aus einer N-terminalen DNA-bindenden Domäne (DBD), einer im Zentrum liegenden Transaktivierungsdomäne (TAD) und einer C-terminalen negativ regulierenden Domäne (NRD). Verschiedene Co-Aktivatoren (FLASH, CBP/p300) bzw. -Repressoren (N-CoR, TIP60) können die Erkennung der Konsensussequenz an der DBD oder die Transaktivierung an der TAD beeinflussen, während die NRD nur Repressoren (Tif1β) rekrutiert, die *c*-MYB durch posttranslationale Modifikationen inaktivieren.[164]

Transkriptionsfaktoren galten aufgrund fehlender niedermolekularer Bindungsstellen lange Zeit als nicht medikamentös zugänglich, und obwohl inzwischen einige Strategien zur Hemmung MYB-assoziierter Effekte untersucht wurden, konnten bisher nur mäßige therapeutische Erfolge erzielt werden.[165] Die vielversprechendste Strategie besteht darin, die Bindung des Co-Aktivators CBP/p300 zu unterbrechen und so die Aktivität zu regulieren (Abb. 13).

CBP/p300 abhängige Inhibitoren

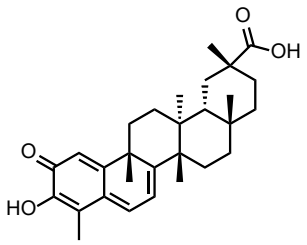

Celastol (34)

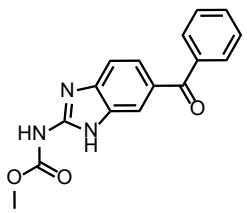

Mebendazol (35)

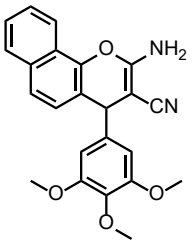

Bcr-TMP (36)

Indirekte c-MYB Inhibition (MYB-NFIB)

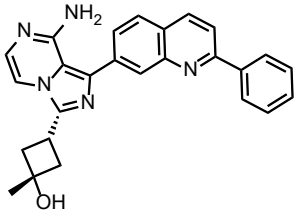

Linsitinib (37)

Abbildung 13: Strukturformeln *c*-MYB-inhibierender Substanzen, die entweder die Co-Aktivierung von CBP/p300 hemmen oder im Fall eines translozierten MYB-Gens (MYB-NFIB) die *c*-MYB-Expression indirekt durch IGF1R- oder EGF-Inhibition verringern.

Dies kann sowohl durch *small molecule inhibitors* (Celastrol **34**, Mebandazol **35** oder Bcr-TMP **36**) als auch durch Peptidmimetika (MYBMIM) erreicht werden.[166–169] In adenoid-zystischen Karzinomen liegt MYB besonders häufig transloziert als MYB-NFIB-Fusionsgen vor, das sich durch verstärkte Transkription am neuen Genlokus und eine Inaktivierung der C-terminalen NRD auszeichnet.[170] Da das MYB-NFIB-Onkogen IGF1R- und EGF-abhängig reguliert wird, kann der Einsatz von Linsitinib **37** oder Figitumumab in diesem Fall zu einer verminderten Expression führen.[171,172] Der in Form eines Plasmid-Vektors (pVAX1) verabreichte DNA-Impfstoff (TetMYB) stellt einen Versuch dar, durch Fusion von Tetanospasmin-Epitopen mit inaktiviertem MYB eine tumorspezifische Immunantwort zu induzieren und wird bereits in einer ersten klinischen Studie getestet.[173]

2. Synopsis

2.1 Übersicht der Teilprojekte

Die vorliegende kumulative Dissertation setzt sich aus drei Publikationen zusammen, die Ihren Fokus auf die wirkmechanistische Aufklärung sowie die strukturelle Optimierung verschiedener LY290181(**38**)-abgeleiteter Naphthopyran-Analoga legen (Abb. 14). Dabei sollten durch die Variation des Tubulin-bindenden 3,4,5-Trimethoxyphenyl-Strukturmotivs (CA4 **20**) neue multimodale Wirkstoffe mit verbesserten Eigenschaften generiert werden, um gleichzeitig mehrere *Cancer Hallmarks* zu adressieren. Bei allen Substanzserien konzentrieren sich die Studien auf die Mikrotubuli-destabilisierende Wirkung und die daraus resultierenden antiproliferativen Eigenschaften, sowie antiangiogene Effekte *in vitro* und *in vivo*. Zudem wurden weitere therapeutisch relevante Targets zur Aufklärung des Wirkprinzips untersucht. Die in Publikation I beschriebenen Dihydropyranchromene zeichneten sich durch die Inhibition des in vielen Tumorarten auftretenden *centrosomal clustering* aus, welches einen wichtigen Mechanismus bei der Vermeidung von multipolaren Zellteilungen in Krebszellen spielt. Publikationen II (Naphthopyrane) und III (Arylchromene) knüpften an der 2022 von M. V. Yusenko *et al.* beschriebenen Inhibition des Transkriptionsfaktors *c*-MYB durch das Naphthopyran-Derivat Bcr-TMP **36** an, wobei zwei neue Substanzklassen auf Ihren Einfluss gegenüber Zytoskelett, Angiogenese und potenzielle *c*-MYB-Aktivität gescreent wurden.

Die im Rahmen dieser Arbeit untersuchten Verbindungen wurden vollständig von Dr. Bernhard Biersack am Lehrstuhl für Organische Chemie I der Universität Bayreuth hergestellt. Einzelne Assays wurden von Kooperationspartnern des Biochemie-Instituts der Westfälische-Wilhelms-Universität in Münster, des *Department of Chemistry & Post Graduate Research Center* des Abeda Inamdar Senior College (Indien) und der Arbeitsgruppe Entwicklungsbiologie der Universität Bayreuth durchgeführt.

Leitstrukturen

Naphthopyrane

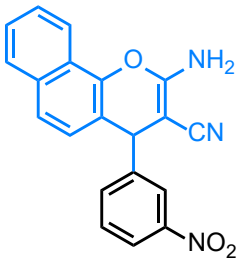

LY290181 (38)

+

Stilbene

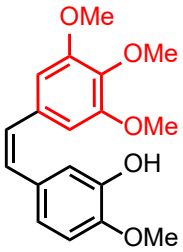

Combretastatin A4 (20)

Teilprojekte

Publikation I	**Publikation II**	**Publikation III**
ChemMedChem 2022	*Med. Chem. Lett 2022*	*Cancer Drug Resist 2023*

Dihydropyranochromene

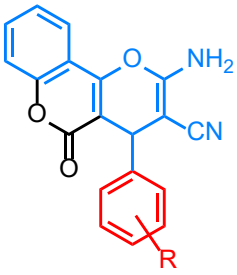

1a-m

Naphtopyrane

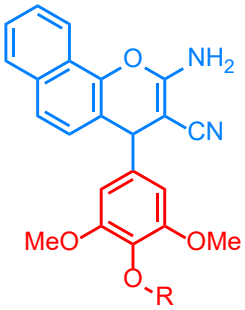

3a-g

Arylchromene

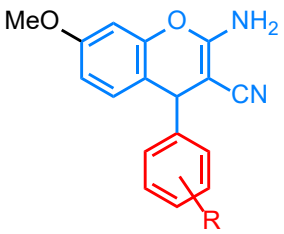

2a-r

Abbildung 14: Übersicht der untersuchten Substanzen mit Zuordnung zu den entsprechenden Publikationen: Das 4-Aryl-4*H*-naphthopyran LY290181 sowie das Stilben CA4 dienten als Leitstruktur für die in dieser Arbeit untersuchten Substanzserien. Die davon abgeleiteten multifunktionalen Dihydropyranchromene (Publikation I), Naphthopyrane (Publikation II) und Arylchromene (Publikation III) stellen neue Verbindungen dar, welche neben Mikrotubuli-destabilisierenden und Angiogenese-hemmenden Eigenschaften auch das *centrosome clustering* oder die *c*-MYB-Aktivität beeinträchtigen.

2.2 Publikation 1: 2-Amino-4-aryl-5-oxo-4,5-dihydropyran[3,2-*c*]chromen-3-carbonitrile mit Mikrotubuli-disruptiven, Zentrosom Declustering und antiangiogenen Effekten *in vitro* und *in vivo*.

Im Fokus dieser Arbeit steht die Untersuchung fünfzehn neuer Dihydropyranchromene, welche sich strukturell vom 4-Aryl-4*H*-Naphthopyran LY290181 **38** ableiten lassen. Das Naphthopyran-Grundgerüst wurde mit einem δ-Lacton an 5,6-Position (4-Hydroxycumarin) versehen und die Reste des 4-Phenylrings mit verschiedenen Heteroatomen und funktionellen Gruppen substituiert (Abb. 15).

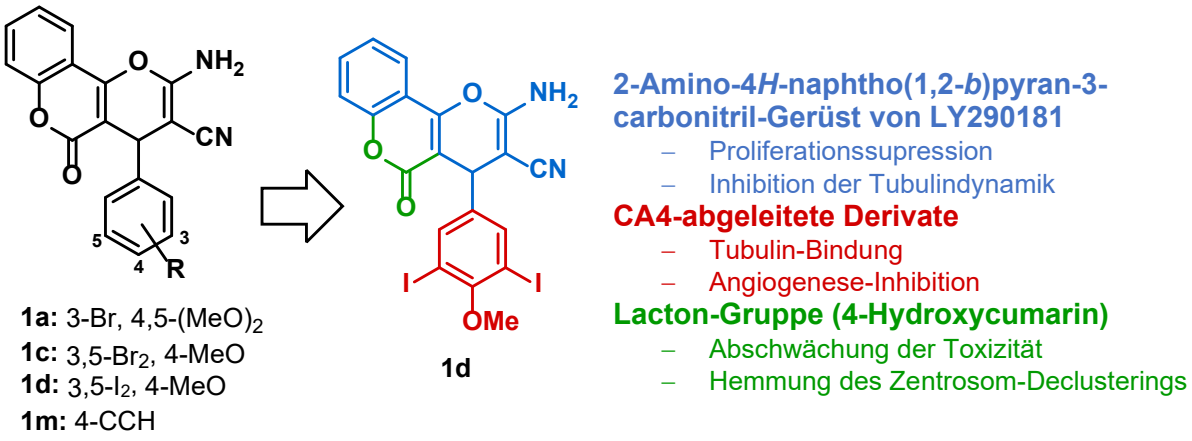

1a: 3-Br, 4,5-$(MeO)_2$
1c: 3,5-Br_2, 4-MeO
1d: 3,5-I_2, 4-MeO
1m: 4-CCH

Abbildung 15: Strukturen der untersuchten Dihydropyranchromene (**1a**, **1c**, **1d**) und die biologischen Targets der wirksamsten Substanz **1d**.

Substanz **1f** wurde bereits 2016 von Y. Hu *et al.* ohne sichtlichen Erfolg auf ihr antibakterielles Potential hin untersucht, zeigte jedoch gegenüber einigen humanen Krebszelllinien zytotoxische Effekte.[174] Die drei Derivate **1a** (3-Brom-4,5-dimethoxyphenyl-Motiv), **1c** (3,5-Dibrom-5-methoxyphenyl-Motiv) und **1d** (3,5-Diiod-5-methoxyphenyl-Motiv) stachen bei ersten Zytotoxizitätsstudien mit einstellig mikromolaren IC_{50}-Werten (halbmaximale inhibitorische Konzentration) gegenüber neun verschiedene Krebs- und Hybridzelllinien hervor. Das meta-halogenierte Methoxyphenylmotiv, welches bereits in vorangegangenen Studien zu einer Wirkungsverbesserung geführt hat, leitet sich vom Tubulin-bindenden und vaskular-disruptiven CA4 **20** ab.[175,176] Neben einer deutlichen Selektivität gegenüber malignen Zellen waren die Derivate zudem in der Lage, *in vitro* die Tubulinpolymerisation zu inhibieren sowie das Mikrotubuli-Zytoskelett innerhalb von 518A2 Melanomzellen zu zerstören. Dabei konnte die Häufung von multiplen Mitosespindeln innerhalb substanzbehandelter Zellen beobachtet werden, was auf die Störung eines Krebs-

assoziierten Überlebensmechanismus, dem sogenannten *centrosome clustering,* zurückgeführt werden könnte (Abb. 16, A und B).[148]

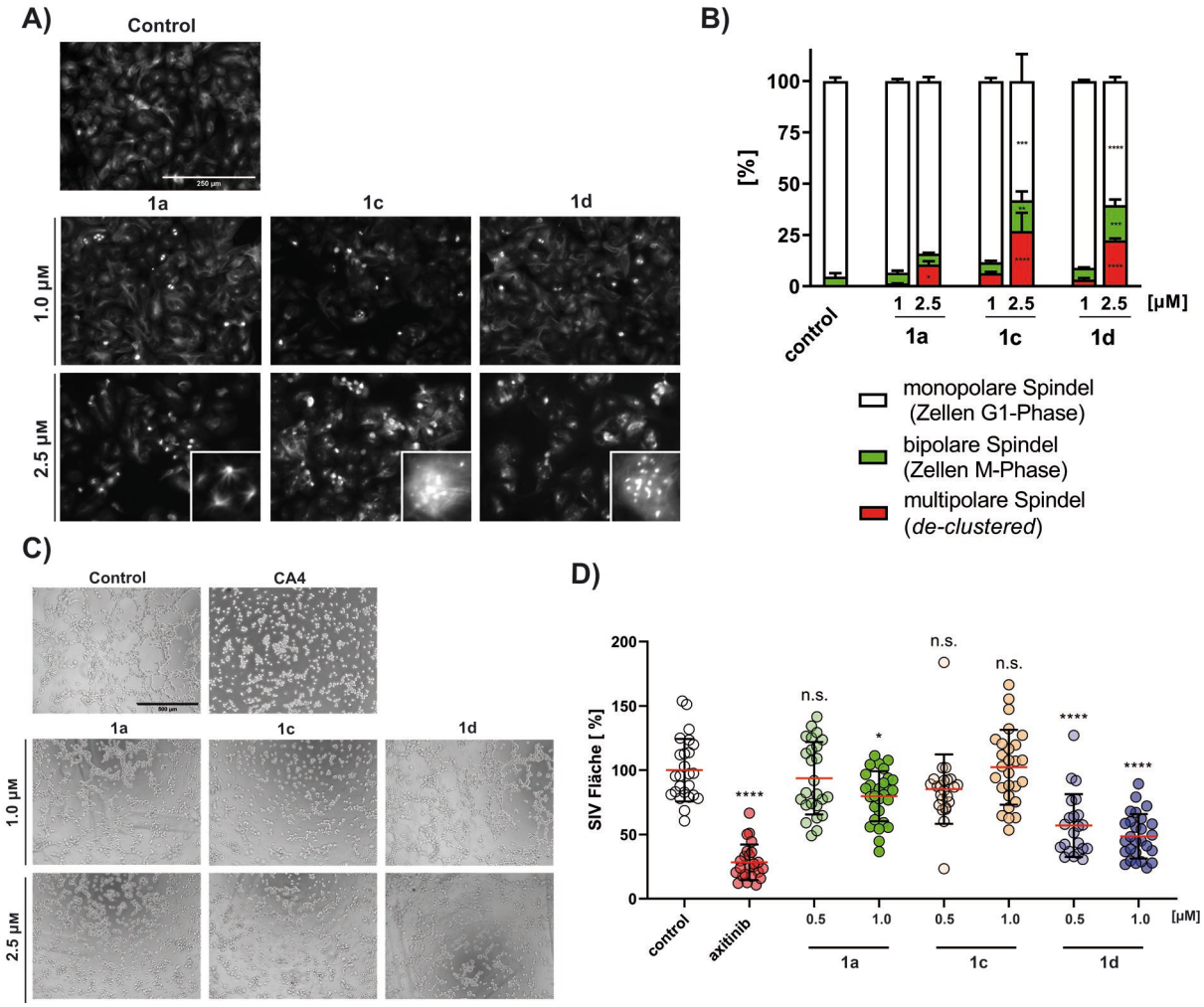

Abbildung 16: (A) Wirkung der Verbindungen **1a**, **1c** und **1d** (1 und 2,5 µM) auf die Bildung des Spindelapparats und die Häufung von multipolaren Spindeln. Die Bilder zeigen die Färbung von α-Tubulin und sind repräsentativ für mindestens drei unabhängige Experimente. Vergrößerung 100×. Maßstabsleiste: 250 µm. Vergrößerte Bildausschnitte zeigen Einzelzellen mit multipolaren Spindeln. (B) Die Histogramme zeigen den prozentualen Anteil der Zellen mit bipolarem Spindelapparat (grün) und Zellen mit multipolarem Spindelapparat (rot). Es wurden 500-800 Zellen pro Wirkstoffkonzentration von 3 unabhängigen Experimenten gezählt. (C) Konzentrationsabhängige Effekte der Testsubstanzen (1 und 2,5 µM) auf die Fähigkeit von EA.hy926 Endothelhybridzellen, gefäßähnliche Strukturen auf Matrigel® zu bilden. Die Positivkontrolle wurde mit 100 nM CA4 **20** behandelt. Die Aufnahmen repräsentieren drei unabhängige Experimente mit vitalen Zellen >80% (MTT-Assays) im Vergleich zur Negativkontrolle. Vergrößerung 100×. Maßstabsleiste: 500 µm. (D) Die Fläche der Subintestinalen Venen (SIV) von Zebrafischembryos nach 48-stündiger Behandlung mit den Testsubstanzen (0.5 und 1 µM) ist als Dotplot dargestellt. Die Negativkontrolle wurde mit DMSO, die Positivkontrolle mit Axitinib (1 µM) behandelt. Die Signifikanz wurde gegenüber der Kontrolle für jede Konzentration angegeben mit: *p<0,05; **p<0,01; ***p<0,001; ****p<0,0001. [Reprinted with permission from L. H. F. Köhler *et al.*, *ChemMedChem* **2022**, *17*, e202200064. DOI: 10.1002/cmdc.202200064]

Obwohl die zugrundeliegenden Mechanismen noch teilweise unbekannt sind, stellt dies ein krebsspezifisches Target für selektive Therapieansätze dar.[177] Eine für MDAs typische Veränderung des Zellzyklus konnte hauptsächlich bei **1d** in Form eines G2/M-Arrests nachgewiesen werden, was zudem durch eine Inhibition der Mitose-

regulierenden CDK1 verstärkt wurde. Die intrazelluläre Lokalisierung des Ethinyl-substituierten Derivats **1m** mittels Alkin-Azid-Click-Reaktion zeigte eine Anreicherung im Zellkern und teilweise im Zytoplasma der behandelten Zellen. Ein weiteres Target der untersuchten Verbindungen stellt die Angiogenese bzw. vaskuläre Mimikry dar, welche bei der Sauerstoff- und Nährstoffversorgung sowie der Metastasierung von Tumoren eine zentrale Rolle spielen.[152] Anhand des EA.hy926-Tube-Formation-Assays konnten Substanz-induzierte Effekte auf Migration, Zell-Zell-Adhäsion oder Sprossung beobachtet werden, welche für die Angiogenese essentiell sind (Abb. 16, C). Signifikant verringerte SIV-Flächen (*subintestinal veins*) von heranwachsenden Zebrafischembryonen belegt zudem die antiangiogenen Eigenschaften von **1d** *in vivo* (Abb. 16, D).

Weitere Details: L. H. F. Köhler, S. Reich, G. Begemann, R. Schobert, B. Biersack

2-Amino-4-aryl-5-oxo-4,5-dihydropyrano[3,2-c]chromene-3-carbonitriles with Microtubule-Disruptive, Centrosome-Declustering, and Antiangiogenic Effects in vitro and in vivo

ChemMedChem **2022**, doi.org/10.1002/cmdc.202200064

2.3 Publikation 2: Ein neues Naphthopyranderivat mit kombinierter Hemmung von *c*-MYB, auf Mikrotubuli abziehlender Effekte und antiangiogener Eigenschaften.

Die vorliegende Studie baut auf der Arbeit von YUSENKO *et al.* (2022, *Cancers*) auf, in der 2-Amino-4-(3,4,5-trimethoxyphenyl)-4*H*-naphtho[1,2-*b*]pyran-3-carbonitril Bcr-TMP **1b** als neuer und vielversprechender *c*-MYB-Inhibitor mit Mikrotubuli-destabilisierenden Eigenschaften identifiziert wurde. Ziel der Studie ist die weitere Analyse der Wirkmechanismen sowie die strukturelle Optimierung dieser Substanzklasse. (Abb. 17).[168]

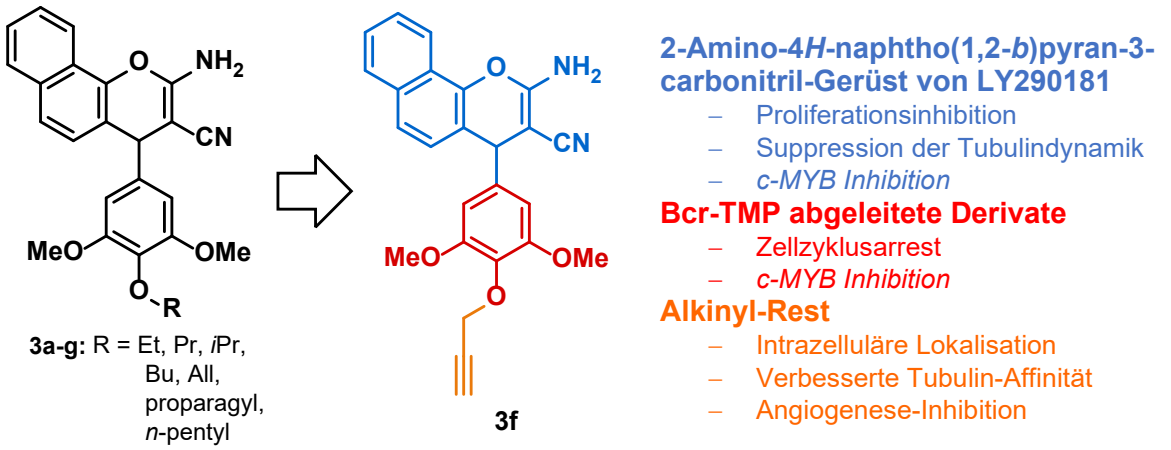

Abbildung 17: Strukturenübersicht der untersuchten Naphthopyran-Derivate **3a-g** und die biologische Aktivität der effektivsten Substanz **3f**.

Zu diesem Zweck wurde eine Serie neu synthetisierter sowie Literatur-bekannter Substanzen mittels eines neuartigen Luciferase-Reporter-Assays hinsichtlich Ihrer *c*-MYB-inhibierenden Eigenschaften verglichen, wobei sechs von **1b** abgeleitete Strukturen expliziter untersucht wurden.[178] Diese an der 4-Methoxygruppe des Phenylrings modifizierten Derivate zeigten mit zunehmender Kettenlänge generell eine Wirkungsabnahme, wobei das Alkinderivat **3f** eine Ausnahme darstellte. Die ursprünglich für die intrazelluläre Lokalisation hergestellte Substanz erwies sich als besonders aktiv mit IC_{50}-Werten im ein- bis zweistelligen nanomolaren Bereich. Eine Akkumulation im Zytoplasma konnte mit der Alkin-Azid-Click-Reaktion nachgewiesen werden. Neben einer mit CA4 **20** vergleichbaren Hemmung der Tubulinpolymerisation und einer Destabilisierung des Mikrotubuli-Zytoskeletts in 518A2-Melanomzellen mit nanomolaren Substanzkonzentrationen wurde die hohe Affinität zur Colchicin-Bindestelle des Tubulins in Dockingstudien bestätigt (Abb. 18, A, B und C).

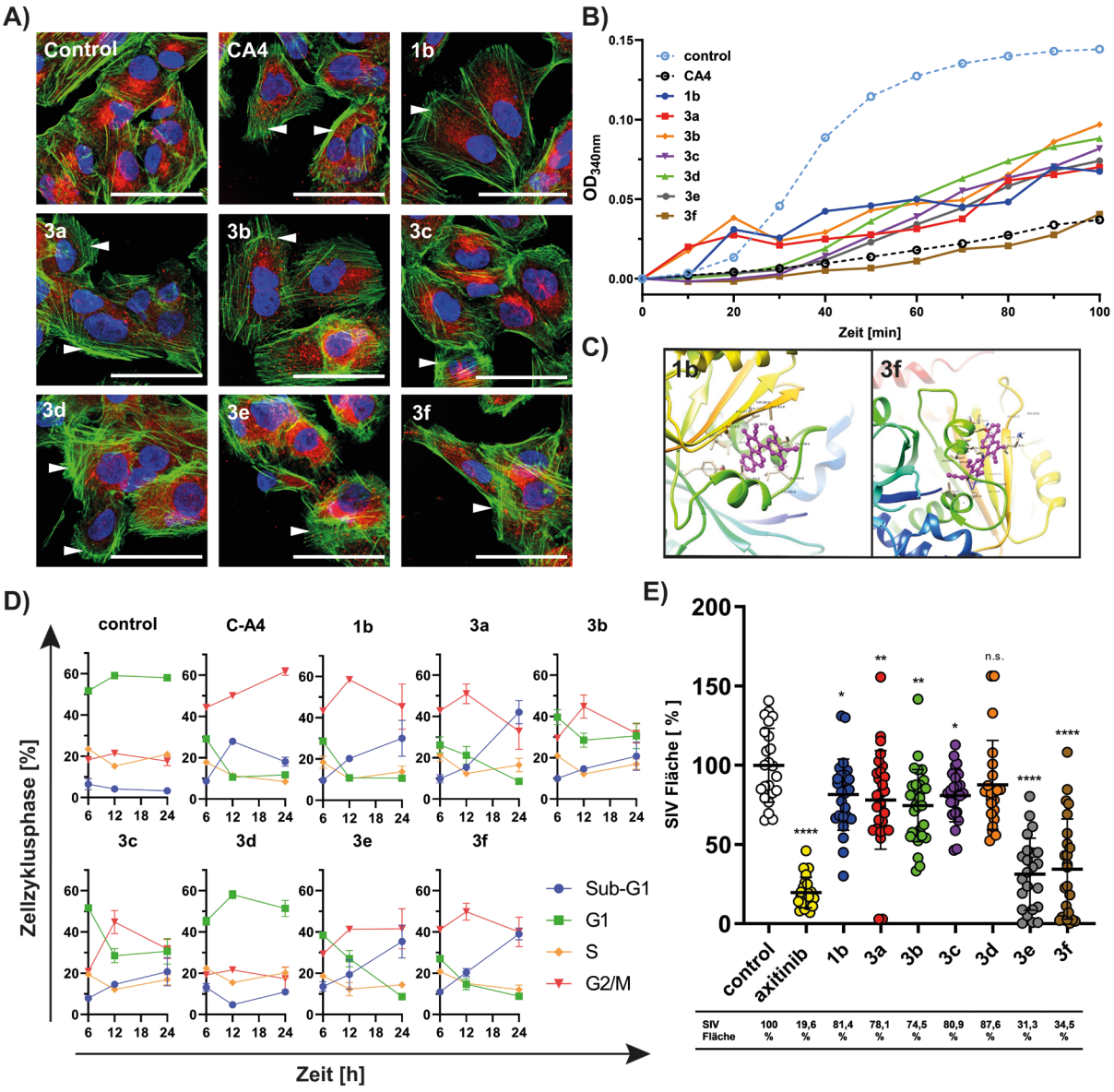

Abbildung 18: (A) Wirkung der Testsubstanzen **1b** und **3a-3f** (25 µM) auf das Tubulin- und Aktin-Zytoskelett von 518A2 Melanomzellen nach 24-stündiger Behandlung. Als Positivkontrolle wurde CA4 **20** (25 nM) verwendet. Die Immunofluoreszenzbilder zeigen die Mikrotubuli (rot), Aktinfilamente (grün) und Zellkerne (blau) und sind repräsentativ für mindestens drei unabhängige Experimente. Aktin-Stressfasern sind mit weißen Pfeilen gekennzeichnet. Vergrößerung 630×. Maßstabsleiste: 50 µm. (B) Zeitabhängige Inhibition der *in-vitro*-polymerisation von Tubulin durch Substanzbehandlung (5 µM) in Doppelbestimmung. (C) Docking-Simulation von **1b** und **3f** in der Colchicin-Bindestelle von Tubulin (1sa0) mittels PYMOL. (D) Zeitlicher Verlauf (6, 12 und 24 h) der Zellzyklusphasen behandelter 518A2 Melanomzellen (25 nM) in Prozent. Die Datenpunkte sind Mittelwerte und repräsentativ für mindestens zwei unabhängige Experimente mit 10000 gezählten Zellen. (E) Die Flächen der subintestinalen Venen (SIV) von Zebrafischembryos 48 h nach Testsubstanzbehandlung (100 µM) sind als Dotplot und in Prozent zur Kontrolle aufgetragen. Die Positivkontrolle wurde mit 500 nM Axitinib behandelt. Die Signifikanz wurde gegenüber der Kontrolle für jede Konzentration angegeben mit: *p<0,05; **p<0,01; ****p<0,0001. [Reprinted with permission from L. H. F. Köhler *et al.; ACS Med. Chem. Lett.* **2022**, *13*, 1783. DOI: 10.1021/acsmedchemlett.2c00403]

Die Zellzyklusanalyse substanzbehandelter Zellen zeigte bereits nach 6 h einen starken G2/M-Arrest sowie einen kontinuierlichen Anstieg der Sub-G1-Zellpopulation (Abb. 18, D). In Zusammenhang mit einer Aktivitätssteigerung der Effektorcaspasen 3

und 7 ist möglicherweise die Induktion von Apoptose die Ursache. Antimigratorische Effekte wurden durch verminderte Motilität und Ausprägung von Zell-Zell-Kontakten im EA.hy926 Tube-Formation Assay und durch stressinduzierte Bildung von Aktinfilamenten in behandelten 518A2 Zellen mit geschädigten Mikrotubuli nachgewiesen. Die Untersuchungen des antiangiogenen Potentials ergaben eine geringere *in-vivo*-Toxizität im Zebrafischmodell und erstaunlicherweise nur für zwei der Substanzen (**3e** und **3f**) eine deutliche Reduktion der Angiogenese (Abb 18, E). Die Substanzspezifität könnte hierbei ein Hinweis darauf sein, dass nicht die MTA-assoziierte Hemmung der Angiogenese, sondern andere antiangiogene Mechanismen die Ursache für diesen Effekt darstellen. Auch vorteilhafte Eigenschaften wie eine hohe gastrointestinale Resorption konnten in ADME-Simulationen der pharmakokinetischen Eigenschaften demonstriert werden. Zusammenfassend konnte die erfolgreiche Kombination von *c*-MYB-Hemmung, MTA-assoziierten Effekten und antiangiogenen Eigenschaften in einem intrazellulär lokalisierbaren pleiotropen Wirkstoff gezeigt werden.

Weitere Details: Leonhard H. F. Köhler, Sebastian Reich, Maria Yusenko, Karl-Heinz Klempnauer, Amin H. Shaikh, Khursheed Ahmed, Gerrit Begemann, Rainer Schobert und Bernhard Biersack.

A New Naphthopyran Derivative Combines c-Myb Inhibition, Microtubule-Targeting Effects, and Antiangiogenic Properties

Med. Chem. Lett. **2022**, doi.org/10.1021/acsmedchemlett.2c00403

2.4 Publikation 3: Multimodale 4-Arylchromen-Derivate mit Mikrotubuli-destabilisierender, antiangiogener und *c*-Myb inhibierender Wirkung

In der dritten Publikation dieser Dissertation wurden sechzehn neue 2-Amino-3-cyano-4-(aryl)-7-methoxy-4H-chromen-Derivate untersucht, um durch Strukturoptimierungen die Wirksamkeit gegen humane Krebszellen zu erhöhen (Abb. 19).

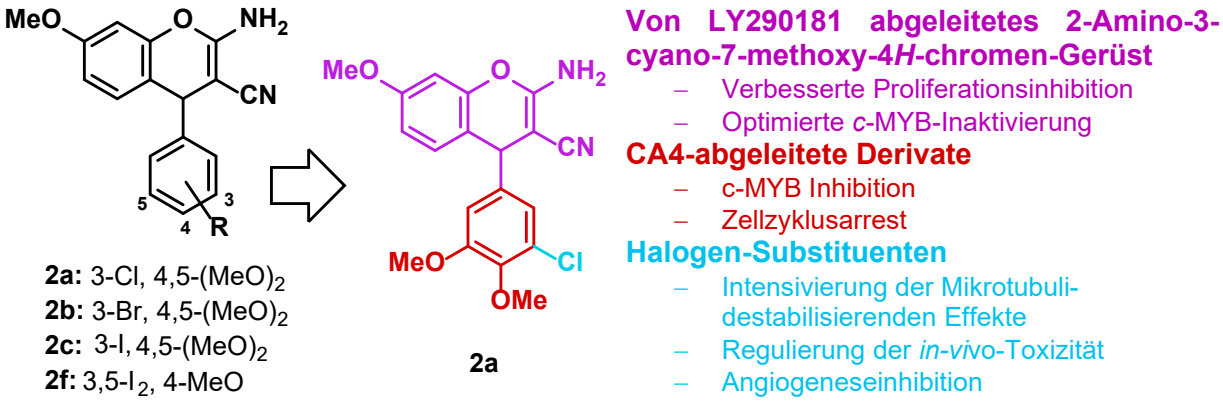

Abbildung 19: Strukturen der untersuchten 4-Arylchromen-Derivate (**2a-c** und **2f**) und biologische Aktivität der vielversprechendsten Verbindung **2a**.

Wie bereits in früheren Publikationen beschrieben, erwies sich sowohl das Substitutionsmuster des 4-Aryl-Restes als auch das 2-Amino-4*H*-chromen-3-carbonitril-Gerüst als besonders entscheidend für die Wirkungsoptimierung. Zytotoxizitätsstudien konnten vier Substanzen (**2a-c**, **2f**) mit ausgezeichneter antiproliferativer Wirkung und Selektivität gegenüber malignen Zellen identifizieren. Die Auswertung dieser Substanzen ergab, dass sich der 3,5-Diiod-4-methoxyphenylrest (**2f**) durch eine besonders schnelle Zerstörung des Zytoskeletts und eine starke Induktion von G2/M-arretierten Zellen auszeichnet, wobei die monohalogenierten Analoga (**2a-c**) einen verzögerten Wirkungseintritt zeigten (Abb 20, A). Lokalisierungsexperimente mittels Azid-Alkin-Cycloaddition bestätigten eine Anreicherung des 7-Propargylether-Derivats am Wirkort, dem Zytoplasma. Nachdem der *in-vitro*-Tube-Formation-Assay mit EA.hy926 Endothelhybridzellen Indizien für eine antiangiogene Wirkung lieferte, wurde der Substanzeinfluss im Zebrafisch-Modell anhand der SIV-Entwicklung quantifiziert (Abb 20, B). Dieser zeigte nicht nur eine sichtliche Diskrepanz der tolerierten Substanzkonzentrationen gegenüber Vertebraten, sondern verdeutlichte auch die signifikanten Unterschiede der antiangiogenen Wirkung *in vivo*. Im Gegensatz zum bisher aktivsten Derivat **2f**, das gegenüber Zebrafischen deutlich toxischer war, konnte das 3-Chlor-4,5-dimethoxyderivat **2a** trotz hoher Strukturähnlichkeit signifikante antiangiogene Effekte

erzielen. Die Aktivität des Transkriptionsfaktors *c*-MYB unter Substanzeinfluss wurde mit dem bekannten Inhibitor Bcr-TMP **1b** anhand des Luciferase-Reporter-assays verglichen (Abb 20, C).

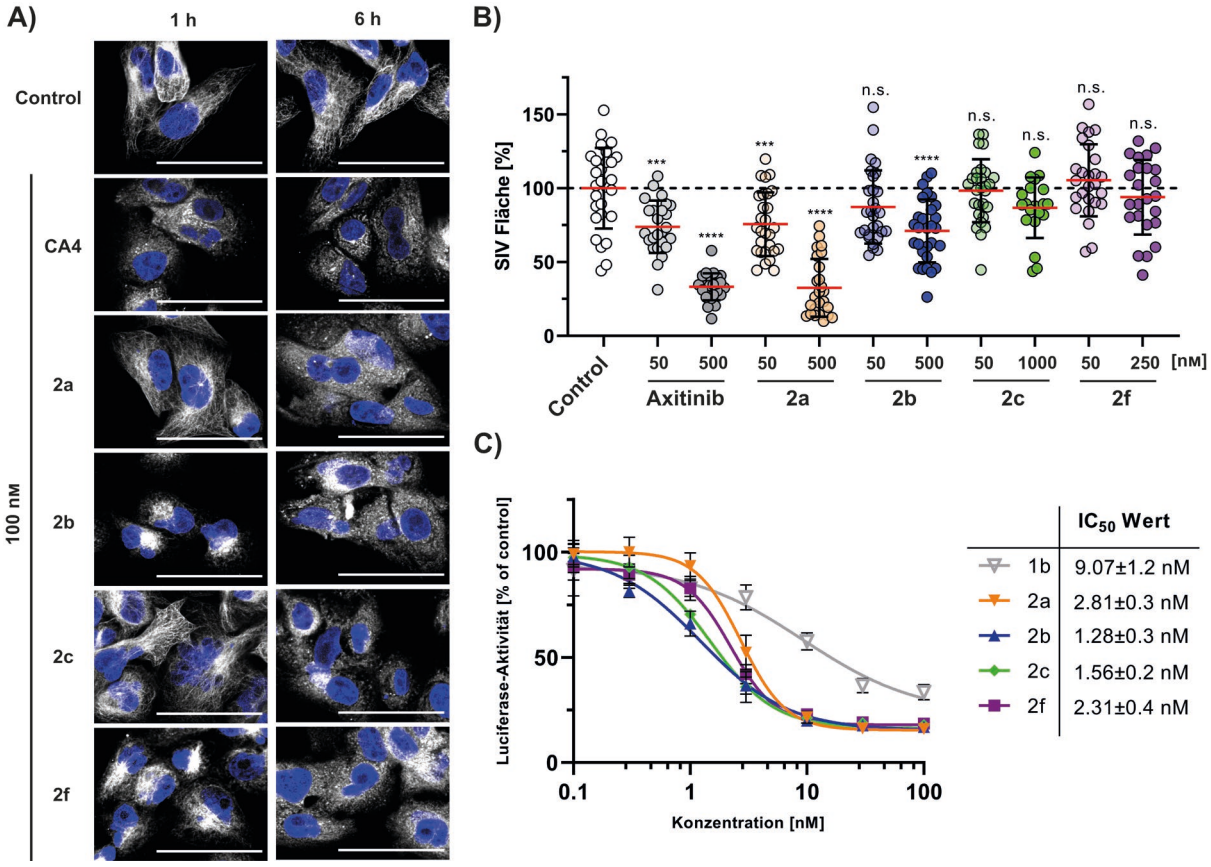

Abbildung 20: (A) Zeitlicher Effekt (1 und 6 h) der Testsubstanzen **2a-c**, **2f** und CA4 (100 nM) auf das Tubulin-Zytoskelett von 518A2 Melanomzellen. Die Immunofluoreszenzbilder zeigen die Mikrotubuli (weiß) und Zellkerne (blau). Sie stehen repräsentativ für mindestens zwei unabhängige Experimente. Vergrößerung 630×. Maßstabsleiste: 100 µm. (B) Die Fläche der subintestinalen Venen (SIV) von Zebrafischembryos nach 48-stündiger Behandlung mit den Testsubstanzen (50, 250, 500 oder 1000 nM) ist als Dotplot dargestellt. Als Positivkontrolle wurde Axitinib (50 und 500 nM) eingesetzt. Die Signifikanz wurde gegenüber der Kontrolle für jede Konzentration angegeben mit: ***p<0,001; ****p<0,0001. (C) Mittels Luciferase-Reporter-Assay quantifizierte *c*-MYB-Inhibition der Testsubstanzen nach 16-stündiger Behandlung. Die halbmaximale Inhibitorische Konzentration (IC_{50}) wurde mittels Konzentrations-Wirkungskurve zwischen 0,1 und 100 nM ermittelt. Jede Konzentration repräsentiert den Mittelwert von mindestens vier unabhängigen Versuchen. [Reprinted with permission from L. H. F. Köhler *et al.*, *Cancer Drug Resist* **2023**, *6,* 59. DOI: 10.20517/cdr.2022.90]

Hier konnte die Wirksamkeit durch das 7-Methoxy-4*H*-chromenmotiv deutlich verbessert werden, die 4-Arylringsubstituenten beeinflussten die Aktivität jedoch nur geringfügig. Als Ergebnis konnte das selektive, antiproliferative und angiogenesehemmende **2a** als potenter Wirkstoffkandidat für die Entwicklung weiterer *c*-MYB-inhibierender MTAs identifiziert werden.

Weitere Details: L. H. F. Köhler, S. Reich, M. Yusenko, K. Klempnauer, A. H. Shaikh, K. Ahmed, G. Begemann, R. Schobert, B. Biersack

Multimodal 4-arylchromene derivatives with microtubule destabilizing, anti-angiogenic, and MYB-inhibitory activity

Cancer Drug Resist **2023**, DOI: 10.20517/cdr.2022.90

3. Literaturverzeichnis

1. Hanahan D., Weinberg R. A. *Cell* **2000;** 100(1):57–70. [DOI:10.1016/s0092-8674(00)81683-9].

2. Hanahan D., Weinberg R. A. *Cell* **2011;** 144(5):646–74. [DOI:10.1016/j.cell.2011.02.013].

3. Hanahan D. *Cancer Discov* **2022;** 12(1):31–46. [DOI:10.1158/2159-8290.CD-21-1059].

4. Futreal P. A., Coin L., Marshall M., Down T., Hubbard T., Wooster R., Rahman N., Stratton M. R. *Nat Rev Cancer* **2004;** 4(3):177–83. [DOI:10.1038/nrc1299].

5. Croce C. M. *N Engl J Med* **2008;** 358(5):502–11. [DOI:10.1056/NEJMra072367].

6. Sieber O. M., Tomlinson S. R., Tomlinson I. P. M. *Nat Rev Cancer* **2005;** 5(8):649–55. [DOI:10.1038/nrc1674].

7. Jackson A. L., Loeb L. A. *Genetics* **1998;** 148(4):1483–90. [DOI:10.1093/genetics/148.4.1483].

8. Yao Y., Dai W. *J Carcinog Mutagen* **2014;** 5. [DOI:10.4172/2157-2518.1000165].

9. Loeb L. A. *Cancer Res* **2016;** 76(8):2057–9. [DOI:10.1158/0008-5472.CAN-16-0794].

10. Loeb L. A. *Nat Rev Cancer* **2011;** 11(6):450–7. [DOI:10.1038/nrc3063].

11. Negrini S., Gorgoulis V. G., Halazonetis T. D. *Nat Rev Mol Cell Biol* **2010;** 11(3):220–8. [DOI:10.1038/nrm2858].

12. Smalley K. S. M., Brafford P. A., Herlyn M. *Semin Cancer Biol* **2005;** 15(6):451–9. [DOI:10.1016/j.semcancer.2005.06.002].

13. Rofstad E. K. *Int J Radiat Biol* **2000;** 76(5):589–605. [DOI:10.1080/095530000138259].

14. Spranger S., Gajewski T. F. *Annu. Rev. Cancer Biol.* **2018;** 2(1):213–28. [DOI:10.1146/annurev-cancerbio-030617-050606].

15. D'Alterio C., Scala S., Sozzi G., Roz L., Bertolini G. *Semin Cancer Biol* **2020;** 60:351–61. [DOI:10.1016/j.semcancer.2019.08.019].

16. Luqmani Y. A. *Med Princ Pract* **2005;** 14 Suppl 1:35–48. [DOI:10.1159/000086183].

17. Tubbs A., Nussenzweig A. *Cell* **2017;** 168(4):644–56. [DOI:10.1016/j.cell.2017.01.002].

18. Niida A., Nagayama S., Miyano S., Mimori K. *Cancer Sci* **2018;** 109(4):884–92. [DOI:10.1111/cas.13510].

19. Albertson D. G., Collins C., McCormick F., Gray J. W. *Nat Genet* **2003;** 34(4):369–76. [DOI:10.1038/ng1215].

20. Fortini P., Pascucci B., Parlanti E., D'Errico M., Simonelli V., Dogliotti E. *Biochimie* **2003;** 85(11):1053–71. [DOI:10.1016/j.biochi.2003.11.003].

21. Zhivotovsky B., Kroemer G. *Nat Rev Mol Cell Biol* **2004;** 5(9):752–62. [DOI:10.1038/nrm1443].

22. Adams J. M. *Genes Dev* **2003;** 17(20):2481–95. [DOI:10.1101/gad.1126903].

23. Trapani J. A., Smyth M. J. *Nat Rev Immunol* **2002;** 2(10):735–47. [DOI:10.1038/nri911].

24. Voskoboinik I., Whisstock J. C., Trapani J. A. *Nat Rev Immunol* **2015;** 15(6):388–400. [DOI:10.1038/nri3839].

25. Fernald K., Kurokawa M. *Trends Cell Biol* **2013;** 23(12):620–33. [DOI:10.1016/j.tcb.2013.07.006].

26. Ledgerwood E. C., Morison I. M. *Clin Cancer Res* **2009;** 15(2):420–4. [DOI:10.1158/1078-0432.CCR-08-1172].

27. Guicciardi M. E., Gores G. J. *FASEB J* **2009;** 23(6):1625–37. [DOI:10.1096/fj.08-111005].

28. Zhu J., Petit P.-F., van den Eynde B. J. *Cancer Immunol Immunother* **2019;** 68(5):835–47. [DOI:10.1007/s00262-018-2269-y].

29. Igney F. H., Krammer P. H. *J Leukocyte Bio* **2002;** 71(6):907–20. [DOI:10.1189/jlb.71.6.907].

30. Carneiro B. A., El-Deiry W. S. *Nat Rev Clin Oncol* **2020;** 17(7):395–417. [DOI:10.1038/s41571-020-0341-y].

31. Macleod K. *Curr Opin Genet Dev* **2000;** 10(1):81–93. [DOI:10.1016/s0959-437x(99)00041-6].

32. Joana D Amaral, Joana M Xavier, Clifford J Steer, Cecilia M Rodrigues. *Discovery Medicine* **2010;** 9(45):145–52.

33. Lavin M. F., Gueven N. *Cell Death Differ* **2006;** 13(6):941–50. [DOI:10.1038/sj.cdd.4401925].

34. Qian Y., Chen X. *Methods Mol Biol* **2013;** 965:37–61. [DOI:10.1007/978-1-62703-239-1_3].

35. Hoischen C., Monajembashi S., Weisshart K., Hemmerich P. *Front Oncol* **2018;** 8:125. [DOI:10.3389/fonc.2018.00125].

36. Zhang C., Liu J., Xu D., Zhang T., Hu W., Feng Z. *J Mol Cell Biol* **2020;** 12(9):674–87. [DOI:10.1093/jmcb/mjaa040].

37. Petitjean A., Mathe E., Kato S., Ishioka C., Tavtigian S. V., Hainaut P., Olivier M. *Hum Mutat* **2007;** 28(6):622–9. [DOI:10.1002/humu.20495].

38. Muller P. A. J., Vousden K. H. *Nat Cell Biol* **2013;** 15(1):2–8. [DOI:10.1038/ncb2641].

39. Levine B., Kroemer G. *Cell* **2008;** 132(1):27–42. [DOI:10.1016/j.cell.2007.12.018].

40. White E., DiPaola R. S. *Clin Cancer Res* **2009;** 15(17):5308–16. [DOI:10.1158/1078-0432.CCR-07-5023].

41. Beauséjour C. M., Krtolica A., Galimi F., Narita M., Lowe S. W., Yaswen P., Campisi J. *EMBO J* **2003;** 22(16):4212–22. [DOI:10.1093/emboj/cdg417].

42. Kumari R., Jat P. *Front Cell Dev Biol* **2021;** 9:645593. [DOI:10.3389/fcell.2021.645593].

43. Beck J., Turnquist C., Horikawa I., Harris C. *Carcinogenesis* **2020;** 41(8):1017–29. [DOI:10.1093/carcin/bgaa071].

44. Lopes-Paciencia S., Saint-Germain E., Rowell M.-C., Ruiz A. F., Kalegari P., Ferbeyre G. *Cytokine* **2019;** 117:15–22. [DOI:10.1016/j.cyto.2019.01.013].

45. Blander H. de, Morel A.-P., Senaratne A. P., Ouzounova M., Puisieux A. *Cancers (Basel)* **2021;** 13(18). [DOI:10.3390/cancers13184561].

46. Lee S., Schmitt C. A. *Nat Cell Biol* **2019;** 21(1):94–101. [DOI:10.1038/s41556-018-0249-2].

47. Milanovic M., Fan D. N. Y., Belenki D., Däbritz J. H. M., Zhao Z., Yu Y., Dörr J. R., Dimitrova L., Lenze D., Monteiro Barbosa I. A., Mendoza-Parra M. A., Kanashova T., Metzner M., Pardon K., Reimann M., Trumpp A., Dörken B., Zuber J., Gronemeyer H., Hummel M., Dittmar G., Lee S., Schmitt C. A. *Nature* **2018;** 553(7686):96–100. [DOI:10.1038/nature25167].

48. Hayflick L., Moorhead P. S. *Exp Cell Res* **1961;** 25:585–621. [DOI:10.1016/0014-4827(61)90192-6].

49. Maniwa Y., Yoshimura M., Obayashi C., Inaba M., Kiyooka K., Kanki M., Okita Y. *Chest* **2001;** 120(2):589–94. [DOI:10.1378/chest.120.2.589].

50. Roake C. M., Artandi S. E. *Nat Rev Mol Cell Biol* **2020;** 21(7):384–97. [DOI:10.1038/s41580-020-0234-z].

51. Cohen S. B., Graham M. E., Lovrecz G. O., Bache N., Robinson P. J., Reddel R. R. *Science* **2007;** 315(5820):1850–3. [DOI:10.1126/science.1138596].

52. Shay J. W., Bacchetti S. *Eur J Cancer* **1997;** 33(5):787–91. [DOI:10.1016/S0959-8049(97)00062-2].

53. Henson J. D., Reddel R. R. *FEBS Lett* **2010;** 584(17):3800–11. [DOI:10.1016/j.febslet.2010.06.009].

54. O'Rourke J. J., Bythell-Douglas R., Dunn E. A., Deans A. J. *Nucleus* **2019;** 10(1):221–30. [DOI:10.1080/19491034.2019.1685246].

55. Ségal-Bendirdjian E., Geli V. *Front Cell Dev Biol* **2019;** 7:332. [DOI:10.3389/fcell.2019.00332].

56. Witsch E., Sela M., Yarden Y. *Physiology (Bethesda)* **2010;** 25(2):85–101. [DOI:10.1152/physiol.00045.2009].

57. Uings I. J., Farrow S. N. *Mol Pathol* **2000;** 53(6):295–9. [DOI:10.1136/mp.53.6.295].

58. Bhowmick N. A., Neilson E. G., Moses H. L. *Nature* **2004;** 432(7015):332–7. [DOI:10.1038/nature03096].

59. Cheng N., Chytil A., Shyr Y., Joly A., Moses H. L. *Mol Cancer Res* **2008;** 6(10):1521–33. [DOI:10.1158/1541-7786.MCR-07-2203].

60. Dick F. A., Rubin S. M. *Nat Rev Mol Cell Biol* **2013;** 14(5):297–306. [DOI:10.1038/nrm3567].

61. Cano A., Pérez-Moreno M. A., Rodrigo I., Locascio A., Blanco M. J., Del Barrio M. G., Portillo F., Nieto M. A. *Nat Cell Biol* **2000;** 2(2):76–83. [DOI:10.1038/35000025].

62. Baldwin L. A., Hoff J. T., Lefringhouse J., Zhang M., Jia C., Liu Z., Erfani S., Jin H., Xu M., She Q.-B., van Nagell J. R., Wang C., Chen L., Plattner R., Kaetzel D. M.,

Luo J., Lu M., West D., Liu C., Ueland F. R., Drapkin R., Zhou B. P., Yang X. H. *Oncotarget* **2014;** 5(23):12203–17. [DOI:10.18632/oncotarget.2622].

63. Carmeliet P., Jain R. K. *Nature* **2000;** 407(6801):249–57. [DOI:10.1038/35025220].

64. Patan S. *Cancer Treat Res* **2004;** 117:3–32. [DOI:10.1007/978-1-4419-8871-3_1].

65. Burri P. H., Hlushchuk R., Djonov V. *Dev Dyn* **2004;** 231(3):474–88. [DOI:10.1002/dvdy.20184].

66. Eilken H. M., Adams R. H. *Curr Opin Cell Biol* **2010;** 22(5):617–25. [DOI:10.1016/j.ceb.2010.08.010].

67. Omorphos N. P., Gao C., Tan S. S., Sangha M. S. *Mol Biol Rep* **2021;** 48(1):941–50. [DOI:10.1007/s11033-020-06108-9].

68. Senger D. R., Davis G. E. *Cold Spring Harb Perspect Biol* **2011;** 3(8):a005090. [DOI:10.1101/cshperspect.a005090].

69. Rundhaug J. E. *J Cell Mol Med* **2005;** 9(2):267–85. [DOI:10.1111/j.1582-4934.2005.tb00355.x].

70. Rabbani S. A., Mazar A. P. *Surgical Oncology Clinics of North America* **2001;** 10(2):393–415. [DOI:10.1016/S1055-3207(18)30072-3].

71. Folkman J. *N Engl J Med* **1971;** 285(21):1182–6. [DOI:10.1056/NEJM197111182852108].

72. Jiang X., Wang J., Deng X., Xiong F., Zhang S., Gong Z., Li X., Cao K., Deng H., He Y., Liao Q., Xiang B., Zhou M., Guo C., Zeng Z., Li G., Li X., Xiong W. *J Exp Clin Cancer Res* **2020;** 39(1):204. [DOI:10.1186/s13046-020-01709-5].

73. Bergers G., Benjamin L. E. *Nat Rev Cancer* **2003;** 3(6):401–10. [DOI:10.1038/nrc1093].

74. Karamysheva A. F. *Biochemistry (Mosc)* **2008;** 73(7):751–62. [DOI:10.1134/s0006297908070031].

75. Adams J. C., Lawler J. *Cold Spring Harb Perspect Biol* **2011;** 3(10):a009712. [DOI:10.1101/cshperspect.a009712].

76. Wu W.-Z., Sun H.-C., Shen Y.-F., Chen J., Wang L., Tang Z.-Y., Iliakis G., Liu K.-D. *J Cancer Res Clin Oncol* **2005;** 131(3):169–78. [DOI:10.1007/s00432-004-0615-2].

77. Semenza G. *Biochemical Pharmacology* **2002;** 64(5-6):993–8. [DOI:10.1016/S0006-2952(02)01168-1].

78. Sottile J. *Biochim Biophys Acta* **2004;** 1654(1):13–22. [DOI:10.1016/j.bbcan.2003.07.002].

79. Nagy J. A., Chang S.-H., Dvorak A. M., Dvorak H. F. *Br J Cancer* **2009;** 100(6):865–9. [DOI:10.1038/sj.bjc.6604929].

80. Dudley A. C. *Cold Spring Harb Perspect Med* **2012;** 2(3):a006536. [DOI:10.1101/cshperspect.a006536].

81. Chang Y. S., Di Tomaso E., McDonald D. M., Jones R., Jain R. K., Munn L. L. *Proc Natl Acad Sci U S A* **2000;** 97(26):14608–13. [DOI:10.1073/pnas.97.26.14608].

82. Di Tomaso E., Capen D., Haskell A., Hart J., Logie J. J., Jain R. K., McDonald D. M., Jones R., Munn L. L. *Cancer Res* **2005;** 65(13):5740–9. [DOI:10.1158/0008-5472.CAN-04-4552].

83. Lugano R., Ramachandran M., Dimberg A. *Cell. Mol. Life Sci.* **2020;** 77(9):1745–70. [DOI:10.1007/s00018-019-03351-7].

84. Folberg R., Hendrix M. J., Maniotis A. J. *Am J Pathol* **2000;** 156(2):361–81. [DOI:10.1016/S0002-9440(10)64739-6].

85. Wei X., Chen Y., Jiang X., Peng M., Liu Y., Mo Y., Ren D., Hua Y., Yu B., Zhou Y., Liao Q., Wang H., Xiang B., Zhou M., Li X., Li G., Li Y., Xiong W., Zeng Z. *Mol Cancer* **2021;** 20(1):7. [DOI:10.1186/s12943-020-01288-1].

86. Sun B., Zhang D., Zhao N., Zhao X. *Oncotarget* **2017;** 8(18):30502–10. [DOI:10.18632/oncotarget.8461].

87. Valastyan S., Weinberg R. A. *Cell* **2011;** 147(2):275–92. [DOI:10.1016/j.cell.2011.09.024].

88. Majidpoor J., Mortezaee K. *Med Oncol* **2021;** 38(1):3. [DOI:10.1007/s12032-020-01447-w].

89. Francou A., Anderson K. V. *Annu. Rev. Cancer Biol.* **2020;** 4:197–220. [DOI:10.1146/annurev-cancerbio-030518-055425].

90. Nieto M. A., Huang R. Y.-J., Jackson R. A., Thiery J. P. *Cell* **2016;** 166(1):21–45. [DOI:10.1016/j.cell.2016.06.028].

91. Kalluri R., Weinberg R. A. *J Clin Invest* **2009;** 119(6):1420–8. [DOI:10.1172/JCI39104].

92. Lamouille S., Xu J., Derynck R. *Nat Rev Mol Cell Biol* **2014;** 15(3):178–96. [DOI:10.1038/nrm3758].

93. Yu Y., Xiao C.-H., Tan L.-D., Wang Q.-S., Li X.-Q., Feng Y.-M. *Br J Cancer* **2014;** 110(3):724–32. [DOI:10.1038/bjc.2013.768].

94. Yamazaki D., Kurisu S., Takenawa T. *Cancer Sci* **2005;** 96(7):379–86. [DOI:10.1111/j.1349-7006.2005.00062.x].

95. Sznurkowska M. K., Aceto N. *FEBS J* **2022;** 289(15):4336–54. [DOI:10.1111/febs.16046].

96. Wheeler L. J., Watson Z. L., Qamar L., Yamamoto T. M., Sawyer B. T., Sullivan K. D., Khanal S., Joshi M., Ferchaud-Roucher V., Smith H., Vanderlinden L. A., Brubaker S. W., Caino C. M., Kim H., Espinosa J. M., Richer J. K., Bitler B. G. *iScience* **2019;** 19:474–91. [DOI:10.1016/j.isci.2019.07.049].

97. Bock K. de, Mazzone M., Carmeliet P. *Nat Rev Clin Oncol* **2011;** 8(7):393–404. [DOI:10.1038/nrclinonc.2011.83].

98. Lo H. C., Xu Z., Kim I. S., Pingel B., Aguirre S., Kodali S., Liu J., Zhang W., Muscarella A. M., Hein S. M., Krupnick A. S., Neilson J. R., Paust S., Rosen J. M., Wang H., Zhang X. H.-F. *Nature cancer* **2020;** 1(7):709–22. [DOI:10.1038/s43018-020-0068-9].

99. Labelle M., Begum S., Hynes R. O. *Cancer Cell* **2011;** 20(5):576–90. [DOI:10.1016/j.ccr.2011.09.009].

100. Summers M. A., McDonald M. M., Croucher P. I. *Cold Spring Harb Perspect Med* **2020;** 10(4). [DOI:10.1101/cshperspect.a037556].

101. Chaffer C. L., Thompson E. W., Williams E. D. *Cells Tissues Organs* **2007;** 185(1-3):7–19. [DOI:10.1159/000101298].

102. Steeg P. S. *Nat Med* **2006;** 12(8):895–904. [DOI:10.1038/nm1469].

103. Gilman A., Philips F. S. *Science* **1946;** 103(2675):409–36. [DOI:10.1126/science.103.2675.409].

104. Goodman L. S., Wintrobe M. M. *J Am Med Assoc* **1946;** 132:126–32. [DOI:10.1001/jama.1946.02870380008004].

105. Faber S., Diamond L. K. *N Engl J Med* **1948;** 238(23):787–93. [DOI:10.1056/NEJM194806032382301].

106. Ansfield F. J., SchroederR J. M., Curreri A. R. *JAMA* **1962;** 181:295–9. [DOI:10.1001/jama.1962.03050300015003].

107. Pratt C. B., Shanks E. C. *Am J Dis Child* **1974;** 127(4):534–6. [DOI:10.1001/archpedi.1974.02110230080012].

108. Chabner B. A., Roberts T. G. *Nat Rev Cancer* **2005;** 5(1):65–72. [DOI:10.1038/nrc1529].

109. Carelle N., Piotto E., Bellanger A., Germanaud J., Thuillier A., Khayat D. *Cancer* **2002;** 95(1):155–63. [DOI:10.1002/cncr.10630].

110. Rebucci M., Michiels C. *Biochemical Pharmacology* **2013;** 85(9):1219–26. [DOI:10.1016/j.bcp.2013.02.017].

111. Arora A., Scholar E. M. *J Pharmacol Exp Ther* **2005;** 315(3):971–9. [DOI:10.1124/jpet.105.084145].

112. Mellman I., Coukos G., Dranoff G. *Nature* **2011;** 480(7378):480–9. [DOI:10.1038/nature10673].

113. Casak S. J., Donoghue M., Fashoyin-Aje L., Jiang X., Rodriguez L., Shen Y.-L., Xu Y., Jiang X., Liu J., Zhao H., Pierce W. F., Mehta S., Goldberg K. B., Theoret M. R., Kluetz P. G., Pazdur R., Lemery S. J. *Clin Cancer Res* **2021;** 27(7):1836–41. [DOI:10.1158/1078-0432.CCR-20-3407].

114. Lamb Y. N. *Drugs* **2017;** 77(14):1603–10. [DOI:10.1007/s40265-017-0802-5].

115. Debela D. T., Muzazu S. G., Heraro K. D., Ndalama M. T., Mesele B. W., Haile D. C., Kitui S. K., Manyazewal T. *SAGE Open Med* **2021;** 9:20503121211034366. [DOI:10.1177/20503121211034366].

116. Sterner R. C., Sterner R. M. *Blood Cancer J.* **2021;** 11(4):69. [DOI:10.1038/s41408-021-00459-7].

117. Conry R. M., Westbrook B., McKee S., Norwood T. G. *Hum Vaccin Immunother* **2018;** 14(4):839–46. [DOI:10.1080/21645515.2017.1412896].

118. Copelan E. A. *N Engl J Med* **2006;** 354(17):1813–26. [DOI:10.1056/NEJMra052638].

119. Frei E., Holland J. F., Schneiderman M. A., Pinkel D., Selkirk G., Freireich E. J., Silver R. T., Gold G. L., RegelsonW. *Blood* **1958;** 13(12):1126–48. [DOI:10.1182/blood.V13.12.1126.1126].

120. Mayer L. D., Janoff A. S. *Mol Interv* **2007;** 7(4):216–23. [DOI:10.1124/mi.7.4.8].

121. Rautio J., Meanwell N. A., Di L., Hageman M. J. *Nat Rev Drug Discov* **2018;** 17(8):559–87. [DOI:10.1038/nrd.2018.46].

122. Csermely P., Agoston V., Pongor S. *Trends Pharmacol Sci* **2005;** 26(4):178–82. [DOI:10.1016/j.tips.2005.02.007].

123. Gao X., Burris III H. A., Vuky J., Dreicer R., Sartor A. O., Sternberg C. N., Percent I. J., Hussain M. H. A., Rezazadeh Kalebasty A., Shen J., Heath E. I., Abesada-Terk G., Gandhi S. G., McKean M., Lu H., Berghorn E., Gedrich R., Chirnomas S. D., Vogelzang N. J., Petrylak D. P. *JCO* **2022;** 40(6_suppl):17. [DOI:10.1200/JCO.2022.40.6_suppl.017].

124. Menichincheri M., Ardini E., Magnaghi P., Avanzi N., Banfi P., Bossi R., Buffa L., Canevari G., Ceriani L., Colombo M., Corti L., Donati D., Fasolini M., Felder E., Fiorelli C., Fiorentini F., Galvani A., Isacchi A., Borgia A. L., Marchionni C., Nesi M., Orrenius C., Panzeri A., Pesenti E., Rusconi L., Saccardo M. B., Vanotti E., Perrone E., Orsini P. *J Med Chem* **2016;** 59(7):3392–408. [DOI:10.1021/acs.jmedchem.6b00064].

125. Alford R., Simpson H. M., Duberman J., Hill G. C., Ogawa M., Regino C., Kobayashi H., Choyke P. L. *Mol Imaging* **2009;** 8(6):7290.2009.00031. [DOI:10.2310/7290.2009.00031].

126. Beatty K. E., Liu J. C., Xie F., Dieterich D. C., Schuman E. M., Wang Q., Tirrell D. A. *Angew. Chem.* **2006;** 118(44):7524–7. [DOI:10.1002/ange.200602114].

127. Wu J., Akhmanova A. *Annu Rev Cell Dev Biol* **2017;** 33:51–75. [DOI:10.1146/annurev-cellbio-100616-060615].

128. Akhmanova A., Steinmetz M. O. *Nat Rev Mol Cell Biol* **2015;** 16(12):711–26. [DOI:10.1038/nrm4084].

129. Brouhard G. J., Rice L. M. *Nat Rev Mol Cell Biol* **2018;** 19(7):451–63. [DOI:10.1038/s41580-018-0009-y].

130. Roostalu J., Thomas C., Cade N. I., Kunzelmann S., Taylor I. A., Surrey T. *Elife* **2020;** 9. [DOI:10.7554/eLife.51992].

131. Sweeney H. L., Holzbaur E. L. F. *Cold Spring Harb Perspect Biol* **2018;** 10(5). [DOI:10.1101/cshperspect.a021931].

132. Goodson H. V., Jonasson E. M. *Cold Spring Harb Perspect Biol* **2018;** 10(6). [DOI:10.1101/cshperspect.a022608].

133. Verhey K. J., Gaertig J. *Cell Cycle* **2007;** 6(17):2152–60. [DOI:10.4161/cc.6.17.4633].

134. Steinmetz M. O., Prota A. E. *Trends Cell Biol* **2018;** 28(10):776–92. [DOI:10.1016/j.tcb.2018.05.001].

135. Prota A. E., Bargsten K., Diaz J. F., Marsh M., Cuevas C., Liniger M., Neuhaus C., Andreu J. M., Altmann K.-H., Steinmetz M. O. *Proc Natl Acad Sci U S A* **2014;** 111(38):13817–21. [DOI:10.1073/pnas.1408124111].

136. Prota A. E., Bargsten K., Northcote P. T., Marsh M., Altmann K.-H., Miller J. H., Díaz J. F., Steinmetz M. O. *Angew Chem Int Ed Engl* **2014;** 53(6):1621–5. [DOI:10.1002/anie.201307749].

137. Singh P., Rathinasamy K., Mohan R., Panda D. *IUBMB Life* **2008;** 60(6):368–75. [DOI:10.1002/iub.42].

138. Tron G. C., Pirali T., Sorba G., Pagliai F., Busacca S., Genazzani A. A. *J Med Chem* **2006;** 49(11):3033–44. [DOI:10.1021/jm0512903].

139. Gigant B., Wang C., Ravelli R. B. G., Roussi F., Steinmetz M. O., Curmi P. A., Sobel A., Knossow M. *Nature* **2005;** 435(7041):519–22. [DOI:10.1038/nature03566].

140. Ranaivoson F. M., Gigant B., Berritt S., Joullié M., Knossow M. *Acta Crystallogr D Biol Crystallogr* **2012;** 68(Pt 8):927–34. [DOI:10.1107/S0907444912017143].

141. Eli S., Castagna R., Mapelli M., Parisini E. *Front Mol Biosci* **2022;** 9:841777. [DOI:10.3389/fmolb.2022.841777].

142. Čermák V., Dostál V., Jelínek M., Libusová L., Kovář J., Rösel D., Brábek J. *European Journal of Cell Biology* **2020;** 99(4):151075. [DOI:10.1016/j.ejcb.2020.151075].

143. Field J. J., Kanakkanthara A., Miller J. H. *Bioorganic & Medicinal Chemistry* **2014;** 22(18):5050–9. [DOI:10.1016/j.bmc.2014.02.035].

144. Vitale I., Galluzzi L., Castedo M., Kroemer G. *Nat Rev Mol Cell Biol* **2011;** 12(6):385–92. [DOI:10.1038/nrm3115].

145. Castedo M., Perfettini J.-L., Roumier T., Andreau K., Medema R., Kroemer G. *Oncogene* **2004;** 23(16):2825–37. [DOI:10.1038/sj.onc.1207528].

146. Sinha D., Duijf P. H. G., Khanna K. K. *Cell Cycle* **2019;** 18(1):7–15. [DOI:10.1080/15384101.2018.1559557].

147. Gordon D. J., Resio B., Pellman D. *Nat Rev Genet* **2012;** 13(3):189–203. [DOI:10.1038/nrg3123].

148. Krämer A., Maier B., Bartek J. *Mol Oncol* **2011;** 5(4):324–35. [DOI:10.1016/j.molonc.2011.05.003].

149. Rebacz B., Larsen T. O., Clausen M. H., Rønnest M. H., Löffler H., Ho A. D., Krämer A. *Cancer Res* **2007;** 67(13):6342–50. [DOI:10.1158/0008-5472.CAN-07-0663].

150. Bates D., Eastman A. *Br J Clin Pharmacol* **2017;** 83(2):255–68. [DOI:10.1111/bcp.13126].

151. Schwartz E. L. *Clin Cancer Res* **2009;** 15(8):2594–601. [DOI:10.1158/1078-0432.CCR-08-2710].

152. Lugano R., Ramachandran M., Dimberg A. *Cell. Mol. Life Sci.* **2020;** 77(9):1745–70. [DOI:10.1007/s00018-019-03351-7].

153. Abdalla A. M. E., Xiao L., Ullah M. W., Yu M., Ouyang C., Yang G. *Theranostics* **2018;** 8(2):533–48. [DOI:10.7150/thno.21674].

154. Kamba T., McDonald D. M. *Br J Cancer* **2007;** 96(12):1788–95. [DOI:10.1038/sj.bjc.6603813].

155. Viallard C., Larrivée B. *Angiogenesis* **2017;** 20(4):409–26. [DOI:10.1007/s10456-017-9562-9].

156. Roskoski R. *Pharmacological Research* **2021;** 165:105463. [DOI:10.1016/j.phrs.2021.105463].

157. Casak S. J., Fashoyin-Aje I., Lemery S. J., Zhang L., Jin R., Li H., Zhao L., Zhao H., Zhang H., Chen H., He K., Dougherty M., Novak R., Kennett S., Khasar S., Helms

W., Keegan P., Pazdur R. *Clinical Cancer Research* **2015;** 21(15):3372–6. [DOI:10.1158/1078-0432.CCR-15-0600].

158. Gaya A., Tse V. *Cancer Treat Rev* **2012;** 38(5):484–93. [DOI:10.1016/j.ctrv.2011.12.008].

159. Smith S. W. *Toxicol Sci* **2009;** 110(1):4–30. [DOI:10.1093/toxsci/kfp097].

160. Sherbet G. V. *Anticancer Research* **2015;** 35(11):5767–72.

161. Faes S., Santoro T., Demartines N., Dormond O. *Cancers (Basel)* **2017;** 9(11):152. [DOI:10.3390/cancers9110152].

162. Oh I. H., Reddy E. P. *Oncogene* **1999;** 18(19):3017–33. [DOI:10.1038/sj.onc.1202839].

163. Prendergast G. C. *Oncogene* **1999;** 18(19):2914–5. [DOI:10.1038/sj.onc.1202784].

164. Pattabiraman D. R., Gonda T. J. *Leukemia* **2013;** 27(2):269–77. [DOI:10.1038/leu.2012.225].

165. Ramsay R. G., Gonda T. J. *Nat Rev Cancer* **2008;** 8(7):523–34. [DOI:10.1038/nrc2439].

166. Uttarkar S., Dassé E., Coulibaly A., Steinmann S., Jakobs A., Schomburg C., Trentmann A., Jose J., Schlenke P., Berdel W. E., Schmidt T. J., Müller-Tidow C., Frampton J., Klempnauer K.-H. *Blood* **2016;** 127(9):1173–82. [DOI:10.1182/blood-2015-09-668632].

167. Walf-Vorderwülbecke V., Pearce K., Brooks T., Hubank M., van den Heuvel-Eibrink M. M., Zwaan C. M., Adams S., Edwards D., Bartram J., Samarasinghe S., Ancliff P., Khwaja A., Goulden N., Williams G., Boer J. de, Williams O. *Leukemia* **2018;** 32(4):882–9. [DOI:10.1038/leu.2017.317].

168. Yusenko M. V., Biyanee A., Frank D., Köhler L. H. F., Andersson M. K., Khandanpour C., Schobert R., Stenman G., Biersack B., Klempnauer K.-H. *Cancers (Basel)* **2021;** 14(1). [DOI:10.3390/cancers14010043].

169. Ramaswamy K., Forbes L., Minuesa G., Gindin T., Brown F., Kharas M. G., Krivtsov A. V., Armstrong S. A., Still E., Stanchina E. de, Knoechel B., Koche R., Kentsis A. *Nat Commun* **2018;** 9(1):110. [DOI:10.1038/s41467-017-02618-6].

170. Mitani Y., Li J., Rao P. H., Zhao Y.-J., Bell D., Lippman S. M., Weber R. S., Caulin C., El-Naggar A. K. *Clinical Cancer Research* **2010;** 16(19):4722–31. [DOI:10.1158/1078-0432.CCR-10-0463].

171. Andersson M. K., Afshari M. K., Andrén Y., Wick M. J., Stenman G. *J Natl Cancer Inst* **2017;** 109(9). [DOI:10.1093/jnci/djx017].

172. Calvo E., Soria J.-C., Ma W. W., Wang T., Bahleda R., Tolcher A. W., Gernhardt D., O'Connell J., Millham R., Giri N., Wick M. J., Adjei A. A., Hidalgo M. *Clinical Cancer Research* **2017;** 23(5):1177–85. [DOI:10.1158/1078-0432.CCR-15-2301].

173. Pham T., Pereira L., Roth S., Galletta L., Link E., Akhurst T., Solomon B., Michael M., Darcy P., Sampurno S., Heriot A., Ramsay R., Desai J. *Contemp Clin Trials Commun* **2019;** 16:100409. [DOI:10.1016/j.conctc.2019.100409].

174. Hu Y., Li J., Lv C.-W., Di Qu, Hou Z., Jia M., Li J.-T., Zhang Z.-D., Luo X.-X., Yuan Z., Li M.-K. *Z fur Phys Chem* **2016;** 230(1):97–110. [DOI:10.1515/zpch-2015-0630].

175. Schmitt F., Gold M., Rothemund M., Andronache I., Biersack B., Schobert R., Mueller T. *Eur J Med Chem* **2019;** 163:160–8. [DOI:10.1016/j.ejmech.2018.11.055].

176. Gold M., Köhler L., Lanzloth C., Andronache I., Anant S., Dandawate P., Biersack B., Schobert R. *Eur J Med Chem* **2020;** 189:112060. [DOI:10.1016/j.ejmech.2020.112060].

177. Sabat-Pośpiech D., Fabian-Kolpanowicz K., Prior I. A., Coulson J. M., Fielding A. B. *Biochem Soc Trans* **2019;** 47(5):1209–22. [DOI:10.1042/BST20190034].

178. Yusenko M., Jakobs A., Klempnauer K.-H. *Sci Rep* **2018;** 8(1):13159. [DOI:10.1038/s41598-018-31620-1].

4. Publikationen

4.1 Darstellung des Eigenanteils

Die in dieser Dissertation aufgeführten Publikationen wurden zum großen Teil in Kooperation mit anderen Arbeitsgruppen erarbeitet. Darunter zählen das Biochemie-Instituts der Westfälische-Wilhelms-Universität in Münster, das *Department of Chemistry & Post Graduate Research Center* des Abeda Inamdar Senior College (Indien) und die Arbeitsgruppe Entwicklungsbiologie der Universität Bayreuth.

Es folgt eine detaillierte Darstellung der Beiträge aller Co-Autoren zu den jeweiligen Publikationen.

4.1.1 zu Publikation I

Die Ergebnisse zu diesem Thema wurden im Journal ***ChemMedChem*** (doi.org/10.1002/cmdc.202200064) unter folgendem Titel veröffentlicht:

„2-Amino-4-aryl-5-oxo-4,5-dihydropyrano[3,2-c]chromene-3-carbonitriles with Microtubule-Disruptive, Centrosome-Declustering, and Antiangiogenic Effects in vitro and in vivo“

Von den Autoren

Leonhard H. F. Köhler, Sebastian Reich, Gerrit Begemann, Rainer Schobert, und Bernhard Biersack.

Der Eigenanteil setzt sich aus Konzeption, Durchführung und Auswertung der biochemischen Assays zusammen. Diese umfassen Zellkultivierung, MTT-Assay, Tubulinpolymerisationsassay, Immunofluoreszenzmikroskopie, Zellzyklusanalysen, CDK1/CyclinA2-Aktivitätstests, Co-Lokalisierungsexperimente, EA.hy926-Tube-Formation-Assay und Zebrafisch-Angiogenese-Assay. Sebastian Reich unterstützte die experimentelle Durchführung im Rahmen eines Forschungsmoduls. Synthese, Aufreinigung und Charakterisierung der untersuchten Testsubstanzen wurde von Dr. Bernhard Biersack durchgeführt. Prof. Gerrit Begemann stellte die Laboratorien und Geräte für den Zebrafisch-Angiogenese-Assay zur Verfügung. Das Manuskript einschließlich der Revision sowie Diskussion und graphische Darstellung der Ergebnisse wurde von mir und Herrn Dr. Bernhard Biersack mit Korrekturen von Herrn Prof. Dr. Rainer Schobert erstellt.

4.1.2 zu Publikation II

Die Ergebnisse zu diesem Thema wurden im Journal ***ACS Medicinal Chemistry Letters*** (DOI: 10.1021/acsmedchemlett.2c00403) unter folgendem Titel veröffentlicht:

„A New Naphthopyran Derivative Combines c -Myb Inhibition, Microtubule-Targeting Effects, and Antiangiogenic Properties“

Von den Autoren

Leonhard H. F. Köhler, Sebastian Reich, Maria Yusenko, Karl-Heinz Klempnauer, Amin H. Shaikh, Khursheed Ahmed, Gerrit Begemann, Rainer Schobert und Bernhard Biersack.

Der Eigenanteil setzt sich aus Konzeption, Durchführung und Auswertung der biochemischen Assays zusammen. Diese umfassen Zellkultivierung, MTT-Assay, Tubulinpolymerisationsassay, Immunofluoreszenzmikroskopie, Zellzyklusanalysen, Caspase-3/7-Aktivitätstests, Co-Lokalisierungsexperimente, EA.hy926-Tube-Formation-Assay, Zebrafisch-Angiogenese-Assay und Stabilitätsmessungen mittels UV-Absorption und RP-HPLC. Die experimentelle Durchführung wurde von Sebastian Reich im Rahmen seiner Bachelorarbeit unterstützt. Dr. Bernhard Biersack war für die Synthese, Aufreinigung und Charakterisierung der untersuchten Testsubstanzen verantwortlich. Maria Yusenko führte den *c*-MYB-Luciferase-Reporter-Assay unter der Leitung von Prof. Dr. Karl-Heinz Klempnauer durch. Molekulare Docking-Studien wurden von Amin H. Shaikh und Prof. Khursheed Ahmed durchgeführt und diskutiert. Das Manuskript einschließlich der Revision sowie Diskussion und graphische Darstellung der Ergebnisse wurde von mir und Herrn Dr. Bernhard Biersack mit Korrektur von Herrn Prof. Rainer Schobert und Prof. Dr. Karl-Heinz Klempnauer erstellt.

4.1.3 zu Publikation III

Die Ergebnisse zu diesem Thema wurden im Journal ***Cancer Drug Resistance*** (DOI: 10.20517/cdr.2022.90) unter folgendem Titel veröffentlicht:

„Multimodal 4-Arylchromene derivatives with microtubule-destabilizing, anti-angiogenic, and MYB-inhibitory activities“

Von den Autoren

Leonhard H. F. Köhler, Sebastian Reich, Maria Yusenko, Karl-Heinz Klempnauer, Gerrit Begemann, Rainer Schobert und Bernhard Biersack.

Der Eigenanteil setzt sich aus Konzeption, Durchführung und Auswertung der biochemischen Assays zusammen. Diese umfassen Zellkultivierung, MTT-Assay, Immunofluoreszenzmikroskopie, Zellzyklusanalysen, Co-Lokalisierungsexperimente, EA.hy926-Tube-Formation-Assay und Zebrafisch-Angiogenese-Assay. Sebastian Reich unterstützte im Rahmen eines Forschungspraktikums die experimentelle Durchführung. Die Synthese der Testsubstanzen sowie deren Aufreinigung und Charakterisierung wurden von Dr. Bernhard Biersack durchgeführt. Maria Yusenko war unter der Leitung von Prof. Dr. Karl-Heinz Klempnauer für die Messung der *c*-MYB-Luciferase-Aktivität zuständig. Das Manuskript einschließlich der Revision sowie Diskussion und graphische Darstellung der Ergebnisse wurde von mir und Herrn Dr. Bernhard Biersack mit Korrektur von Herrn Prof. Dr. Rainer Schobert und Prof. Dr. Karl-Heinz Klempnauer erstellt.

4.2 Publikation I

2-Amino-4-aryl-5-oxo-4,5-dihydropyrano[3,2-*c*]chromene-3-carbonitriles with Microtubule-Disruptive, Centrosome-Declustering, and Antiangiogenic Effects *in vitro* and *in vivo*

Leonhard H. F. Köhler,[a] Sebastian Reich,[a] Gerrit Begemann,[b] Rainer Schobert,[a] und Bernhard Biersack.[a]*

[a] Organic Chemistry Laboratory University of Bayreuth, Universitätsstraße 30, 95440 Bayreuth (Germany)
[b] Developmental Biology, University of Bayreuth, Universitätsstraße 30, Bayreuth 95440 (Germany)

*Corresponding author. E-Mail address: bernhard.biersack@yahoo.com

ChemMedChem **2022**, *17*, e202200064

2-Amino-4-aryl-5-oxo-4,5-dihydropyrano[3,2-*c*]chromene-3-carbonitriles with Microtubule-Disruptive, Centrosome-Declustering, and Antiangiogenic Effects *in vitro* and *in vivo*

Leonhard H. F. Köhler,[a] Sebastian Reich,[a] Gerrit Begemann,[b] Rainer Schobert,[a] and Bernhard Biersack*[a]

A series of fifteen 2-amino-4-aryl-5-oxo-4,5-dihydropyrano[3,2-*c*]chromene-3-carbonitriles (**1 a**–**o**) were synthesized via a three-component reaction of 4-hydroxycoumarin, malononitrile, and diversely substituted benzaldehydes or pyridine carbaldehydes. The compounds were tested for anticancer activities against a panel of eight human tumor cell lines. A few derivatives with high antiproliferative activities and different cancer cell specificity were identified and investigated for their modes of action. They led to microtubule disruption, centrosome de-clustering and G2/M cell cycle arrest in 518 A2 melanoma cells. They also showed anti-angiogenic effects *in vitro* and *in vivo*.

Introduction

The development of new drugs is mainly based on the synthesis and screening of compound libraries, and on the elucidation of target-ligand interactions, structure-activity relationships (SAR) and target/disease selectivities.[1] When following a target-oriented strategy, one-pot multi-component reactions (MCR) are an excellent approach to the synthesis of large libraries of compounds with systematically varied substituents.[2] Prominent examples of such multi-component reactions often-used for drug development are those named after Ugi, Biginelli and Van Leusen, and modifications thereof.[3] The coumarin (1,2-benzopyrone) scaffold is found in quite a few biologically active compounds including anticancer agents.[4] 4-Hydroxycoumarin, in particular, emerged as an important antitumoral pharmacophore (Scheme 1).[5] It is fortunate that 4-hydroxycoumarin reacts readily in one-pot three-component reactions with aryl aldehydes and malononitrile to give pyranochromene derivatives, which were frequently found active against cancer cells, especially when carrying halogen substituents.[6] Analogous reactions using naphthol and phenol derivatives instead of 4-hydroxycoumarin previously led to a plethora of similar anticancer active compounds.[7–9] In continuation of our recent work on anticancer active pyrans derived from 1-naphthol and hydroxyquinoline, we now submitted the most promising substituted aryl aldehydes of these series (e.g., such with methoxyphenyl and fluorinated phenyl residues) to MCR with malononitrile and 4-hydroxycoumarin. This afforded a series of new 2-amino-4-aryl-5-oxo-4,5-dihydropyrano[3,2-*c*]chromene-3-carbonitriles, whose anticancer activities and modes of action were assessed in detail.[8,9] In particular, effects on microtubules, cellular morphology, cell cycle arrest, CDK, and angiogenesis were studied in this work.

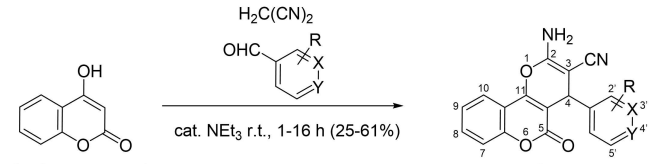

1a: X = Y = C; R = 3′-Br, 4′,5′-$(MeO)_2$
1b: X = Y = C; R = 3′-I, 4′,5′-$(Meo)_2$
1c: X = Y = C; R = 3′,5′-Br_2, 4′-MeO
1d: X = Y = C; R = 3′,5′-I_2, 4′-MeO
1e: X = Y = C; R = 3′,4′-F_2
1f: X = C, Y = CH; R = 3′,5′-F_2
1g: X = Y = C; R = 3′,4′,5′-F_3
1h: X = Y = C; R = 3′,4′-Cl_2
1i: X = CH, Y = C; R = 4′-MeS
1j: X = C, Y = CH; R = 3′-SF_5
1k: X = Y = C; R = 3′-NO_2, 4′-MeO
1l: X = C, Y = CH; R = 3′-CN
1m: X = CH, Y = C; R = 4′-CCH
1n[a]: X = N, Y = CH; R = H
1o[a]: X = CH, Y = N; R = H
1p[a]: X = CH, Y = C, R = 4′-Br
1q[a]: X = CH, Y = C, R = 2′,4′-F_2

Scheme 1. Syntheses of 2-amino-4-aryl-5-oxo-4,5-dihydropyrano[3,2-*c*]chromene-3-carbonitriles **1**.[a] El-Agrody et al.[10]

Results and Discussion

Synthesis

The test compounds **1 a**–**q** were prepared from a mixture of 4-hydroxycoumarin, malononitrile, the corresponding aryl aldehyde, and a catalytic amount of triethyl amine in acetonitrile

[a] *L. H. F. Köhler, S. Reich, Prof. Dr. R. Schobert, Dr. B. Biersack*
Organic Chemistry Laboratory
University of Bayreuth
Universitätsstraße 30, 95447 Bayreuth (Germany)
E-mail: bernhard.biersack@yahoo.com
bernhard.biersack@uni-bayreuth.de
[b] *Prof. Dr. G. Begemann*
Department of Biology
University of Bayreuth
Universitätsstraße 30, 95447 Bayreuth (Germany)

Supporting information for this article is available on the WWW under https://doi.org/10.1002/cmdc.202200064

(Scheme 1). The new compounds **1a**–**m** were obtained as colorless solids in low to moderate yields. NMR, IR, and MS analyses confirmed the proposed structures.

Antiproliferative activity

The compounds **1a**–**o** were initially tested for their antiproliferative activity against a panel of eight tumor cell lines from five different entities and one endothelial hybrid cell line (EA.hy926) using MTT assays (Table 1). The previously published compounds **1p** and **1q** served as reference compounds but showed no activity in our experiments in the tested concentration range.[10] Compounds **1a**–**d** showed generally considerable antiproliferative activities with IC_{50} values in the low one-digit micromolar range. The bromo-derivatives **1a** and **1c** were slightly more active than the iodo analogs **1b** and **1d**. 3,5-Dibromo-4-methoxyphenyl derivative **1c** was especially active against HT-29 colon carcinoma cells ($IC_{50}=0.5$ μM).

Among the fluorophenyl derivatives, only 3,5-difluorophenyl compound **1f** exhibited moderate antiproliferative activities while the 3,4-difluorophenyl and 3,4,5-trifluorophenyl derivatives **1e** and **1g** were virtually inactive. In contrast to the inactive compound **1e**, its dichlorophenyl analog **1h** was active against HT-29, EA.hy926 and HCT-116 cells, while it remained inactive against 518 A2, KB-V1 and MCF-7 cells. Hence, **1h** showed a certain degree of tumor type specificity. Particularly interesting activities and selectivities were observed for the 3-pentafluorothiophenyl derivative **1j**. It was highly active against EA.hy926, HCT-116 p53−/−, and HT-29 cells ($IC_{50}=0.15$, 0.04, and 0.4 μM, respectively), while it was inactive against the other tumor cell lines. In contrast to that, the 3-cyanophenyl derivative **1l** showed moderate but unspecific activity against all tested cancer cell lines. Interestingly, the 4-ethynylphenyl derivative **1m**, which was designed for localization assays (see below), showed moderate activity only against HCT-116, HCT-116 p53−/−, and U87 cells. The 4-methylthiophenyl analog **1i**, the 3-nitro-4-methoxyphenyl analog **1k**, and the pyridyl derivatives **1n** and **1o** showed no antiproliferative activities below concentrations of 50 μM. Some of the compounds, e.g., **1f**, **1g** and **1l**, might be a substrate of efflux transporter P-gp, as cells treated with the P-gp inhibitor verapamil (VER) prior to the application of these compounds gave rise to significantly lower IC_{50} values when compared to those measured in the absence of verapamil. By contrast, **1a**–**d** displayed no significant difference in IC_{50} values of verapamil treated and untreated KB-V1 cervix carcinoma cells. They are thus unlikely to be P-gp substrates, which fact might contribute to their superior activity. To estimate their selectivity for cancer cells the three most active compounds **1a**, **1c** and **1d** were also tested on non-malignant adult human dermal fibroblasts (HDFa) via MTT assays. The selectivity index (SI) for all tested cancer cell lines was calculated from the ratio of the average IC_{50} value and that of HDFa cells (SI=IC_{50} HDFa/average IC_{50} of all cancer cell lines). Since all three compounds showed high SI values (29.3 for **1a**, 52.9 for **1c**, 31.1 for **1d**), they can be considered as selective for cancer cells (Table S1, Supporting Information).[11]

The three most active compounds **1a** (3,5-dibromo-4-methoxy motif), **1c** (3-bromo-4,5-dimethoxy motif) and **1d** (3,5-diiodo-4-methoxy motif) were selected for further mechanistic studies. Despite its selectivity for and low IC_{50} values against EA.hy926, HCT-116p53−/− and HT-29 cells, compound **1j** was excluded because of its lower average cytotoxicity and poor efficacy against the mainly used 518 A2 melanoma cell line.

Effect on tubulin polymerisation and the microtubules

The superior cytotoxicity of the methoxyphenyl derivatives **1a**, **1c** and **1d**, which remotely structurally resemble combretasta-

Table 1. Inhibitory concentrations IC_{50}[a] [μM] of test compounds **1a**–**q** when applied to 518 A2 melanoma, KB-$V1^{Vbl}$ MDR cervix carcinoma (treated with and without 1 μM verapamil), U-87 MG likely glioblastoma, MCF-7 breast carcinoma, HT-29, HCT-116 and HCT-116p53−/− (p53 knockout mutant) colon carcinoma, EA.hy926 endothelial hybrid cells, and HDFa human dermal fibroblasts.

	EA.hy926	518 A2	HCT-116	HCT-116 p53−/−	U87	HT-29	KB–$V1^{Vb.}$	KB–$V1^{Vbl.}$ [1 μM VER]	MCF-7	HDFa
1a	1.8±0.1	1.9±0.1	3.2±0.1	2.2±0.2	4.2±0.2	6.4±0.9	4.9±0.3	4.2±0.2	1.9±0.08	>100
1b	6.2±0.2	2.9±0.1	6.7±0.2	1.7±0.16	12.3±1.4	5.6±0.3	7.8±0.8	7.0±1.4	5.8±0.2	–
1c	1.0±0.06	1.8±0.2	1.5±0.05	1.9±0.1	3.4±0.2	0.5±0.05	3.0±0.2	2.8±0.2	1.1±0.1	>100
1d	2.8±0.07	1.5±0.1	3.1±0.1	2.9±0.06	5.5±0.3	2.5±0.2	3.7±0.06	3.5±0.08	3.4±0.2	>100
1e	>50	–	>50	>50	>50	>50	>50	–	–	–
1f	8.8±0.3	6.7±0.5	7.8±0.6	9.8±0.4	12.6±2.2	13.7±1.5	21.2±2.8	7.4±1.4	5.8±0.2	–
1g	>50	>50	>50	>50	>50	>50	29.3±2.0	>50	>50	–
1h	7.0±0.5	>50	18.2±1.4	42±1.8	49.1±7.1	1.5±0.2	>50	>50	>50	–
1i	–	–	>50	>50	–	>50	–	–	–	–
1j	0.15±0.02	>50	>50	0.04±0.008	>50	0.4±0.02	>50	>50	>50	–
1k	–	–	>50	>50	–	>50	–	–	–	–
1l	10.2±0.7	13.3±1.0	15.3±1.0	16.6±3.3	15.7±1.7	35.1±3.6	14.6±1.2	2.9±0.3	14.4±0.9	–
1m	>50	>50	13.5±1.2	27.4±1.2	7.4±0.8	>50	>50	>50	>50	–
1n	–	–	–	>50	>50	–	>50	–	–	–
1o	–	–	>50	>50	>50	>50	>50	–	–	–
1p	–	>50	–	–	–	–	>50	>50	>50	–
1q	–	>50	–	–	–	–	>50	>50	>50	–

[a] Values are the means of at least four independent experiments (±SD). They were derived from concentration-response curves obtained by measuring the percentage of vital cells relative to untreated controls after 72 h using MTT-assays.

tin A-4 (C–A4), may be due to a C–A4-like interaction with cellular tubulin.[12] Therefore, their effect on the *in vitro* polymerisation of tubulin was investigated (Figure 1A). As a component of the cytoskeleton, microtubules are essential for a variety of cellular processes including cell division, motility, transport, and structure stability, making them a promising target for anticancer therapeutics.[13] Interestingly, compound **1 d** caused the strongest inhibition of the polymerisation of purified tubulin, even though its cytotoxicity was lower than that of **1 c**, suggesting that cellular targets other than tubulin might also play a role in cytotoxicity. To investigate the effects on tubulin within living cancer cells, the microtubules of 518 A2 melanoma cells were fluorescently stained 24 h after treatment with 1 and 2.5 μM of **1 a**, **1 c** or **1 d** (Figure 1B). Vehicle treated cells had a well-organized and structured tubulin-cytoskeleton, contrary to C–A4 (0.1 μM) treated cells, which had no intact microtubules except for some fragments. At concentrations of 1 μM, only **1 d** showed a slight destabilizing effect, apparent from a reduction and shortening of the microtubules. At a concentration of 2.5 μM, **1 a** and **1 c** also led to a strong decrease and fragmentation of intact microtubules, confirming the results of the polymerisation inhibition tests *in vitro*.

Centrosomal de-clustering

In addition to the effects on the cytoskeleton, we observed an increase in bipolar and multipolar mitotic spindles for all three compounds (Figure 2A). After treatment with 2.5 μM of compound, the number of cells with bipolar spindles were slightly increased for **1 c** (10%) and **1 d** (13%), whereas cells with multipolar spindles increased by 11% for **1 a**, by 22% for **1 c** and by 26% for **1 d** (Figure 2B). The increase in bipolar mitotic spindles indicates that cells are prevalent in prometa- or metaphase, which may be the consequence of an improper chromosome alignment resulting in an M phase spindle checkpoint arrest.[14] Unlike healthy somatic cells, most tumor cells have multiple centrosomes, which would normally lead to the formation of multiple mitotic spindles, resulting in deficient chromosome segregation and cell death.[15] Therefore, inhibition of centrosome clustering with the resulting induction of multipolar spindles and subsequent cell death would selectively affect tumor cells.[16] As already described for other antimitotic drugs, compounds **1 a**, **1 c** and **1 d** induced a significant increase in multipolar mitotic spindles, suggesting a mode of action

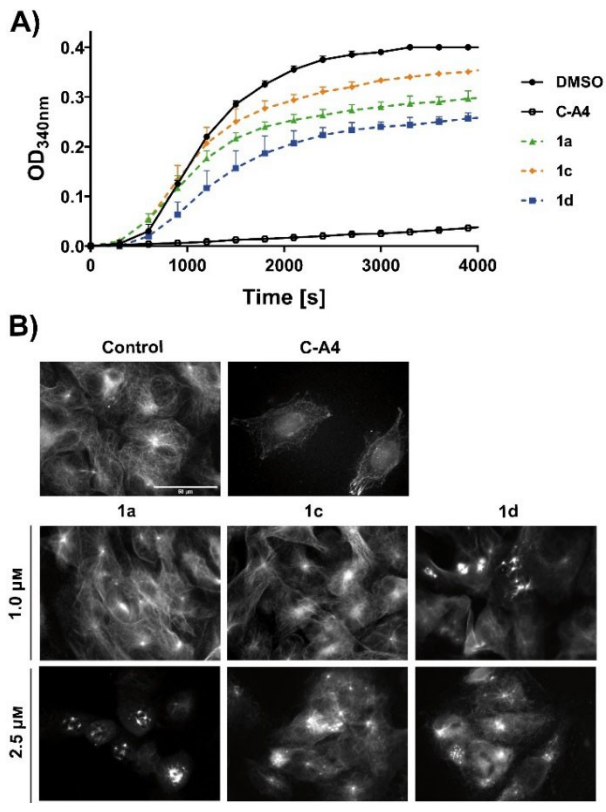

Figure 1. (A) Effect of compounds **1 a**, **1 c** and **1 d** (5 μM) on *in vitro* tubulin polymerisation as determined by a turbidimetric assay. Vehicle (DMSO) and C–A4 (5 μM) served as controls. Data are representative of two independent experiments and quoted as means ± SD. (B) Images illustrating tubulin cytoskeleton stained for α-tubulin in 518 A2 melanoma cells after 24 h incubation with substances **1 a**, **1 c** and **1 d** (1 and 2.5 μM). Negative controls were treated with an equivalent amount of vehicle (DMSO) and positive controls were treated with 100 nM C–A4. Images are representative of at least three independent experiments. Magnification 630×.

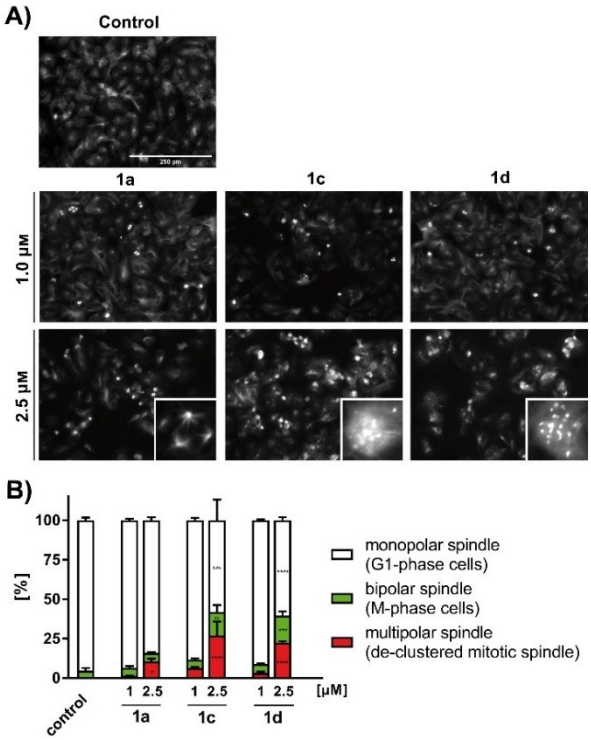

Figure 2. (A) Effect of compounds **1 a**, **1 c** and **1 d** (1 and 2.5 μM) on spindle apparatus formation and accumulation of multipolar spindles with α-tubulin staining. Vehicle (DMSO) served as a control. Images are representative of at least three independent experiments. Magnification 100×. The insets show enlarged image sections with multipolar spindles (B) Histograms represent the percentage of cells with bipolar spindle apparatus (green) displaying cells in mitotic phase and multipolar spindle apparatus (red) displaying defective declustered spindles. 500–800 cells were counted per condition of 3 independent experiments. The significance was given as $^{*}p<0.05$; $^{**}p<0.01$; $^{***}p<0.001$; $^{****}p<0.0001$ against control for each concentration, One-way ANOVA with Dunnett's multiple comparison test (GraphPad Prism 7).

through interference with spindle tension and subsequent inhibition of centrosome clustering.[17] Furthermore, it is possible that **1a**, **1c** and **1d** inhibit other key enzymes involved in centrosome-cluster formation.[18]

In recent studies the inhibition of centrosome clustering has been described as a promising approach for selectively targeting cancer cells.[19] As cancer cells rely on centrosome clustering for survival, whereas healthy cells with normal centrosome complement are hardly affected, centrosome declustering could offer an opportunity for chemotherapy with few side effects.

Effects on cell cycle and CDK1/CyclinA2 activity

To investigate this more closely, substance-treated cells were analysed by FACS and the percentage of cells in the respective cell cycle phase was determined. Upon treatment of 518 A2 melanoma cells with 2.5 μM of **1a**, **1c** or **1d** for 12 h, an arrest in the G2/M-phase was observed for all three substances, most pronounced so for **1d** with an increase of cells in this phase of 26% (Figure 3A). This supports the assumption that the cell cycle is also influenced by the inhibition of tubulin polymerisation as already shown. During cell cycle, the balance between tubulin dimers and microtubules plays a crucial role for successful mitosis.[20] This supports the assumption that the cell cycle is also influenced by the inhibition of tubulin polymerisation as already shown. During cell cycle, the balance between tubulin dimers and microtubules plays a crucial role for successful mitosis.[20]

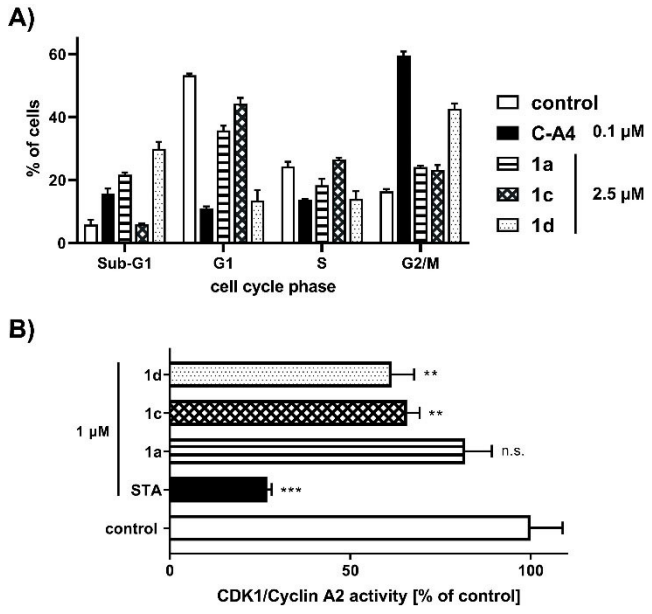

Figure 3. (A) Ratio of cells in different cycle phases of 518 A2 melanoma cells after 12 h incubation with compounds **1a**, **1c** and **1d** (2.5 μM). Negative controls were treated with an equivalent amount of solvent (DMSO) and positive controls with C–A4 (100 nM). The assay was performed in triplicate and quoted as means ± SD. (B) Inhibition of the cell cycle regulating CDK1/Cyclin A2 complex assessed by Kinase Enzyme Assay Kit (Promega). **1a**, **1c**, **1d** and positive control staurosporine (STA; 1 μM) were tested in duplicate and DMSO served as negative control. The significance was given as $^{*}p < 0.05$; $^{**}p < 0.01$; $^{***}p < 0.001$; $^{****}p < 0.0001$ against control, Two-way ANOVA (A), One-way ANOVA (B), with Dunnett's multiple comparison test (GraphPad Prism 7).

Obstruction of tubulin polymerisation also prevents the formation of kinetochore microtubules, which are supposed to separate the sister chromatids during anaphase, consequently leading to a G2/M-phase arrest.[21] A moderate increase of cells in the sub-G1 phase was observed only for **1a** and **1d**, indicating that cell death is already occurring. To clarify whether an apoptotic mechanism was triggered, caspase-3/7 activity was measured after compound treatment. No significant increase of this activity was observed, which supports the notion of an apoptosis-independent cell death (Figure S2, Supporting Information). In line with the effect of centrosome de-clustering, a mitotic catastrophe is the most likely mode of cell death, triggered by aberrant mitosis and leading to the formation of micronuclei and subsequent cell death.[22] Cells that survive are more likely to get aneuploid through incorrect chromosome segregation causing chromosomal instability (CIN).[23] CIN occurs in a variety of cancer types and is responsible for numerical changes in chromosomes.[24] Alterations result in proliferative advantages but also increased susceptibility to the accumulation of chromosomal defects.[25] Cell cycle regulating cyclin dependent kinases (CDKs) play a crucial role, as they control various cell cycle checkpoints and prevent uncontrolled cell division in normal cells.[26] Furthermore, it has been shown that certain CDKs are overexpressed in tumor cells, which makes them an interesting target in cancer therapy.[27] The CDKs 1, 2, 4, and 6 with their regulatory cyclin-subunits A, B, D, and E are directly involved in cell cycle progression and essential for proliferation.[28] Apart from CDK1, all other CDKs are redundant and are therefore not essential for successful cell division.[29] The CDK1/Cyclin A2 ADP-Glo assay system (Promega) was used to determine the inhibitory potential of **1a**, **1c** and **1d** (Figure 3B). Although inferior to the positive control staurosporine (STA), **1c** and **1d** caused a significant decrease in CDK1-activity at concentrations of 1 μM. In addition to their antimitotic properties, this is another mode of action that explains the G2/M-arrest and provides a reason for the high selectivity for cancer over non-malignant cells.

Intracellular localization

The cellular localization of the ethynyl-substituted derivative **1m** in 518 A2 melanoma cells was investigated via copper catalysed azide-alkyne click reactions using 3-azido-7-hydroxycoumarin, $CuSO_4$ and sodium ascorbate in bovine serum albumin (BSA) buffer (Figure 4).[30]

This fluorogenic method employs a bio-orthogonal reaction proceeding under mild conditions and applicable to a variety of bioconjugations.[31] Pearsons Correlation Coefficient (PCC) and Li's Intensity Correlation Quotient (LICQ) of cells co-stained with DAPI (4′,6-diamidino-2-phenylindole) were calculated using imageJ (Coloc2 plugin).[32] High PCC and LICQ values of 0.86 (1 corresponds to a complete colocalization) and 0.441 (0.5 cor-

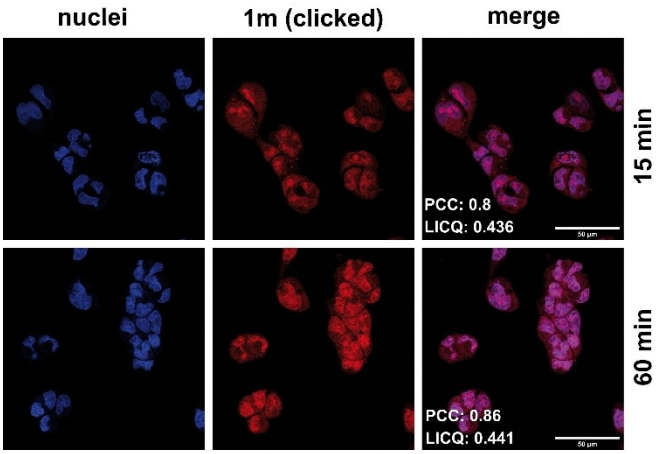

Figure 4. Localization of alkyne-substituted compound **1 m** (50 μM) in 518 A2 melanoma cells after incubation for 15 and 60 min. The internalised compound was then fluorescently labelled using a copper(I)-catalysed azide-alkyne cycloaddition with 3-azido-7-hydroxycoumarin (red, $\lambda_{ex}=404/\lambda_{em}=477$ nm). Colocalized nuclei were stained with Nuclear Green (blue, $\lambda_{ex}=503/\lambda_{em}=526$ nm). The experiment was carried out in triplicate. Magnification 630×. Pearson correlation coefficient (PCC) and Li's colocalization quotient (LICQ) were calculated for the merged images via imageJ (Coloc2 plugin).

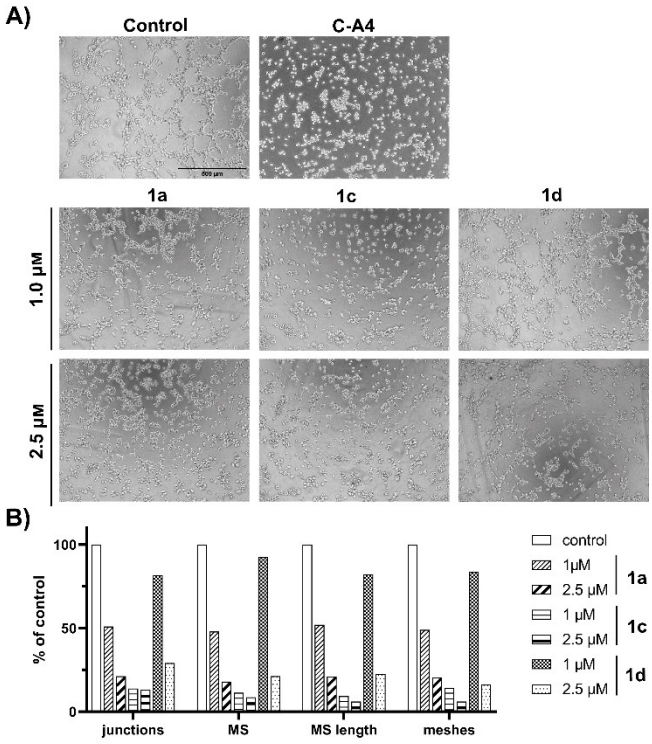

Figure 5. (A) Effect of compounds **1 a**, **1 c** and **1 d** (1 and 2.5 μM) on the ability of EA.hy926 endothelial hybrid cells to form vessel-like structures on Matrigel® after 3 h. Negative controls were treated with vehicle (DMSO) and positive controls with C–A4 (100 nM). Images are representative of three independent experiments. The vitality (assessed by MTT-assay) of treated cells was >80% compared to controls set to 100%. Magnification 100×. (B) Number of junctions, master segments (MS), MS length and meshes as representative parameters of tube-formation assays as percent of control measured with imageJ (angiogenesis analysing plugin).[41]

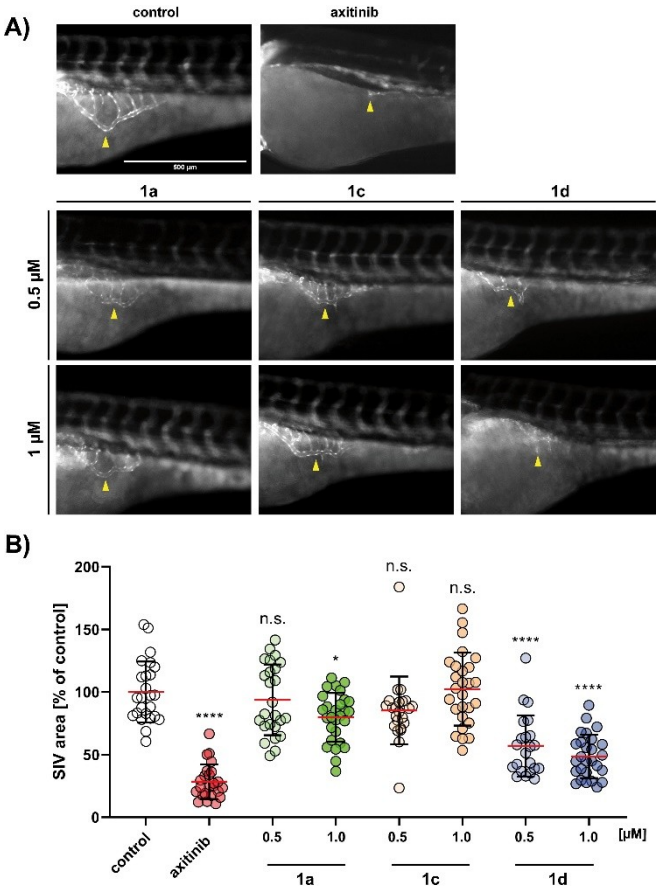

Figure 6. (A) Antiangiogenic effects of **1 a**, **1 c** and **1 d** (0.5 and 1 μM) on the subintestinal veins (SIV) of zebrafish embryos (24 hpf) after 48 h exposure. Negative controls were treated with vehicle DMSO and positive controls with axitinib (1 μM). Images are representative of at least 22 identically treated zebrafish. (B) Area of SIVs illustrated as the mean ± SD of each measurement was quantified using ImageJ. For **1 c** and **1 d**, concentrations above 1 μM were too toxic to be tested. The significance was given as $^{*}p<0.05$; $^{****}p<0.0001$ against control, One-way ANOVA, with Dunnett's multiple comparison test (GraphPad Prism 7).

responds to a complete colocalization) after 60 min, indicated an accumulation of **1 m** mainly in the nuclei. Assuming that compounds **1 a**, **1 c**, and **1 d** accumulate in the nuclei, too, this finding is consistent with the observed CDK1 interference of the latter. Albeit not as strong as in the nucleus, a slight fluorescence occurs in the cytoplasm, that falls in line with the observed inhibition of tubulin polymerization, and correct spindle formation that take place predominantly in the cytoplasm.[33]

Inhibition of tube-formation by EA.hy926 cells

Microtubule-targeting agents (MTAs) do not only affect cell division and proliferation, but also the formation of new blood vessels.[34] The recruitment of new blood vessels (angiogenesis) is essential for the growth of solid tumors, as it facilitates the supply of nutrients and oxygen.[35] In addition, highly vascularized tumors have a considerably higher metastatic potential,

due to a likelier intravasation of migrating cancer cells.[36,37] For several MTAs such as paclitaxel, colchicine or C–A4, anti-angiogenic effects were demonstrated in various studies, which primarily identified microtubule-dependent processes like migration, cell-adhesion or sprouting as targets.[38,39] The *in vitro* tube formation assay was now used to determine the anti-angiogenic properties of compounds **1a**, **1c**, and **1d** (Figure 5A).[40]

This angiogenesis model is based on the ability of Ea.hy926 endothelial hybrid cells to form tubular and vessel-like structures on a basement membrane matrix.[42] For all three compounds, a concentration-dependent effect was demonstrated. Compound **1c** led to a complete inhibition of tube formation at concentrations as low as 1 μM, like the positive control C–A4. Compound **1a** at 1 μM caused a decrease in cord-like junctions but cells were still able to form small tubes and cell agglomerates. Compound **1d** caused a significant reduction of vessel-like structures only at 2.5 μM. The images were analysed with imageJ (angiogenesis-analysing tool) and compared for the number of junctions, meshes, master segments (MS) and length of MS (Figure 5B). The vitality of the cells was determined by MTT assay to be higher than 80% compared to negative controls (Table S3, Supporting Information).

Antiangiogenic effects in zebrafish

As an *in vivo* study, the angiogenesis of zebrafish larvae 24 hours post fertilization (hpf) was observed by monitoring the development of the subintestinal veins (SIV) during treatment with **1a**, **1c** and **1d** (0.5 and 1 μM).[43] Transgenic *casper*-zebrafish embryos (*fli1:EGFP*), lacking melanocytes and reflecting iridophores and expressing enhanced green fluorescent protein (EGFP) in their blood vessels, were used to analyse the anti-angiogenic effects by fluorescence microscopy (Figure 6A).[44,45]

Surprisingly, the most potent compound in tube formation inhibition, **1c**, failed to show significant anti-angiogenic effects *in vivo*. Concentrations above 1 μM of **1c** and **1d** were too toxic for the zebrafish larvae. **1a** and **1d**, however, showed a decrease in SIV-area by 24% (**1a**, 1 μM) and 43% (**1d**, 1 μM) compared to untreated zebrafish (Figure 6B). In summary, while **1d** had the strongest anti-angiogenic effect, **1a** was less toxic to vertebrates at concentrations above 1 μM.

Conclusion

The evaluation of the fifteen 2-amino-4-aryl-5-oxo-4,5-dihydropyrano[3,2-*c*]chromene-3-carbonitriles **1a**–**o** against a panel of tumor cell lines revealed that in particular, **1a** (3,5-dibromo-4-methoxyphenyl motif), **1c** (3-bromo-4,5-dimethoxyphenyl motif) and **1d** (3,5-diiodo-4-methoxyphenyl motif) with halogen-substituted aryl residues proved highly active and selective against cancer cells of five different entities. Although not as potent as the remotely related vascular disrupting natural combretastatin-A4, the compounds **1a**, **1c** and **1d** inhibited tubulin polymerization and destabilized the microtubule cytoskeleton of cancer cells. Cancer cells treated with any one of these three compounds showed the phenomenon of centrosomal de-clustering, normally appearing in cancer cells that cannot build a bipolar spindle apparatus, resulting in genome instability and subsequent cell death. Although many mechanisms of centrosome clustering are still unknown, it provides an effective and cancer-specific target for future therapies.[46] Intracellular localization of the ethynyl-substituted derivative **1m** via an alkyne-azide click reaction to give a fluorescent triazole revealed its accumulation in the nucleus. This finding nicely matched the observed inhibition of CDK1/CyclinA2 and mitotic arrest by the **1m**-analogues **1a**, **1c** and **1d**. Furthermore, concentration dependent anti-angiogenic effects of these compounds were demonstrated *in vitro* by their inhibition of tube formation by EA.hy926 endothelial hybrid cells and *in vivo* by a significantly reduced development of subintestinal veins of zebrafish embryos treated with them. The development of new blood vessels, which is important for the growth and spread of tumors, can be inhibited by these substances, reducing cancer cell invasion and metastasis.[36,37] In summary, the 3′,5′-diiodo-4′-methoxy derivative **1d** stood out as the most promising compound of this new series of 2-amino-4-aryl-5-oxo-4,5-dihydropyrano[3,2-*c*]chromene-3-carbonitriles with pleiotropic character. Based on its antiproliferative and antimetastatic properties, as well as its distinct selectivity for cancer cells and its rare centrosome declustering effect in cancer cells, **1d** might be a good starting point for further optimization and investigation.

Experimental Section

General

All starting compounds were purchased from Aldrich, Alfa Aesar and TCI. The known compounds **1n**–**q** were prepared according to literature procedures.[10,47] The following instruments were applied for this study: melting points (uncorrected), Gallenkamp; IR spectra, Perkin-Elmer Spectrum One FT-IR spectrophotometer with ATR sampling unit; nuclear magnetic resonance spectra, BRUKER Avance 300 spectrometer; chemical shifts are given in parts per million (δ) downfield from tetramethylsilane as internal standard; mass spectra, Varian MAT 311 A (EI), UPLC/Orbitrap (ESI); microanalyses, Perkin-Elmer 2400 CHN elemental analyzer. All tested compounds were >95% pure by elemental analysis.

Chemistry and Synthesis

2-Amino-4-(3-bromo-4,5-dimethoxyphenyl)-5-oxo-4,5-dihydropyrano[3,2-c]chromene-3-carbonitrile (1a)

3-Bromo-4,5-dimethoxybenzaldehyde (245 mg, 1.0 mmol) and malononitrile (70 mg, 1.0 mmol) were dissolved in MeCN (5 mL) and three drops of Et_3N were added. The reaction mixture was stirred at room temperature for 30 min. 4-Hydroxycoumarin (162 mg, 1.0 mmol) was added and the reaction mixture was stirred at room temperature for 16 h. The formed precipitate was collected, washed with MeCN and *n*-hexane and dried in vacuum. Yield: 156 mg (0.34 mmol, 34%); colorless solid of m.p. 237 °C; IR (ATR): ν_{max} =

3418, 3316, 3186, 2938, 2202, 1703, 1664, 1603, 1567, 1492, 1457, 1428, 1415, 1375, 1306, 1280, 1258, 1236, 1208, 1176, 1152, 1131, 1114, 1048, 998, 961, 904, 860, 833, 797, 769, 757, 784, 710, 676, 655, 629, 617, 577 cm^{-1}; ^1H NMR (300 MHz, [D_6]DMSO): $\delta = 3.71$ (s, 3H), 3.80 (s, 3H), 4.48 (s, 1H), 6.98 (d, $J = 2.0$ Hz, 1H), 7.02 (d, $J = 2.0$ Hz, 1H), 7.4–7.5 (m, 4H), 7.7–7.8 (m, 1H), 7.89 (dd, $J = 7.9$ Hz, 1.4 Hz, 1H); ^{13}C NMR (75.5 MHz, [D_6]DMSO): $\delta = 36.5$, 56.1, 57.4, 60.0, 103.1, 112.3, 113.1, 116.6, 119.1, 122.6, 123.0, 124.6, 132.9, 140.8, 144.7, 152.2, 153.2, 153.7, 158.0, 159.6; MS (70 eV): *m/z* (%): 456 (63) $[M]^+$, 454 (66) $[M]^+$, 425 (7), 423 (8), 390 (12), 388 (12), 375 (53), 359 (7), 309 (15), 239 (100), 121 (32), 66 (10); elemental analysis calcd (%) for $C_{21}H_{15}BrN_2O_5$: C 55.40, H 3.32, N 6.15; found: C 55.50, H 3.39, N 6.08.

2-Amino-4-(3-iodo-4,5-dimethoxyphenyl)-5-oxo-4,5-dihydropyrano[3,2-c]chromene-3-carbonitrile (1 b)

3-Iodo-4,5-dimethoxybenzaldehyde (292 mg, 1.0 mmol) and malononitrile (70 mg, 1.0 mmol) were dissolved in MeCN (5 mL) and three drops of Et_3N were added. The reaction mixture was stirred at room temperature for 30 min. 4-Hydroxycoumarin (162 mg, 1.0 mmol) was added and the reaction mixture was stirred at room temperature for 16 h. The formed precipitate was collected, washed with MeCN and *n*-hexane and dried in vacuum. Yield: 156 mg (0.34 mmol, 34%); colorless solid of m.p. 237 °C; IR (ATR): $\nu_{max} =$ 3415, 3317, 3184, 2936, 2203, 1704, 1663, 1603, 1564, 1476, 1457, 1425, 1412, 1377, 1306, 1276, 1258, 1235, 1207, 1177, 1152, 1131, 1115, 1038, 998, 961, 903, 860, 820, 796, 767, 756, 721, 709, 675, 652, 628, 617 cm^{-1}; ^1H NMR (300 MHz, [D_6]DMSO): $\delta = 3.68$ (s, 3H), 3.77 (s, 3H), 4.45 (s, 1H), 6.97 (s, 1H), 7.17 (s, 1H), 7.4–7.6 (m, 4H), 7.7–7.8 (m, 1H), 7.89 (d, $J = 7.9$ Hz, 1H); ^{13}C NMR (75.5 MHz, [D_6]DMSO): $\delta = 36.3$, 56.0, 57.5, 59.7, 92.7, 103.3, 113.1, 116.6, 119.1, 122.6, 124.6, 128.6, 132.9, 141.5, 147.2, 152.1, 152.2, 153.6, 158.0, 159.6; MS (70 eV): *m/z* (%): 502 (63) $[M]^+$, 436 (37), 309 (42), 239 (100), 121 (42); $C_{21}H_{15}IN_2O_5$: C 50.22, H 3.01, N 5.58; found: C 50.31, H 3.06, N 5.50.

2-Amino-4-(3,5-dibromo-4-methoxyphenyl)-5-oxo-4,5-dihydropyrano[3,2-c]chromene-3-carbonitrile (1 c)

3,5-Dibromo-4-methoxybenzaldehyde (293 mg, 1.0 mmol) and malononitrile (70 mg, 1.0 mmol) were dissolved in MeCN (5 mL) and three drops of Et_3N were added. The reaction mixture was stirred at room temperature for 30 min. The formed precipitate was redissolved by heating and 4-hydroxycoumarin (162 mg, 1.0 mmol) was added. The reaction mixture was stirred at room temperature for 2 h. The formed precipitate was collected, washed with MeCN and *n*-hexane and dried in vacuum. Yield: 240 mg (0.48 mmol, 48%); colorless solid of m.p. 274–275 °C; IR (ATR): $\nu_{max} =$ 3388, 3322, 3256, 3215, 3194, 2944, 2923, 2857, 2822, 2197, 1714, 1667, 1639, 1605, 1547, 1495, 1466, 1456, 1420, 1398, 1381, 1324, 1307, 1276, 1257, 1207, 1176, 1115, 1050, 987, 957, 904, 872, 801, 772, 762, 749, 737, 719, 712, 676 cm^{-1}; ^1H NMR (300 MHz, [D_6]DMSO): $\delta = 3.78$ (s, 3H), 4.53 (s, 1H), 7.4–7.5 (m, 2H), 7.51 (s, 2H), 7.60 (s, 2H), 7.7–7.8 (m, 1H), 7.8–7.9 (m, 1H); ^{13}C NMR (75.5 MHz, [D_6]DMSO): $\delta = 35.9$, 57.0, 60.4, 102.6, 113.1, 116.6, 117.4, 119.0, 122.7, 124.6, 132.1, 133.0, 142.6, 152.3, 154.0, 158.0, 159.7; MS (70 eV): *m/z* (%): 506 (9) $[M]^+$, 504 (18) $[M]^+$, 502 (9) $[M]^+$, 438 (9), 425 (15), 423 (16), 359 (12), 357 (11), 239 (100), 121 (23); $C_{20}H_{12}Br_2N_2O_4$: C 47.65, H 2.40, N 5.56; found: C 47.72, H 2.45, N 5.49.

2-Amino-4-(3,5-diiodo-4-methoxyphenyl)-5-oxo-4,5-dihydropyrano[3,2-c]chromene-3-carbonitrile (1 d)

3,5-Diiodo-4-methoxybenzaldehyde (388 mg, 1.0 mmol) and malononitrile (70 mg, 1.0 mmol) were dissolved in MeCN (3 mL) and three drops of Et_3N were added. The reaction mixture was stirred at room temperature for 30 min. 4-Hydroxycoumarin (162 mg, 1.0 mmol) was added, the reaction mixture was stirred at room temperature for 1 h. The formed precipitate was collected, washed with MeCN/H_2O, and dried in vacuum. Yield: 322 mg (0.54 mmol, 54%); colorless solid of m.p. 277–278 °C; IR (ATR): $\nu_{max} =$ 3655, 3322, 3288, 3254, 3209, 2177, 2932, 2197, 1712, 1673, 1637, 1607, 1538, 1492, 1457, 1412, 1400, 1376, 1327, 1310, 1284, 1272, 1251, 1211, 1171, 1112, 1059, 995, 958, 907, 800, 768, 746, 736, 710, 699 cm^{-1}; ^1H NMR (300 MHz, [D_6]DMSO): $\delta = 3.73$ (s, 3H), 4.47 (s, 1H), 7.4–7.5 (m, 4H), 7.7–7.8 (m, 3H), 7.89 (d, $J = 7.9$ Hz, 1H); ^{13}C NMR (75.5 MHz, [D_6]DMSO): $\delta = 35.3$, 57.1, 60.2, 91.4, 102.8, 113.1, 116.6, 119.0, 122.6, 124.6, 133.0, 138.7, 143.1, 152.2, 153.8, 157.4, 158.0, 159.6; MS (70 eV): *m/z* (%): 598 (20) $[M]^+$, 532 (15), 405 (31), 239 (100), 121 (23); $C_{20}H_{12}I_2N_2O_4$: C 40.16, H 2.02, N 4.68; found: C 40.28, H 2.08, N 4.62.

2-Amino-4-(3,4-difluorophenyl)-5-oxo-4,5-dihydropyrano[3,2-c]-chromene-3-carbonitrile (1 e)

3,4-Difluorobenzaldehyde (142 mg, 1.0 mmol) and malononitrile (70 mg, 1.0 mmol) were dissolved in MeCN (5 mL) and three drops of Et_3N were added. The reaction mixture was stirred at room temperature for 30 min. The formed precipitate was redissolved by heating and 4-hydroxycoumarin (162 mg, 1.0 mmol) was added. The reaction mixture was stirred at room temperature for 16 h. The formed precipitate was collected, washed with MeCN and *n*-hexane and dried in vacuum. Yield: 180 mg (0.51 mmol, 51%); colorless solid of m.p. 248–249 °C; IR (ATR) $\nu_{max} =$ 3366, 3323, 3301, 3261, 3193, 2942, 2200, 1716, 1673, 1641, 1606, 1578, 1519, 1493, 1456, 1436, 1411, 1376, 1326, 1315, 1288, 1274, 1257, 1208, 1171, 1137, 1112, 1056, 1023, 960, 932, 922, 905, 871, 838, 823, 808, 778, 763, 753, 745, 722, 710, 698, 677, 648, 626, 615, 599, 588, 576 cm^{-1}; ^1H NMR (300 MHz, [D_6]DMSO): $\delta = 4.53$ (s, 1H), 7.1–7.2 (m, 1H), 7.3–7.5 (m, 6H), 7.7–7.8 (m, 1H), 7.89 (dd, $J = 7.9$ Hz, 1.4 Hz, 1H); ^{13}C NMR (75.5 MHz, [D_6]DMSO): $\delta = 36.3$, 57.3, 103.0, 113.0, 116.5, 116.7, 116.9, 117.2, 117.4, 119.0, 122.6, 124.6, 133.0, 141.1, 147.6, 150.2, 152.2, 153.7, 157.9, 159.6; MS (70 eV): *m/z* (%): 352 (34) $[M]^+$, 239 (100), 121 (31); $C_{19}H_{10}F_2N_2O_3$: C 64.78, H 2.86, N 7.95; found: C 64.84, H 2.90, N 7.89.

2-Amino-4-(3,5-difluorophenyl)-5-oxo-4,5-dihydropyrano[3,2-c]-chromene-3-carbonitrile (1 f)

3,5-Difluorobenzaldehyde (142 mg, 1.0 mmol) and malononitrile (70 mg, 1.0 mmol) were dissolved in MeCN (5 mL) and three drops of Et_3N were added. The reaction mixture was stirred at room temperature for 30 min. The formed precipitate was redissolved by heating and 4-hydroxycoumarin (162 mg, 1.0 mmol) was added. The reaction mixture was stirred at room temperature for 16 h. The formed precipitate was collected, washed with MeCN and *n*-hexane and dried in vacuum. Yield: 95 mg (0.27 mmol, 27%); colorless solid of m.p. 238 °C; IR (ATR): $\nu_{max} =$ 3406, 3322, 3256, 3218, 3193, 3086, 3055, 2195, 1694, 1664, 1622, 1606, 1594, 1495, 1456, 1445, 1416, 1382, 1305, 1276, 1253, 1205, 1179, 1154, 1124, 1115, 1063, 1022, 993, 970, 945, 905, 856, 796, 782, 766, 759, 720, 688, 672 cm^{-1}; ^1H NMR (300 MHz, $CDCl_3$/ D_6]DMSO): $\delta = 4.50$ (s, 1H), 6.46 (s, 2H), 6.6–6.7 (m, 1H), 6.8–6.9 (m, 2H), 7.3–7.4 (m, 2H), 7.5–7.6 (m, 1H), 7.83 (dd, $J = 9.5$ Hz, 1.6 Hz, 1H); ^{13}C NMR (75.5 MHz, D_6]DMSO): $\delta = 36.4$, 58.2, 102.0, 102.4, 102.7, 103.0, 110.2, 110.5, 112.4, 116.2, 118.2, 122.3, 124.1, 132.4, 146.0, 152.1, 153.6, 158.0, 159.5, 160.6, 160.8,

164.1; MS (70 eV): *m/z* (%): 352 (42) $[M]^+$, 240 (23), 239 (100), 121 (23); $C_{19}H_{10}F_2N_2O_3$: C 64.78, H 2.86, N 7.95; found: C 64.82, H 2.91, N 7.90.

2-Amino-4-(3,4,5-trifluorophenyl)-5-oxo-4,5-dihydropyrano[3,2-c]chromene-3-carbonitrile (1 g)

3,4,5-Trifluorobenzaldehyde (160 mg, 1.0 mmol) and malononitrile (70 mg, 1.0 mmol) were dissolved in MeCN (3 mL) and three drops of Et_3N were added. The reaction mixture was stirred at room temperature for 30 min. 4-Hydroxycoumarin (162 mg, 1.0 mmol) was added, the reaction mixture was stirred at room temperature for 1 h. The formed precipitate was collected, washed with MeCN/H_2O, and dried in vacuum. Yield: 145 mg (0.39 mmol, 39%); colorless solid of m.p. 236–237 °C; IR (ATR): ν_{max} = 3402, 3319, 3257, 3212, 3191, 2198, 1708, 1665, 1629, 1604, 1528, 1495, 1448, 1414, 1380, 1342, 1307, 1275, 1254, 1239, 1204, 1178, 1151, 1114, 1056, 1040, 972, 953, 905, 865, 809, 796, 780, 757, 715, 706, 684, 662 cm^{-1}; ^1H NMR (300 MHz, [D_6]DMSO): δ = 4.57 (s, 1H), 7.3–7.4 (m, 2H), 7.5–7.6 (m, 4H), 7.7–7.8 (m, 1H), 7.89 (d, *J* = 7.9 Hz, 1H); ^{13}C NMR (75.5 MHz, [D_6]DMSO): δ = 36.4, 56.8, 102.3, 112.4, 112.7, 113.1, 116.5, 118.8, 122.7, 124.6, 133.0, 140.7, 148.5, 152.3, 154.1, 158.0, 159.6; MS (70 eV): *m/z* (%): 370 (28) $[M]^+$, 239 (100), 121 (44), 92 (23); $C_{19}H_9F_3N_2O_3$: C 61.63, H 2.45, N 7.57; found: C 61.71, H 2.50, N 7.51.

2-Amino-4-(3,4-dichlorophenyl)-5-oxo-4,5-dihydropyrano[3,2-c]-chromene-3-carbonitrile (1 h)

3,4-Dichlorobenzaldehyde (175 mg, 1.0 mmol) and malononitrile (70 mg, 1.0 mmol) were dissolved in MeCN (3 mL) and three drops of Et_3N were added. The reaction mixture was stirred at room temperature for 30 min. 4-Hydroxycoumarin (162 mg, 1.0 mmol) was added, the reaction mixture was stirred at room temperature for 1 h. The formed precipitate was collected, washed with MeCN/H_2O, and dried in vacuum. Yield: 190 mg (0.49 mmol, 49%); colorless solid of m.p. 244–245 °C; IR (ATR): ν_{max} = 3394, 3320, 3250, 3209, 3192, 2206, 1694, 1666, 1604, 1496, 1468, 1456, 1399, 1378, 1312, 1275, 1254, 1208, 1177, 1147, 1114, 1061, 1027, 958, 906, 838, 780, 761, 730, 699, 675 cm^{-1}; ^1H NMR (300 MHz, [D_6]DMSO): δ = 4.55 (s, 1H), 7.3–7.4 (m, 1H), 7.4–7.6 (m, 6H), 7.7–7.8 (m, 1H), 7.89 (d, *J* = 7.8 Hz, 1H); ^{13}C NMR (75.5 MHz, [D_6]DMSO): δ = 36.2, 57.0, 102.8, 113.0, 116.6, 118.9, 122.6, 124.6, 128.3, 129.7, 129.9, 130.6, 131.0, 133.0, 144.4, 152.3, 153.9, 158.0, 159.6; MS (70 eV): *m/z* (%): 386 (11) $[M]^+$, 384 (16) $[M]^+$, 239 (100), 121 (22); $C_{19}H_{10}Cl_2N_2O_3$: C 59.24, H 2.62, N 7.27; found: C 59.32, H 2.68, N 7.22.

2-Amino-4-(4-methylthiophenyl)-5-oxo-4,5-dihydropyrano[3,2-c]chromene-3-carbonitrile (1 i)

4-Methylsulfanylbenzaldehyde (152 mg, 1.0 mmol) and malononitrile (70 mg, 1.0 mmol) were dissolved in MeCN (5 mL) and three drops of Et_3N were added. The reaction mixture was stirred at room temperature for 30 min. The formed precipitate was redissolved by heating and 4-hydroxycoumarin (162 mg, 1.0 mmol) was added. The reaction mixture was stirred at room temperature for 16 h. The formed precipitate was collected, washed with MeCN and *n*-hexane and dried in vacuum. Yield: 150 mg (0.41 mmol, 41%); colorless solid of m.p. 235 °C; IR (ATR): ν_{max} = 3388, 3321, 3253, 3192, 2917, 2193, 1705, 1667, 1605, 1493, 1456, 1435, 1407, 1378, 1328, 1305, 1273, 1253, 1206, 1175, 1112, 1090, 1047, 1014, 957, 903, 834, 773, 755, 727, 700, 676, 646, 618, 578, 558 cm^{-1}; ^1H NMR (300 MHz, [D_6]DMSO): δ = 2.44 (s, 3H), 4.42 (s, 1H), 7.1–7.2 (m, 4H), 7.4–7.5 (m, 4H), 7.7–7.8 (m, 1H), 7.90 (dd, *J* = 7.9 Hz, 1.4 Hz, 1H); ^{13}C NMR (75.5 MHz, [D_6]DMSO): δ = 14.7, 36.5, 57.8, 103.9, 113.0, 116.6, 119.2, 122.5, 124.7, 126.0, 128.3, 132.9, 136.8, 140.0, 152.1, 153.3, 157.9, 159.5; MS (70 eV): *m/z* (%): 362 (96) $[M]^+$, 315 (70). 296 (25), 249 (42), 239 (100), 121 (24); $C_{20}H_{14}N_2O_3S$: C 66.29, H 3.89, N 7.73; found: C 66.35, H 3.96, N 7.77.

2-Amino-4-(3-pentafluorothiophenyl)-5-oxo-4,5-dihydropyrano[3,2-c]chromene-3-carbonitrile (1 j)

3-Pentafluorothiobenzaldehyde (232 mg, 1.0 mmol) and malononitrile (70 mg, 1.0 mmol) were dissolved in MeCN (5 mL) and three drops of Et_3N were added. The reaction mixture was stirred at room temperature for 30 min. The formed precipitate was redissolved by heating and 4-hydroxycoumarin (162 mg, 1.0 mmol) was added. The reaction mixture was stirred at room temperature for 16 h. The formed precipitate was collected, washed with MeCN and *n*-hexane and dried in vacuum. Yield: 270 mg (0.61 mmol, 61%); colorless solid of m.p. 285 °C; IR (ATR): ν_{max} = 3416, 3326, 3256, 3222, 3194, 3117, 3076, 2200, 1706, 1668, 1636, 1604, 1495, 1484, 1456, 1435, 1411, 1380, 1331, 1305, 1275, 1260, 1206, 1176, 1114, 1053, 956, 907, 881, 851, 835, 817, 789, 771, 761, 747, 725, 710, 687 cm^{-1}; ^1H NMR (300 MHz, [D_6]DMSO): δ = 4.70 (s, 1H), 7.4–7.6 (m, 6H), 7.7–7.9 (m, 3H), 7.91 (dd, *J* = 7.9 Hz, 1.4 Hz, 1H); ^{13}C NMR (75.5 MHz, [D_6]DMSO): δ = 36.8, 57.1, 102.9, 112.9, 116.6, 118.9, 122.6, 124.7, 125.1, 129.8, 131.7, 133.1, 145.0, 152.3, 152.6, 153.9, 158.1, 159.6; MS (70 eV): *m/z* (%): 442 (18) $[M]^+$, 314 (8), 239 (100), 121 (17); $C_{19}H_{11}F_5N_2O_3S$: C 51.59, H 2.51, N 6.33; found: C 51.67, H 2.56, N 6.30.

2-Amino-4-(3-nitro-4-methoxyphenyl)-5-oxo-4,5-dihydropyrano[3,2-c]chromene-3-carbonitrile (1 k)

4-Methoxy-3-nitrobenzaldehyde (181 mg, 1.0 mmol) and malononitrile (70 mg, 1.0 mmol) were dissolved in MeCN (5 mL) and three drops of Et_3N were added. The reaction mixture was stirred at room temperature for 30 min. The formed precipitate was redissolved by heating and 4-hydroxycoumarin (162 mg, 1.0 mmol) was added. The reaction mixture was stirred at room temperature for 16 h. The formed precipitate was collected, washed with MeCN and *n*-hexane and dried in vacuum. Yield: 180 mg (0.46 mmol, 46%); colorless solid of m.p. 246–247 °C; IR (ATR): ν_{max} = 3368, 3329, 3298, 3284, 3249, 3211, 3187, 3055, 2947, 2846, 2196, 1716, 1698, 1671, 1619, 1604, 1578, 1526, 1497, 1458, 1411, 1378, 1356, 1321, 1308, 1281, 1251, 1210, 1181, 1114, 1087, 1063, 1017, 963, 906, 845, 824, 763, 702, 672 cm^{-1}; ^1H NMR (300 MHz, [D_6]DMSO): δ = 3.90 (s, 3H), 4.57 (s, 1H), 7.30 (d, *J* = 8.8 Hz, 1H), 7.4–7.5 (m, 4H), 7.6–7.8 (m, 2H), 7.79 (d, *J* = 2.3 Hz, 1H), 7.9–8.0 (m, 1H); ^{13}C NMR (75.5 MHz, [D_6]DMSO): δ = 35.9, 56.7, 57.2, 103.0, 113.1, 114.2, 116.6, 119.1, 122.6, 123.9, 124.6, 133.0, 133.8, 135.8, 139.2, 150.9, 152.2, 153.7, 158.0, 159.6; MS (70 eV): *m/z* (%): 391 (22) $[M]^+$, 374 (20), 325 (20), 239 (100), 121 (27); $C_{20}H_{13}N_3O_6$: C 61.38, H 3.35, N 10.74; found: C 61.46, H 3.41, N 10.66.

2-Amino-4-(3-cyanophenyl)-5-oxo-4,5-dihydropyrano[3,2-c]-chromene-3-carbonitrile (1 l)

3-Cyanobenzaldehyde (131 mg, 1.0 mmol) and malononitrile (70 mg, 1.0 mmol) were dissolved in MeCN (3 mL) and three drops of Et_3N were added. The reaction mixture was stirred at room temperature for 30 min. The formed precipitate was redissolved by heating and 4-hydroxycoumarin (162 mg, 1.0 mmol) was added. The reaction mixture was stirred at room temperature for 1 h. The formed precipitate was collected, washed with MeCN and *n*-hexane and dried in vacuum. Yield: 197 mg (0.58 mmol, 58%); colorless solid of m.p. 278 °C; IR (ATR): ν_{max} = 3400, 3322, 3291, 3253, 3215, 3194, 3076, 2233, 2201, 1722, 1675, 1638, 1602, 1495, 1456, 1435,

1417, 1376, 1327, 1302, 1273, 1255, 1213, 1196, 1171, 1112, 1098, 1056, 1012, 957, 928, 901, 876, 817, 789, 779, 762, 744, 703 cm^{-1}; ^1H NMR (300 MHz, [D_6]DMSO): $\delta = 4.59$ (s, 1H), 7.4–7.6 (m, 5H), 7.6–7.8 (m, 3H),7.8–7.9 (m, 2H); ^{13}C NMR (75.5 MHz, [D_6]DMSO): $\delta = 36.6$, 57.1, 102.7, 111.4, 113.1, 116.6, 118.7, 119.0, 122.6, 124.6, 129.7, 131.0, 131.5, 132.9, 133.0, 144.9, 152.3, 154.0, 158.0, 159.6; MS (70 eV): *m/z* (%): 341 (33) $[M]^+$, 275 (19), 274 (24), 240 (22), 239 (100), 121 (26); $C_{20}H_{11}N_3O_3$: C 70.38, H 3.25, N 12.31; found: C 70.42, H 3.30, N 12.27.

2-Amino-4-(4-ethynylphenyl)-5-oxo-4,5-dihydropyrano[3,2-c]-chromene-3-carbonitrile (1 m)

3-Ethynylbenzaldehyde (130 mg, 1.0 mmol) and malononitrile (70 mg, 1.0 mmol) were dissolved in MeCN (5 mL) and three drops of Et_3N were added. The reaction mixture was stirred at room temperature for 30 min. The formed precipitate was redissolved by heating and 4-hydroxycoumarin (162 mg, 1.0 mmol) was added. The reaction mixture was stirred at room temperature for 1 h. The formed precipitate was collected, washed with MeCN and *n*-hexane and dried in vacuum. Yield: 85 mg (0.25 mmol, 25%); off-white solid of m.p. >395 °C; IR (ATR): $\nu_{max} = 3390$, 3322, 3285, 3212, 2196, 1709, 1669, 1639, 1605, 1498, 1456, 1417, 1381, 1328, 1307, 1275, 1257, 1210, 1177, 1115, 1052, 1018, 958, 904, 852, 833, 787, 773, 740, 661 cm^{-1}; ^1H NMR (300 MHz, [D_6]DMSO): $\delta = 4.15$ (s, 1H), 4.49 (s, 1H), 7.28 (dd, $J = 8.3$ Hz, 1.9 Hz, 2H), 7.4–7.5 (m, 6H), 7.7–7.8 (m, 1H), 7.9–8.0 (m, 1H); ^{13}C NMR (75.5 MHz, [D_6]DMSO): $\delta = 36.8$, 57.4, 80.8, 83.3, 103.5, 112.9, 116.6, 119.1, 120.5, 122.5, 124.7, 128.1, 131.9, 133.0, 144.2, 152.2, 153.6, 158.0, 159.6; MS (70 eV): *m/z* (%): 340 (52) $[M]^+$, 273 (24), 239 (100), 121 (37); $C_{19}H_{10}F_2N_2O_3$: C 64.78, H 2.86, N 7.95; found: C 64.84, H 2.90, N 7.89; $C_{21}H_{12}N_2O_3$: C 74.11, H 3.55, N 8.23; found: C 74.22, H 3.48, N 8.19.

Cell lines and culture conditions

518 A2 melanoma (Department of Radiotherapy, Medical University of Vienna, Austria),[48] KB-V1^{Vbl} (ACC-149) multidrug-resistant (MDR) cervix carcinoma, U-87 glioblastoma, MCF-7 (ACC-115) breast carcinoma, HT-29 (ACC-299), HCT-116 (ACC-581) and HCT-116p53−/− (p53 knockout mutant) colon carcinoma, EA.hy926 (ATCC® CRL-2922™) endothelial hybrid cells, and HDFa (ATCC® PCS-201-012™) human dermal fibroblasts were cultivated in Dulbecco's Modified Eagle Medium (DMEM) supplemented with 10% fetal bovine serum (20% for HDFa cells), and 1% antibiotic-antimycotic at 37 °C, 5% CO_2, and 95% humidity. To keep KB-V1^{Vbl} cells resistant, 340 nM vinblastine was added to the cell culture medium 24 h after every passage. Cells were grown at 5% CO_2, and 95% humidity. Only mycoplasma-free cell cultures were used.

Cell viability assay (MTT assay)

MTT assays were carried out for cytotoxicity evaluation of compounds **1 a**–**q**. The cancer and hybrid cells (5×10^4 cells/mL, 100 μL/well), as well as HDFa cells (1×10^5 cells/mL, 100 μL/well) were grown in 96-well plates for 24 h under cell culture conditions. Then, they were treated with various concentrations (100 μM–0.5 nM) of compounds **1 a**–**q**, or vehicle (DMSO) for another 72 h. After the addition of 12.5 μL of a 0.5% MTT solution in PBS the cells were incubated for 2 h at 37 °C so that the water-soluble MTT could be converted to formazan crystals. The plates were centrifuged (300 g, 5 min, 4 °C), the medium was withdrawn, and the formazan dissolved in 25 μL of DMSO containing 10% SDS and 0.6% acetic acid for at least 1 h at 37 °C. The absorbance of formazan ($\lambda =$ 570 nm), and background ($\lambda = 630$ nm) was measured with a microplate reader (Tecan infinite F200). The IC_{50} values were derived from dose-inhibition curves as the means ± SD of four independent experiments with respect to vehicle treated control cells set to 100% (GraphPad Prism). The cytotoxic selectivity was determined by calculating the selectivity index (SI) according to following equation: SI=IC_{50} (nonmalignant HDFa cells)/IC_{50} (average cancer cell lines).

Tubulin polymerisation

In a black 96-well half-area clear bottom plate, 50 μL of Brinkley's Buffer 80 (BRB80: 400 mM PIPES, 5 mM $MgCl_2$, 5 mM EGTA, pH = 6.8) containing 20% glycerol and 2 mM GTP was pipetted. Test compounds were added to the wells to reach a concentration of 5 μM. To start the polymerization reaction 50 μL porcine brain tubulin (10 mg/mL in BRB80) was added and the plate was immediately placed in the microplate reader (Tecan infinite F200). The optical density was measured at 37 °C by recording the absorption at 340 nm for 100 min. Data are representative as the means ± SD of at least two independent experiments.

Immunofluorescence staining of tubulin cytoskeleton

518 A2 melanoma cells (1×10^5 cells/mL, 0.5 mL/well) were seeded on coverslips in 24-well cell culture plates and incubated for 24 h under cell culture conditions (37 °C, 5% CO_2 and 95% humidity). After treatment with different concentrations of test compounds **1 a**, **1 c** and **1 d** (1 and 2.5 μM) or the vehicle DMSO, the cells were incubated for another 24 h (37 °C, 5% CO_2, 95% humidity). The cells were washed with cytoskeletal buffer (100 mm PIPES, 3 mM $MgCl_2$, 138 mM KCl, 2 mM EGTA, 300 mM sucrose, pH 6.8), fixed and permeabilized in 3.7% formaldehyde and 0.2% Triton X-100 in cytoskeletal buffer for 5 min at rt. As additional fixation step, the cells were incubated with ice-cold EtOH for 10 s and rehydrated in PBS. After blocking with 1% BSA in PBS for 30 min the cells were treated for 2 h with a primary antibody against alpha-tubulin (anti alpha-tubulin, mouse monoclonal antibody), washed two times with PBS, followed by 1 h incubation with a secondary antibody AlexaFluor®-546 conjugate (goat anti-mouse IgG-AF-546, Invitrogen). Actin and nuclei staining was done with Phallodin-iFluor™ 488 Conjugate (AAT Bioquest) and DAPI (1 μg/mL) for 1 h in the dark. Finally, the cells were washed three times with PBS and the coverslips were embedded in ProLong™ Glass Antifade Mountant. Nuclei, actin filaments and microtubules were documented by fluorescence microscopy (Zeiss Imager A1 AX10, 100× and 630× magnification) and edited with imageJ. The ratio of bipolar and multipolar spindle apparatus to the total cell count was determined with the cell count tool (imageJ).

Cell cycle analysis

518 A2 melanoma cells (1×10^5 cells/mL, 3 mL/well) were seeded in 6-well cell culture plates for 24 h under cell culture conditions (37 °C, 5% CO_2, 95% humidity). The treatment with 1 μM each of compounds **1 a**, **1 c**, **1 d**, vehicle (DMSO) or positive control C–A4 (25 nM) was carried out for another 12 h. Cells were fixed in 70% EtOH after trypsinization and centrifugation (5 min, 300×g, 4 °C) for at least 24 h at 4 °C. Before flow-cytometric measurement with a Beckmann Coulter Cytomics FC500 flow cytometer ($\lambda_{em} = 570$ nm, $\lambda_{ex} = 488$ nm laser source) the cells were washed with PBS and stained with propidium iodide solution (50 μg/mL PI, 0.1% sodium citrate, 50 μg/mL RNAse A in PBS). The DNA content of at least 10,000 single cells was measured and the ratio of the cell cycle phases (sub-G1, G1, S, G2/M) were determined by CXP software (Beckman Coulter).

CDK1/CyclinA2 activity assay

The CDK1/CyclinA2 kinase enzyme system (Promega) was used to profile the effect of substance **1 a**, **1 c**, **1 d**, staurosporine, or vehicle DMSO on kinase activity.[49] The released ADP was quantified by ADP-Glo™ Assay (Promega).[50] Reactions were carried out in white 96-well plates with 2 ng of CDK1/CyclinA2 protein complex, 5 μg histone H1 substrate, and test compounds in reaction buffer (40 mM Tris-HCl, 20 mM $MgCl_2$, 0.1 mg/mL BSA, pH 7.5). The kinase reaction was initiated by adding 5 μL of ATP solution (250 μM), bringing the final volume up to 25 μL. The reaction was terminated after 15 min at 30 °C and remaining ATP was depleted by addition 25 μL of ADP-Glo reagent for 40 min at rt. 50 μL of kinase detection reagent was added for another 30 min of incubation and followed by luminescence measurement with a FLUOstar microplate reader (Omega). Each concentration was measured in duplicate and solvent controls were set to 100%. Significant decrease in CDK1/Cyclin A2 activity compared to vehicle control was determined using a *t*-test; $*p<0.05$; $**p<0.01$; $***p<0.001$; $****p<0.0001$, One-way ANOVA with Dunnett's multiple comparison test (GraphPad Prism 7).

Colocalization via intracellular click-reaction

518 A2 melanoma cells (1×10^5 cells/mL, 0.5 mL/well) were grown on coverslips in 24-well cell culture plates for 24 h under cell culture conditions (37 °C, 5% CO_2, 95% humidity). Then the cells were incubated with 50 μM **1 m** (solution in 0.2% Tween 80) for 15, 30 and 60 min under cell culture conditions. After washing with PBS, the cells were fixed (3.7% formaldehyde in PBS) for 10 min and again washed with PBS. The "click-reagents" (2 mM $CuSO_4$, 5 mM sodium ascorbate, 0.1 mM 3-azido-7-hydroxycoumarin, 1% BSA in PBS) were incubated before 200 μL was pipetted to the cells and incubated in the dark for 30 min. Nuclei were counterstained with Nuclear Green (1:1000, 50 μg/mL RNase, 1% BSA in PBS). The cells were washed once more with PBS and ddH_2O before the coverslips were embedded in Roti®Mount FluorCare and documented using a Leica TCS SP5 confocal microscope (630× magnification). Pearson correlation coefficient (PC) and Li's colocalization quotient (LICQ) were calculated for the merged images via imageJ (Coloc2).

EA.hy926 tube formation assay

Ibidi μ-Slides were coated with the basement membrane-like matrix Matrigel® (Corning). EA.hy926 endothelial hybrid cells were cultivated for 24 h in EndoPrime low serum (Capricorn) endothelial medium and seeded (50 μL/well, 3×10^5 cells/mL) on Matrigel®. The cells were treated with **1 a**, **1 c**, **1 d** (1 and 2.5 μM) or solvent (DMSO) for 4 h under cell culture conditions (37 °C, 5% CO_2, and 95% humidity), until tubular structures had formed in the control wells. Anti-angiogenic effects were documented via light microscopy (Zeiss Axiovert 135, 100× magnification). The measurements were carried out in triplicate. Cell vitality was reviewed via MTT assay (higher than 75% with DMSO treated cells set to 100%) as described above (2.4.). The images were analysed with imageJ (angiogenesis-analysing tool) and compared for the number of junctions, meshes, master segments (MS) and length of MS to quantify the tube formation process.[39]

Zebrafish angiogenesis assay

Transgenic zebrafish of the strain *Tg(fli1:EGFP)* and *casper* mutant background were raised under standard conditions at about 28 °C.[44,51] The eggs were cultivated in E3 medium (5 mM NaCl, 0.17 mM KCl, 0.33 mM $CaCl_2$, 0.33 mM $MgSO_4$, 0.01% methylene blue, pH 7.2) for 24 h, manually dechorionated and distributed in 6-well plates with 5 mL E3 medium each. The embryos were treated with **1 a**, **1 c** and **1 d** (0.5, 1 and 2.5 μM), axitinib (1 μM), or solvent DMSO for 48 h. The SIV (subintestinal vein) area was used to determine the vascular development and angiogenesis respectively, and was documented by fluorescence microscopy ($\lambda_{ex}=488$ nm, $\lambda_{em}=509$ nm; Leica MZ10F with Zeiss AxioCam Mrc and Mrc-ZEN pro 2012 software). SIV areas were quantified with imageJ of at least 22 identically treated zebrafish larvae per concentration as means ± SD with solvent control set to 100%. Significance in SIV decrease compared to vehicle control was determined using a *t*-test; $*p<0.05$; $**p<0.01$; $***p<0.001$; $****p<0.0001$, One-way ANOVA with Dunnett's multiple comparison test (GraphPad Prism 7).

Acknowledgements

We thank Denise Erbe and Philipp Augsburger for technical assistance and Prof. Dr. Olaf Stemmann, Prof. Dr. Carlo Unverzagt and Prof. Dr. Claus Kuhn for the provision of laboratory equipment. Open Access funding enabled and organized by Projekt DEAL.

Conflict of Interest

The authors declare no conflict of interest.

Data Availability Statement

The data that support the findings of this study are available from the corresponding author upon reasonable request.

Keywords: Pyrano[3,2-*c*]chromene · Centrosome de-clustering · Antiangiogenic agents · Anticancer drugs

[1] C. G. L. Veale, *ChemMedChem* **2021**, *16*, 1199–1225.
[2] a) R. V. Orru, M. de Greef, *Synthesis* **2003**, *34*, 1471–1499; b) L. Weber, *Drug Discovery Today* **2002**, *7*, 143–147; c) A. Dömling, I. Ugi, *Angew. Chem. Int. Ed.* **2000**, *39*, 3168–3210; *Angew. Chem.* **2000**, *112*, 3300–3344.
[3] a) M. A. Fouad, H. Abdel-Hamid, M. S. Ayoup, *RSC Adv.* **2020**, *10*, 42644–42681; b) H. Nagarajaiah, A. Mukhopadhyay, J. N. Moorthy, *Tetrahedron Lett.* **2016**, *57*, 5135–5149; c) X. Zheng, W. Liu, D. Zhang, *Molecules* **2020**, *25*, 1594; d) L. Wang, K. W. Woods, Q. Li, K. J. Barr, R. W. McCroskey, S. M. Hannick, L. Gherke, R. B. Credo, Y.-H. Hui, K. Marsh, et al., *J. Med. Chem.* **2002**, *45*, 1697–1711.
[4] K. Venkata Sairam, B. M. Gurupadayya, R. S. Chandan, D. K. Nagesha, B. Vishwanathan, *Curr. Drug Delivery* **2016**, *13*, 186–201.
[5] a) M. M. Abdou, R. A. El-Saeed, S. Bondock, *Arab. J. Chem.* **2019**, *12*, 88–121; b) G. Pilli, N. Dumala, J. S. Sreeja, R. John, S. Sengupta, P. Grover, J. Prakash M, *ChemistrySelect* **2019**, *4*, 10805–10809; c) S. Stanchev, G. Momekov, F. Jensen, I. Manolov, *Eur. J. Med. Chem.* **2008**, *43*, 694–706; d) N. A. Abdel Latif, R. Z. Batran, M. A. Khedr, M. M. Abdalla, *Bioorg. Chem.* **2016**, *67*, 116–129; e) R. Z. Batran, D. H. Dawood, S. A. El-Seginy, M. M. Ali, T. J. Maher, K. S. Gugnani, A. N. Rondon-Ortiz, *Arch. Pharm.* **2017**, *350*, 1700064.
[6] a) R. Ghorbani-Vaghei, Z. Toghraei-Semiromi, R. Karimi-Nami, *J. Braz. Chem. Soc.* **2011**, *5*, 905–909; b) A. M. El-Agrody, A. M. Fouda, M. A. Assiri, A. Mora, T. E. Ali, M. M. Alam, M. Y. Alfaifi, *Med. Chem. Res.* **2020**,

29, 617–629; c) N. Daneshvar, O. Goli-Jolodar, R. Karimi-Chayjani, M. S. Nikoo Langarudi, F. Shirini, *ChemistrySelect* **2019**, *4*, 1562–1566; d) K. S. Pandit, P. V. Chavan, U. V. Desai, M. A. Kulkarni, P. P. Wadgaonkar, *New J. Chem.* **2015**, *39*, 4452–4463.
[7] a) W. Kemnitzer, S. Kasibhatla, S. Jiang, H. Zhang, J. Zhao, S. Jia, L. Xu, C. Crogan-Grundy, R. Denis, N. Barriault, et al., *Bioorg. Med. Chem. Lett.* **2005**, *15*, 4745–4751; b) I. G. Tsygankova, S. M. Zhenodarova, *Russ. J. Gen. Chem.* **2014**, *84*, 89–97.
[8] F. Schmitt, M. Gold, M. Rothemund, I. Andronache, B. Biersack, R. Schobert, T. Mueller, *Eur. J. Med. Chem.* **2019**, *163*, 160–168.
[9] F. Schmitt, R. Schobert, B. Biersack, *Med. Chem. Res.* **2019**, *28*, 1694–1703.
[10] A. M. El-Agrody, A. M. Fouda, M. A. Assiri, A. Mora, T. E. Ali, M. M. Alam, M. Y. Alfaifi, *Med. Chem. Res.* **2020**, *29*, 617–629.
[11] M. López-Lázaro, *Oncoscience* **2015**, *2*, 91–98.
[12] C. M. Lin, S. B. Singh, P. S. Chu, R. O. Dempcy, J. M. Schmidt, G. R. Pettit, E. Hamel, *Mol. Pharmacol.* **1988**, *34*, 200–208.
[13] M. A. Jordan, L. Wilson, *Nat. Rev. Cancer.* **2004**, *4*, 253–265.
[14] K. Vermeulen, D. R. van Bockstaele, Z. N. Berneman, *Cell Prolif.* **2003**, *36*, 131–149.
[15] a) G. A. Pihan, A. Purohit, J. Wallace, H. Knecht, B. Woda, P. Quesenberry, S. J. Doxsey, *Cancer Res.* **1998**, *58*, 3974–3985; b) N. J. Ganem, S. A. Godinho, D. Pellman, *Nature* **2009**, *460*, 278–282.
[16] B. Rebacz, T. O. Larsen, M. H. Clausen, M. H. Rønnest, H. Löffler, A. D. Ho, A. Krämer, *Cancer Res.* **2007**, *67*, 6342–6350.
[17] a) J. Shi, J. D. Orth, T. Mitchison, *Cancer Res.* **2008**, *68*, 3269–3276; b) J.-G. Chen, S. B. Horwitz, *Cancer Res.* **2002**, *62*, 1935–1938.
[18] a) M. Kwon, S. A. Godinho, N. S. Chandhok, N. J. Ganem, A. Azioune, M. Thery, D. Pellman, *Genes Dev.* **2008**, *22*, 2189–2203; b) B. Leber, B. Maier, F. Fuchs, J. Chi, P. Riffel, S. Anderhub, L. Wagner, A. D. Ho, J. L. Salisbury, M. Boutros, et al., *Sci. Transl. Med.* **2010**, *2*, 33–38.
[19] a) A. Ogden, P. C. G. Rida, R. Aneja, *Cell Death Differ.* **2012**, *19*, 1255–1267; b) M. H. Choe, J. Kim, J. Ahn, S.-G. Hwang, J. S. Oh, J.-S. Kim, *Anticancer Res.* **2018**, *38*, 3393–3400; c) V. Pannu, P. C. G. Rida, B. Celik, R. C. Turaga, A. Ogden, G. Cantuaria, J. Gopalakrishnan, R. Aneja, *Cell Death Dis.* **2014**, *5*, e1538; d) A. Krämer, B. Maier, J. Bartek, *Mol. Oncol.* **2011**, *5*, 324–335.
[20] K. H. Downing, *Annu. Rev. Cell Dev. Biol.* **2000**, *16*, 89–111.
[21] T. U. Tanaka, A. Desai, *Curr. Opin. Cell Biol.* **2008**, *20*, 53–63.
[22] a) I. B. Roninson, E. V. Broude, B. D. Chang, *Drug Resist. Updates* **2001**, *4*, 303–313; b) L. E. Bröker, F. A. E. Kruyt, G. Giaccone, *Clin. Cancer Res.* **2005**, *11*, 3155–3162.
[23] B. D. Vitre, D. W. Cleveland, *Curr. Opin. Cell Biol.* **2012**, *24*, 809–815.
[24] G. J. P. L. Kops, B. A. A. Weaver, D. W. Cleveland, *Nat. Rev. Cancer* **2005**, *5*, 773–785.
[25] M. Malumbres, M. Barbacid, *Trends Biochem. Sci.* **2005**, *30*, 630–641.
[26] a) A. Satyanarayana, P. Kaldis, *Oncogene* **2009**, *28*, 2925–2939; b) M. B. Kastan, J. Bartek, *Nature* **2004**, *432*, 316–323.
[27] a) S. L. Carter, A. C. Eklund, I. S. Kohane, L. N. Harris, Z. Szallasi, *Nat. Genet.* **2006**, *38*, 1043–1048; b) G. I. Shapiro, *Am. J. Clin. Oncol.* **2006**, *24*, 1770–1783.
[28] a) M. Malumbres, M. Barbacid, *Nat. Rev. Cancer* **2009**, *9*, 153–166; b) A. Ammazzalorso, M. Agamemnone, B. de Filippis, M. Fantacuzzi, *Molecules* **2021**, *26*, 1488–1514.
[29] D. Santamaría, C. Barrière, A. Cerqueira, S. Hunt, C. Tardy, K. Newton, J. F. Cáceres, P. Dubus, M. Malumbres, M. Barbacid, *Nature* **2007**, *448*, 811–815.
[30] S. Li, L. Wang, F. Yu, Z. Zhu, D. Shobaki, H. Chen, M. Wang, J. Wang, G. Qin, U. J. Erasquin, et al., *Chem. Sci.* **2017**, *8*, 2107–2114.
[31] C. Le Droumaguet, C. Wang, Q. Wang, *Chem. Soc. Rev.* **2010**, *39*, 1233–1239.
[32] a) J. Benesty, J. Chen, Y. Huang, I. Cohen, *Noise Reduction in Speech Processing* (Eds.: I. Cohen, Y. Huang, J. Chen, J. Benesty), Springer Berlin Heidelberg, Berlin, Heidelberg **2009**, pp. 1–4; b) Q. Li, A. Lau, T. J. Morris, L. Guo, C. B. Fordyce, E. F. Stanley, *J. Neurosci.* **2004**, *24*, 4070–4081; c) W. Stauffer, H. Sheng, H. N. Lim, *Sci. Rep.* **2018**, *8*, 15764.
[33] L. A. Porter, D. J. Donoghue, *Prog. Cell Cycle Res.* **2003**, *5*, 335–347.
[34] E. Pasquier, S. Honoré, D. Braguer, *Drug Resist. Updates* **2006**, *9*, 74–86.
[35] M. Guppy, *Biochem. Biophys. Res. Commun.* **2002**, *299*, 676–680.
[36] B. R. Zetter, *Annu. Rev. Med.* **1998**, *49*, 407–424.
[37] D. R. Bielenberg, B. R. Zetter, *Cancer J. (Sudbury, Mass.)* **2015**, *21*, 267–273.
[38] a) C. Dumontet, M. A. Jordan, *Nat. Rev. Drug Discovery* **2010**, *9*, 790–803; b) S. J. Stafford, J. Schwimer, C. T. Anthony, J. L. Thomson, Y. Z. Wang, E. A. Woltering, *J. Surg. Res.* **2005**, *125*, 104–108; c) M. Su, J. Huang, S. Liu, Y. Xiao, X. Qin, J. Liu, C. Pi, T. Luo, J. Li, X. Chen, et al., *Sci. Rep.* **2016**, *6*, 28139; d) E. L. Schwartz, *Clin. Cancer Res.* **2009**, *15*, 2594–2601; e) D. Bates, A. Eastman, *Br. J. Clin. Pharmacol.* **2017**, *83*, 255–268.
[39] D. S. Grant, T. L. Williams, M. Zahaczewsky, A. P. Dicker, *Int. J. Cancer* **2003**, *104*, 121–129.
[40] I. Arnaoutova, H. K. Kleinman, *Nat. Protoc.* **2010**, *5*, 628–635.
[41] G. Carpentier, S. Berndt, S. Ferratge, W. Rasband, M. Cuendet, G. Uzan, P. Albanese, *Sci. Rep.* **2020**, *10*, 11568.
[42] E. Aranda, G. I. Owen, *Biol. Res.* **2009**, *42*.
[43] H. Draut, T. Rehm, G. Begemann, R. Schobert, *Chem. Biodiversity* **2017**, *14*.
[44] N. D. Lawson, B. M. Weinstein, *Dev. Biol.* **2002**, *248*, 307–318.
[45] G. D'Agati, R. Beltre, A. Sessa, A. Burger, Y. Zhou, C. Mosimann, R. M. White, *Dev. Biol.* **2017**, *430*, 11–17.
[46] a) E. Kawamura, A. B. Fielding, N. Kannan, A. Balgi, C. J. Eaves, M. Roberge, S. Dedhar, *Oncotarget* **2013**, *4*, 1763–1776; b) G. Konotop, E. Bausch, T. Nagai, A. Turchinovich, N. Becker, A. Benner, M. Boutros, K. Mizuno, A. Krämer, M. S. Raab, *Cancer Res.* **2016**, *76*, 6690–6700; c) D. Sabat-Pośpiech, K. Fabian-Kolpanowicz, I. A. Prior, J. M. Coulson, A. B. Fielding, *Biochem. Soc. Trans.* **2019**, *47*, 1209–1222.
[47] M. Khoobi, M. Alipour, A. Sakhteman, H. Nadri, A. Moradi, M. Ghandi, S. Emami, A. Foroumadi, A. Shafiee, *Eur. J. Med. Chem.* **2013**, *68*, 260–269.
[48] B. Jansen, S. A. Inoue, H. Wadl, H.-G. Eichler, K. Wolff, A. van Elsas, P. I. Schrier, H. Pehamberger, *Int. J. Cancer* **1996**, *67*, 821–825.
[49] A. W. Tai, N. Bojjireddy, T. Balla, *Anal. Biochem.* **2011**, *417*, 97–102.
[50] H. Zegzouti, M. Zdanovskaia, K. Hsiao, S. A. Goueli, *Assay Drug Dev. Technol.* **2009**, *7*, 560–572.
[51] R. M. White, A. Sessa, C. Burke, T. Bowman, J. LeBlanc, C. Ceol, C. Bourque, M. Dovey, W. Goessling, C. E. Burns, et al., *Cell Stem Cell* **2008**, *2*, 183–189.

Manuscript received: February 2, 2022
Revised manuscript received: February 25, 2022
Accepted manuscript online: February 28, 2022
Version of record online: March 16, 2022

ChemMedChem

Supporting Information

2-Amino-4-aryl-5-oxo-4,5-dihydropyrano[3,2-*c*]chromene-3-carbonitriles with Microtubule-Disruptive, Centrosome-Declustering, and Antiangiogenic Effects *in vitro* and *in vivo*

Leonhard H. F. Köhler, Sebastian Reich, Gerrit Begemann, Rainer Schobert, and Bernhard Biersack*

Table of Contents

Experimental section

NMR Spectra

^{1}H NMR spectrum of **1a**

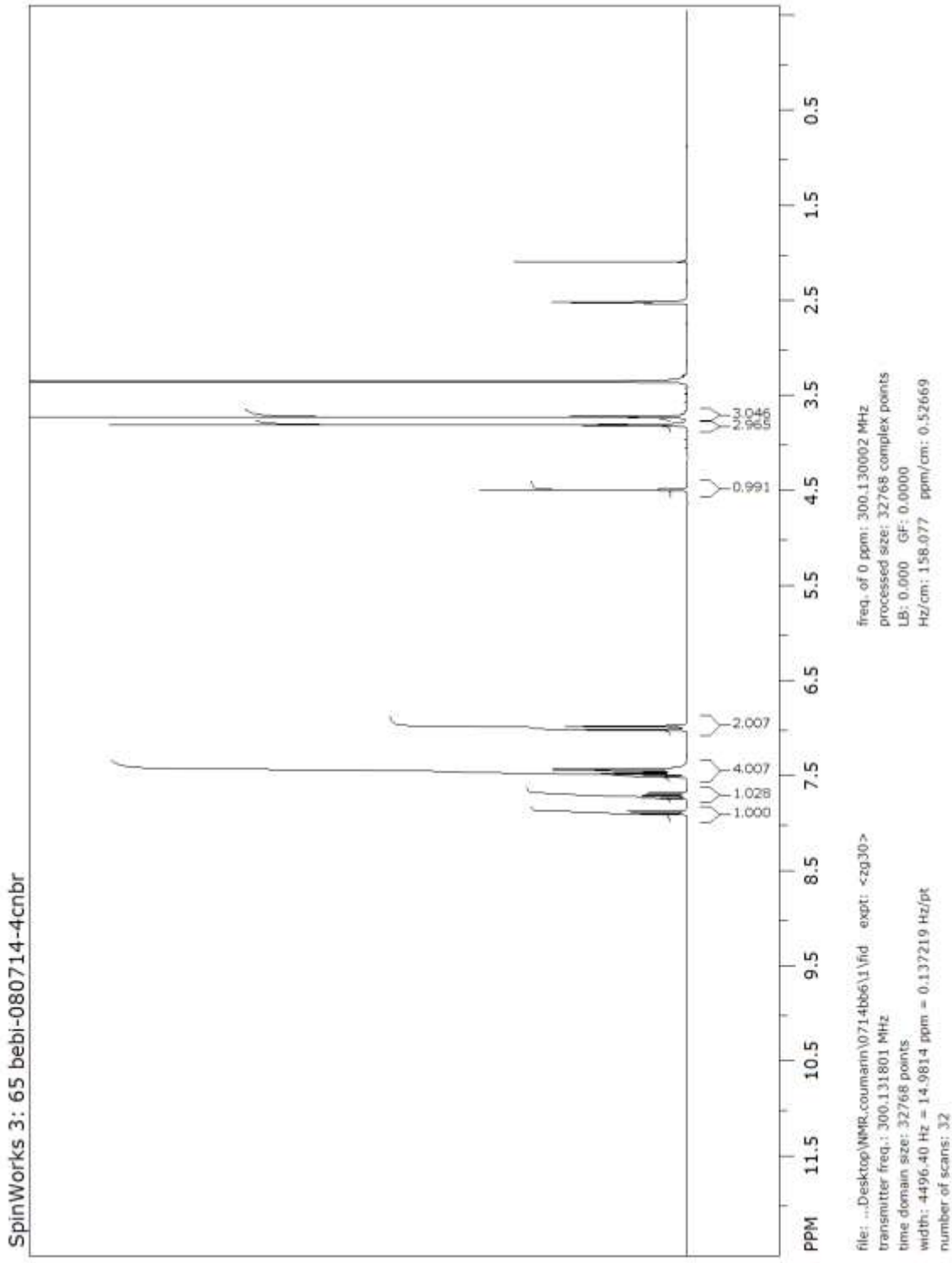

^{13}C NMR spectrum of **1a**

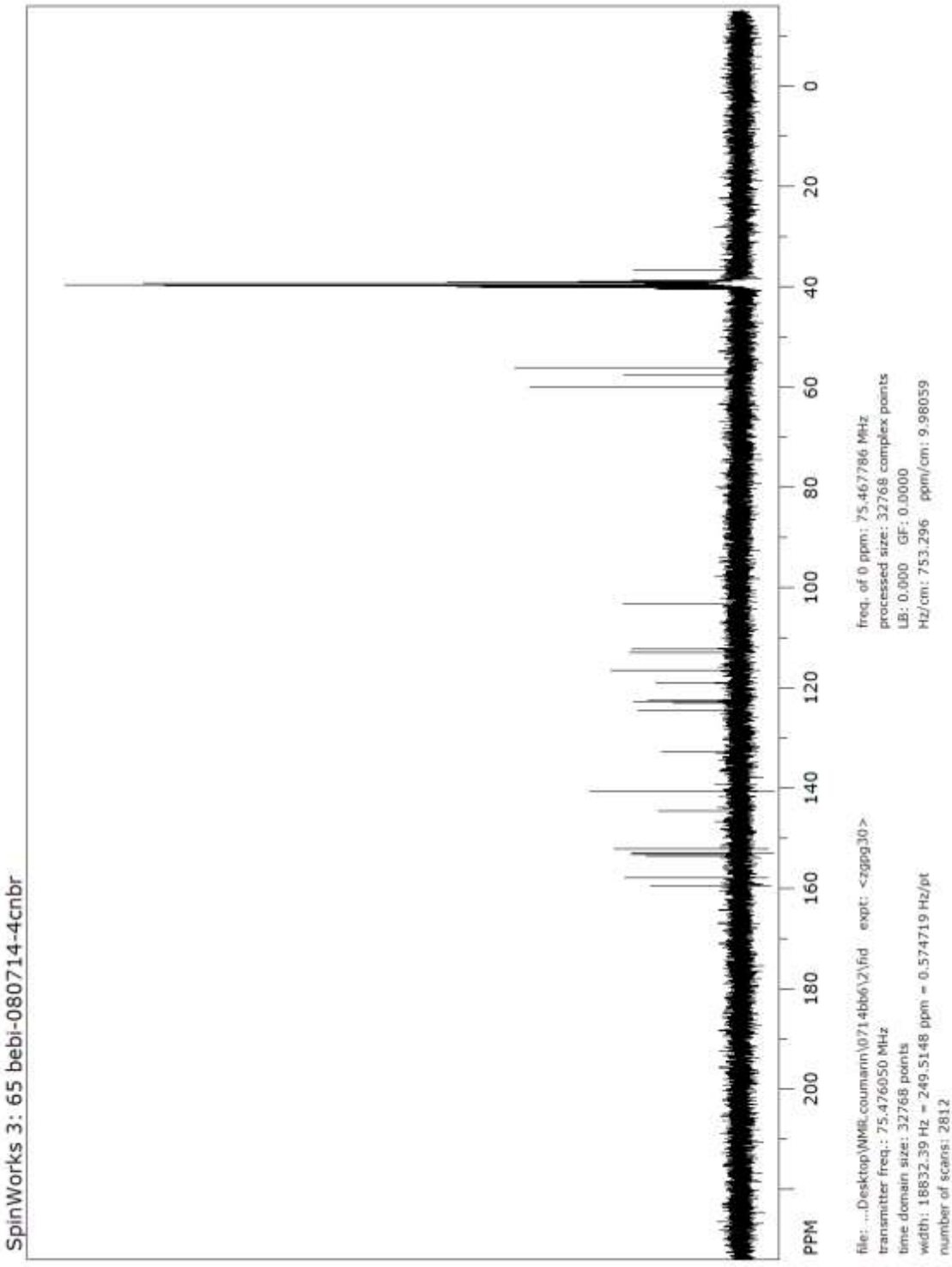

^{1}H NMR spectrum of **1b**

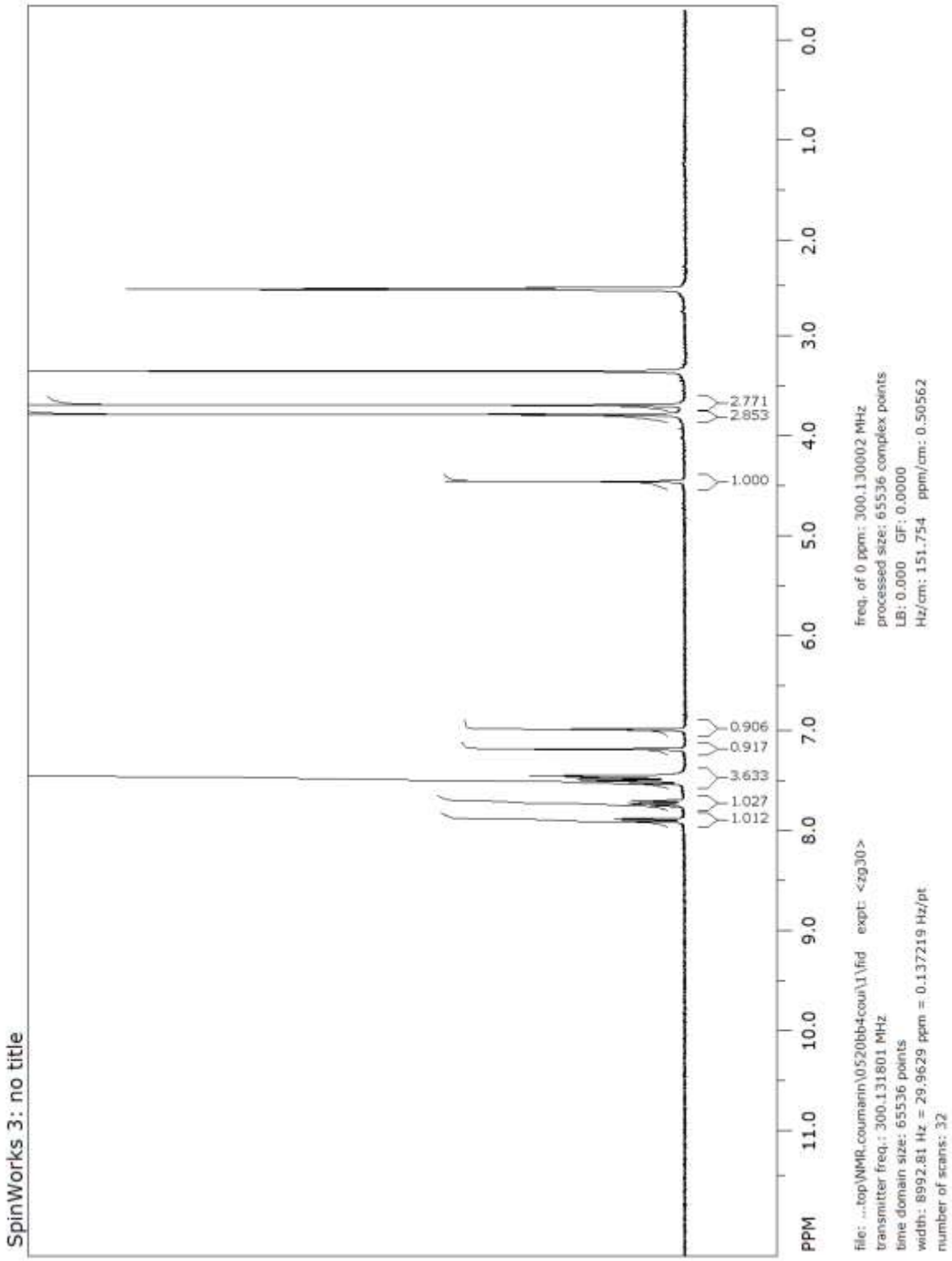

^{13}C NMR spectrum of **1b**

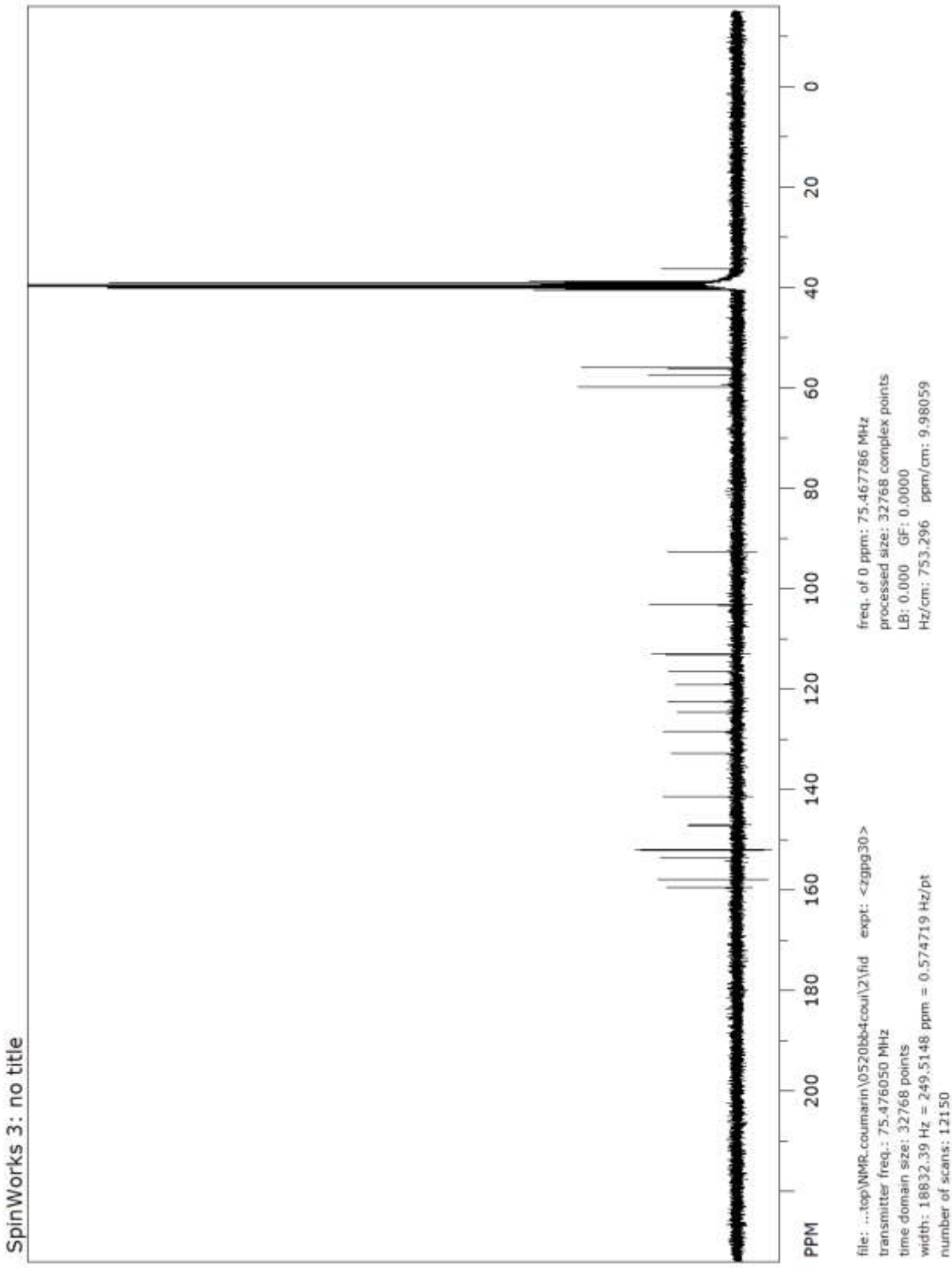

^{1}H NMR spectrum of **1c**

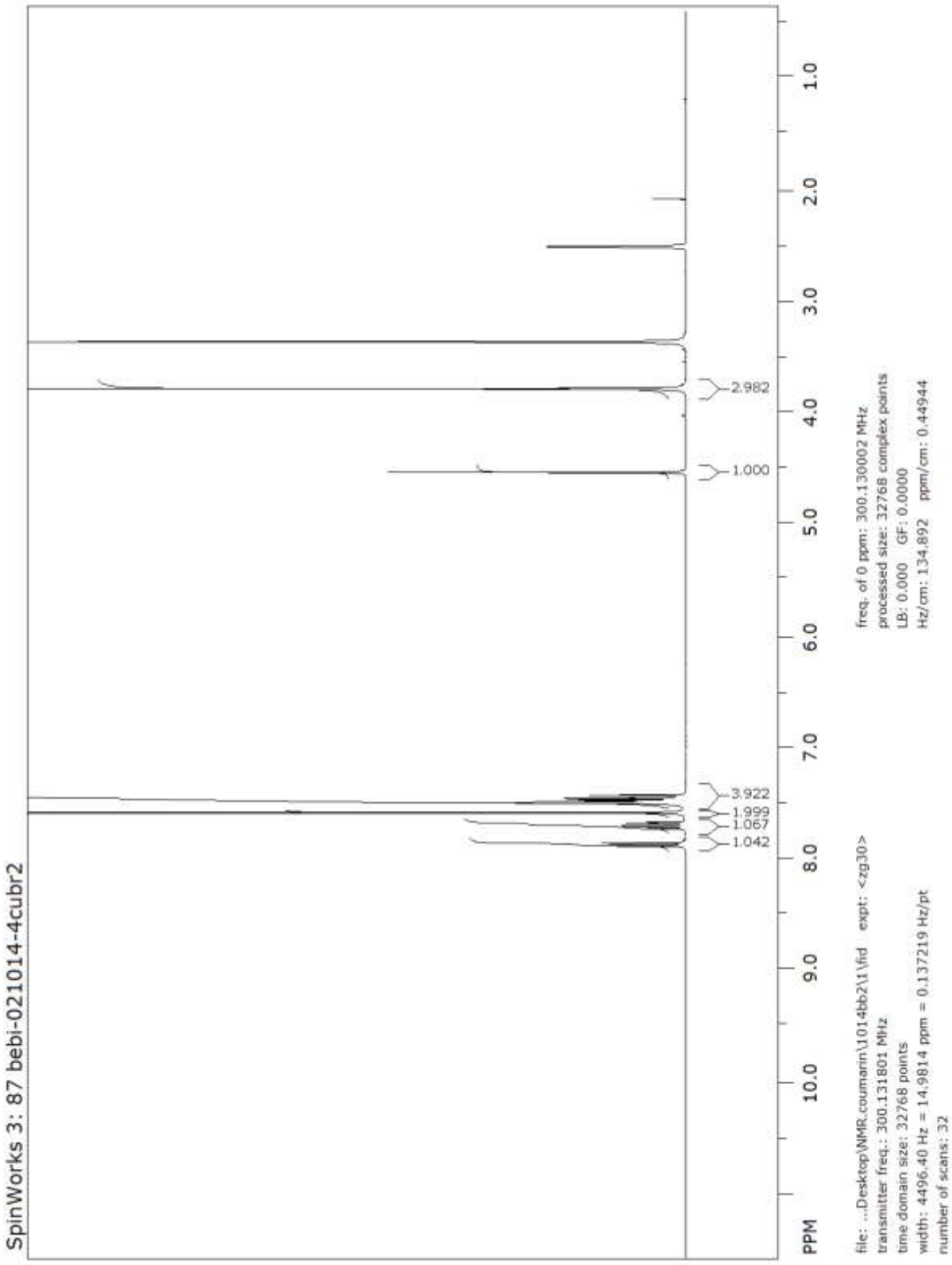

^{13}C NMR spectrum of **1c**

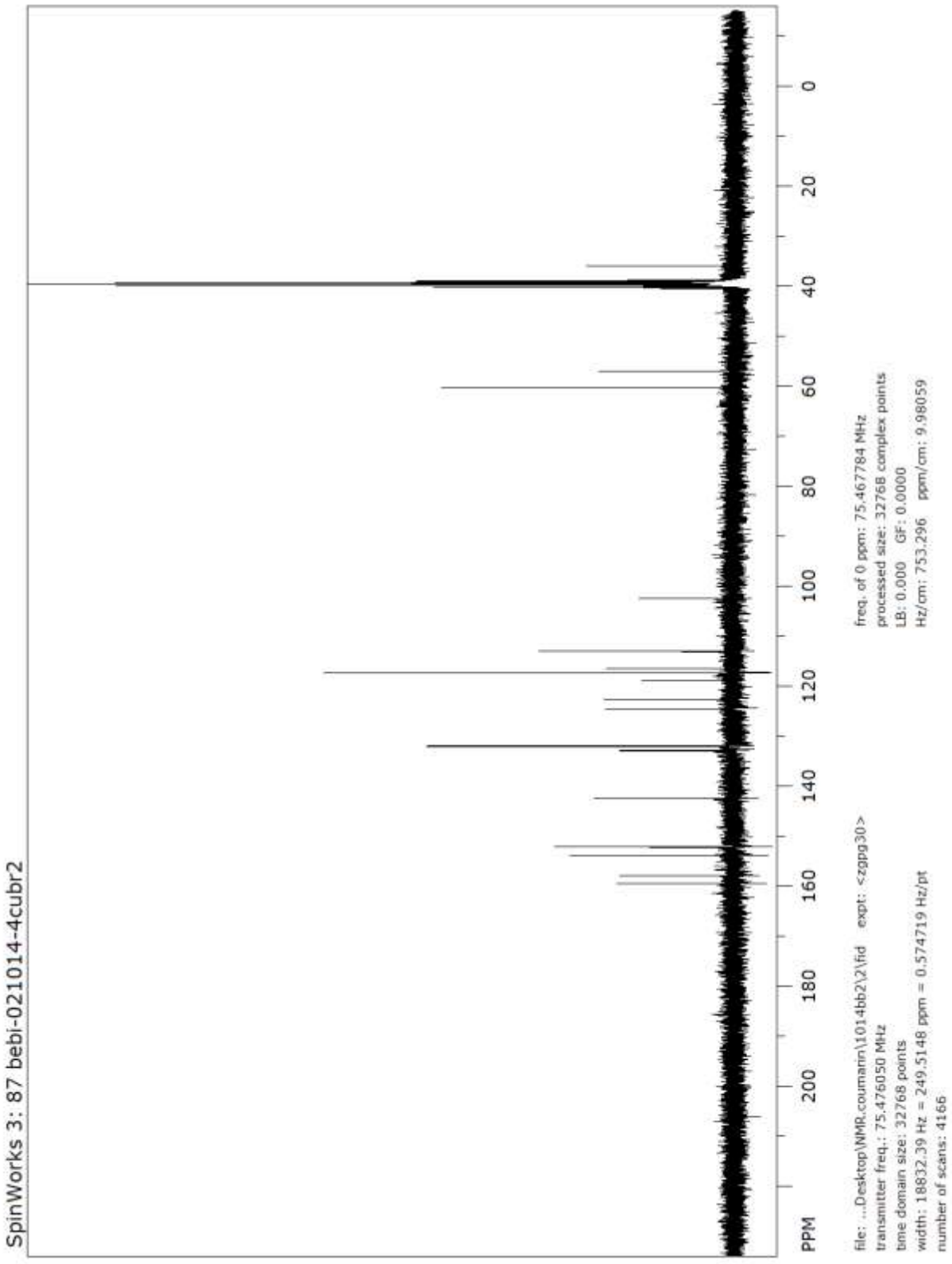

^{1}H NMR spectrum of **1d**

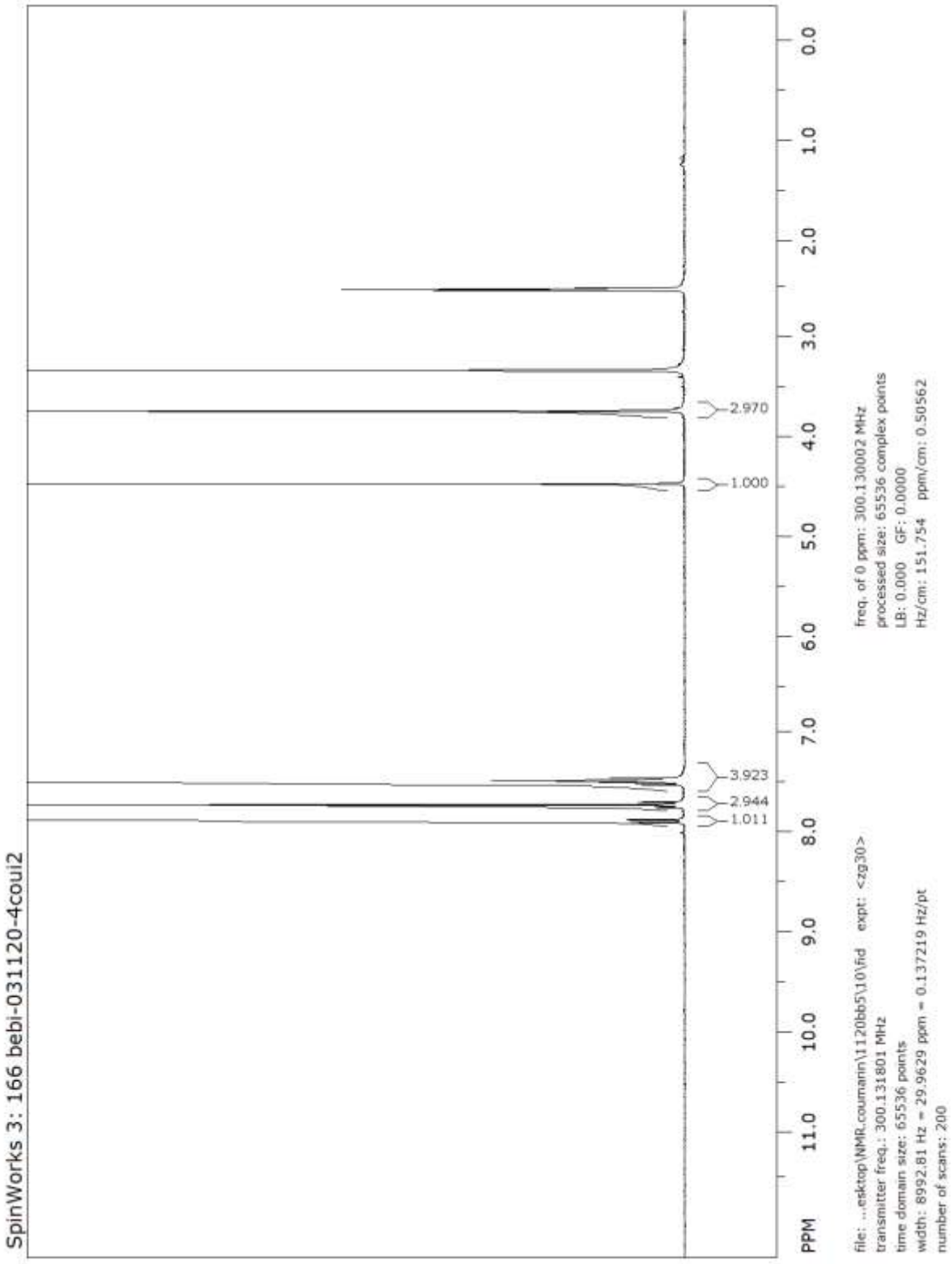

^{13}C NMR spectrum of **1d**

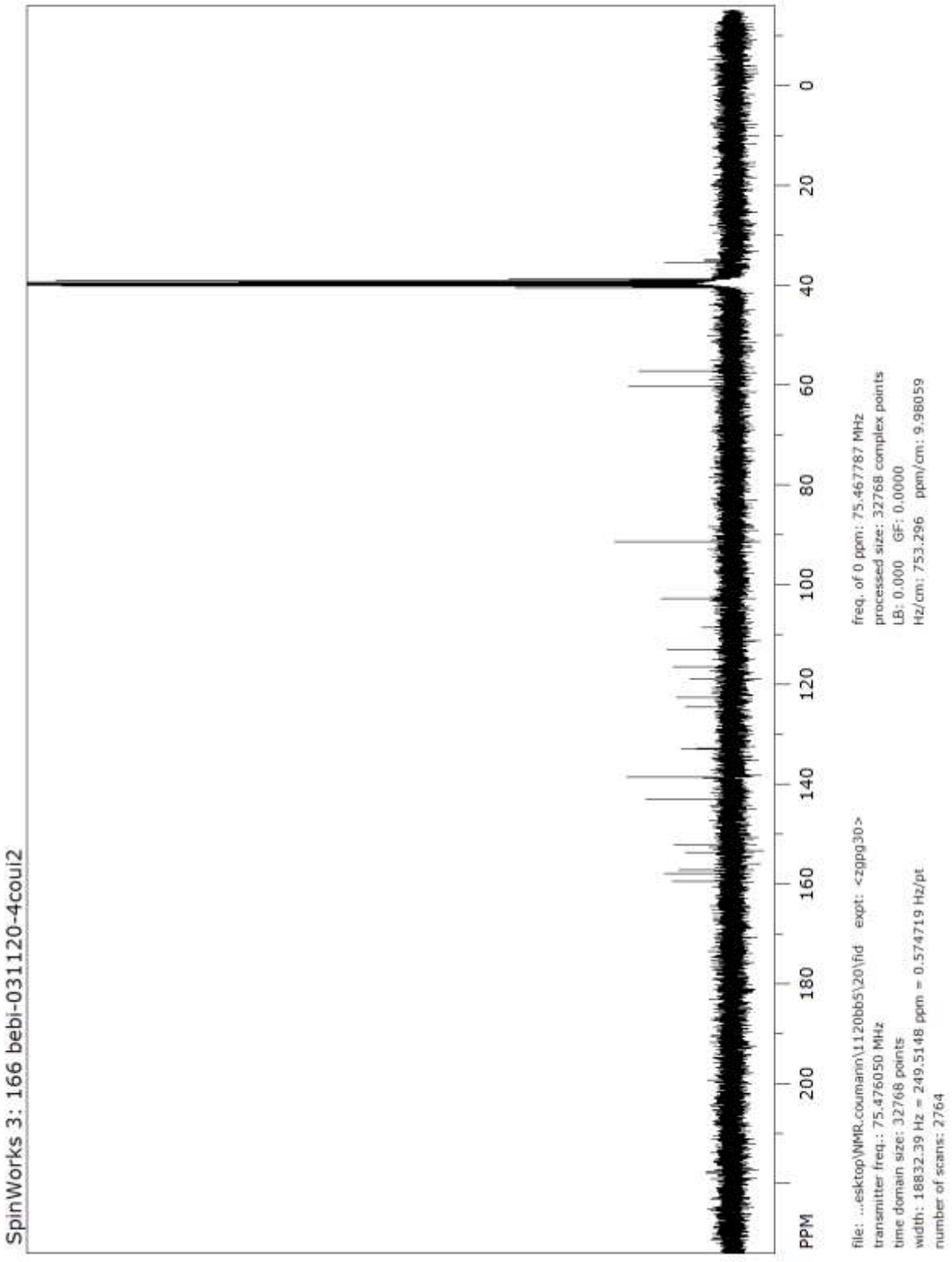

^{1}H NMR spectrum of **1e**

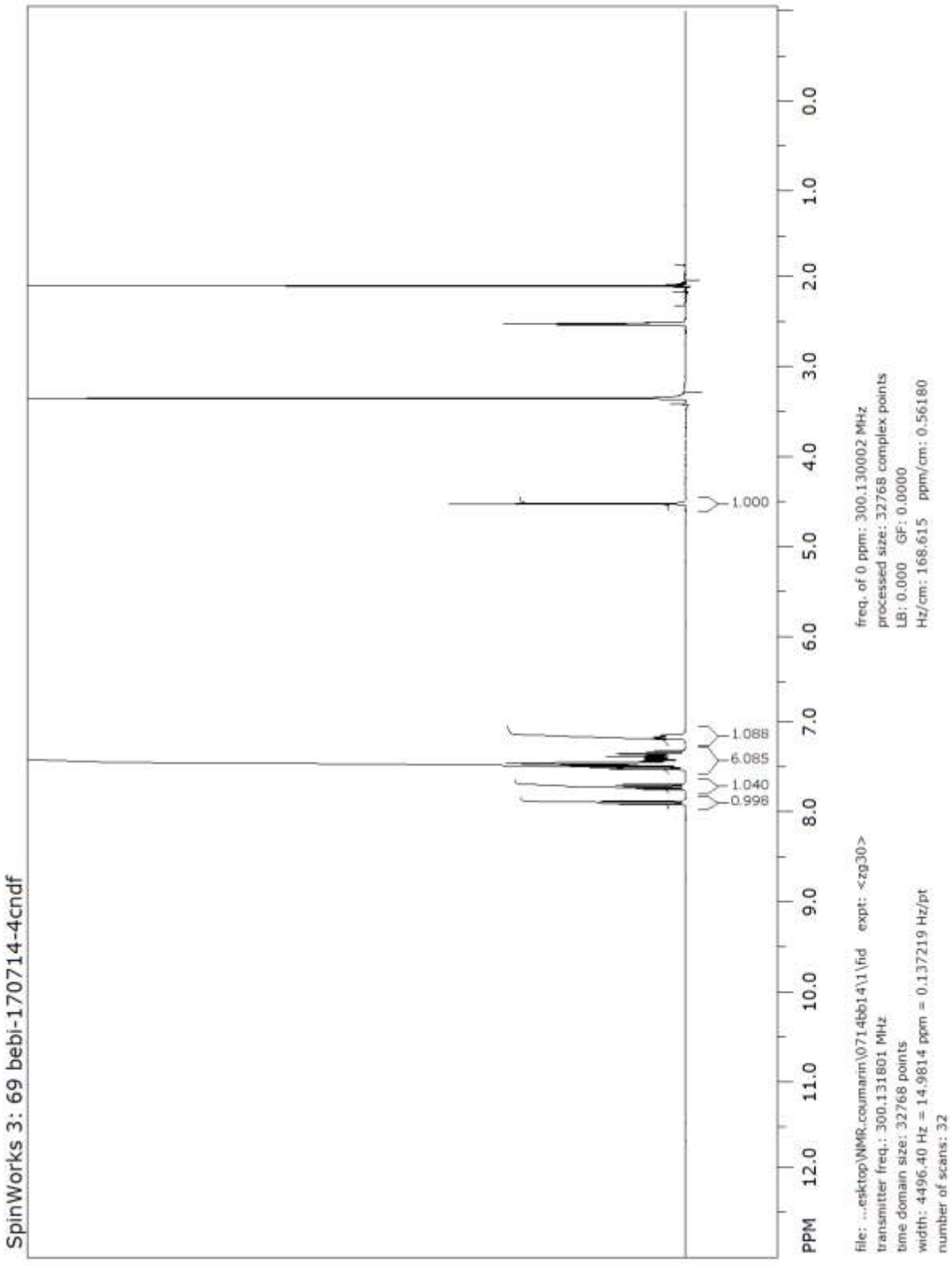

^{13}C NMR spectrum of **1e**

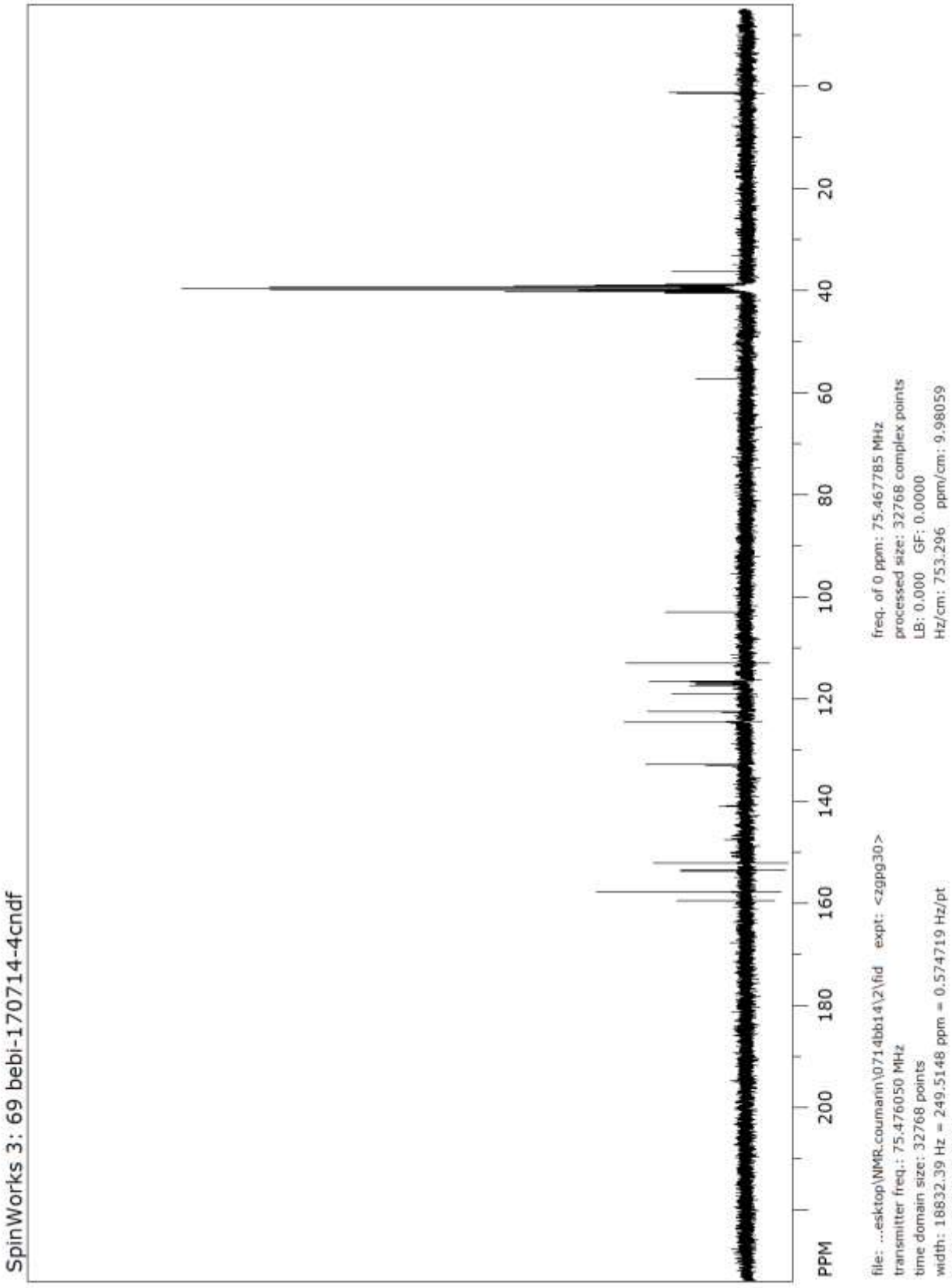

^{1}H NMR spectrum of **1f**

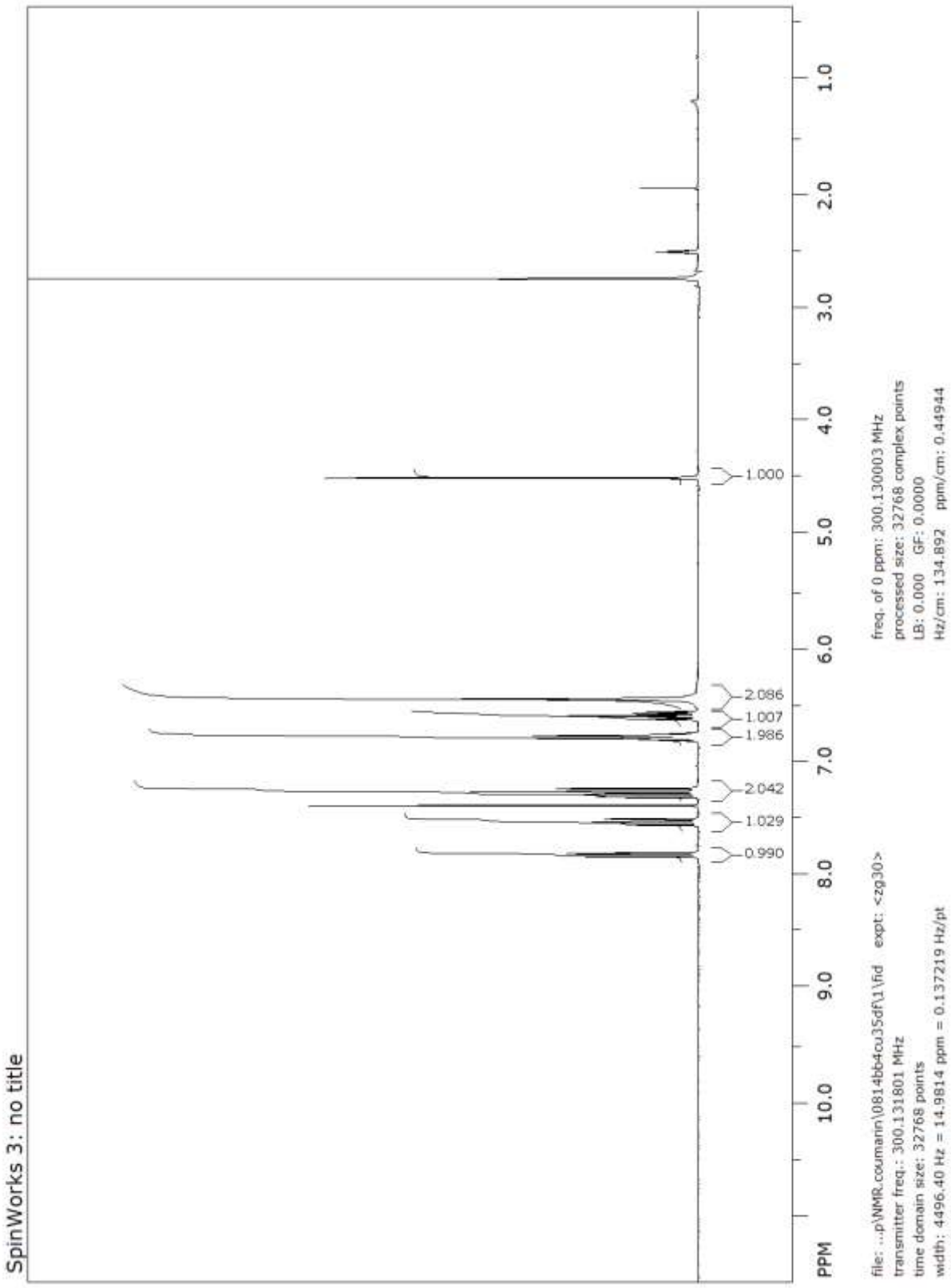

^{13}C NMR spectrum of **1f**

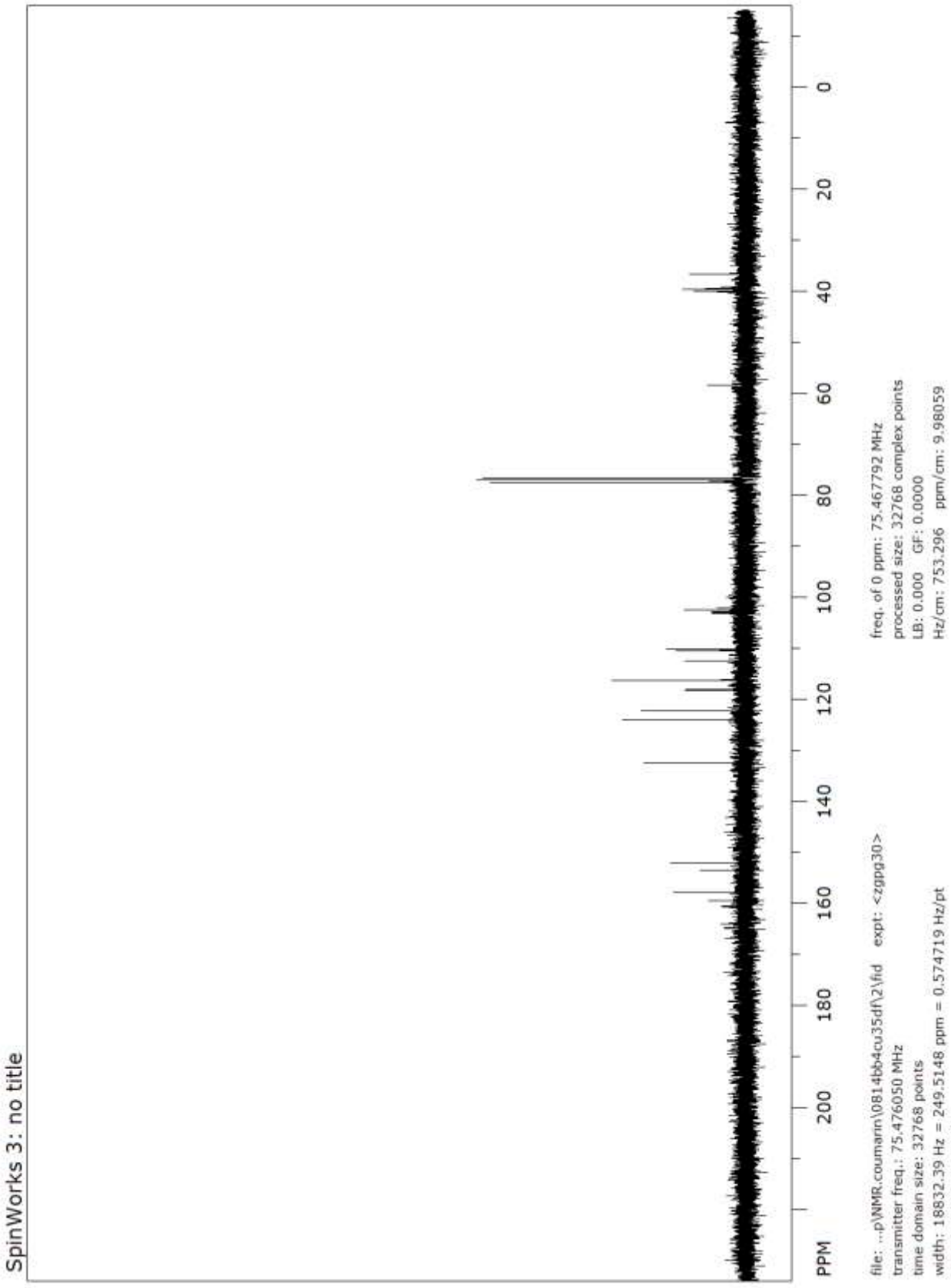

^{1}H NMR spectrum of **1g**

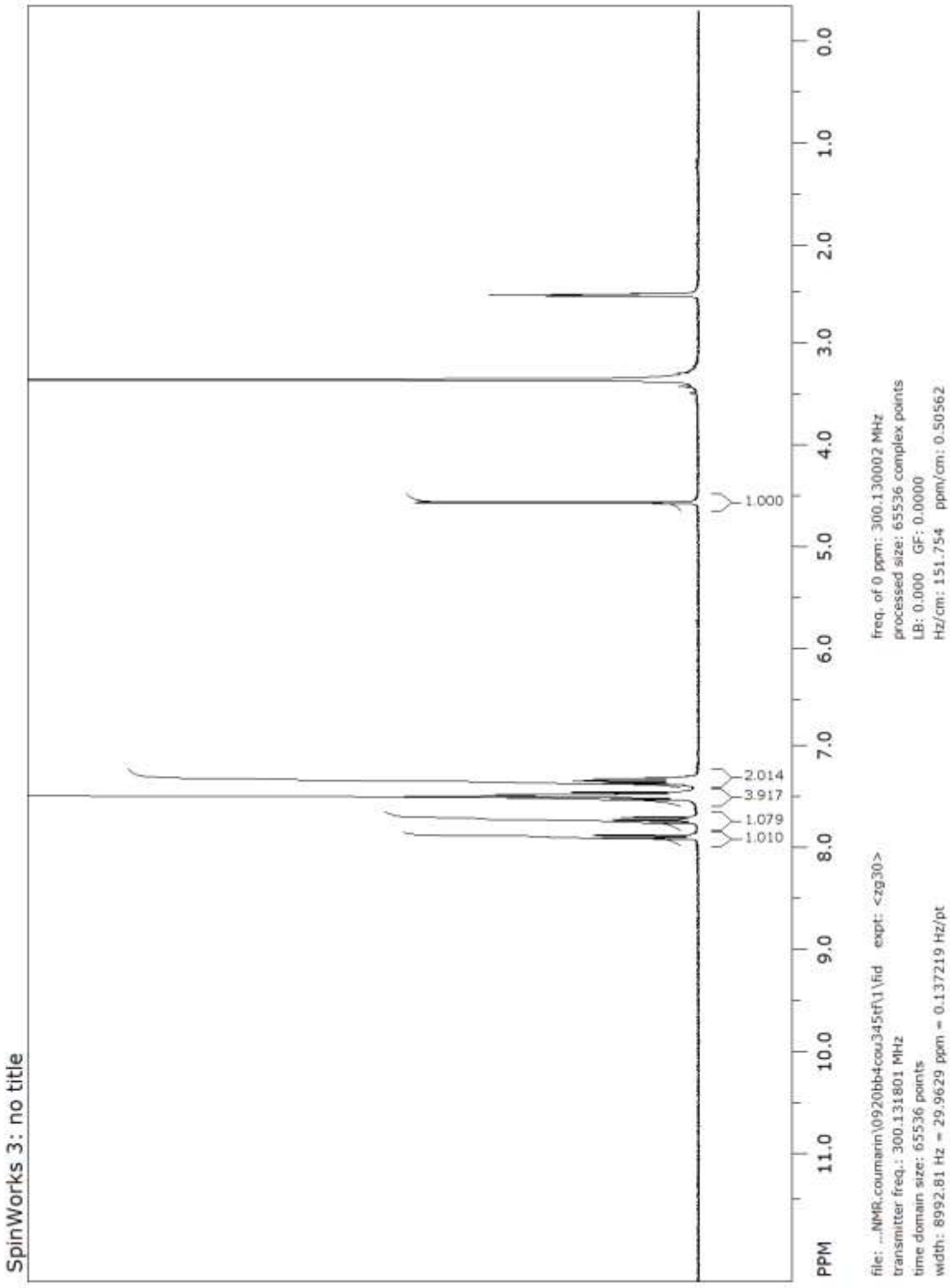

^{13}C NMR spectrum of **1g**

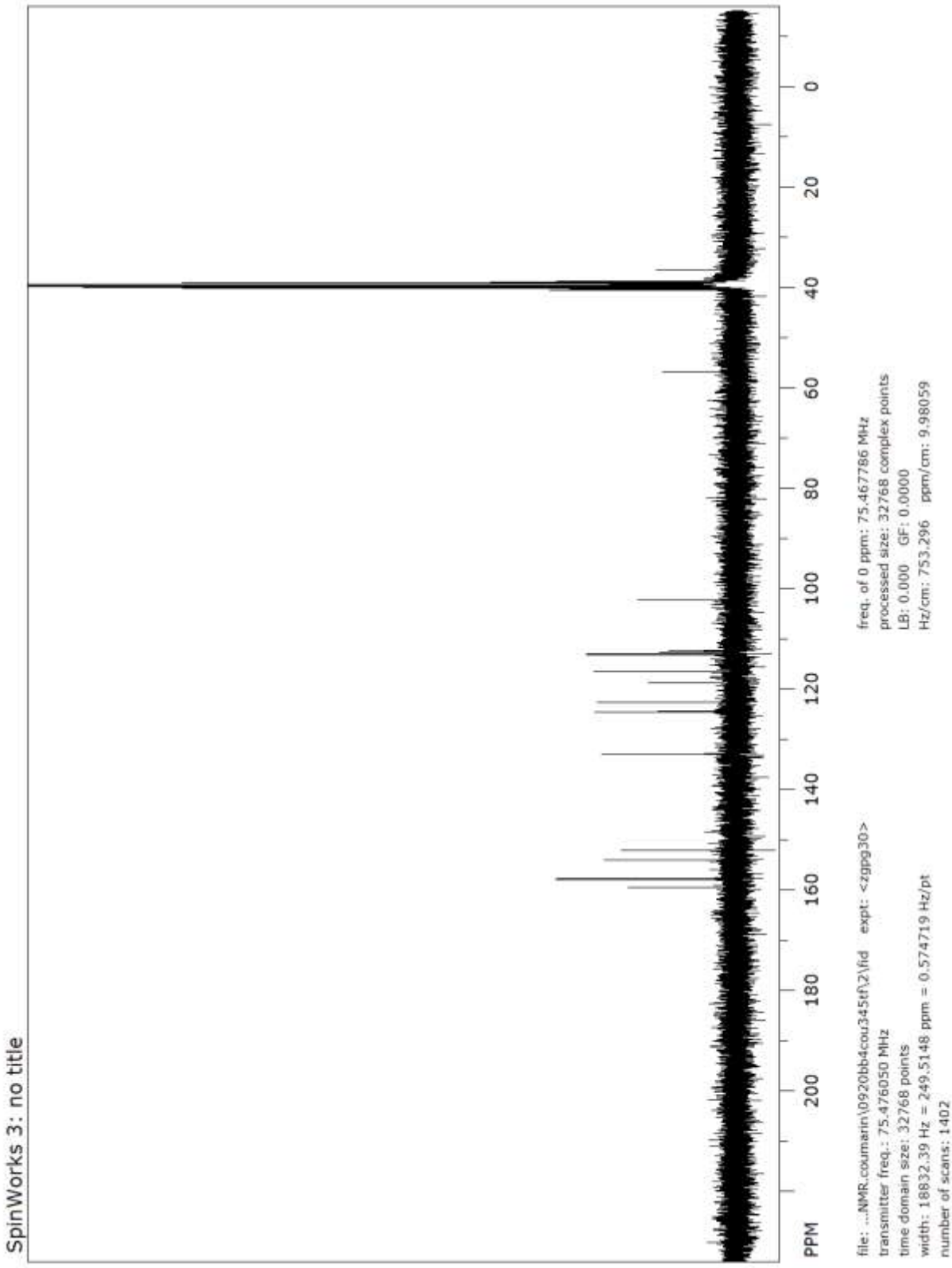

^{1}H NMR spectrum of **1h**

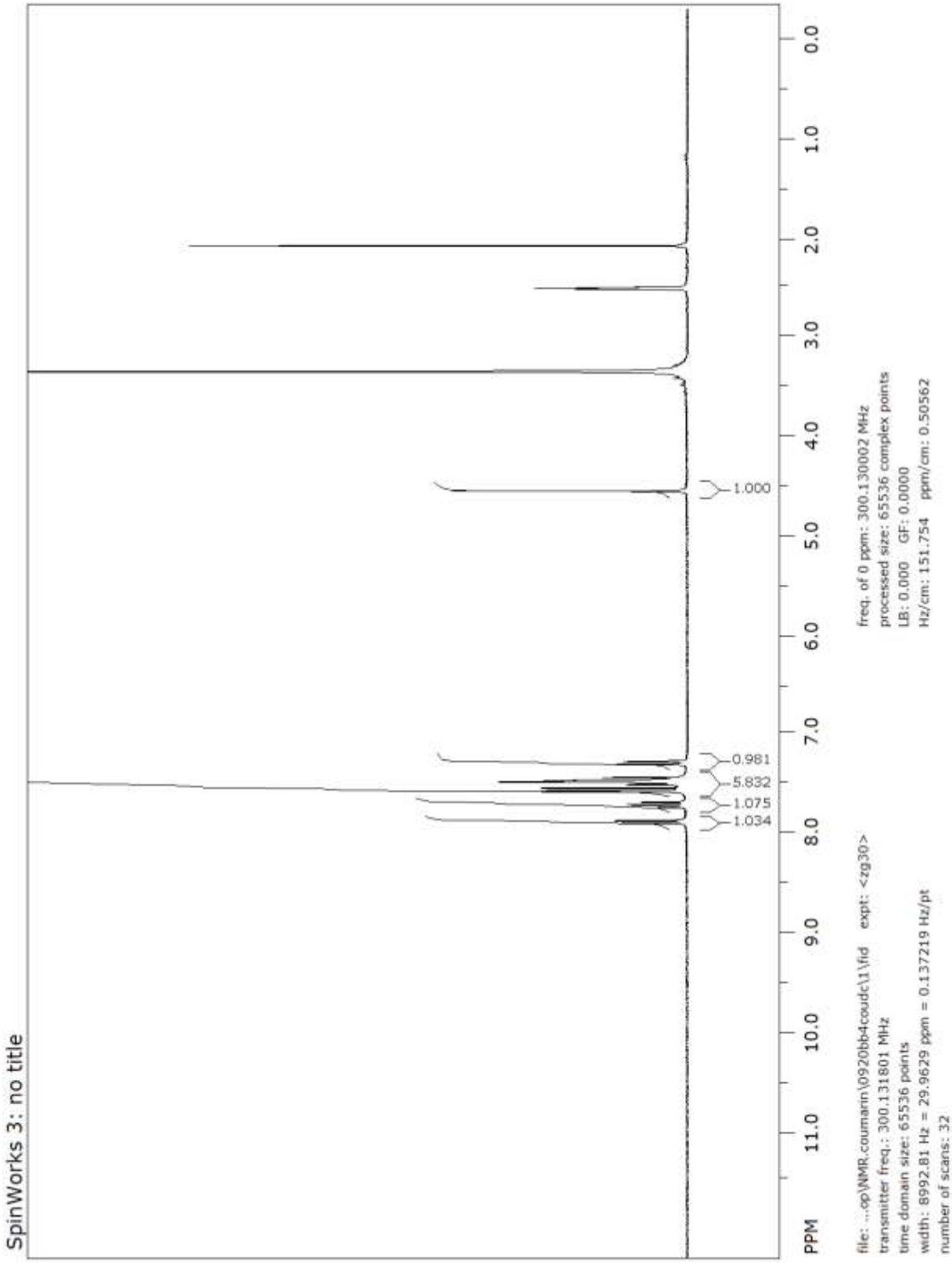

^{13}C NMR spectrum of **1h**

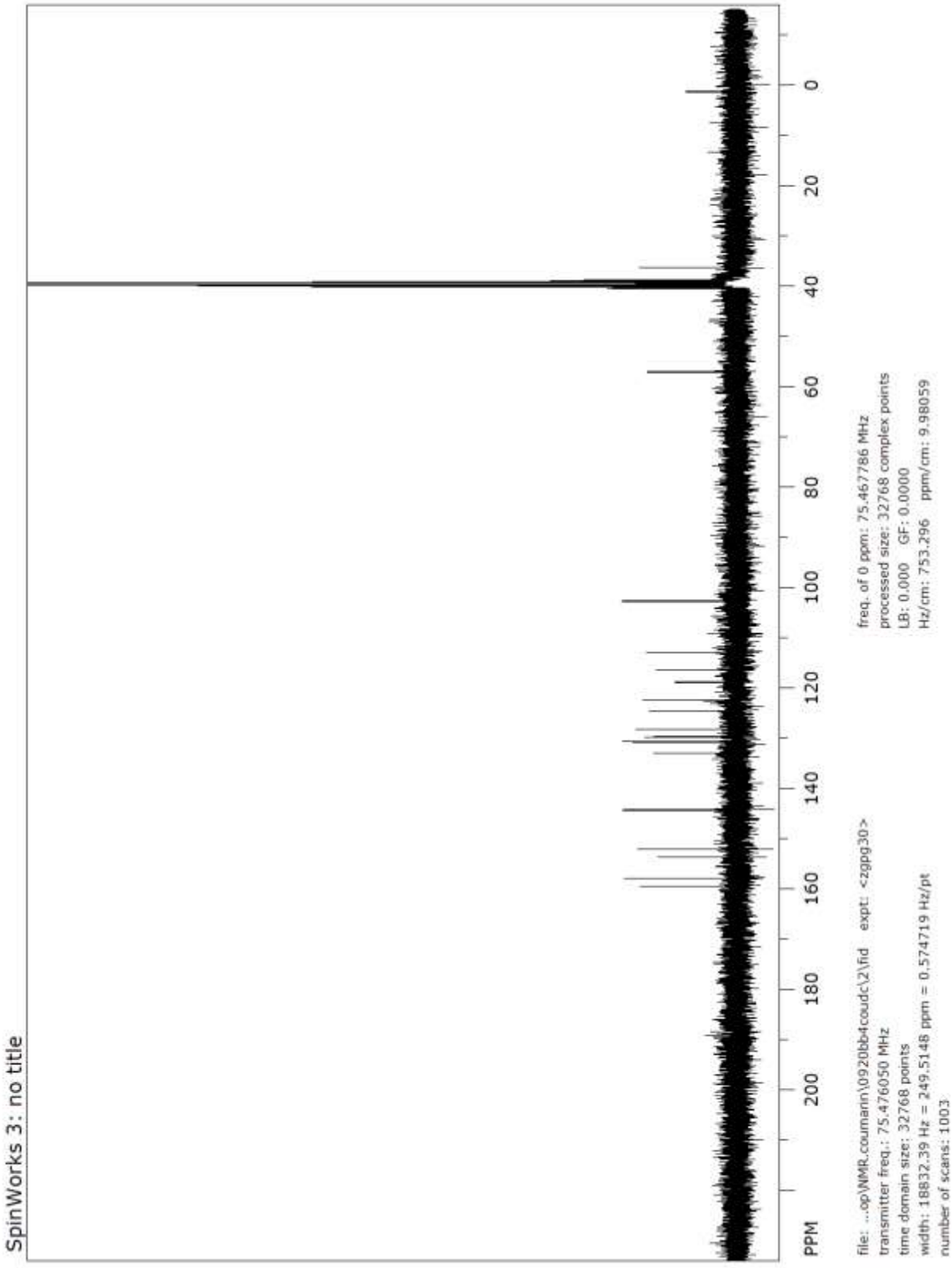

^{1}H NMR spectrum of **1i**

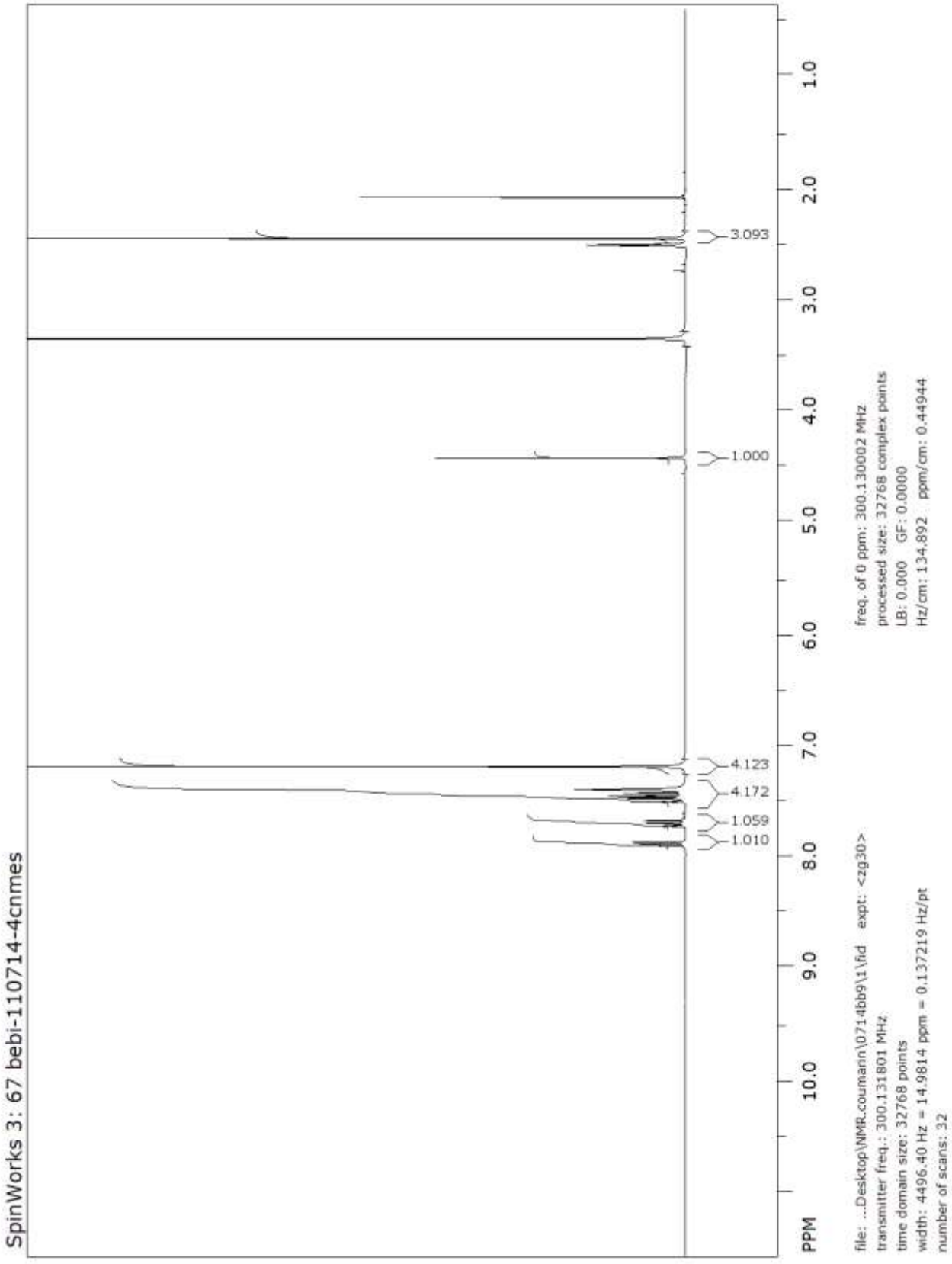

^{13}C NMR spectrum of **1i**

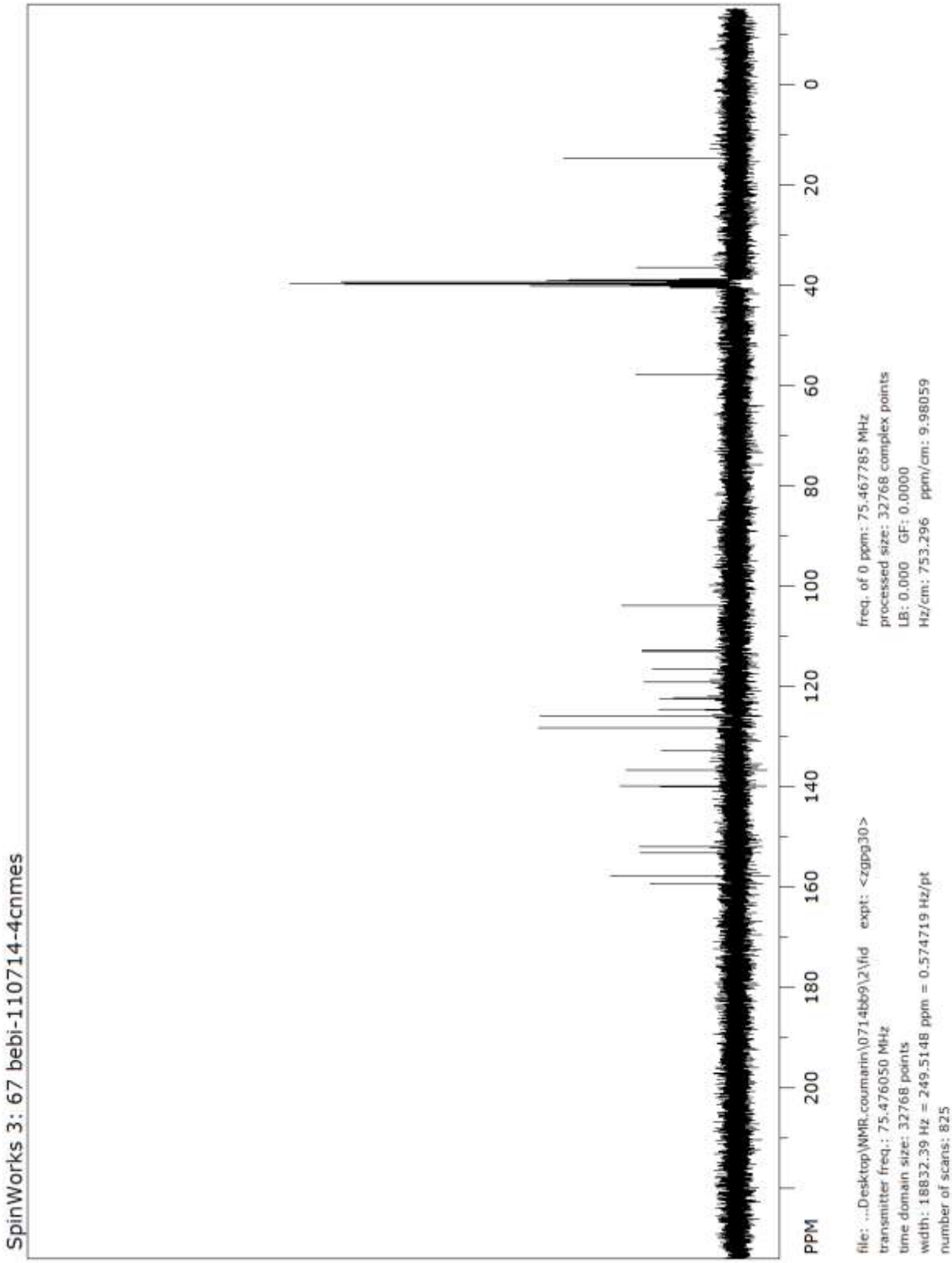

^{1}H NMR spectrum of **1j**

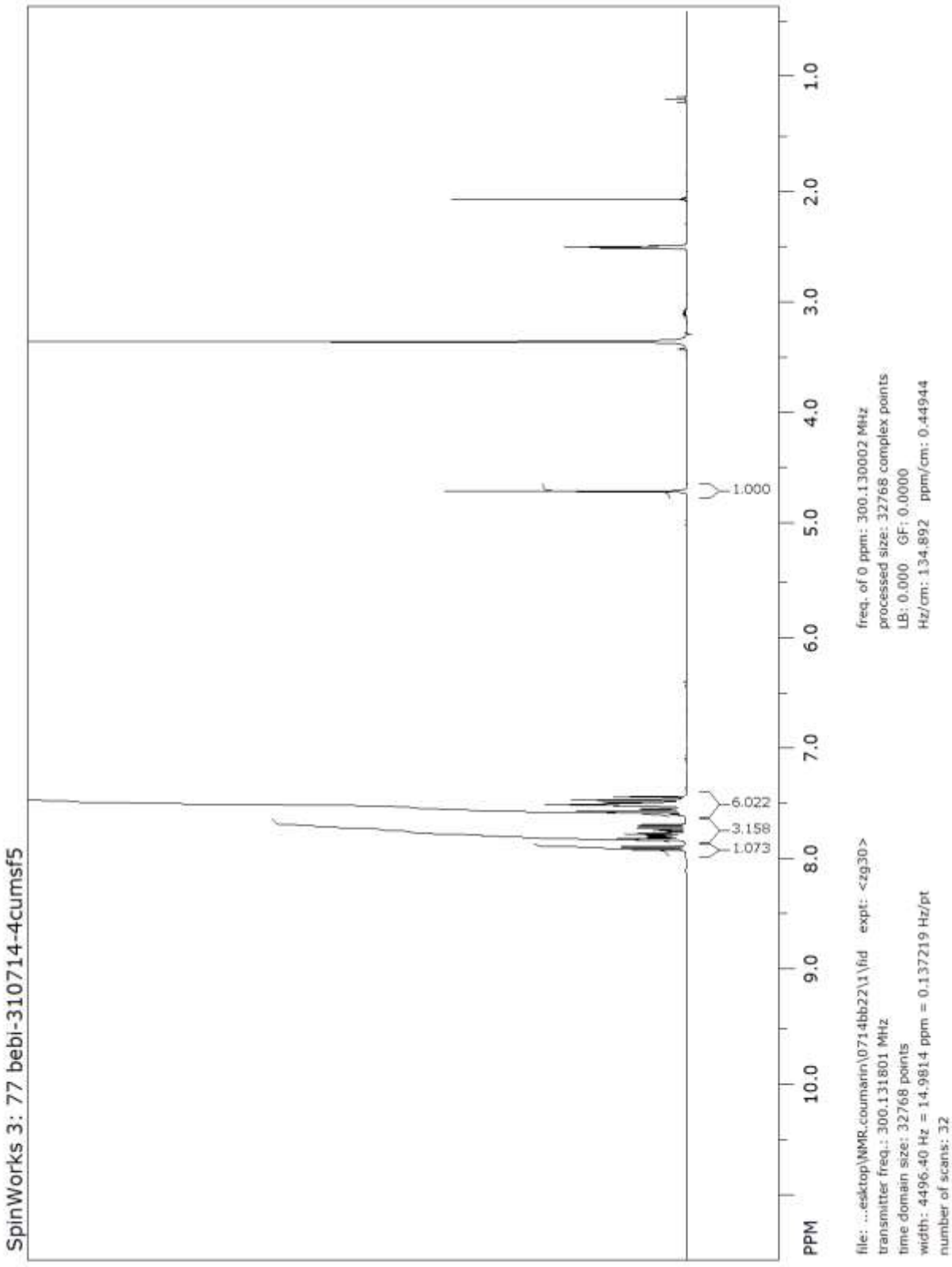

^{13}C NMR spectrum of **1j**

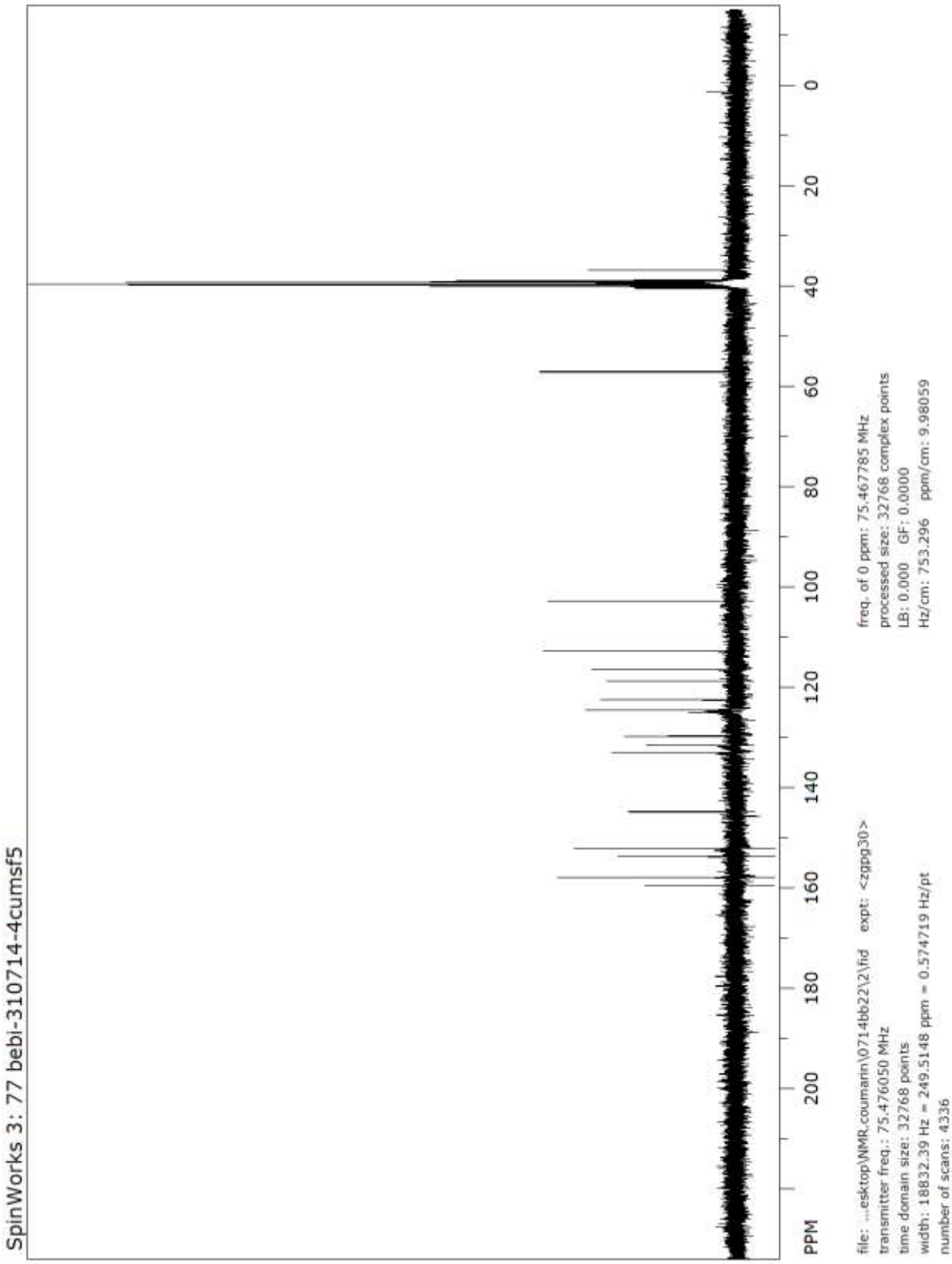

^{1}H NMR spectrum of **1k**

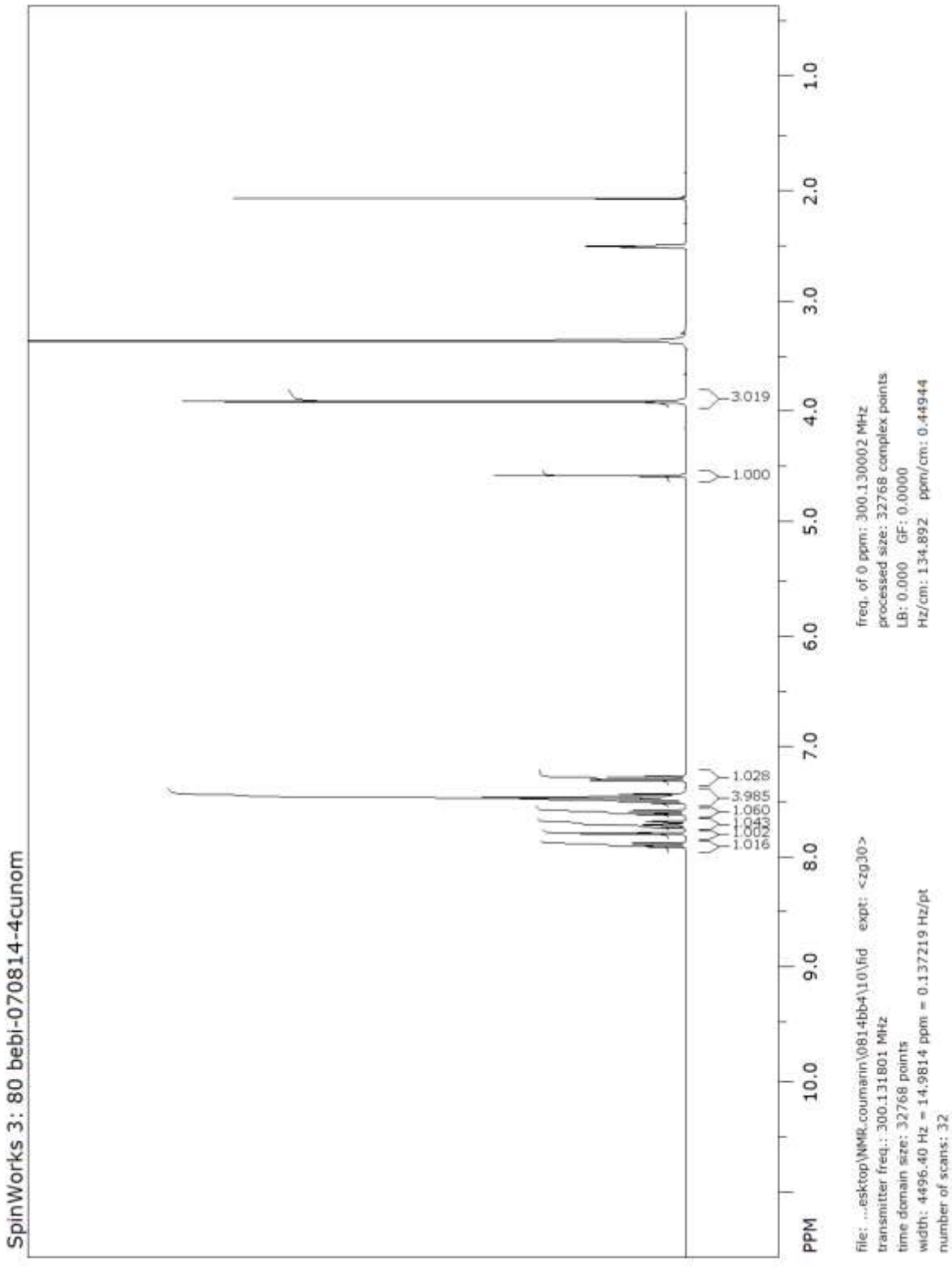

^{13}C NMR spectrum of **1k**

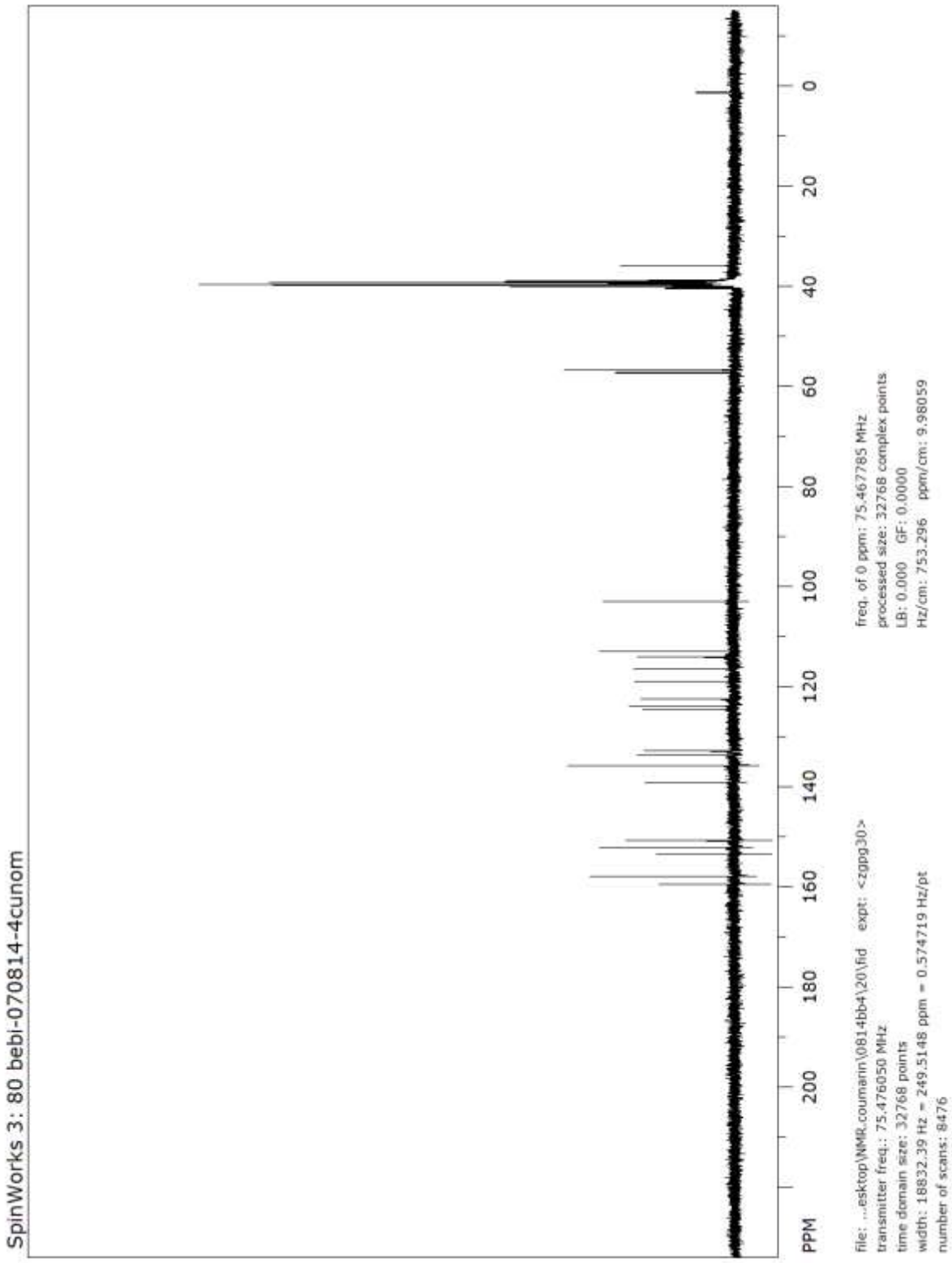

^{1}H NMR spectrum of **1l**

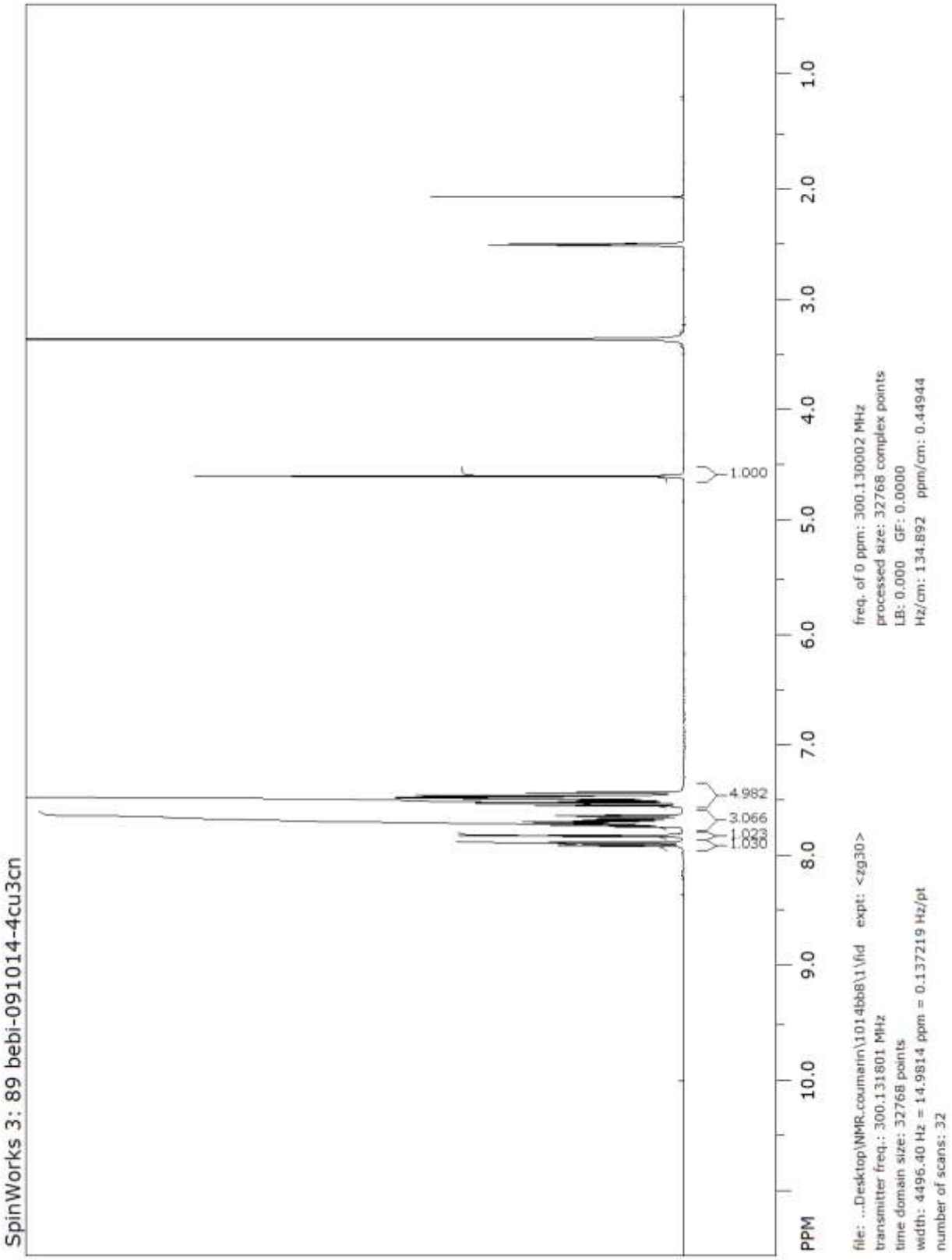

^{13}C NMR spectrum of **1l**

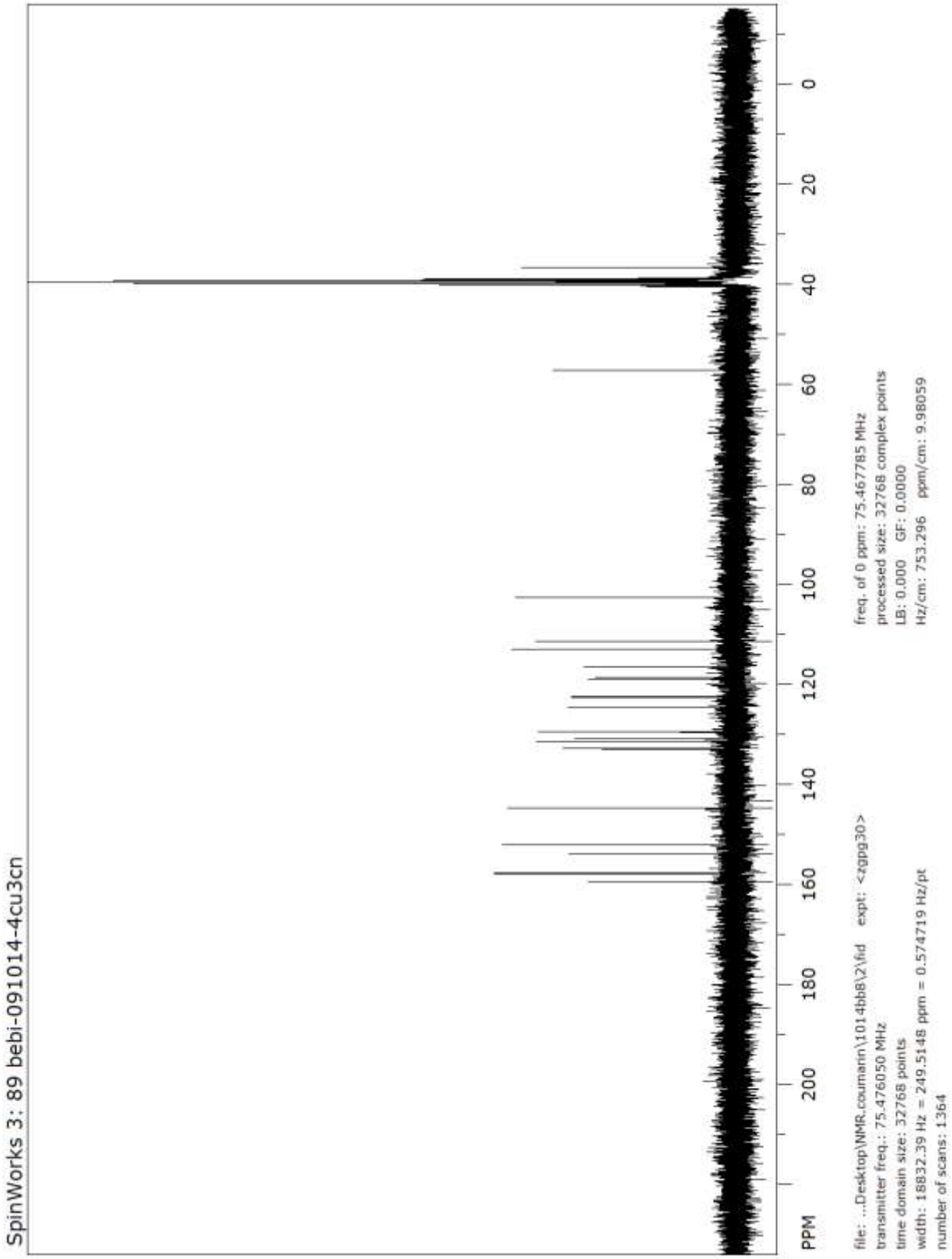

^{1}H NMR spectrum of **1m**

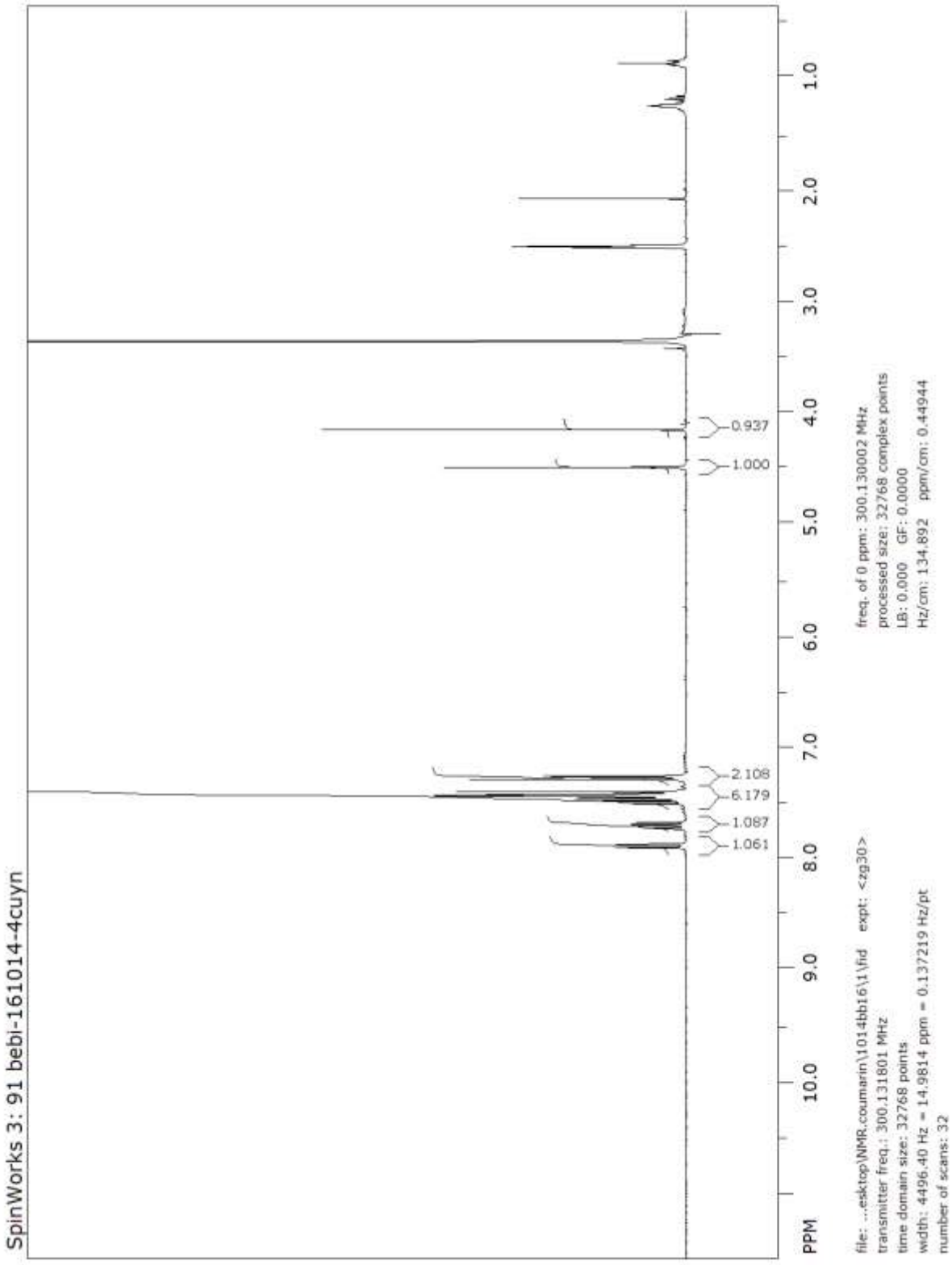

^{13}C NMR spectrum of **1m**

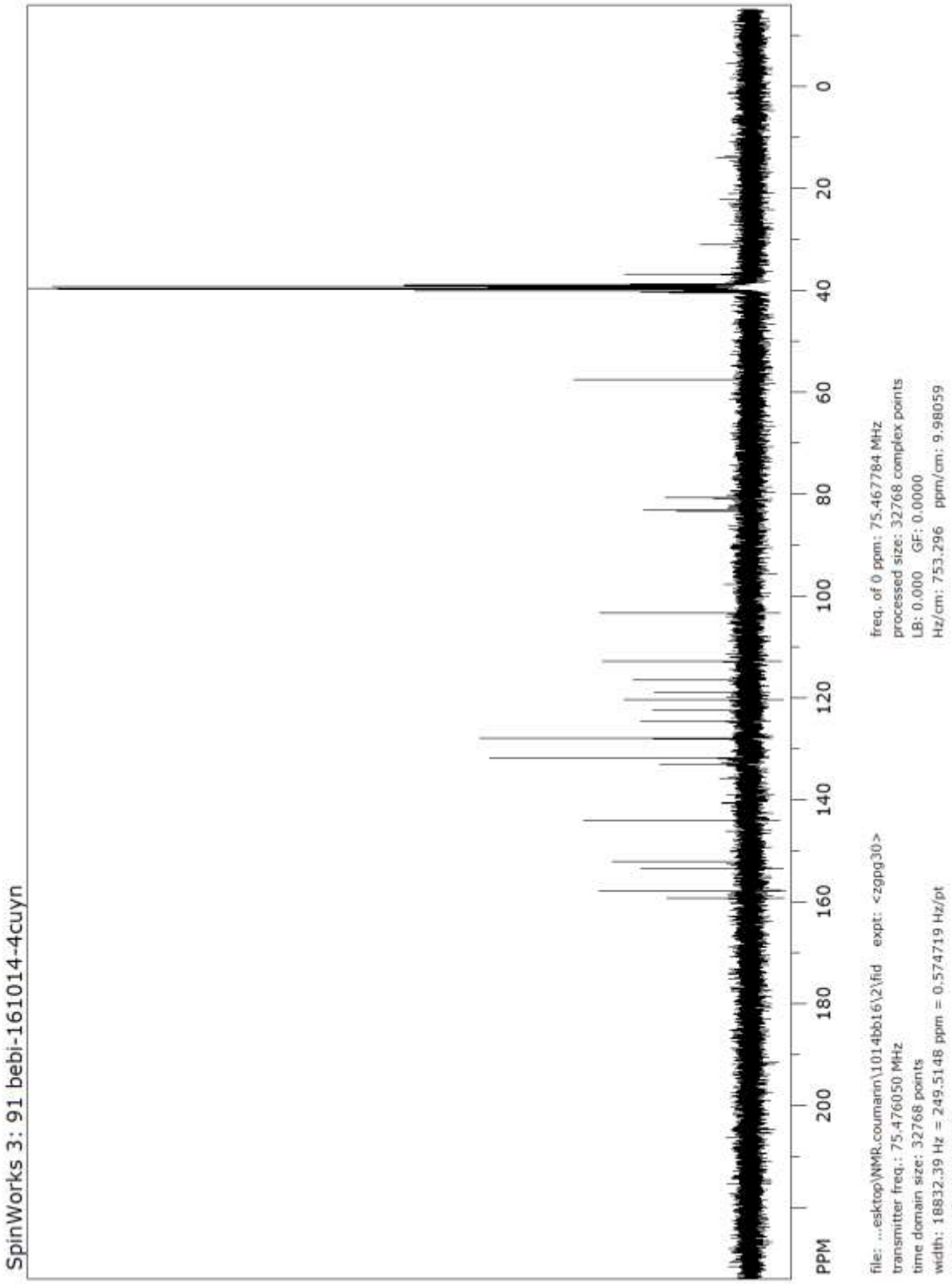

^{1}H NMR spectrum of **1n**

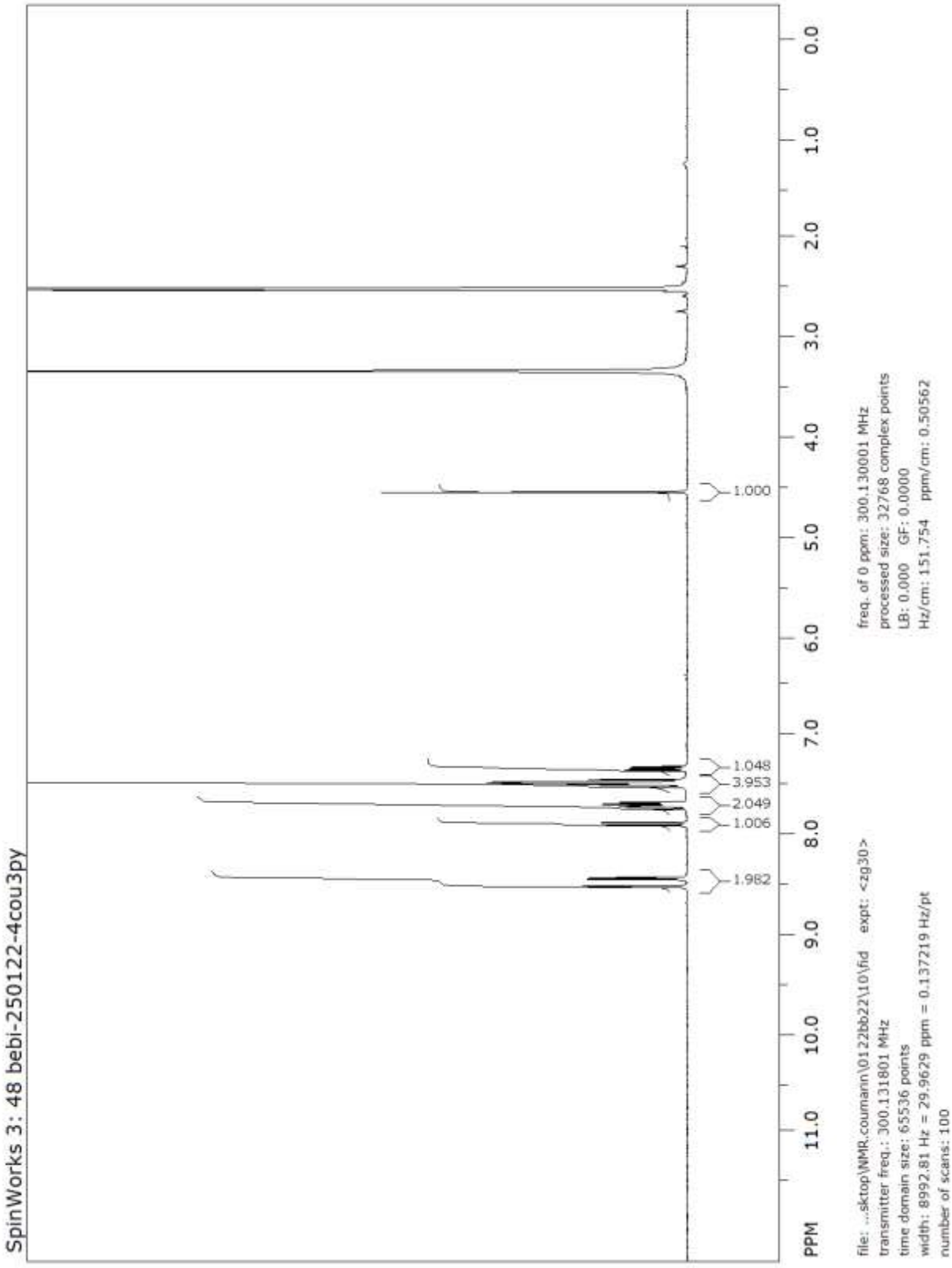

^{1}H NMR spectrum of **1m**

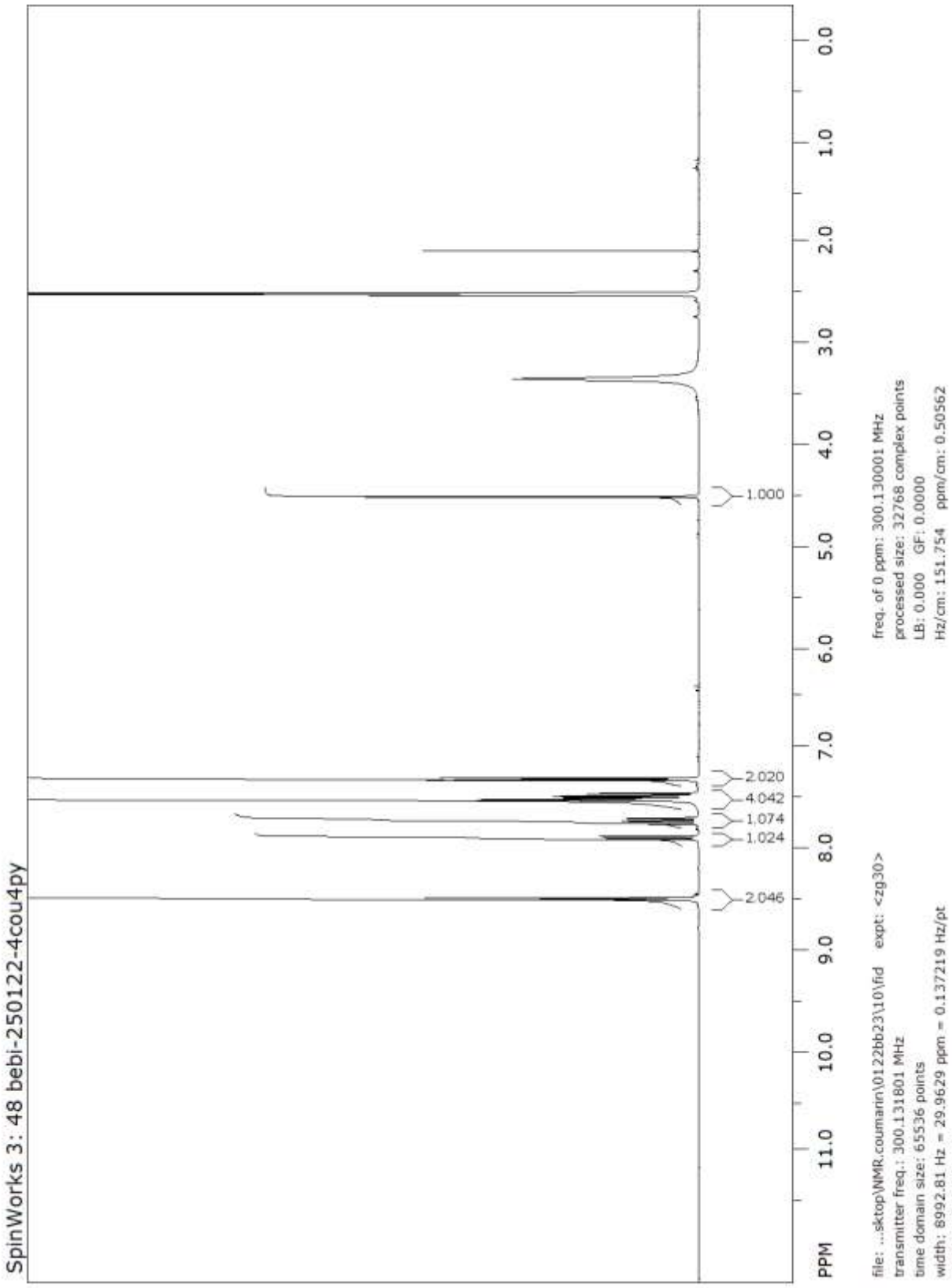

^{1}H NMR spectrum of **1o**

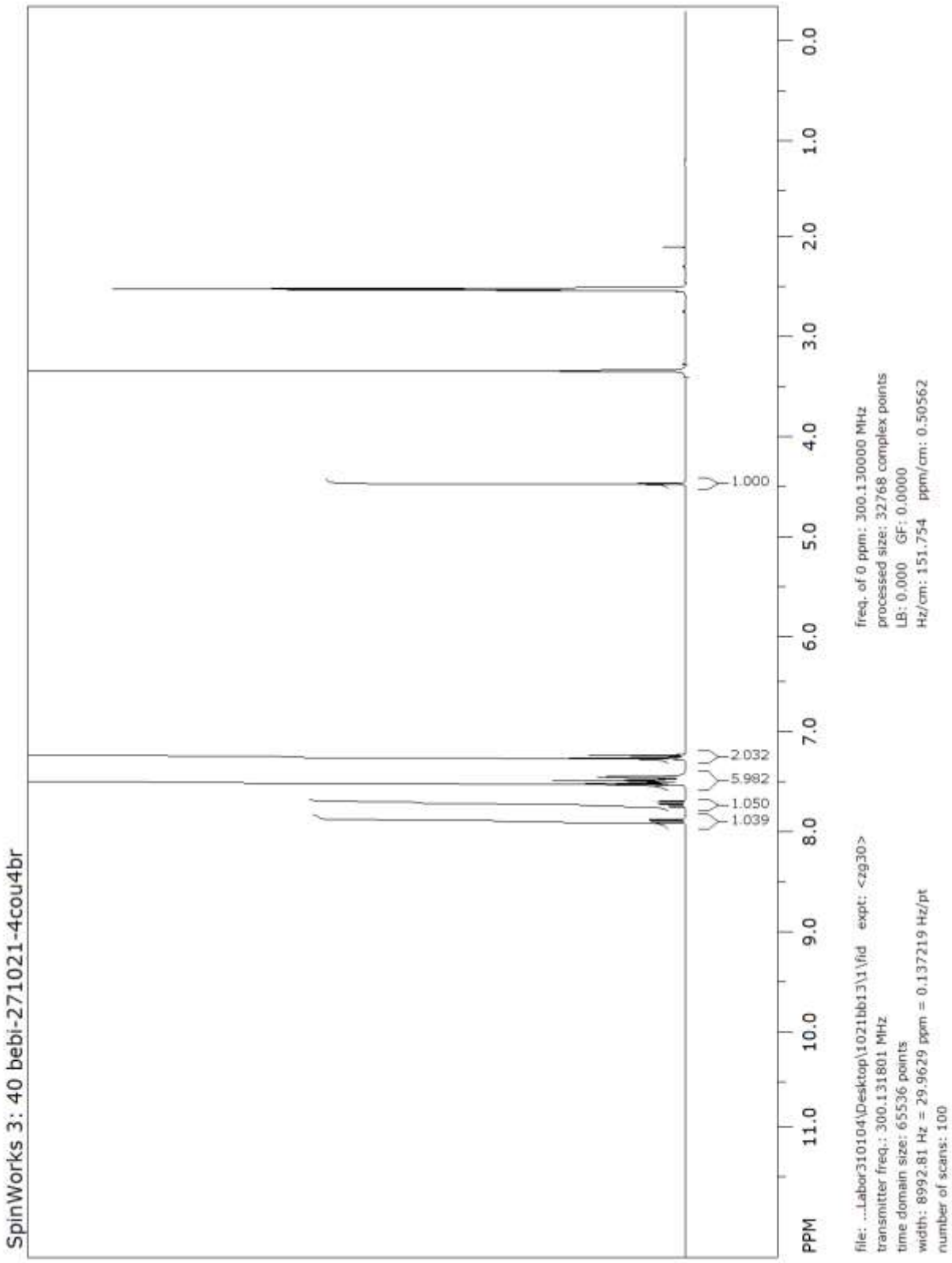

^{1}H NMR spectrum of **1p**

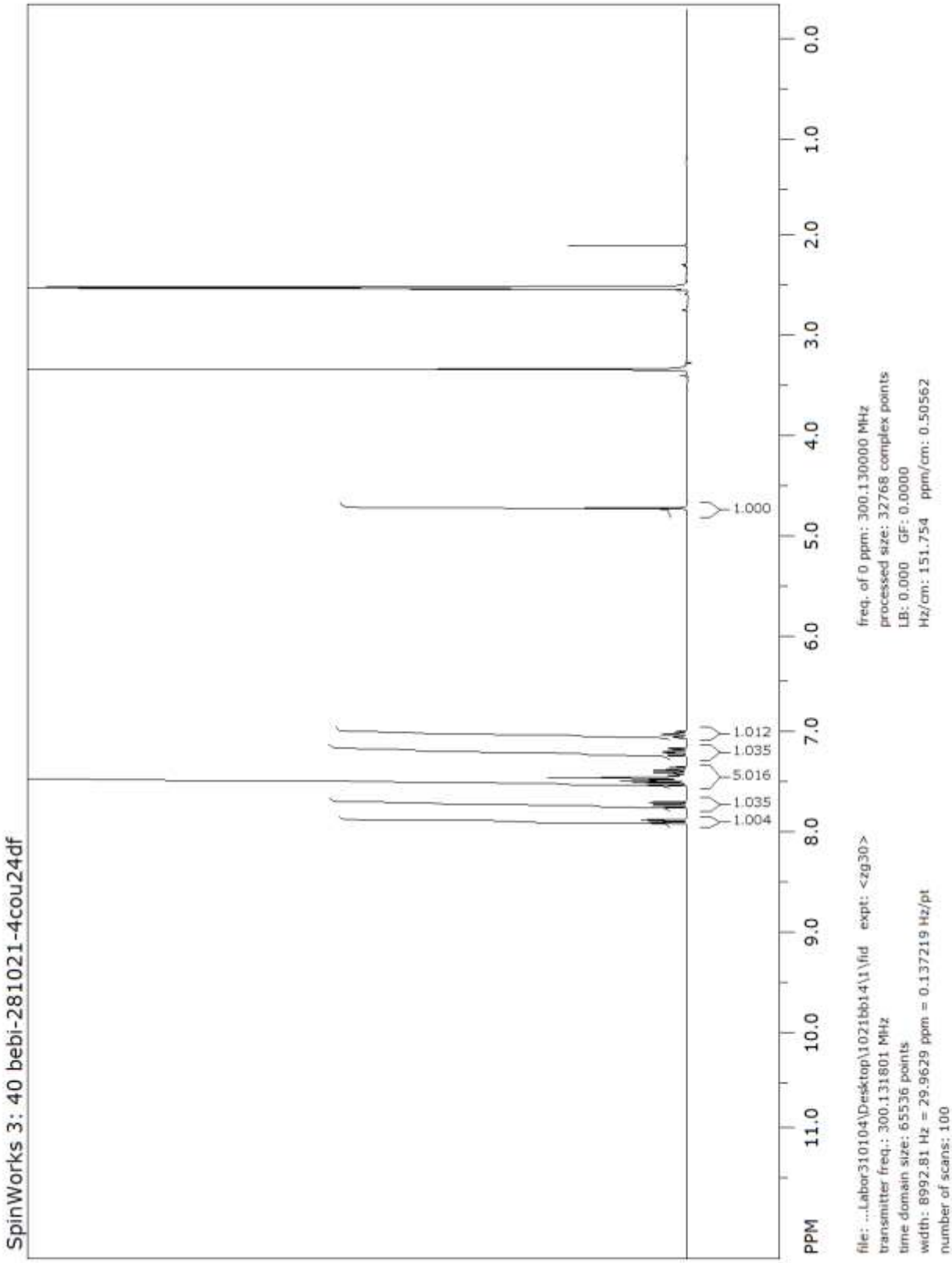

^{13}C NMR spectrum of **1p**

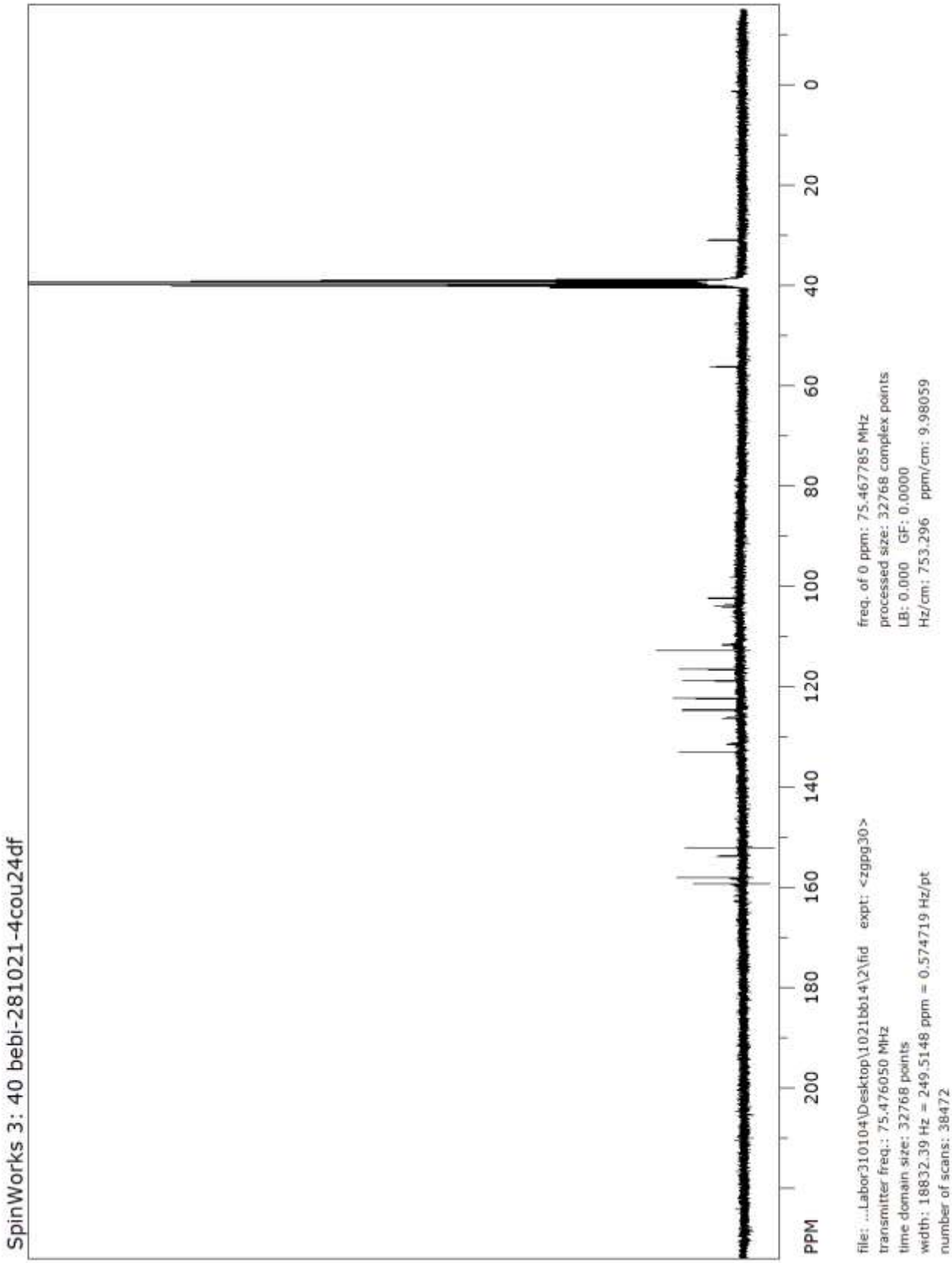

Results

Selectivity Index

To estimate their selectivity for cancer cells the three most active compounds **1a**, **1c**, **1d** were also tested on non-malignant adult human dermal fibroblasts (HDFa) via MTT-assays. The selectivity index (SI) for all tested cancer cell lines was calculated from the ratio of the average IC_{50} value and that of HDFa cells (Tab S1).

Table S1. Average IC_{50} value [µM] of all tested cancer cell lines the for compounds 1a, 1c and 1d and the calculated selectivity index (SI = IC_{50} nonmalignant HDFa cells / IC_{50} average of cancer cell lines). [1]

	Average IC_{50} value [µM]	Selectivity index (SI)
1a	3.41±1.5	29.3
1c	1.89±0.9	52.9
1d	3.21±1.0	31.1

Effects on the cell cycle

Effect of compounds **1a**, **1c**, **1d** as well as C-A4 and solvent (DMSO) on the cell cycle of 518A2 melanoma cells were assessed via PI staining and subsequent flow cytometry (Fig. S2).

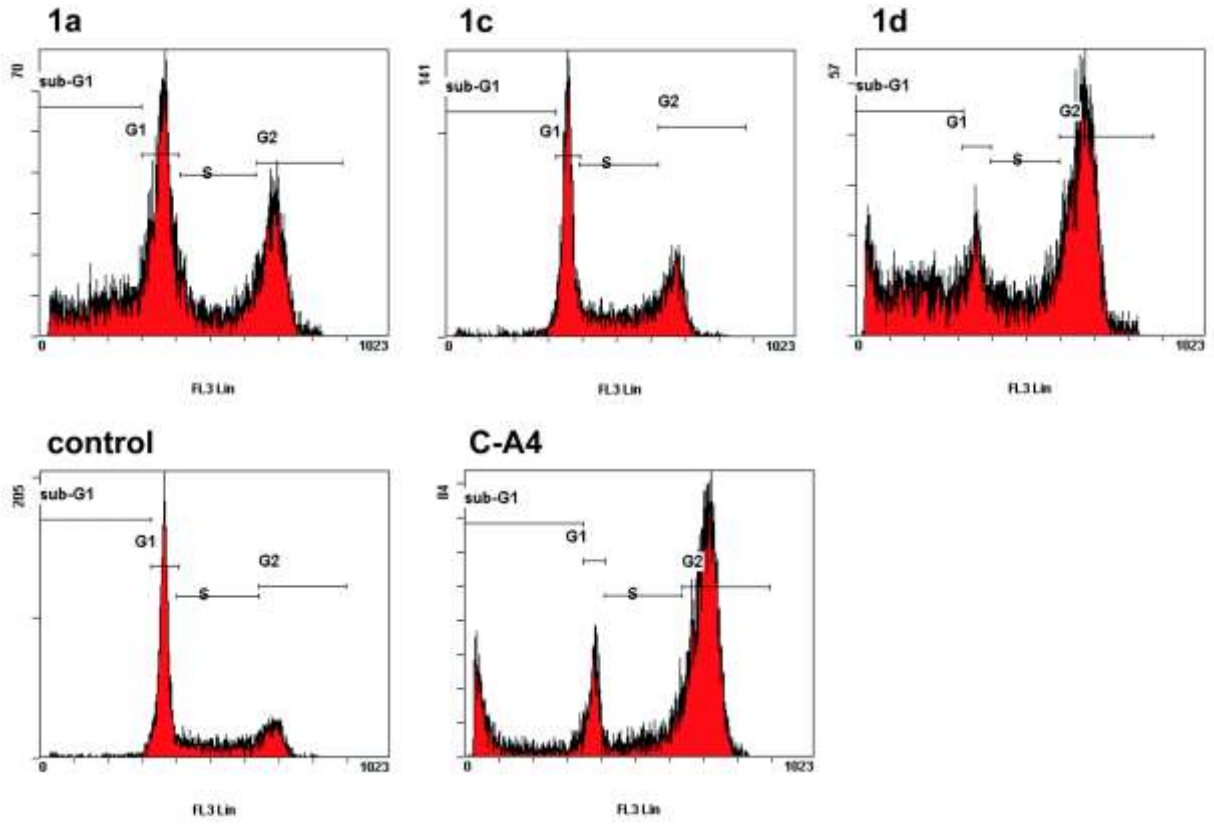

Figure S2. Representative cell cycle Histograms of 518A2 melanoma cells treated with 2.5 µM of **1a**, **1c**, **1d** or Combretastatin A4 (100 nM) for 12 h. Negative controls were treated with an equivalent amount of solvent (DMSO).

Caspase-3/7 activity

The activation of effector caspases 3 and 7 was investigated through an Apo-One® Homogenous Caspase-3/7 Assay Kit (Promega) after 6h of incubation with substances **1a**, **1c**, **1d** as well as C-A4 and vehicle DMSO (Fig S3).

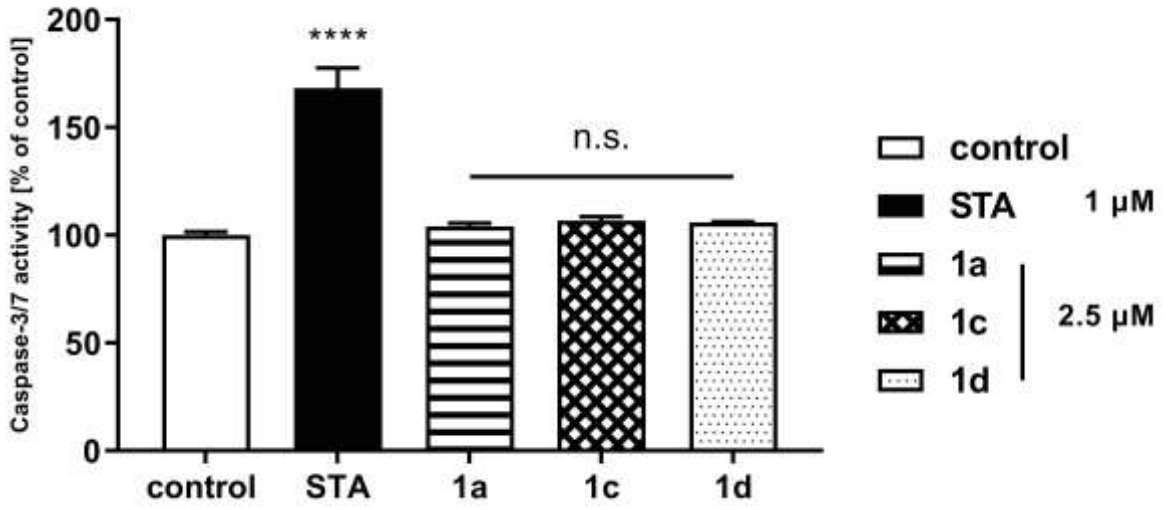

Figure S3. Measurement of caspase-3/7 activity via Apo-ONE® Homogenous Caspase-3/7 Assay Kit (Promega) after treatment of 518A2 melanoma cells with test compounds **1a**, **1c**, **1d** (2.5 µM) and staurosporine (1 µM). Solvent (DMSO) treated cells served as positive control and were set to 100%. Experiments were performed in triplicate and quoted as means ± SD. The significance was given as: ****: p <0.0001 against control, One-way ANOVA, with Dunnett's multiple comparison test (GraphPad Prism 7).

Tube-Formation viability (MTT-assay)

The vitality of the cells after treatment with **1a**, **1c**, **1d** as well as C-A4 and solvent (DMSO) for 3 h was determined by MTT assay to be higher than 80% compared to negative controls (Tab. S4).

Table S4. Viability of 518A2 melanoma cells after treatment with test compound 1a, 1c, 1d (1 and 2.5 µM) or C-A4 (100 nM) with vehicle (DMSO) treated cells set to 100%. Values were assessed by MTT-assay after 3 h of incubation under cell culture conditions.

	Concentration [µM]	Viability [% of control]
control	-	100.0
C-A4	0.1	81.1
1a	1.0	100.2
	2.5	106.9
1c	1.0	93.2
	2.5	81.0
1d	1.0	91.3
	2.5	84.7

References

[1] M. López-Lázaro, *Oncoscience* **2015**, *2*, 91.

4.3 Publikation II

New Naphthopyran Derivative Combines *c*-Myb Inhibition, Microtubule-Targeting Effects, and Antiangiogenic Properties

Leonhard H. F. Köhler,[a] Sebastian Reich,[a] Maria Yusenko,[b] Karl-Heinz Klempnauer,[b] Amin H. Shaikh,[c] Hhursheed Ahmed,[c] Gerrit Begemann,[d] Rainer Schobert,[a] und Bernhard Biersack.[a]*

[a] Organic Chemistry Laboratory University of Bayreuth, Universitätsstraße 30, 95440 Bayreuth (Germany)
[b] Institute for Biochemistry, Westfälische-Wilhelms-Universität, Wilhelm-Klemm-Strasse 2, 48149 Münster (Germany)
[c] Department of Chemistry & Post Graduate Research Center, Abeda Inamdar Senior College, Camp, Pune 411001 (India)
[d] Developmental Biology, University of Bayreuth, Universitätsstraße 30, Bayreuth 95440 (Germany)

*Corresponding author. E-Mail address: bernhard.biersack@yahoo.com

ACS Med. Chem. Lett. **2022**, *13, 1783*

ACS Medicinal Chemistry Letters

pubs.acs.org/acsmedchemlett Letter

A New Naphthopyran Derivative Combines *c*-Myb Inhibition, Microtubule-Targeting Effects, and Antiangiogenic Properties

Leonhard H. F. Köhler, Sebastian Reich, Maria Yusenko, Karl-Heinz Klempnauer, Amin H. Shaikh, Khursheed Ahmed, Gerrit Begemann, Rainer Schobert, and Bernhard Biersack*

Cite This: https://doi.org/10.1021/acsmedchemlett.2c00403 Read Online

ACCESS | Metrics & More | Article Recommendations | Supporting Information

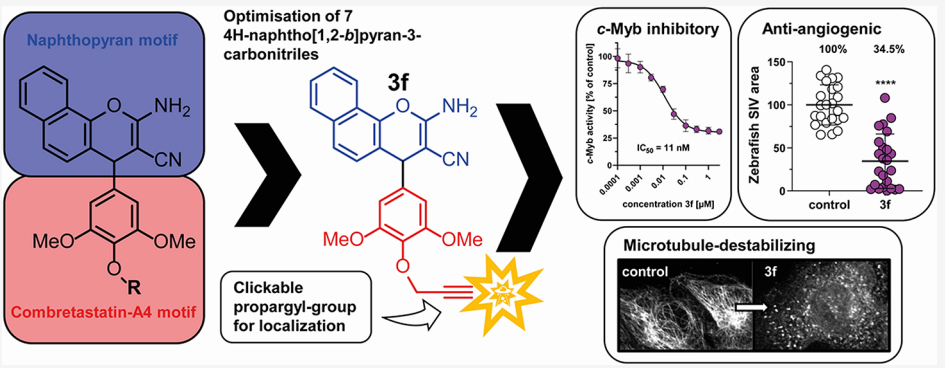

ABSTRACT: Based on the promising *c*-Myb inhibitor **1b**, a series of 2-amino-4-aryl-4*H*-naphtho[1,2-*b*]pyran-3-carbonitriles (**1a**, **2a**−**q**, **3a**−**g**) were repurposed or newly synthesized via a three-component reaction of 1-naphthol, and various aryl aldehydes and malononitrile and screened for their *c*-Myb inhibitory activities. **1b** also served as a lead compound for seven new naphthopyran derivatives (**3a**−**f**), which were cytotoxic with nanomolar IC_{50} values, to inhibit the polymerization of tubulin, and to destabilize microtubules in living cells. Especially, the alkyne **3f**, originally made for intracellular localization studies using click chemistry, showed an overall high activity in all assays performed. A strong G2/M cell cycle arrest was detected, which resulted in a distinct increase in sub-G1 cells through the induction of effector caspases 3 and 7. Inhibition of angiogenesis was confirmed *in vitro* and *in vivo*. In summary, **3f** was found to be a pleiotropic compound with high selectivity for cancer cells, combining *c*-Myb inhibitory, microtubule destabilizing, and antiangiogenic effects.

KEYWORDS: *Naphthopyran, Multitargeting, c-Myb, Microtubule, Antiangiogenesis*

The transcription factor *c*-Myb (encoded by the *MYB* proto-oncogene) plays a crucial role in hematopoietic cells and other tissues.[1] The coactivator and histone acetyltransferase p300 is a prominent interaction partner of *c*-Myb.[2] *c*-Myb is upregulated in leukemias and various solid cancers such as colon cancers, indicating its importance for tumorigenesis.[3−6] Hence, inhibitors of *c*-Myb activity and disruptors of the *c*-Myb/p300 interaction are suitable drug candidates for the treatment of leukemias and solid cancers. Until now, small molecules of various compound classes such as sesquiterpene lactones (e.g., mexicanin-I), naphthols (e.g., naphthol AS-E phosphate), naphthoquinones (plumbagin, shikonin, and naphthazarin), and podophyllotoxins (teniposide and etoposide) were identified as inhibitors of *c*-Myb function.[7−10]

Drug development, when target-oriented, is generally based on the screening of compound libraries, the elucidation of target-ligand interactions as well as of SAR and target/disease selectivities.[11] Multicomponent or domino reactions are excellent tools for the design of biologically active compounds since they allow the fast generation of compound libraries with variance in residues and stereo configurations by the ever same efficient carbon−carbon and/or carbon-heteroatom bond formation reactions in one pot and without the need of isolating and purifying intermediates. The starting materials and required reagents and catalysts are commercially available in most cases.[12]

Prominent examples of multicomponent reactions applied for drug development are those named after Ugi, Biginelli, Van Leusen, and modifications thereof.[13−15] An efficient synthesis of biologically active pyrans was reported, and multicomponent reactions using derivatives led to anticancer active com-

Received: August 25, 2022
Accepted: October 28, 2022

pounds.[16,17] The antiproliferative 2-amino-4-(3-nitrophenyl)-4*H*-naphtho(1,2-*b*)pyran-3-carbonitrile (LY290181, **1a**) was prepared by Dell et al. and identified as a microtubule-targeting agent (MTA) (Scheme 1).[18] Its 4-(3,4,5-trimethoxyphenyl)

Scheme 1. Reagents and Conditions: (i) Malononitrile, Aryl Aldehyde, Cat. Et_3N, MeCN, rt, 3−16 h, 35−79%. Structures of LY290181 (1a), c-Myb Inhibitor H (1b), and the Naphthopyrans 2a−q and 3a−g

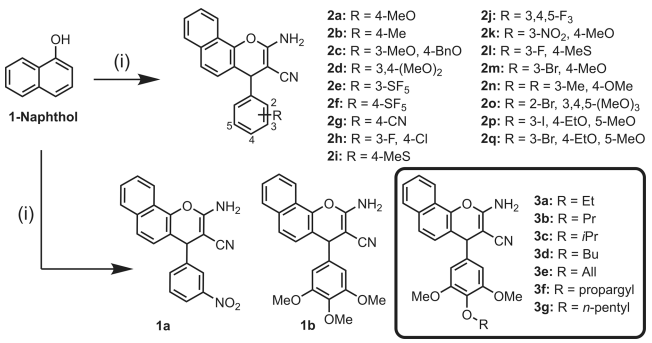

analogue **1b** (a.k.a. Bcr-TMP) was recently reported to be a highly potent inhibitor of *c*-Myb activity, which surpassed the *c*-Myb inhibitory activities of the above-mentioned *c*-Myb inhibitors by far.[19] Based on published works on related anticancer active pyrans derived from 1-naphthol, we tested a number of known anticancer active 2-amino-4-aryl-4*H*-naphtho[1,2-*b*]pyran-3-carbonitriles for *c*-Myb inhibition, as well as a series of close analogues of the *c*-Myb inhibitor **1b**, prepared for the first time.[16,17,19] The pronounced *c*-Myb inhibitory activity of **1b** warranted a deeper investigation of this class of naphthopyrans in order to identify structure−activity relationships and eventually improved *c*-Myb inhibitors. Among the test compounds **2**, halogenated analogues refer to known pro-apoptotic bromophenyl-substituted pyrans highlighting the relevance of halogens for drug design.[16] The new series **3** compounds have a 3,5-dimethoxy-4-alkoxy motif derived from **1b** and were investigated for *c*-Myb inhibition and tubulin-binding properties. In order to find out the underlying mechanisms of action of these compounds, further experiments on their microtubule destabilization, cell cycle arrest, cell death induction, intracellular localization, and antiangiogenic effects were carried out in this study.

The test compounds **1a−b**, **2a−q**, and **3a−g** were prepared from a mixture of 1-naphthol, malononitrile, the corresponding aryl aldehyde, and a catalytic amount of triethylamine in acetonitrile (Scheme 1). **1a−b**, **2a**, and **2d** are known from literature and have already been tested for c-Myb inhibition.[19] Here, some more substances should be investigated and structurally compared based on their c-Myb inhibition IC_{50} value. Based on the lead substance **1b**, a series of new naphthopyrans (**3a−g**) was prepared. The synthesis and analysis of the known compounds **1a**, **1b**, **2a−j**, and **2n** followed literature procedures.[16,17,20−23] The new compounds **2k−m**, **2o−q**, and **3a−g** were obtained as colorless solids in low to moderate yields. NMR, IR, and MS analyses confirmed the proposed structures. The stability of the substances **1a**, **1b**, and **3f** in aqueous solution was confirmed by ^1H NMR over 7 days (Figure S7, SI). Except for the isotopic exchange of the amino group with D_2O (7−7.5 ppm/δ) after 24 h, no changes in the spectrum were observed. The susceptibility of compounds to biotransformation could be excluded by treatment with cell lysate and subsequent UV absorption measurement after 24 h and RP-HPLC analysis after 72 h (Figures S9 and S10, SI). Drug-like properties are crucial for the design of new drug molecules and are typically based on the five guiding principles outlined by Lipinski (Table S2, SI). High gastrointestinal absorption (GI) but no blood-brain barrier permeability (BBB) was exhibited by all compounds. These features are observed in the BOILED-Egg model and bioavailability radar graphs (Figure S8, SI).

All compounds **1a−b**, **2a−q**, and **3a−g** were initially tested for their *c*-Myb inhibitory activity (Figure 1). Their half-

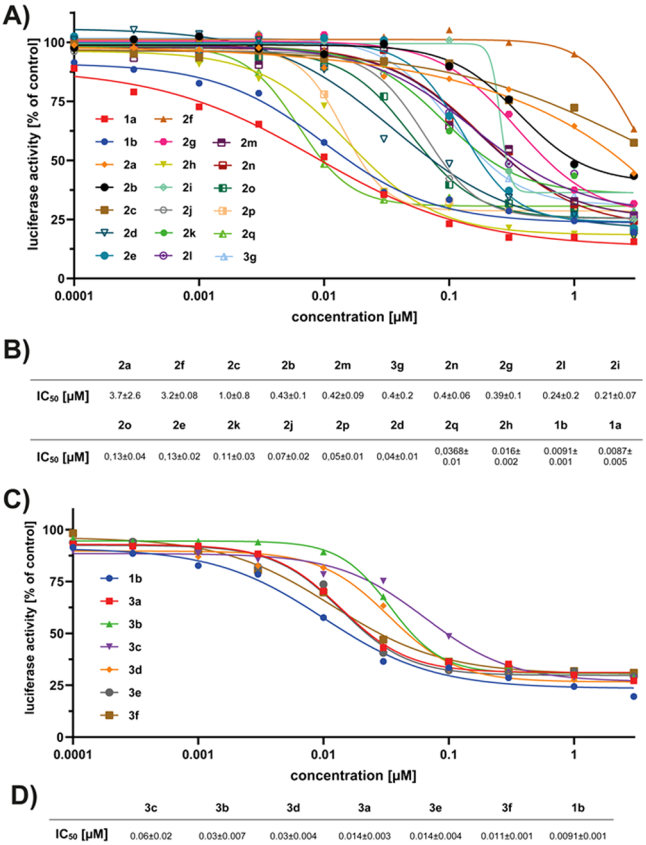

Figure 1. Values are representing the relative luciferase activity in HEKT cells transfected with the reporter plasmid pGL4−5xMRE-(GG)-Myc and the expression vector for MYB-2KR, treated with compounds **1a−b**, **2a−q**, and **3a−g** for 16 h (A and C). Values are means of at least four independent experiments. IC_{50} values were calculated using GraphPad Prism 9 and sorted by size (B and D).

maximal inhibitory concentrations ranged from single-digit micromolar to single-digit nanomolar values, showing a conspicuous dependency on the phenyl-substituents. Sterically demanding residues, such as Bn (**2c**) or SF_5 (**2f**), at the para position led to derivatives with weak *c*-Myb inhibition. The 4-SF_5 derivative **2f** showed an activity, weaker by more than an order of magnitude than that of its 3-SF_5 analogue **2e**. A comparably large loss of activity was observed for **1a** (3-NO_2) with an additional 4-methoxy group **2k** (3-NO_2, 4-MeO) or a methyl instead of a nitro group **2n** (3-Me, 4-MeO). Fluorination of the 3-position in **2l** led to distinctly increased activity when compared with **2i**, which lacks this fluorine. Other fluorinated derivatives such as **2h** and **2j** had an even higher activity. Most surprising was the large difference in IC_{50} values between anisyl, veratryl, and 3,4,5-trimethoxyphenyl

https://doi.org/10.1021/acsmedchemlett.2c00403
ACS Med. Chem. Lett. XXXX, XXX, XXX−XXX

compounds **2a** (3.7 μM), **2d** (0.04 μM) and **1b** (0.009 μM), showing activities increasing with the number of methoxy substituents. Another interesting aspect was a 10-fold decrease in activity of the trimethoxy motif (**1b**) when a bromine group was inserted at position 2 (**2o**). As already shown by Yusenko et al., the amino- and cyano-groups of the naphthopyran scaffold are important for anti-*c*-Myb activity.[19] However, the functional groups at the phenyl ring appear to be quite flexible and allow multiple functional groups for optimization. Here we showed that H-bond acceptors like methoxy- (**1b**), nitro- (**1a**), pentafluorosulfanyl- (**2e**) or halogen substituents (**2h**) can have a positive effect on activity, whereas nonpolar groups like methyl- (**2b**), benzyloxy- (**2c**), or pentoxy- (**3g**) are decreasing it.

Next, we used the structure of **1b** as a lead for the design of refined *c*-Myb inhibitors **3**, bearing modified 4-alkoxy groups (Scheme 1). The compounds **3a** (R = ethyl), **3e** (R = allyl), and **3f** (R = propargyl) were only slightly less active *c*-Myb inhibitors when compared with **1b**. In contrast, compounds **3b**, **3c**, and **3d** bearing longer-chained or bulkier saturated alkoxy residues showed distinctly weaker *c*-Myb inhibitory activities, which, however, still exceeded most of the compound **2** series. Analogously, the 4-ethoxy compounds **2p** and **2q** containing a 3-iodo or 3-bromo substituent exhibited slightly lower *c*-Myb inhibitory activities when compared with the 3,5-dimethoxy-4-ethoxyphenyl compound **3a**, with the bromo-substituent being slightly superior to the iodo-substituent. **3g** was not investigated further because of its significantly lower inhibitory activity against *c*-Myb indicating distinctly reduced inhibitory effects by compounds bearing longer alkoxy chains in *para*-position. When restricted to variations of the phenyl substituents, the SAR studies suggested the 3,4,5-trimethoxyphenyl motif of **1b** near the optimum in terms of *c*-Myb inhibition, also reached only by compounds **2h**, **3a**, **3e**, and **3f**.

The new compounds **3a**−**f** and controls **1a**−**b** were tested for their antiproliferative activity against a panel of nine tumor cell lines of five different entities and one endothelial hybrid cell line (EA.hy926) via MTT assays and compared with some previously published compounds **2c** and **2e**−**i** (Table 1). Looking at the IC_{50} values, *c*-Myb inhibition roughly correlates with cytotoxicity. The positive controls **1a** and **1b** as well as compound **3f** showed excellent antiproliferative activities (low nanomolar IC_{50} values) in most tumor cell lines. Compounds **2c**,**f**,**g**,**i** had shown comparatively low activities (single to double-digit micromolar IC_{50} values) in previous tests on cell lines 518A2 and HT-29, while **2e** and **2h** had been more active with submicromolar IC_{50} values.[17] In general, HT-29 was the cell line most insensitive to all compounds tested, except for **3f** (IC_{50} = 36.9 nM). The IC_{50} values averaged over all cell lines, showed that **3a** and **3f** were the most active compounds with mean IC_{50} values of ca. 27 nM (**3f**) and ca. 43 nM (**3a**), followed by **3b** (ca. 55 nM), **3e** (ca. 73 nM), **3d** (ca. 150 nM), and **3c** (ca. 564 nM).

To investigate the selectivity for cancer cells, the compounds **1b** and **3a**−**f** were also tested on nonmalignant adult human dermal fibroblasts (HDFa) by the MTT assay. Although the dose−response curves showed a concentration-dependent decrease in proliferation, a clear resistance of the HDFa cells to the test substances was observed (Figures S1 and S2, SI).

The compounds **1a** and **1b** have already been shown to inhibit tubulin polymerization and to destroy microtubules in a manner comparable to that of combretastatin-A4 (C-A4).[18,19] Naphthopyran **1b** carries a 3,4,5-trimethoxyphenyl motif,

Table 1. Inhibitory Concentrations IC_{50} [nM][a] of Compounds 1a−b, 2c, 2e−i, and 3a−f When Applied to EA.hy926 Endothelial Hybrid Cells, 518A2 Melanoma, HCT-116, HCT-116p53−/− (p53 knockout mutant), and HT-29 Colon Carcinomas, KB-V1Vbl Multidrug-Resistant (MDR) Cervix Carcinoma, U-87 Glioblastoma, MCF-7 Breast Carcinoma, and HeLa Cervix Carcinoma

	EA.hy 926	518A2	HCT-116^{wt}	HCT-116$^{p53-/-}$	HT-29	KB-V1$^{Vbl.}$	KB-V1$^{Vbl.c}$	U-87	MCF-7	HeLa	average IC_{50}
1a	29.5 ± 1.2	10.8 ± 1.4	7.57 ± 0.68	28.2 ± 2.7	32.1 ± 2.82	23.7 ± 2.31	76.1 ± 2.4	67.7 ± 8.9	182.5 ± 19.0	36.1 ± 1.67	49.4
1b	19.9 ± 1.2	28.8 ± 0.01	22.2 ± 1.91	27.6 ± 1.9	324 ± 30	26.4 ± 1.2	8.8 ± 1.3	5.2 ± 0.15	34.1 ± 2.45	11.3 ± 1.1	50.8
2c	-	1660 ± 430[b]	-	-	5820 ± 570[b]	-	-	-	-	-	-
2e	-	505 ± 38[b]	-	-	570 ± 41[b]	-	-	-	-	-	-
2f	-	7130 ± 900[b]	-	-	9970 ± 410[b]	-	-	-	-	-	-
2g	-	939 ± 122[b]	-	-	1227 ± 117[b]	-	-	-	-	-	-
2h	-	425 ± 62[b]	-	-	172 ± 18[b]	-	-	-	-	-	-
2i	-	1980 ± 189[b]	-	-	1102 ± 72[b]	-	-	-	-	-	-
3a	6.2 ± 0.04	25 ± 1.4	22.7 ± 2.03	13.1 ± 0.5	269 ± 8.6	20.9 ± 2.3	16.5 ± 0.7	10.6 ± 0.8	28.1 ± 1.78	21.9 ± 2.3	43.4
3b	11.9 ± 0.8	26.1 ± 3.2	68.5 ± 7.4	33.1 ± 0.2	284 ± 25.4	23.1 ± 2.1	16.3 ± 1.5	27.4 ± 3.0	21.4 ± 1.08	33.1 ± 2.8	54.5
3c	65.8 ± 4.1	266 ± 10.7	274 ± 16.7	137 ± 6.7	4314 ± 166	89 ± 10	105 ± 7.3	53.1 ± 4.2	265 ± 6	72 ± 5.04	564
3d	78 ± 7.1	143 ± 36.6	67.4 ± 5.	172 ± 11.9	671 ± 28	84.5 ± 8.2	41.6 ± 6.4	46.3 ± 6.9	103 ± 10.4	98.9 ± 9.9	151
3e	15.7 ± 1.4	3.6 ± 0.3	193 ± 12.3	15.9 ± 0.7	395 ± 26	18.7 ± 1	15.9 ± 1.9	5.7 ± 0.4	43.3 ± 2.7	22.2 ± 2.2	72.9
3f	17.1 ± 0.3	20.6 ± 1.3	75.2 ± 4.3	19.9 ± 0.6	36.9 ± 0.9	60.6 ± 2.6	10.6 ± 1.1	5.2 ± 0.06	2.6 ± 0.3	24 ± 1.2	27.3

[a]Values are the means of at least four independent experiments ± SD. They were derived from concentration−response curves obtained by measuring the percentage of vital cells relative to untreated controls after 72 h using MTT-assay. [b]Values taken from Schmitt et al.[17] [c]Compound treatment plus verapamil (1 μM).

https://doi.org/10.1021/acsmedchemlett.2c00403
ACS Med. Chem. Lett. XXXX, XXX, XXX−XXX

which is frequently found in tubulin binders such as C-A4 and colchicine.[24] We now investigated the influence of the 3,4,5-trialkoxyphenyl analogues **3a–f** (5 μM) on the *in vitro* polymerization of tubulin (Figure 2A). Again, the 4-

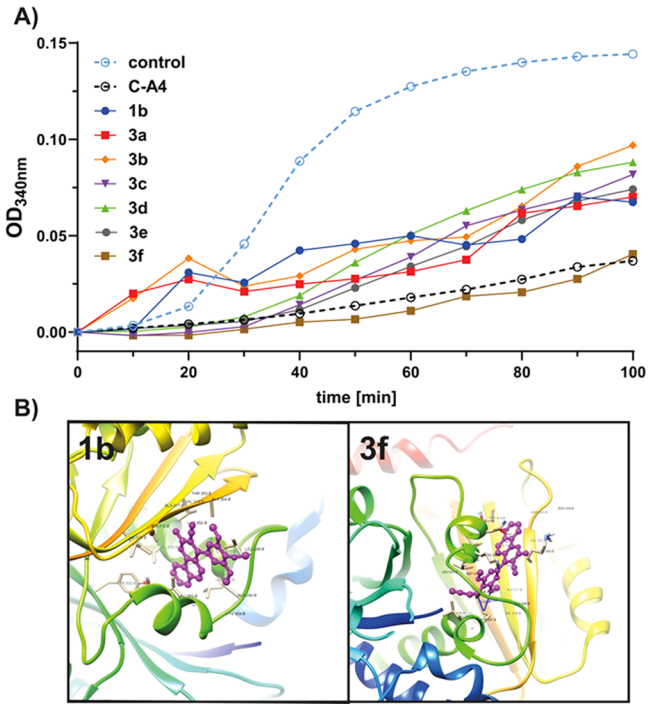

Figure 2. (A) Inhibition of *in vitro* polymerization of tubulin by **1b** and **3a–f** (5 μM) measured by a turbidimetric assay at 340 nm at 10 min intervals for 100 min. The vehicle DMSO and C-A4 (5 μM) served as controls. Values are means of at least two independent experiments. (B) Visualization of **1b** and **3f** docked in the colchicine binding pocket of tubulin (1sa0) using PYMOL (18 × 22 × 20 Å simulation box).

propargyloxy derivative **3f** stood out as the most potent inhibitor surpassing even the positive control C-A4. However, the other test compounds also showed a distinct inhibitory effect on tubulin polymerization with no discernible gradation. This superiority of the 4-propargyloxy group for the interaction with purified tubulin has so far never been reported or been taken into account for the optimization of tris(alkoxy) phenyl substituted tubulin binders.[17,25] A comparative molecular docking analysis for the interaction of compounds **1b** and **3f** with the colchicine binding site of tubulin was carried out using AutoDock 4.2.6 with Lamarckian genetic algorithm and empirical free energy scoring function (Figure 2B).[26] The arrangement of the substances within the colchicine binding site showed two different possible orientations, but the exact binding mode can only be confirmed by X-ray crystallography.

For **1b**, the naphthopyran motif was located within the binding pocket, whereas for **3f**, the 3,5-dimethoxy-4-propargylphenyl moiety was located within the binding site.

The docking afforded binding energies and inhibition constants of −7.93 kcal/mol and 1.53 μM (**1b**) or −8.69 kcal/mol and 0.43 μM (**3f**), and they revealed the H-bonds and amino acids are mainly involved (Table S1, SI). This proves a stronger interaction of **3f** with the binding pocket and explains the stronger inhibition of in vitro tubulin polymerization.

The compounds **1b** and **3a–f** (25 nM) were then applied to 518A2 melanoma cells. The microtubules and actin filaments of treated cells were immunostained after 24 h and the effects on the cytoskeletons documented (Figure 3). A disruption of the microtubular cytoskeleton comparable to that of positive control C-A4 (25 nM), as evidenced by fragmented microtubules and intensely fluorescent areas within the cells, was observed with all substances except **3c**. The loss of structural integrity due to a destroyed tubulin cytoskeleton not only affects the mobility and proliferation of the cells but also can lead to a RhoA-dependent formation of so-called actin stress fibers.[27] In epithelial cells, such as the 518A2 melanoma cells used, actin stress fibers are particularly abundant and serve cell adhesion and morphogenesis.[28] The microscopic images of phalloidin-stained actin (green) showed the formation of actin stress fibers (white arrows), especially in the cells with destroyed microtubules. In contrast to the DMSO control, areas with dorsal stress fibers and transverse arcs can be seen, mainly in C-A4, **1b**, **3a–b**, and **3d–f** treated cells.[29]

Using copper(I)-catalyzed azide–alkyne click reactions, the alkyne derivative **3f** was linked to 3-azido-7-hydroxycoumarin via cycloaddition, producing a fluorescent triazole which was visualized by confocal microscopy in 518A2 melanoma cells (Figure S4, SI).[30] Within 15 min, the uptake of **3f** into the cells was observed, with accumulation mainly in the cytoplasm. This is consistent with the prior identified target, tubulin, predominantly occurring in the cytoplasm.

The impairment of the tubulin cytoskeleton is always accompanied by effects on the cell cycle of proliferating cells.[31] The perturbation of chromosome segregation activates the spindle assembly checkpoint (SAC) leading to mitotic arrest and subsequent cell death.[32,33] The time-dependent effect of compounds **1b** and **3a–f** (25 nM), as well as C-A4 (25 nM) and solvent (DMSO) on the cell cycle of 518A2 melanoma cells was examined by FACS analysis. The treated cells were analyzed after 6, 12, and 24 h of incubation and the percentage ratio of cells in individual cell cycle phases was depicted as line graphs (Figure 4).

Except for **3d** all tested compounds gave rise to a distinct increase in sub-G1 and G2/M-phase cells, when compared with solvent-treated cells. **1b**, **3a**, **3e**, and **3f** turned out to induce a strong G2/M cell cycle arrest comparable with that of the positive control C-A4. Cells arrested in the G2/M phase reached their maximum after 12 h and partially entered the sub-G1-phase after 24 h. In contrast to C-A4 treated cells, the cells arrested in G2/M entered the sub-G1 phase more quickly, which would suggest a more rapid induction of cell death by substances **1b**, **3a**, **3e**, and **3f**. Since it is not possible to differentiate between apoptotic and necrotic cells within the sub-G1 population, the activity of effector caspases 3 and 7 was determined after 6 and 24 h (Figure S5, SI). While staurosporine (STA) triggered caspase-3/7 activity after 6 h through direct caspase activation, the test compounds and C-A4 led to a significant increase after only 24 h. The late induction of effector caspases indicates an apoptosis mechanism through mitotic arrest and subsequent initiation of caspase cascades, as proposed for C-A4.[34]

Since the impairment of the cytoskeleton and cell cycle can also affect angiogenesis, the influence of the test substances on the formation of vessel-like 2D structures in the EA.hy926 endothelial tube-formation model was investigated (Figure S6, SI).[35] Clear indications of an antiangiogenic mode of action of the substances were shown, with **1b**, **3b**, and **3f** standing out.

https://doi.org/10.1021/acsmedchemlett.2c00403
ACS Med. Chem. Lett. XXXX, XXX, XXX–XXX

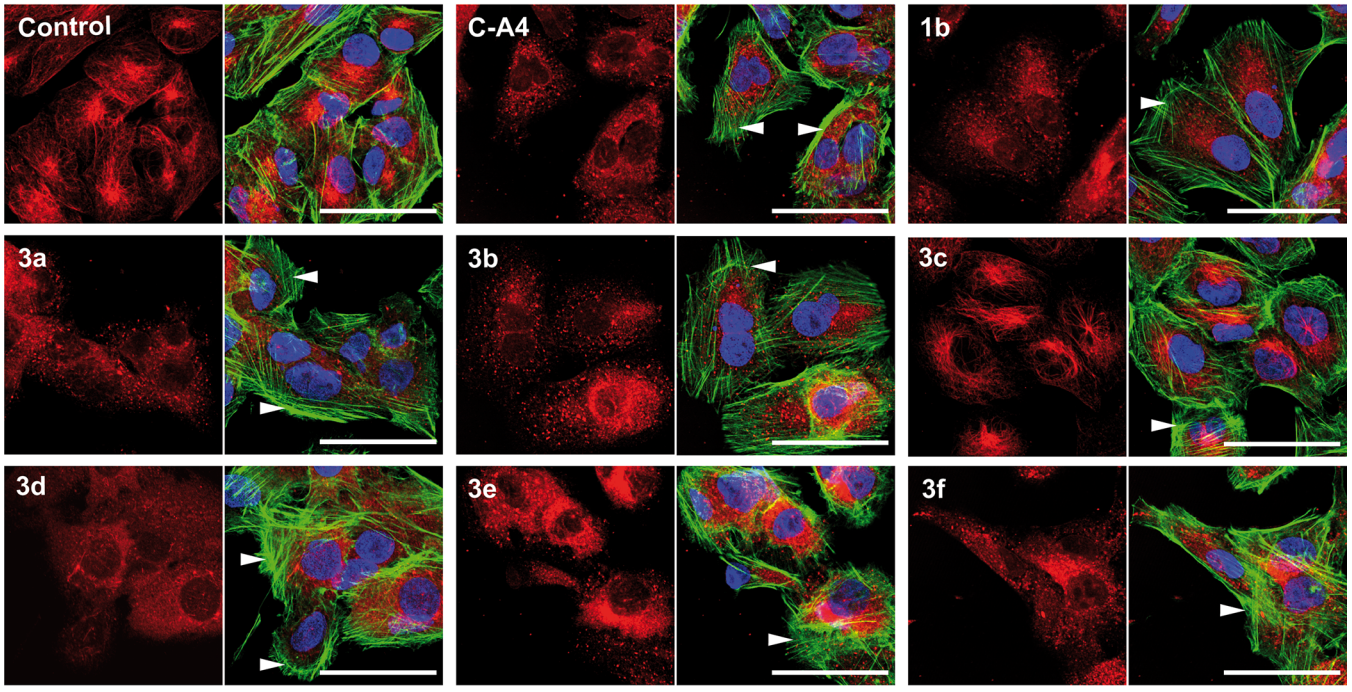

Figure 3. Effects of compounds **1b** and **3a–f** (25 nM) on the tubulin and actin cytoskeleton of 518A2 melanoma cells after 24 h of treatment. Vehicle DMSO and C-A4 (25 nM) served as controls. The left panels show the microtubules (red), the right panels the merge of actin filaments (green), nuclei (blue) and tubulin (red). White arrows indicate the formation of actin stress fibers. Images are representative of at least three independent experiments. Magnification 630×, scale bars correspond to 50 μm.

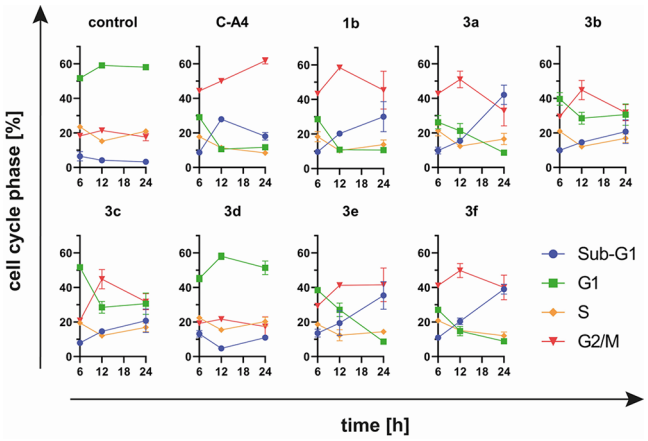

Figure 4. Effect of compounds **1b**, **3a–f**, C-A4 (25 nM) or solvent (DMSO) on the cell cycle phases of 518A2 melanoma cells after 6, 12, and 24 h of treatment. Experiments were performed at least in duplicate with 10 000 counted cells each and quoted as means ± SD.

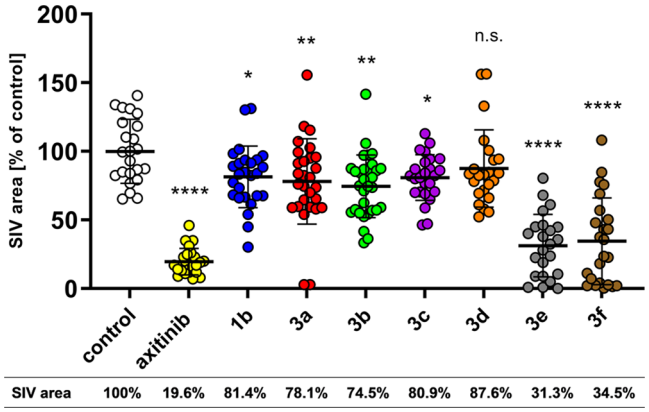

Figure 5. Antiangiogenic effects of **1b** and **3a–f** (100 nM) on the SIVs of zebrafish embryos after 48 h exposure. Negative controls were treated with vehicle DMSO and positive controls with axitinib (500 nM). Area of SIVs illustrated as the mean ± SD of at least 23 zebrafish quantified using ImageJ. The significance was given as n.s.: $p > 0.05$; *: $p < 0.05$; **: $p < 0.01$; ****: $p < 0.0001$ against control, one-way ANOVA, with Dunnett's multiple comparison test (GraphPad Prism 9).

The growth of the so-called subintestinal vessels (SIVs) during the embryonal development of zebrafish larvae is another reliable evaluation indicator for angiogenesis affecting substances.[36] Treatment of transgenic casper-zebrafish embryos (fli1:EGFP) 24 h post fertilization (hpf) for 48 h with substances **1b**, **3a–f** (100 nM), axitinib (500 nM) or C-A4 (10 nM) revealed several interesting insights (Figure S11, SI). In terms of substance concentration, the 10-fold higher tolerance for the test substances compared to the positive control C-A4 (results not shown) stands out and suggests a lower *in vivo* toxicity to vertebrates. SIV area quantification revealed a significant decrease through **3e** (31.3%) and **3f** (34.5%) when compared with solvent-treated fish (Figure 5B). The well-known angiogenesis inhibitor axitinib achieved a reduction to 19.6%, though with a 5-fold higher concentration.[37] The compounds **1b** and **3a–d** had a merely weak effect with a reduction to 75.5–87.6%.

With the growing interest in multitarget drugs as therapeutic agents, the purpose of this work was to get deeper insight into the therapeutic potential of the *MYB*-inhibitory, and microtubule destabilizing compound **1b** and some of its derivatives.[19] Structurally, the compounds are a combination of the microtubule destabilizing and cell cycle arresting naphthopyran LY290282 (**1a**) and the vascular targeting C-A4. SAR studies of various known naphthopyrans (**1a–b** and **2a–q**) revealed

https://doi.org/10.1021/acsmedchemlett.2c00403
ACS Med. Chem. Lett. XXXX, XXX, XXX–XXX

the importance of the 3,5-dimethoxy-4-alkoxyphenyl motif for *c*-Myb inhibition. Despite an attenuation by larger alkyl residues, the propargyl derivative **3f** impressed with high cytotoxicity and strong tubulin depolymerization. Compound **3f** stood out with low nanomolar IC_{50} values surpassing even the effects of C-A4 and **1a**. Its high selectivity for cancer over nonmalignant cells bodes well for a conceivable applicability in man. According to SwissADME *in silico* predictions, most of the substances are suitable for oral application and possess drug-like properties, which makes them candidates for detailed *in vivo* studies. The inhibition of tubulin polymerization, its high affinity toward the colchicine binding site and the microtubule destabilization properties in 518A2 melanoma cells of **3f** showed that the so far poorly studied 3,5-dimethoxy-4-propargylphenyl moiety could represent an interesting structural motif for new MTAs. A practical bonus aspect of this structural motif is that it can be monitored within living cells by means of fluorescent labeling via click reactions, which greatly simplifies the observation of uptake and accumulation. Compound **3f** was found to accumulate mainly in the cytoplasm of 518A2 melanoma cells, which is another hint at tubulin being a major target. The destruction of the microtubular cytoskeleton of cells by **3f** resulted in further beneficial effects, such as the formation of actin stress fibers and a strong G2/M cell cycle arrest. The transition of mitotic arrest to sub-G1 phase (cell death) occurred faster than for C-A4, suggesting a quicker apoptosis mechanism for the tested naphthopyrans. In contrast to C-A4, which isomerizes and loses its activity in aqueous solution, these naphthopyrans are stable for at least 7 days. Even under metabolic conditions, no biotransformation of **3f** could be detected after 72 h. It is worthy of note that loss of *MYB* function can sensitize tumor cells to apoptosis, suggesting a bimodal mechanism of mitotic arrest and subsequent mitotic catastrophe coupled with accelerated apoptosis induction by *c*-Myb inhibition.[38] It is known that the effect of MTAs is not limited to inhibition of cancer cell proliferation but can also attenuate the recruitment of blood vessels within a growing tumor.[39,40] The antiangiogenic potential was investigated using *in vitro* (EA.hy926 tube formation assay) and *in vivo* (SIV angiogenesis in zebrafish) models. The zebrafish model allowed both the demonstration of a 10-fold lower *in vivo* toxicity compared to C-A4 and the identification of **3e** and **3f** as potent angiogenesis inhibitors in a vertebrate system. It therefore seems likely that the inhibition of SIV growth is related to the alkenyl (**3e**) or alkynyl (**3f**) residue. More specific statements regarding the mechanism cannot be made at this point. The antiangiogenic properties make **3f** an especially interesting new lead structure superior to **1b** in this regard. This finding implies an additional mechanism of action of **3f** and highlights the novel 3,5-dimethoxy-4-propargyloxyphenyl motif as a potent pharmacophore. Simulations of drug likeness using SwissADME revealed favorable pharmacokinetic properties, as well as high gastrointestinal absorption. Taken together, compound **3f** represents a multimodal agent that combines *c*-Myb inhibition, MTA-associated effects, and antiangiogenic properties. Thus, the fusion of the 2-amino-4*H*-naphtho(1,2-*b*)pyran-3-carbonitrile backbone of **1a** (LY290181) with an intracellular localizable 3,5-dimethoxy-4-proparagyloxy moiety (**3f**) derived from C-A4, generated a promising pleiotropic compound and potential lead structure for further studies.

■ ASSOCIATED CONTENT

Supporting Information

The Supporting Information is available free of charge at https://pubs.acs.org/doi/10.1021/acsmedchemlett.2c00403.

Experimental section, NMR spectra, HDFa vitality-decrease, molecular docking analysis, Intracellular localization via copper catalyzed click reaction, caspases 3/7 assay, EA.hy926 tube-formation assay, Hydrolytic stability testing via ^{1}H NMR, drug-likeness and pharmacokinetic studies, metabolic stability monitored by UV-absorption, RP-HPLC analysis of substance stability, zebrafish angiogenesis assay (PDF)

■ AUTHOR INFORMATION

Corresponding Author

Bernhard Biersack − *Organic Chemistry Laboratory, University of Bayreuth, 95440 Bayreuth, Germany;* orcid.org/0000-0001-7305-346X; Email: bernhard.biersack@uni-bayreuth.de

Authors

Leonhard H. F. Köhler − *Organic Chemistry Laboratory, University of Bayreuth, 95440 Bayreuth, Germany*

Sebastian Reich − *Organic Chemistry Laboratory, University of Bayreuth, 95440 Bayreuth, Germany*

Maria Yusenko − *Institute for Biochemistry, Westfälische-Wilhelms-Universität, 48149 Münster, Germany*

Karl-Heinz Klempnauer − *Institute for Biochemistry, Westfälische-Wilhelms-Universität, 48149 Münster, Germany;* orcid.org/0000-0002-5239-7690

Amin H. Shaikh − *Department of Chemistry & Post Graduate Research Center, Abeda Inamdar Senior College, Camp, Pune 411001, India*

Khursheed Ahmed − *Department of Chemistry & Post Graduate Research Center, Abeda Inamdar Senior College, Camp, Pune 411001, India*

Gerrit Begemann − *Developmental Biology, University of Bayreuth, 95440 Bayreuth, Germany*

Rainer Schobert − *Organic Chemistry Laboratory, University of Bayreuth, 95440 Bayreuth, Germany;* orcid.org/0000-0002-8413-4342

Complete contact information is available at: https://pubs.acs.org/10.1021/acsmedchemlett.2c00403

Author Contributions

The manuscript was written through contributions of all authors. All authors have given approval to the final version of the manuscript.

Funding

M.Y. and K.H.K. are grateful to the Wilhelm-Sander-Stiftung (2020.071.1).

Notes

The authors declare no competing financial interest.

■ ACKNOWLEDGMENTS

We thank Sebastian Schleser (Organic Chemistry Laboratory, University of Bayreuth) for technical assistance with the ^{1}H NMR drug stability studies. We also thank Ole Bundgaard (Bioorganic Chemistry, University of Bayreuth) for his support in the method development of the RP-HPLC analytic and the measurements performed. We would further like to thank Prof.

Dr. Carlo Unverzagt for providing the Waters ACQUITY UPLC system.

■ ABBREVIATIONS

MTA, microtubule-targeting agent; MDR, multi drug resistant; IC_{50}, half maximal inhibitory concentration; HDFa, adult human dermal fibroblasts; C-A4, combretastatin A4; SAC, spindle assembly checkpoint; STA, staurosporine; SIVs, subintestinal vessels; hpf, hours post fertilization

■ REFERENCES

(1) Ramsay, R. G.; Gonda, T. J. MYB function in normal and cancer cells. *Nat. Rev. Cancer* **2008**, *8* (7), 523−534.
(2) Zor, T.; De Guzman, R. N.; Dyson, H.J.; Wright, P. E. Solution structure of the KIX domain of CBP bound to the transactivation domain of c-Myb. *J. Mol. Biol.* **2004**, *337* (3), 521−534.
(3) Anfossi, G.; Gewirtz, A. M.; Calabretta, B. An oligomer complementary to c-myb-encoded mRNA inhibits proliferation of human myeloid leukemia cell lines. *Proc. Natl. Acad. Sci. U.S.A.* **1989**, *86* (9), 3379−3383.
(4) Calabretta, B.; Sims, R. B.; Valtieri, M.; Caracciolo, D.; Szczylik, C.; Venturelli, D.; Ratajczak, M.; Beran, M.; Gewirtz, A. M. Normal and leukemic hematopoietic cells manifest differential sensitivity to inhibitory effects of c-myb antisense oligodeoxynucleotides: an in vitro study relevant to bone marrow purging. *Proc. Natl. Acad. Sci. U.S.A.* **1991**, *88* (6), 2351−2355.
(5) Biroccio, A.; Benassi, B.; D'Agnano, I.; D'Angelo, C.; Buglioni, S.; Mottolese, M.; Ricciotti, A.; Citro, G.; Cosimelli, M.; Ramsay, R. G.; Calabretta, B.; Zupi, G. c-Myb and Bcl-x overexpression predicts poor prognosis in colorectal cancer. *Am. J. Clin. Pathol.* **2001**, *158* (4), 1289−1299.
(6) Hugo, H.; Cures, A.; Suraweera, N.; Drabsch, Y.; Purcell, D.; Mantamadiotis, T.; Phillips, W.; Dobrovic, A.; Zupi, G.; Gonda, T. J.; Iacopetta, B.; Ramsay, R. G. Mutations in the MYB intron I regulatory sequence increase transcription in colon cancers. *Genes Chromosom. Cancer* **2006**, *45* (12), 1143−1154.
(7) Bujnicki, T.; Wilczek, C.; Schomburg, C.; Feldmann, F.; Schlenke, P.; Müller-Tidow, C.; Schmidt, T. J.; Klempnauer, K.-H. Inhibition of Myb-dependent gene expression by the sesquiterpene lactone mexicanin-I. *Leukemia* **2012**, *26* (4), 615−622.
(8) Uttarkar, S.; Dukare, S.; Bopp, B.; Goblirsch, M.; Jose, J.; Klempnauer, K.-H. Naphthol AS-E phosphate inhibits the activity of the transcription factor Myb by blocking the interaction with the KIX domain of the coactivator p300. *Mol. Cancer Ther.* **2015**, *14* (6), 1276−1285.
(9) Uttarkar, S.; Piontek, T.; Dukare, S.; Schomburg, C.; Schlenke, P.; Berdel, W. E.; Müller-Tidow, C.; Schmidt, T. J.; Klempnauer, K.-H. Small-molecule disruption of the Myb/p300 cooperation targets acute myeloid leukemia cells. *Mol. Cancer Ther.* **2016**, *15* (12), 2905−2915.
(10) Yusenko, M.; Jakobs, A.; Klempnauer, K.-H. A novel cell-based screening assay for small-molecule MYB inhibitors identifies podophyllotoxins teniposide and etoposide as inhibitors of MYB activity. *Sci. Rep.* **2018**, *8* (1), 13159.
(11) Veale, C. G. L. Into the fray! A beginner's guide to medicinal chemistry. *ChemMedChem.* **2021**, *16* (8), 1199−1225.
(12) Orru, R. V.; de Greef, M. Recent advances in solution phasemulticomponent methodology for the synthesis of heterocyclic compounds. *Synthesis* **2003**, No. 10, 1471−1499.
(13) Fouad, M. A.; Abdel-Hamid, H.; Ayoup, M. S. Two decades of recent advances of Ugi reactions: synthetic and pharmaceutical applications. *RSC Adv.* **2020**, *10* (70), 42644−42681.
(14) Nagarajaiah, H.; Mukhopadhyay, A.; Moorthy, J. N. Biginelli reaction: an overview. *Tetrahedron Lett.* **2016**, *57* (47), 5135−5149.
(15) Zheng, X.; Liu, W.; Zhang, D. Recent advances in the synthesis of oxazole-based molecules via van Leusen oxazole synthesis. *Molecules* **2020**, *25* (7), 1594.
(16) Kemnitzer, W.; Drewe, J.; Jiang, S.; Zhang, H.; Zhao, J.; Crogan-Grundy, C.; Xu, L.; Lamothe, S.; Gourdeau, H.; Denis, R.; Tseng, B.; Kasibhatla, S.; Cai, S. X. Discovery of 4-aryl-4*H*-chromenes as a new series of apoptosis inducers using a cell- and caspase-based high-throughput screening assay. 3. Structure-activity relationships of fused rings at the 7,8-positions. *J. Med. Chem.* **2007**, *50* (12), 2858−2864.
(17) Schmitt, F.; Gold, M.; Rothemund, M.; Andronache, I.; Biersack, B.; Schobert, R.; Mueller, T. New naphthopyran analogues of LY290181 as potential tumor vascular-disrupting agents. *Eur. J. Med. Chem.* **2019**, *163*, 160−168.
(18) Wood, D. L.; Panda, D.; Wiernicki, T. R.; Wilson, L.; Jordan, M. A.; Singh, J. P. Inhibition of mitosis and microtubule function through direct tubulin binding by a novel antiproliferative naphthopyran LY290181. *Mol. Pharmacol.* **1997**, *52* (3), 437−444.
(19) Yusenko, M. V.; Biyanee, A.; Frank, D.; Köhler, L. H. F.; Andersson, M. K.; Khandanpour, C.; Schobert, R.; Stenman, G.; Biersack, B.; Klempnauer, K.-H. Bcr-TMP, a novel nanomolar-active compound that exhibits both MYB- and microtubule-inhibitory activity. *Cancers* **2022**, *14* (1), 43.
(20) Smith, C. W.; Bailey, J. M.; Billingham, M. E.; Chandrasekhar, S.; Dell, C. P.; Harvey, A. K.; Hicks, C. A.; Kingston, A. E.; Wishart, G. N. The anti-rheumatic potential of a series of 2,4-di-substituted-4*H*-naphtho[1,2-*b*]pyran-3-carbonitriles. *Bioorg. Med. Chem. Lett.* **1995**, *5* (23), 2783−2788.
(21) Maalej, E.; Chabchoub, F.; Oset-Gasque, M. J.; Esquivias-Perez, M.; Gonzalez, M. P.; Monjas, L.; Perez, C.; de los Rios, C.; Rodriguez-Franco, M. I.; Iriepa, I.; Moraleda, I.; Chioua, M.; Romero, A.; Marco-Contelles, J.; Samadi, A. Synthesis, biological assessment, and molecular modeling of racemic 7-aryl-9,10,11,12-tetrahydro-7*H*-benzo[7,8]chromeno[2,3-*b*]quinolin-8-amines as potential drugs for the treatment of Alzheimer's disease. *Eur. J. Med. Chem.* **2012**, *54*, 750−763.
(22) Guenes, C.; Hoffman, E. M.; Rudolph, K. L. Specific inhibitors of protein p21 as therapeutic agents. U.S. Patent No. US20150210717A1, July 30, 2015.
(23) Boutros, M.; Maskey, R.-P.; Koch, C.; Fuchs, F.; Steinbrink, S.; Gilbert, D. Chromene derivatives and their analoga as Wnt pathway antagonists. U.S. Patent US20130303550A1, Nov. 14, 2013.
(24) Lu, Y.; Chen, J.; Xiao, M.; Li, W.; Miller, D. D. An overview of tubulin inhibitors that interact with the colchicine binding site. *Pharm. Res.* **2012**, *29* (11), 2943−2971.
(25) Köhler, L. H. F.; Reich, S.; Begemann, G.; Schobert, R.; Biersack, B. 2-Amino-4-aryl-5-oxo-4,5-dihydropyrano[3,2-*c*]-chromene-3-carbonitriles with microtubule-disruptive, centrosome-declustering, and antiangiogenic effects *in vitro* and *in vivo*. *ChemMedChem* **2022**, *17*, e202200064.
(26) Morris, G. M.; Goodsell, D. S.; Halliday, R. S.; Huey, R.; Hart, W. E.; Belew, R. K.; Olson, A. J. Automated docking using a Lamarckian genetic algorithm and an empirical binding free energy function. *J. Comput. Chem.* **1998**, *19* (14), 1639−1662.
(27) Chitaley, K.; Webb, R. C. Microtubule depolymerization facilitates contraction of vascular smooth muscle via increased activation of RhoA/Rho-kinase. *Med. Hypotheses* **2001**, *56* (3), 381−385.
(28) Tojkander, S.; Gateva, G.; Lappalainen, P. Actin stress fibers-assembly, dynamics and biological roles. *J. Cell Sci.* **2012**, *125* (Pt 8), 1855−1864.
(29) Naumanen, P.; Lappalainen, P.; Hotulainen, P. Mechanisms of actin stress fibre assembly. *J. Microsc.* **2008**, *231* (3), 446−454.
(30) Li, S.; Wang, L.; Yu, F.; Zhu, Z.; Shobaki, D.; Chen, H.; Wang, M.; Wang, J.; Qin, G.; Erasquin, U. J.; Ren, L.; Wang, Y.; Cai, C. Copper-catalyzed click reaction on/in live cells. *Chem. Sci.* **2017**, *8* (3), 2107−2114.
(31) Zhou, J.; Giannakakou, P. Targeting microtubules for cancer chemotherapy. *Curr. Med. Chem. Anticancer Agents* **2005**, *5* (1), 65−71.

https://doi.org/10.1021/acsmedchemlett.2c00403
ACS Med. Chem. Lett. XXXX, XXX, XXX−XXX

(32) Walczak, C. E.; Cai, S.; Khodjakov, A. Mechanisms of chromosome behaviour during mitosis. *Nat. Rev. Mol. Cell Biol.* **2010**, *11* (2), 91−102.
(33) Foley, E. A.; Kapoor, T. M. Microtubule attachment and spindle assembly checkpoint signalling at the kinetochore. *Nat. Rev. Mol. Cell Biol.* **2013**, *14* (1), 25−37.
(34) Kanthou, C.; Greco, O.; Stratford, A.; Cook, I.; Knight, R.; Benzakour, O.; Tozer, G. The tubulin-binding agent combretastatin A-4-phosphate arrests endothelial cells in mitosis and induces mitotic cell death. *Am. J. Pathol.* **2004**, *165* (4), 1401−1411.
(35) Aranda, E.; Owen, G. I. A semi-quantitative assay to screen for angiogenic compounds and compounds with angiogenic potential using the EA.hy926 endothelial cell line. *Biol. Res.* **2009**, *42* (3), 377−389.
(36) Serbedzija, G. N.; Flynn, E.; Willett, C. E. Zebrafish angiogenesis: a new model for drug screening. *Angiogenesis* **1999**, *3* (4), 353−359.
(37) Ma, J.; Waxman, D. J. Modulation of the antitumor activity of metronomic cyclophosphamide by the angiogenesis inhibitor axitinib. *Mol. Cancer Ther.* **2008**, *7* (1), 79−89.
(38) Fry, E. A.; Inoue, K. c-MYB and DMTF1 in Cancer. *Cancer Invest.* **2019**, *37* (1), 46−65.
(39) Pasquier, E.; André, N.; Braguer, D. Targeting microtubules to inhibit angiogenesis and disrupt tumour vasculature: implications for cancer treatment. *Curr. Cancer Drug Targets* **2007**, *7* (6), 566−581.
(40) Schwartz, E. L. Antivascular actions of microtubule-binding drugs. *Clin. Cancer Res.* **2009**, *15* (8), 2594−2601.

https://doi.org/10.1021/acsmedchemlett.2c00403
ACS Med. Chem. Lett. XXXX, XXX, XXX−XXX

Supporting Information

A new naphthopyran derivative combines *c*-Myb inhibition, microtubule-targeting effects, and anti-angiogenic properties

Leonhard H. F. Köhler,[1] Sebastian Reich,[1] Maria Yusenko,[2] Karl-Heinz Klempnauer,[2] Amin H. Shaikh,[3] Khursheed Ahmed,[3] Gerrit Begemann,[4] Rainer Schobert,[1] and Bernhard Biersack[1]*

[1] Organic Chemistry Laboratory, University of Bayreuth Universitätsstrasse 30, 95440 Bayreuth, Germany

[2] Institute for Biochemistry, Westfälische-Wilhelms-Universität, Wilhelm-Klemm-Strasse 2, 48149 Münster, Germany

[3] Department of Chemistry & Post Graduate Research Center, Abeda Inamdar Senior College, Camp, Pune 411001, India

[4] Developmental Biology, University of Bayreuth, Universitätsstrasse 30, 95440 Bayreuth, Germany

Correspondence:

Dr. Bernhard Biersack, Organic Chemistry Laboratory,

University of Bayreuth, Universitätsstrasse 30,

95440 Bayreuth, Germany.

Email: bernhard.biersack@uni-bayreuth.de

Table of contents

Experimental Section

Safety statement

No unexpected or unusually high safety hazards were encountered.

Chemistry - Syntheses

All starting compounds were purchased from Aldrich. The known compounds **1a**, **1b**, **2a-d**, **2h**, **2i**, and **2n** were prepared according to literature procedures.[24,25,27,30-33] The following instruments were applied for this study: melting points (uncorrected), Gallenkamp; IR spectra, Perkin-Elmer Spectrum One FT-IR spectrophotometer with ATR sampling unit; nuclear magnetic resonance spectra, BRUKER Avance 300 spectrometer; chemical shifts are given in parts per million (δ) downfield from tetramethylsilane as internal standard; mass spectra, Varian MAT 311A (EI), UPLC/Orbitrap (ESI); microanalyses, Perkin-Elmer 2400 CHN elemental analyzer. All tested compounds were > 95% pure by elemental analysis.

2-Amino-4-(3-nitro-4-methoxyphenyl)-4H-naphtho(1,2-b)pyran-3-carbonitrile (2k)

4-Methoxy-3-nitrobenzaldehyde (181 mg, 1.0 mmol) and malononitrile (70 mg, 1.0 mmol) were dissolved in MeCN (5 mL) and three drops of Et_3N were added. The reaction mixture was stirred at room temperature for 30 min. 1-Naphthol (144 mg, 1.0 mmol) was added and the reaction mixture was stirred at room temperature for 16 h. The formed precipitate was collected, washed with MeCN and *n*-hexane and dried in vacuum. Yield: 235 mg (0.63 mmol, 63%); pale brown solid of m.p. 199-200 °C; υ_{max}(ATR)/cm^{-1} 3435, 3325, 3203, 3058, 2946, 2189, 1656, 1637, 1608, 1574, 1527, 1440, 1412, 1397, 1376, 1351, 1321, 1279, 1262, 1183, 1152, 1101, 1085, 1041, 1021, 966, 934, 898, 861, 840, 826, 805, 768, 739, 706, 675; ^{1}H NMR (300 MHz, DMSO-d$_6$) δ3.89 (3 H, s), 5.04 (1 H, s), 7.12 (1 H, d, J = 8.6 Hz), 7.24 (2 H, s), 7.33 (1 H, d, J = 8.8 Hz), 7.5-7.7 (4 H, m), 7.80 (1 H, d, J = 2.3 Hz), 7.8-7.9 (1 H, m), 8.24 (1 H, dd, J = 9.0 Hz, 1.6 Hz); ^{13}C NMR (75.5 MHz, DMSO-d$_6$) δ 40.4, 55.5, 56.7, 114.9, 117.0, 120.3, 120.8, 122.7, 123.7, 124.1, 126.0, 126.8, 126.9, 127.7, 132.8, 133.7, 138.1, 139.0, 142.7, 151.0, 160.2; *m/z* (EI) 373 (25) [M$^+$], 221 (100); Anal calcd for $C_{21}H_{15}N_3O_4$ (%): C, 67.56; H, 4.05; N, 11.25. Found (%): C, 67.33; H, 3.99; N, 11.17.

2-Amino-4-(3-fluoro-4-methylthiophenyl)-4H-naphtho(1,2-b)pyran-3-carbonitrile (2l)

3-Fluoro-4-methylsulfanylbenzaldehyde (170 mg, 1.0 mmol) and malononitrile (70 mg, 1.0 mmol) were dissolved in MeCN (5 mL) and three drops of Et_3N were added. The reaction mixture was stirred at room temperature for 30 min. 1-Naphthol (144 mg, 1.0 mmol) was added and the reaction mixture was stirred at room temperature for 16 h. The formed precipitate was collected, washed with MeCN and *n*-hexane and dried in vacuum. Yield: 265 mg (0.73 mmol, 73%); colorless solid of m.p. 234 °C; υ_{max}(ATR)/cm^{-1} 3443, 3332, 3197, 3058, 2198, 1664, 1637, 1605, 1574, 1478, 1407, 1374, 1317, 1283, 1261, 1225, 1191, 1148, 1104, 1065, 1038, 1021, 959, 933, 883, 817, 790, 766, 756, 744; ^{1}H NMR (300 MHz, DMSO-d$_6$) δ 2.44 (3 H, s), 4.94 (1 H, s), 7.0-7.1 (3 H, m), 7.22 (2 H, s), 7.3-7.4 (1 H, m), 7.5-7.7 (3 H, m), 7.8-7.9 (1 H, m), 8.2-8.3 (1 H, m); ^{13}C NMR (75.5 MHz, DMSO-d$_6$) δ 14.0, 40.4, 55.6, 114.1, 114.4, 117.2, 120.3, 120.7, 122.7, 123.6, 123.9, 124.0, 124.3, 124.4, 126.0, 126.7, 126.9, 127.7, 127.9, 128.0, 132.8, 142.7, 144.9, 145.0, 157.3, 160.2, 160.5; *m/z* (EI) 362 (62) [M$^+$], 221 (100); Anal calcd for $C_{21}H_{15}N_2OS$ (%): C, 69.60; H, 4.17; N, 7.73. Found (%): C, 69.52; H, 4.12; N, 7.68.

2-Amino-4-(3-bromo-4-methoxyphenyl)-4H-naphtho(1,2-b)pyran-3-carbonitrile (2m)

3-Bromo-4-methoxybenzaldehyde (215 mg, 1.0 mmol) and malononitrile (70 mg, 1.0 mmol) were dissolved in MeCN (5 mL) and three drops of Et_3N were added. The reaction mixture was stirred at room temperature for 30 min. 1-Naphthol (144 mg, 1.0 mmol) was added and the reaction mixture was stirred at room temperature for 16 h. The formed precipitate was collected, washed

with MeCN and *n*-hexane and dried in vacuum. Yield: 246 mg (0.60 mmol, 60%); colorless solid of m.p. 229-230°C; υ_{max}(ATR)/cm^{-1} 3451, 3330, 3282, 3255, 3202, 3071, 2943, 2840, 2195, 1661, 1600, 1574, 1495, 1464, 1438, 1398, 1374, 1309, 1277, 1256, 1191, 1149, 1104, 1052, 1016, 954, 898, 879, 825, 814, 802, 787, 770, 761, 744, 670, 659, 644; ^{1}H NMR (300 MHz, $CDCl_3$) δ3.84 (3 H, s), 4.76 (2 H, s), 4.79 (1 H, s), 6.83 (1 H, d, J = 8.4 Hz), 6.98 (1 H, d, J = 8.4 Hz), 7.1-7.2 (1 H, m), 7.34 (1 H, s), 7.4-7.6 (3 H, m), 7.7-7.8 (1 H, m), 8.1-8.2 (1 H, m); ^{13}C NMR (75.5 MHz, $CDCl_3$) δ40.5, 56.3, 61.2, 112.0, 112.2, 116.8, 119.5, 120.8, 123.2, 124.8, 126.0, 127.8, 128.2, 132.9, 133.3, 138.2, 143.2, 155.2, 158.9; *m/z* (%) 408 (13) [M$^+$], 406 (12) [M$^+$], 221 (100), 166 (11); Anal calcd for $C_{21}H_{15}BrN_2O_2$ (%): C, 61.93; H, 3.71; N, 6.88. Found (%): C, 61.97; H, 3.77; N, 6.82.

2-Amino-4-(2-bromo-3,4,5-trimethoxyphenyl)-4H-naphtho(1,2-b)pyran-3-carbonitrile (2o)

2-Bromo-3,4,5-trimethoxybenzaldehyde (244 mg, 0.89 mmol) and malononitrile (62 mg, 0.89 mmol) were dissolved in MeCN (5 mL) and three drops of Et_3N were added. The reaction mixture was stirred at room temperature for 30 min. 1-Naphthol (128 mg, 0.89 mmol) was added and the reaction mixture was stirred at room temperature for 16 h. The formed precipitate was collected, washed with MeCN and *n*-hexane and dried in vacuum. Yield: 150 mg (0.32 mmol, 36%); colorless solid; υ_{max}(ATR)/cm^{-1} 3397, 3278, 3172, 2999, 2938, 2830, 2199, 1654, 1634, 1597, 1575, 1479, 1462, 1426, 1393, 1374, 1328, 1293, 1263, 1239, 1189, 1159, 1148, 1101, 1056, 1001, 973, 920, 883, 867, 849, 827, 789, 770, 755, 743, 679, 653, 636, 604; ^{1}H NMR (300 MHz, $CDCl_3$) δ3.66 (3 H, s), 3.86 (3 H, s), 3.91 (3 H, s), 4.78 (2 H, s), 5.59 (1 H, s), 7.07 (1 H, d, J = 8.6 Hz), 7.5-7.6 (3 H, m), 7.7-7.8 (1 H, m), 8.1-8.2 (1 H, m); ^{13}C NMR (75.5 MHz, $CDCl_3$) δ40.1, 56.1, 60.4, 61.0, 109.5, 110.6, 116.9, 119.3, 120.7, 123.1, 124.8, 125.7, 126.7, 126.8, 127.8, 133.4, 142.6, 143.1, 153.3, 159.5; *m/z* (%) 468 (17) [M$^+$], 466 (17) [M$^+$], 387 (12), 221 (100); Anal calcd for $C_{23}H_{19}BrN_2O_4$ (%): C, 59.11; H, 4.10; N, 5.99. Found (%): C, 59.04; H, 4.13; N, 6.05.

2-Amino-4-(3-iodo-4-ethoxy-5-methoxyphenyl)-4H-naphtho(1,2-b)pyran-3-carbonitrile (2p)

4-Ethoxy-3-iodo-5-methoxybenzaldehyde (306 mg, 1.0 mmol) and malononitrile (70 mg, 1.0 mmol) were dissolved in MeCN (5 mL) and three drops of Et_3N were added. The reaction mixture was stirred at room temperature for 30 min. 1-Naphthol (144 mg, 1.0 mmol) was added and the reaction mixture was stirred at room temperature for 16 h. The formed precipitate was collected, washed with MeCN and *n*-hexane and dried in vacuum. Yield: 220 mg (0.44 mmol, 44%); colorless solid; υ_{max}(ATR)/cm^{-1} 3488, 3415, 3385, 3321, 3200, 2973, 2930, 2190, 1658, 1635, 1608, 1592, 1574, 1481, 1462, 1411, 1373, 1311, 1262, 1224, 1186, 1136, 1104, 1031, 891, 868, 830, 803, 767, 749, 732, 669, 652; ^{1}H NMR (300 MHz, $CDCl_3$) δ1.41 (3 H, t, J = 7.0 Hz), 3.77 (3 H, s), 4.00 (2 H, q, J = 7.0 Hz), 4.7-4.8 (3 H, m), 6.74 (1 H, s), 7.01 (1 H, d, J = 8.5 Hz), 7.12 (1 H, s), 7.5-7.6 (3 H, m), 7.8-7.9 (1 H, m), 8.1-8.2 (1 H, m); ^{13}C NMR (75.5 MHz, $CDCl_3$) δ15.8, 40.9, 56.1, 61.0, 69.0, 93.7, 112.9, 116.6, 119.5, 120.8, 123.2, 124.8, 126.0, 126.8, 126.9, 127.8, 130.0, 133.4, 141.9, 143.2, 147.7, 152.8, 159.0; *m/z* (%) 498 (42) [M$^+$], 469 (6), 221 (100), 166 (9); Anal calcd for $C_{23}H_{19}IN_2O_3$ (%): C, 55.44; H, 3.84; N, 5.62. Found (%): C, 55.50; H, 3.79; N, 5.68.

2-Amino-4-(3-bromo-4-ethoxy-5-methoxyphenyl)-4H-naphtho(1,2-b)pyran-3-carbonitrile (2q)

3-Bromo-4-ethoxy-5-methoxybenzaldehyde (259 mg, 1.0 mmol) and malononitrile (70 mg, 1.0 mmol) were dissolved in MeCN (5 mL) and three drops of Et_3N were added. The reaction mixture was stirred at room temperature for 30 min. 1-Naphthol (144 mg, 1.0 mmol) was added and the reaction mixture was stirred at room temperature for 16 h. The formed precipitate was collected, washed with MeCN and *n*-hexane and dried in vacuum. Yield: 190 mg (0.42 mmol, 42%); colorless solid of m.p. 188°C; υ_{max}(ATR)/cm^{-1} 3463, 3334, 3198, 2970, 2929, 2894, 2192, 1666, 1637, 1606, 1572, 1487, 1416, 1397, 1372, 1325, 1278, 1260, 1229, 1207, 1188, 1142, 1103, 1037, 903, 884, 864, 831, 796, 784, 766, 755, 667, 651; ^{1}H NMR (300 MHz, $CDCl_3$) δ1.38 (3 H, t, J = 7.0 Hz), 3.79 (3

H, s), 4.02 (2 H, q, J = 7.0 Hz), 4.7-4.8 (3 H, m), 6.73 (1 H, s), 6.91 (1 H, s), 7.01 (1 H, d, J = 8.7 Hz), 7.5-7.6 (3 H, m), 7.8-7.9 (1 H, m), 8.1-8.2 (1 H, m); ^{13}C NMR (75.5 MHz, $CDCl_3$) δ 15.6, 41.1, 56.2, 61.0, 69.1, 111.6, 116.5, 118.5, 119.5, 120.8, 123.2, 124.3, 124.8, 126.0, 126.8, 126.9, 127.8, 133.4, 141.2, 143.2, 145.1, 154.0, 159.0; *m/z* (%) 452 (9) [M$^+$], 450 (10) [M$^+$], 221 (100), 166 (8); Anal calcd for $C_{23}H_{19}BrN_2O_3$ (%): C, 61.21; H, 4.24; N, 6.21. Found (%): C, 61.14; H, 4.20; N, 6.16.

2-Amino-4-(3,5-dimethoxy-4-ethoxyphenyl)-4H-naphtho(1,2-b)pyran-3-carbonitrile (3a)

3,5-Dimethoxy-4-ethoxybenzaldehyde (240 mg, 1.14 mmol) and malononitrile (80 mg, 1.14 mmol) were dissolved in MeCN (5 mL) and three drops of Et_3N were added. The reaction mixture was stirred at room temperature for 30 min. 1-Naphthol (165 mg, 1.14 mmol) was added and the reaction mixture was stirred at room temperature for 4 h. The formed precipitate was collected, washed with MeCN and *n*-hexane and dried in vacuum. Yield: 363 mg (0.90 mmol, 79%); colorless solid of m.p. 168°C; υ_{max}(ATR)/cm^{-1} 3461, 3338, 3203, 3059, 2990, 2937, 2841, 2191, 1653, 1631, 1612, 1592, 1575, 1504, 1463, 1456, 1426, 1397, 1376, 1325, 1279, 1263, 1240, 1229, 1188, 1147, 1124, 1105, 1033, 919, 900, 860, 811, 786, 757, 691, 667, 655; ^{1}H NMR (300 MHz, $CDCl_3$) δ 1.07 (3 H, t, J = 7.1 Hz), 3.53 (6 H, s), 3.75 (2 H, q, J = 7.1 Hz), 4.56 (1 H, s), 5.5-5.6 (2 H, br s), 6.20 (2 H, s), 6.83 (1 H, d, J = 8.6 Hz), 7.2-7.3 (3 H, m), 7.5-7.6 (1 H, m), 8.0-8.1 (1 H, m); ^{13}C NMR (75.5 MHz, $CDCl_3$/DMSO-d_6) δ 15.0, 41.4, 55.6, 58.5, 68.1, 104.7, 116.6, 119.9, 120.5, 122.8, 123.6, 125.6, 125.9, 126.1, 127.1, 132.7, 135.4, 139.9, 142.7, 153.0, 159.3; *m/z* (%) 402 (33) [M$^+$], 221 (100); Anal calcd for $C_{24}H_{22}N_2O_4$ (%): C, 71.63; H, 5.51; N, 6.96. Found (%): C, 71.71; H, 5.47; N, 7.00.

2-Amino-4-(3,5-dimethoxy-4-propoxyphenyl)-4H-naphtho(1,2-b)pyran-3-carbonitrile (3b)

3,5-Dimethoxy-4-propoxybenzaldehyde (287 mg, 1.28 mmol) and malononitrile (90 mg, 1.28 mmol) were dissolved in MeCN (5 mL) and three drops of Et_3N were added. The reaction mixture was stirred at room temperature for 30 min. 1-Naphthol (185 mg, 1.28 mmol) was added and the reaction mixture was stirred at room temperature for 3 h. The formed precipitate was collected, washed with MeCN and *n*-hexane and dried in vacuum. Yield: 348 mg (0.84 mmol, 66%); colorless solid of m.p. 194-195°C; υ_{max}(ATR)/cm^{-1} 3464, 3343, 3200, 3059, 2963, 2936, 2875, 2839, 2192, 1655, 1610, 1591, 1575, 1504, 1466, 1455, 1425, 1397, 1375, 1324, 1281, 1264, 1240, 1229, 1188, 1149, 1118, 1104, 1064, 1024, 999, 955, 918, 882, 863, 843, 817, 804, 786, 757, 691, 667, 655; ^{1}H NMR (300 MHz, $CDCl_3$) δ 0.96 (3 H, t, J = 7.4 Hz), 1.7-1.8 (2 H, m), 3.75 (6 H, s), 3.88 (2 H, t, J = 7.0 Hz), 4.75 (2 H, s), 4.79 (1 H, s), 6.40 (2 H, s), 7.04 (1 H, d, J = 8.6 Hz), 7.5-7.6 (3 H, m), 7.8-7.9 (1 H, m), 8.1-8.2 (1 H, m); ^{13}C NMR (75.5 MHz, $CDCl_3$) δ 10.3, 23.3, 41.7, 56.2, 61.5, 75.1, 105.5, 117.0, 119.7, 120.8, 123.2, 124.6, 126.2, 126.7, 127.8, 133.4, 136.7, 139.6, 143.2, 153.7, 158.9; *m/z* (%) 416 (47) [M$^+$], 373 (13), 221 (100), 166 (18), 41 (22); Anal calcd for $C_{25}H_{24}N_2O_4$ (%): C, 72.10; H, 5.81; N, 6.73. Found (%): C, 72.20; H, 5.85; N, 6.69.

2-Amino-4-(3,5-dimethoxy-4-isopropyloxyphenyl)-4H-naphtho(1,2-b)pyran-3-carbonitrile (3c)

3,5-Dimethoxy-4-isopropoxybenzaldehyde (224 mg, 1.0 mmol) and malononitrile (66 mg, 1.0 mmol) were dissolved in MeCN (5 mL) and three drops of Et_3N were added. The reaction mixture was stirred at room temperature for 30 min. 1-Naphthol (144 mg, 1.0 mmol) was added and the reaction mixture was stirred at room temperature for 4 h. The formed precipitate was collected, washed with MeCN and *n*-hexane and dried in vacuum. Yield: 160 mg (0.38 mmol, 38%); colorless solid of m.p. 182-183°C; υ_{max}(ATR)/cm^{-1} 3462, 3332, 3198, 2969, 2838, 2194, 1667, 1637, 1605, 1588, 1573, 1501, 1462, 1425, 1397, 1370, 1326, 1282, 1259, 1235, 1185, 1148, 1123, 1102, 1053, 1036, 1022, 935, 853, 826, 815, 785, 768, 759, 734, 688, 668; ^{1}H NMR (300 MHz, $CDCl_3$) δ 1.25 (6 H, d, J = 6.2 Hz), 3.74 (6 H, s), 4.2-4.4 (1 H, m), 4.73 (2 H, s), 4.79 (1 H, s), 6.39 (2 H, s), 7.05 (1 H, d, J = 8.6 Hz), 7.5-7.6 (3 H, m), 7.7-7.8 (1 H, m), 8.1-8.2 (1 H, m); ^{13}C NMR (75.5 MHz, $CDCl_3$) δ 22.5, 41.7, 56.1, 61.5, 75.2, 105.4, 117.1, 119.7, 120.8, 123.2, 124.6, 126.2, 126.6, 126.8, 127.8, 133.3,

135.5, 139.5, 143.2, 154.0, 158.9; *m/z* (%) 414 (23) [M$^+$], 373 (100), 221 (83), 41 (27); Anal calcd for $C_{25}H_{24}N_2O_4$ (%): C, 72.10; H, 5.81; N, 6.73. Found (%): C, 72.23; H, 5.87; N, 6.70.

2-Amino-4-(4-butoxy-3,5-dimethoxyphenyl)-4H-naphtho(1,2-b)pyran-3-carbonitrile (3d)

3,5-Dimethoxy-4-butoxybenzaldehyde (304 mg, 1.276 mmol) and malononitrile (84 mg, 1.276 mmol) were dissolved in MeCN (5 mL) and three drops of Et_3N were added. The reaction mixture was stirred at room temperature for 30 min. 1-Naphthol (184 mg, 1.276 mmol) was added and the reaction mixture was stirred at room temperature for 4 h. The formed precipitate was collected, washed with MeCN and *n*-hexane and dried in vacuum. Yield: 190 mg (0.44 mmol, 35%); colorless solid of m.p. 201-202°C; υ_{max}(ATR)/cm^{-1} 3464, 3331, 3198, 3000, 2955, 2934, 2869, 2839, 2193, 1667, 1637, 1590, 1573, 1506, 1462, 1425, 1397, 1371, 1327, 1282, 1260, 1236, 1186, 1153, 1125, 1103, 1062, 1037, 1022, 957, 856, 826, 815, 800, 785, 760, 688, 669, 654; ^{1}H NMR (300 MHz, $CDCl_3$) δ 0.92 (3 H, t, J = 7.4 Hz), 1.4-1.5 (2 H, m), 1.7-1.8 (2 H, m), 3.75 (6 H, s), 3.92 (2 H, t, J = 6.8 Hz), 4.73 (2 H, s), 4.79 (1 H, s), 6.40 (2 H, s), 7.05 (1 H, d, J = 8.6 Hz), 7.5-7.6 (3 H, m), 7.8-7.9 (1 H, m), 8.1-8.2 (1 H, m); ^{13}C NMR (75.5 MHz, $CDCl_3$) δ 13.9, 19.1, 32.2, 41.7, 56.2, 61.5, 73.2, 105.6, 117.1, 119.7, 120.8, 123.2, 124.6, 126.2, 126.7, 126.8, 127.8, 133.4, 136.8, 139.6, 143.2, 153.7, 158.9; *m/z* (%) 430 (37) [M$^+$], 374 (18), 221 (100), 41 (31); Anal calcd for $C_{26}H_{26}N_2O_4$ (%): C, 72.54; H, 6.09; N, 6.51. Found (%): C, 72.66; H, 6.03; N, 6.60.

2-Amino-4-(4-allyloxy-3,5-dimethoxyphenyl)-4H-naphtho(1,2-b)pyran-3-carbonitrile (3e)

3,5-Dimethoxy-4-allyloxybenzaldehyde (255 mg, 1.15 mmol) and malononitrile (81 mg, 1.15 mmol) were dissolved in MeCN (5 mL) and three drops of Et_3N were added. The reaction mixture was stirred at room temperature for 30 min. 1-Naphthol (166 mg, 1.15 mmol) was added and the reaction mixture was stirred at room temperature for 4 h. The formed precipitate was collected, washed with MeCN and *n*-hexane and dried in vacuum. Yield: 276 mg (0.67 mmol, 58%); colorless solid of m.p. 195-196°C; υ_{max}(ATR)/cm^{-1} 3473, 3353, 3196, 3057, 2921, 2842, 2191, 1657, 1633, 1592, 1575, 1503, 1467, 1457, 1445, 1426, 1398, 1376, 1324, 1282, 1263, 1228, 1149, 1117, 1053, 1026, 1012, 990, 939, 923, 862, 843, 820, 806, 787, 758, 693, 667, 655; ^{1}H NMR (300 MHz, $CDCl_3$/DMSO-d_6) δ 3.58 (6 H, s), 4.2-4.3 (2 H, m), 4.61 (1 H, s), 4.9-5.0 (1 H, m), 5.0-5.1 (1 H, m), 5.52 (2 H, s), 5.8-5.9 (1 H, m), 6.25 (2 H, s), 6.88 (1 H, d, J = 8.6 Hz), 7.3-7.4 (3 H, m), 7.6-7.7 (1 H, m), 8.0-8.1 (1 H, m); ^{13}C NMR (75.5 MHz, $CDCl_3$/DMSO-d_6) δ 41.5, 55.7, 58.9, 73.6, 104.9, 116.7, 117.1, 120.0, 122.9, 123.8, 125.7, 126.1, 126.3, 127.2, 132.8, 134.1, 135.4, 140.1, 142.8, 153.1, 159.3; *m/z* (%) 416 (22) [M$^+$], 374 (33), 221 (100), 166 (14); Anal calcd for $C_{25}H_{22}N_2O_4$ (%): C, 72.45; H, 5.35; N, 6.76. Found (%): C, 72.55; H, 5.31; N, 6.70.

2-Amino-4-(3,5-dimethoxy-4-propargyloxyphenyl)-4H-naphtho(1,2-b)pyran-3-carbonitrile (3f)

3,5-Dimethoxy-4-propargyloxybenzaldehyde (220 mg, 1.0 mmol) and malononitrile (66 mg, 1.0 mmol) were dissolved in MeCN (5 mL) and three drops of Et_3N were added. The reaction mixture was stirred at room temperature for 30 min. 1-Naphthol (144 mg, 1.0 mmol) was added and the reaction mixture was stirred at room temperature for 4 h. The formed precipitate was collected, washed with MeCN and *n*-hexane and dried in vacuum. Yield: 180 mg (0.44 mmol, 44%); colorless solid of m.p. 194-195°C; υ_{max}(ATR)/cm^{-1} 3445, 3353, 3271, 3199, 3054, 3002, 2937, 2842, 2188, 1659, 1634, 1590, 1572, 1503, 1464, 1424, 1405, 1397, 1373, 1327, 1279, 1261, 1235, 1216, 1188, 1129, 1101, 1051, 1034, 1023, 994, 921, 856, 839, 820, 791, 766, 758, 689, 667, 655; ^{1}H NMR (300 MHz, $CDCl_3$/DMSO-d_6) δ 2.87 (1 H, s), 3.70 (6 H, s), 4.5-4.6 (2 H, m), 4.72 (1 H, s), 6.00 (1 H, s), 6.38 (2 H, s), 6.99 (1 H, d, J = 8.6 Hz), 7.5-7.6 (3 H, m), 7.7-7.8 (1 H, m), 8.1-8.2 (1 H, m); ^{13}C NMR (75.5 MHz, $CDCl_3$/DMSO-d_6) δ 41.2, 55.3, 57.6, 59.0, 74.5, 78.8, 104.4, 116.3, 119.7, 120.4, 122.5, 123.4, 125.3, 125.7, 125.9, 126.8, 132.4, 133.8, 140.7, 142.5, 152.7, 159.3; *m/z* (%) 412 (25) [M$^+$], 373

(100), 221 (77); Anal calcd for $C_{25}H_{20}N_2O_4$ (%): C, 72.80; H, 4.89; N, 6.79. Found (%): C, 72.69; H, 4.95; N, 6.73.

2-Amino-4-(3,5-dimethoxy-4-pentyloxyphenyl)-4H-naphtho(1,2-b)pyran-3-carbonitrile (3g)

3,5-Dimethoxy-4-pentoxybenzaldehyde (308 mg, 1.22 mmol) and malononitrile (86 mg, 1.22 mmol) were dissolved in MeCN (5 mL) and three drops of Et_3N were added. The reaction mixture was stirred at room temperature for 30 min. 1-Naphthol (177 mg, 1.22 mmol) was added and the reaction mixture was stirred at room temperature for 4 h. The formed precipitate was collected, washed with MeCN and *n*-hexane and dried in vacuum. Yield: 290 mg (0.65 mmol, 53%); colorless solid of m.p. 191-192°C; υ_{max}(ATR)/cm^{-1} 3463, 3331, 3196, 2998, 2954, 2931, 2863, 2840, 2194, 1667, 1636, 1606, 1590, 1572, 1505, 1462, 1425, 1396, 1370, 1327, 1281, 1260, 1238, 1226, 1206, 1185, 1154, 1125, 1102, 1070, 1047, 1037, 1023, 972, 920, 899, 878, 857, 845, 826, 810, 786, 767, 758, 725, 688, 669, 654; ^{1}H NMR (300 MHz, $CDCl_3$) δ 0.89 (3 H, t, J = 7.1 Hz), 1.3-1.4 (4 H, m), 1.7-1.8 (2 H, m), 3.75 (6 H, s), 3.91 (2 H, t, J = 6.9 Hz), 4.74 (2 H, s), 4.79 (1 H, s), 6.40 (2 H, s), 7.04 (1 H, d, J = 8.6 Hz), 7.5-7.6 (3 H, m), 7.7-7.8 (1 H, m), 8.1-8.2 (1 H, m); ^{13}C NMR (75.5 MHz, $CDCl_3$) δ 14.1, 22.5, 28.0, 29.8, 41.7, 56.2, 61.4, 73.5, 105.5, 117.0, 119.7, 120.8, 123.2, 124.6, 126.2, 126.6, 126.8, 127.8, 133.3, 136.8, 139.6, 143.2, 153.7, 158.9; *m/z* (%) 444 (13) [M$^+$], 374 (15), 221 (100), 43 (14); Anal calcd for $C_{27}H_{28}N_2O_4$ (%): C, 72.95; H, 6.35; N, 6.30. Found (%): C, 73.08; H, 6.40; N, 6.33.

Cell lines and culture conditions

518A2 melanoma (Department of Radiotherapy, Medical University of Vienna, Austria)[1], HeLa cervix carcinoma, KB-V1^{Vbl} (ACC-149) multi drug resistant (MDR) cervix carcinoma, U-87 glioblastoma, MCF-7 (ACC-115) breast carcinoma, HT-29 (ACC-299), HCT-116 (ACC-581) and HCT-116p53-/- (p53 knockout mutant) colon carcinoma, EA.hy926 (ATCC® CRL-2922™) endothelial hybrid cells, and HDFa (ATCC® PCS-201-012™) adult human dermal fibroblasts were cultivated in Dulbecco's Modified Eagle Medium (DMEM) supplemented with 10% fetal bovine serum (20% for HDFa cells), and 1% antibiotic-antimycotic or 1 % ZellShield® at 37 °C, 5% CO_2, and 95% humidity. To keep KB-V1Vbl cells resistant, 340 nM vinblastine was added to the cell culture medium 24 h after every passage. Cells were grown at 5% CO_2, and 95% humidity. Only mycoplasma-free cell cultures were used.

MYB Luciferase screening Assay

Compounds were tested using the HEC-Luc and HEK-MYB-Luc reporter cell lines, which allow a doxycycline dependent induction of MYB expression and harbor a MYB-dependent luciferase reporter plasmid as described before.[2,3] After 16 h of substance treatment (0.0001 – 3 µM), luciferase activities were analyzed with Steady-Glo luciferase kit (Promega), using a TECAN microplate reader.

MTT-assay (Cell viability assay)

The water-soluble tetrazolium salt 3-(4,5-dimethylthiazol-2-yl)-2,5- diphenyltetrazolium bromide (= MTT) was used to identify viable cells, which reduce it to violet formazan crystals. Therefore, the cancer and hybrid cells (5 × 104 cells/mL,100 µL/well), as well as HDFa cells (1 × 105 cells/mL, 100 µL/well) were grown in 96-well plates for 24h under cell culture conditions. After the treatment with various concentrations (100 µM – 0.5 nM) of compounds **1b**, **3a-f** and DMSO for 72h, 12.5µL of a 0.5% MTT solution in PBS were added to the cells and incubated for another 2h at 37°C. Subsequently the microplates were centrifuged (300g, 5 min, 4°C), the supernatant medium was discarded, and the formazan dissolved in 25 µL of DMSO containing 10 % SDS and 0.6% acetic acid for at least 1 h (37°C) in the dark. The absorbance of formazan (λ: 570 nm), and the background (λ: 630 nm) was measured with a microplate reader (Tecan infinite

F200). The IC_{50} values were derived from dose-inhibition curves as the means ± SD of four independent experiments with respect to vehicle treated control cells set to 100%. For these data the "log(inhibitor) vs. normalized response-Variable slope" – curve fitting function was used (GraphPad Prism9).

Tubulin polymerisation

In a black 96-well half-area clear bottom plate, 50µL of Brinkley's Buffer 80 (BRB80: 400 mm PIPES, 5 mm $MgCl_2$, 5 mm EGTA, pH = 6.8) containing 10 % glycerol and 1,5 mm GTP was pipetted. After adding the test compounds **1b** and **3a-f** (5 µM), the polymerisation was started by giving 50 µL porcine brain tubulin (10 mg/mL in BRB80) to the wells. The measurement of the optical density at 340 nm was immediately started in a Tecan infinite F200 plate reader for 120 min at 37°C. The measured data are representative as the means ± SD of at least two independent experiments.

Molecular docking analysis

For molecular docking analysis, the 3D-structure of the Tubulin-colchicine complex (PDB ID: 1sa0) was retrieved from protein data bank (www.rcsb.org). Before actual molecular docking, the health of the protein was assured by plotting Ramachandran's plot in Discovery studio visualizer. The compounds **1b** and **3f** were docked in the active site of target enzymes. In the present work, flexible docking was accomplished using AutoDock 4.2.6. The software executes the molecular docking using Lamarckian Genetic Algorithm and empirical free energy scoring function. The polar hydrogen atoms and Kollman charges were added to the protein. The Water molecules, hetero-atoms and ligands present in the tubulin-colchicine complex were removed from the structure in Autodock 1.5.7. Simulation boxes were centered on the originally crystallized ligand colchicine. Residues Lys254, Lys352, Asn101, Val318 and Ile378 were treated as flexible residues. An 18×22×20 Å simulation box was used in the docking calculations. Docking results were visualized and analyzed in Discovery studio visualizer, UCSF Chimera visualization tools and PYMOL programs.

Immunofluorescence staining of tubulin and actin cytoskeleton

518A2 melanoma cells (1×10^5 cells/mL, 0.5 mL/well) were seeded on coverslips in 24-well cell culture plates and incubated for 24 h under cell culture conditions (37 °C, 5% CO_2 and 95% humidity). Afterwards the cells were treated for 24 h with test compounds **1b**, **3a-f** and C-A4 (25 µM) or solvent (DMSO). After incubation the cells were washed with cytoskeletal buffer (100 mm PIPES, 3 mm $MgCl_2$, 138 mm KCl, 2 mM EGTA, 300 mm sucrose, pH 6.8), fixed and permeabilized with 3.7% formaldehyde and 0.2% Triton X-100 in cytoskeletal buffer for 5 min at rt. As additional fixation step, the cells were incubated with ice-cold EtOH for 10 s and rehydrated in PBS. The cells were blocked with 1% BSA in PBS for 30 min, followed by at least 2 h treatment with a primary antibody against alpha-tubulin (anti alpha-tubulin, mouse monoclonal antibody). Afterwards the cells were washed two times with PBS, subsequently incubated for another 1 h with a secondary antibody AlexaFluor®-546 conjugate (goat anti-mouse IgG-AF-546, Invitrogen). For the immunofluorescence staining of actin and nuclei, Phallodin-iFluor™ 488 Conjugate (AAT Bioquest) and DAPI (1 µg/mL) was used for 1 h in the dark. Consecutively the cells were washed three times with PBS and the coverslips were embedded in ProLong™ Glass Antifade Mountant. Nuclei, actin filaments and microtubules were documented by fluorescence microscopy (Leica TCS SP5 confocal microscope, 630× magnification) and edited with *ImageJ.*

Cell cycle analysis

518A2 melanoma cells (1×10^5 cells/mL, 3 mL/well) were seeded in 6-well cell culture plates for 24 h under cell culture conditions (37 °C, 5% CO_2, 95% humidity). The treatment with 25 nM each of compounds **1b**,**3a-f** (25 nM) and positive control C-A4 (25 nM) or solvent (DMSO) was carried

out for 6 h, 12 h and 24 h. The cells were separated through trypsinization, centrifuged (5 min, 300 × g, 4 °C) and fixed in 70% EtOH for at least 24h at 4°C. Before flow-cytometric measurement the cells were washed with PBS and stained with propidium iodide solution (50 µg/mL PI, 0.1% sodium citrate, 50 µg/mL RNAse A in PBS, pH = 7.4). The DNA content of at least 10000 single cells was measured with a Beckmann Coulter Cytomics FC500 flow cytometer (λ_{em}: 570 nm, λ_{ex}: 488 nm laser source) and the ratio of the cell cycle phases (sub-G1, G1, S, G2/M) were determined as means from duplicates by CXP software (Beckman Coulter).

Caspase-3/7 Activity Assay

Caspase-3/7 activity was measured using the Cell Meter™ Caspase 3/7 Activity Apoptosis Assay Kit (ATT Bioquest®). Therefore, 518A2 melanoma cells (1 × 10^5 cells/mL, 67.5 µL/well) were grown under cell culture conditions (37 °C, 5% CO_2, 95% humidity) in black 96-well plates for 24 h. The cells were incubated with **1b**, **3a-f**, and C-A4 (25 nM), positive control Staurosporine (1 µM) or solvent (DMSO) for 6 or 24 h under cell culture conditions, following by addition of fluorogenic caspase-3/7 substrate solution and 60 min incubation at rt. The fluorescence intensity (λ_{ex}: 485 nm, λ_{em}: 521 nm) was measured using a microplate reader (Tecan infinite F200). The blank values without cells were subtracted to reduce the background signals of the in triplicated performed measurement. The results were quoted as means ± SEM. 518A2 cells were reviewed on their vitality via MTT-assay as described above.

Co-localization via intracellular click-reaction

518A2 melanoma cells (1 × 10^5 cells/mL, 0.5 mL/well) were grown on coverslips in 24-well cell culture plates for 24 h under cell culture conditions (37 °C, 5% CO_2, 95% humidity). Under the same conditions the cells were incubated with **3f** (25 µM) for 0, 5 and 15 min. After the treatment the cells were washed twice with PBS, fixed (3.7% formaldehyde in PBS) for 10 min and washed again with PBS. Subsequently 200 µL of the click-reagent (2 mm $CuSO_4$, 5 mm sodium ascorbate, 0.1 mm 3-azido-7-hydroxycoumarin, 1% BSA in PBS) were pipetted to the cells and incubated for 30 min in the dark. Nuclei were counterstained with Nuclear Green (1:1000, 50 µg/mL RNAse, 1% BSA in PBS) before the cells were washed again with PBS and ddH_2O. The coverslips were embedded in Roti®Mount FluorCare and documented using a Leica TCS SP5 confocal microscope (630× magnification). The localization of **3f** was identified for each point of time (0, 5, 15 min) in at least two independent experiments.

EA.hy926 tube formation assay

EA.hy926 endothelial hybrid cells (100 µL/well, 5 × 10^5 cells/mL) were seeded on thin layers of basement membrane-like matrix Matrigel® (Corning) in µ-Slides (Ibidi) and cultivated for 24 h in EndoPrime low serum (Capricorn) endothelial medium. The cells were treated with **1b**, **3a-f** and **C-A4** (25 nM) or solvent (DMSO) for 5 h under cell culture conditions (37 °C, 5% CO_2, and 95% humidity), till tubular structures had been formed in the control wells. Anti-angiogenic effects were documented via light microscopy (Zeiss Axiovert 135, 100× magnification), in which the determination of the substances was carried out in duplicates. EA.hy926 cells were reviewed on their vitality via MTT-assay as described above. Therefore, a viability higher than 80% of negative control set to 100% were confirmed. The images were analysed with ImageJ (angiogenesis-analysing tool) and compared for the number of junctions, meshes, master segments (MS) and length of MS to quantify the tube formation process.[4]

Zebrafish angiogenesis assay

Transgenic zebrafish of the strain *Tg(fli1:EGFP)* with *casper* mutant background were raised under standard conditions at about 28 °C.[5,6] The eggs (0 hpf) were cultivated in E3 medium (5 mm NaCl, 0.17 mm KCl, 0.33 mm CaCl, 0.33 mm $MgSO_4$, 0.01% methylene blue, pH 7.2) for 24 h, then manually dechorionated and transferred in 6-well plates with 5 mL E3 medium each. The

fluorescent embryos (24 hpf) were treated with **1b** and **3a-f** (100 nM), Axitinib (0.5 µM), solvent (DMSO) for 48 h. Afterwards the development of the vascular system of the embryos (72 hpf), especially the SIV (subintestinal veins) area, was documented by fluorescence microscopy (λ_{ex}: 488 nm, λ_{em}: 509 nm; Leica MZ10F with Zeiss AxioCam MRrc and Mrc-ZEN pro 2012 software). SIV areas of at least 23 identically treated zebrafish larvae per concentration were quantified as means ± SD with control (DMSO) set to 100%. The significant levels of the decreased SIV areas from substance treated individuals compared with solvent control (DMSO) was determined with a One-way ANOVA, *: $p < 0.05$; **: $p < 0.01$; ***: $p < 0.001$; ****: $p < 0.0001$, with Dunnett´s multiple comparison test (GraphPad Prism 9).

Drug-likeness and Pharmacokinetic studies

ADME (Absorption, Distribution, Metabolism and Excretion) and pharmacokinetic properties were checked using SwissADME (an online search tool, link: http://www.swissadme.ch).[7] Chem Draw 12.0 software was used to draw and compute the structures of all the synthesized compounds and their physicochemical characteristics. Simultaneously, the SMILE file format required to obtain the pharmacokinetic parameters of all the compounds was obtained from Chem Draw 12.0. Swiss ADME predictor provides information about absorption parameters like gastrointestinal absorption (GI), oral bioavailability, and distribution parameters like blood brain barrier (BBB).

Preparation of 518A2 cell lysate

518A2 melanoma cells were cultivated under cell culture conditions (125 cm^2 cell culture flask) until confluence was reached. Cells were washed with PBS, detached by cell scraper, and centrifuged (400g, 5 min, 4°C). The cell pellet was resuspended in hypotonic buffer (10 mM KCl, 1.5 mM $MgCl_2$, 10 mM HEPES, pH 7.9) for 10 min, centrifuged and homogenised with a typ B dounce homogenizer (50 strokes) in 1 mL of hypotonic buffer (1:100 Inhibitorcocktail plus, Roth). The concentration of the supernatant after centrifugation (10000g, 10 min, 4°C) was adjusted to 1 mg/mL using a NanoDrop 1000 Spectrophotometer and aliquots were frozen at -80 °C.

Metabolic stability monitored by UV-absorption

The test compound **3f** (100 µM) was treated with 518A2 cell lysate and the stability was monitored via UV-absorbance between 275 nm and 400 nm (Varioskan LUX, Thermo). Solubility of the test substances was enhanced with 4 % tween 80 in PBS (EK=0.4 %). The probes (160 µL PBS, 20 µL Substance dilution in PBS with 4 % tween 80, 20 µL cell lysate 1 mg/mL) were measured in 96-well plates after 0, 3 and 24 h and subtracted by blanks without substances.

RP-HPLC analysis of substance stability

The stability of substance **3f** was verified by RP-HPLC analysis (Waters ACQUITY UPLC H Class System) after 0 and 72 h incubation with 518A2 melanoma cell lysate. The reaction was prepared in PBS with 10 % substance pre-dilution (4 mM in DMSO with 4 % tween 80) and 10 % cell lysate (1 mg/mL in hypotonic buffer). A reference for each measurement was prepared without cell lysate. The reaction was quenched with MeCN (1:1) and stored at -20 °C. RP-HPLC: column hydro C18, 50-95 % MeCN/H_2O + 0.1 % HCOOH over 5 min, 0.5 mL/min, 30 µL.

Supplementary data NMR-Spectra

^{1}H NMR spectrum of **2k**

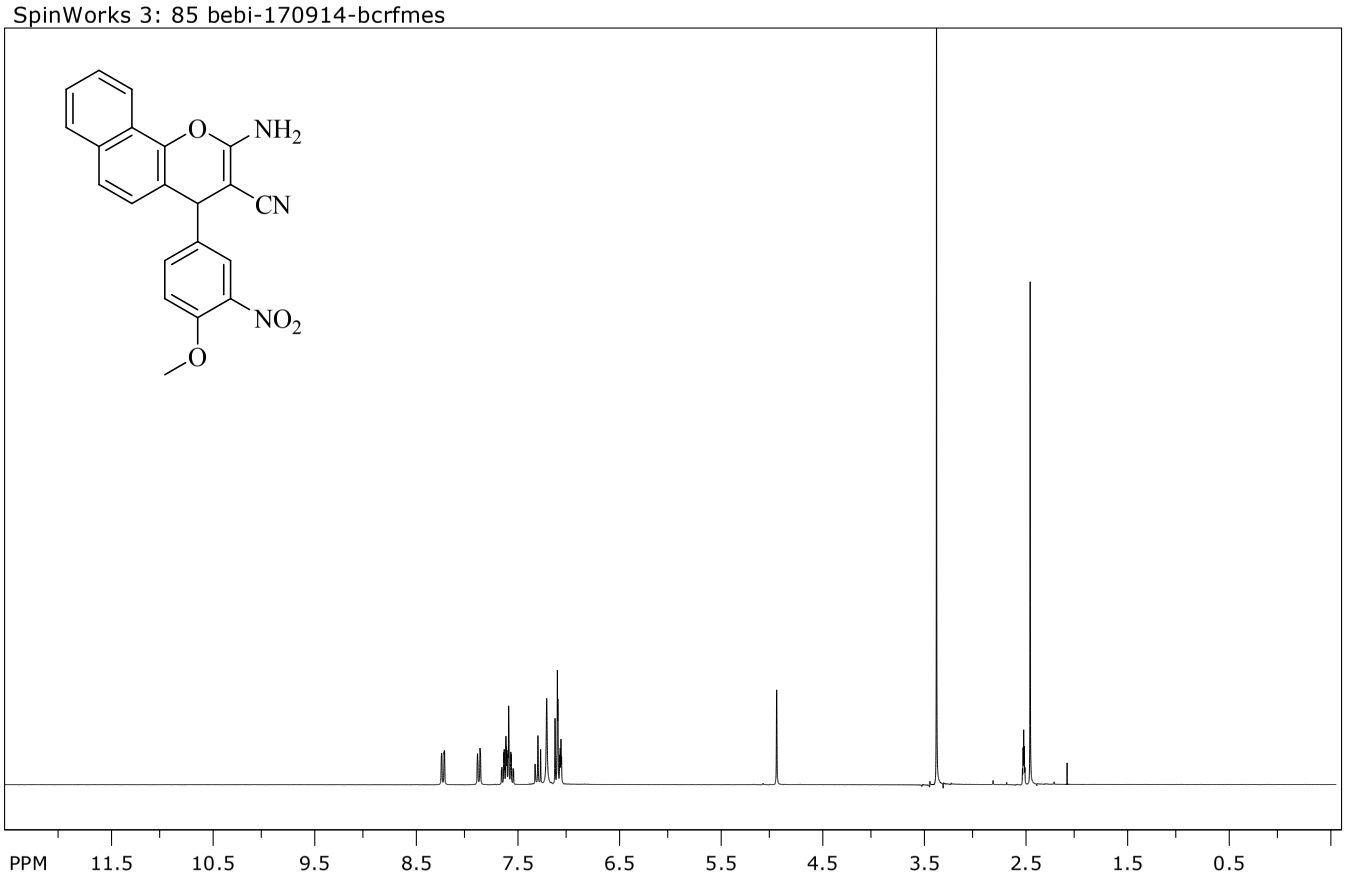

file: ...0104\Desktop\NMR.Bcr\0914bb3\1\fid expt: <zg30>
transmitter freq.: 300.131801 MHz
time domain size: 32768 points
width: 4496.40 Hz = 14.9814 ppm = 0.137219 Hz/pt
number of scans: 32

freq. of 0 ppm: 300.130002 MHz
processed size: 32768 complex points
LB: 0.000 GF: 0.0000
Hz/cm: 158.077 ppm/cm: 0.52669

^{13}C NMR spectrum of **2k**

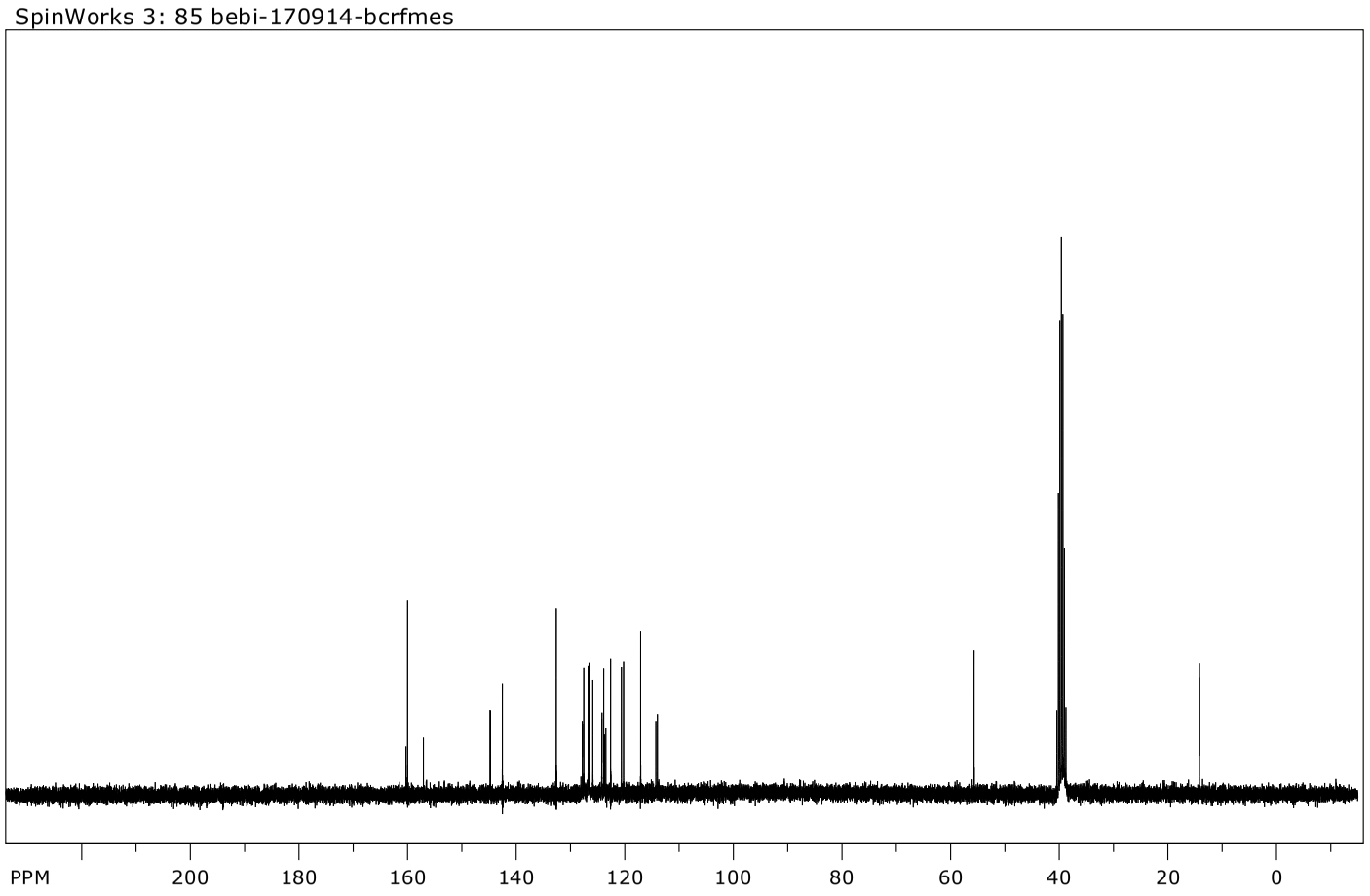

file: ...0104\Desktop\NMR.Bcr\0914bb3\2\fid expt: <zgpg30>
transmitter freq.: 75.476050 MHz
time domain size: 32768 points
width: 18832.39 Hz = 249.5148 ppm = 0.574719 Hz/pt
number of scans: 3905

freq. of 0 ppm: 75.467784 MHz
processed size: 32768 complex points
LB: 0.000 GF: 0.0000
Hz/cm: 753.296 ppm/cm: 9.98059

^{1}H NMR spectrum of **2l**

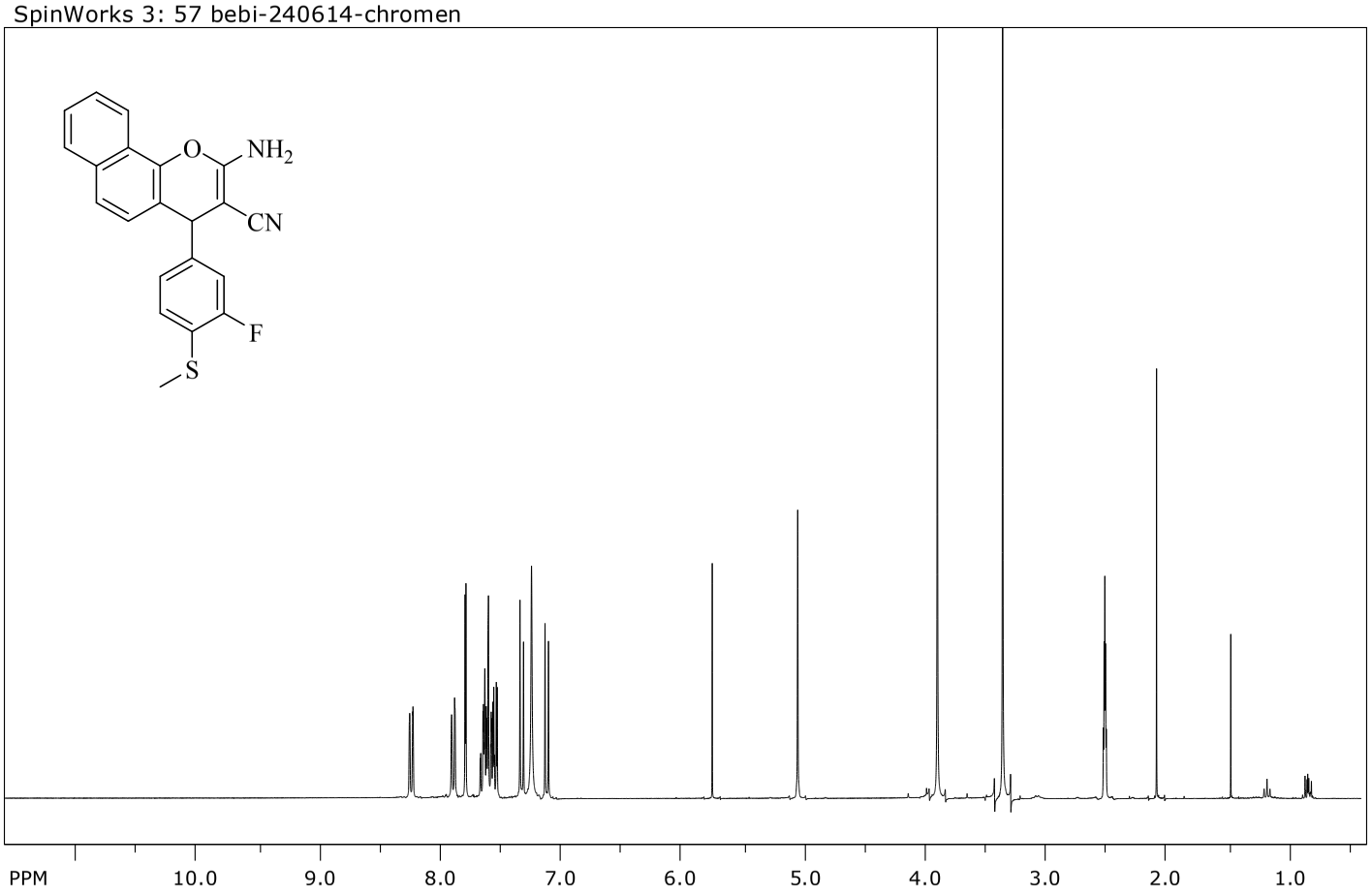

file: ...104\Desktop\NMR.Bcr\0614bb19\1\fid expt: <zg30>
transmitter freq.: 300.131801 MHz
time domain size: 32768 points
width: 4496.40 Hz = 14.9814 ppm = 0.137219 Hz/pt
number of scans: 32

freq. of 0 ppm: 300.130001 MHz
processed size: 32768 complex points
LB: 0.000 GF: 0.0000
Hz/cm: 134.892 ppm/cm: 0.44944

^{13}C NMR spectrum of **2l**

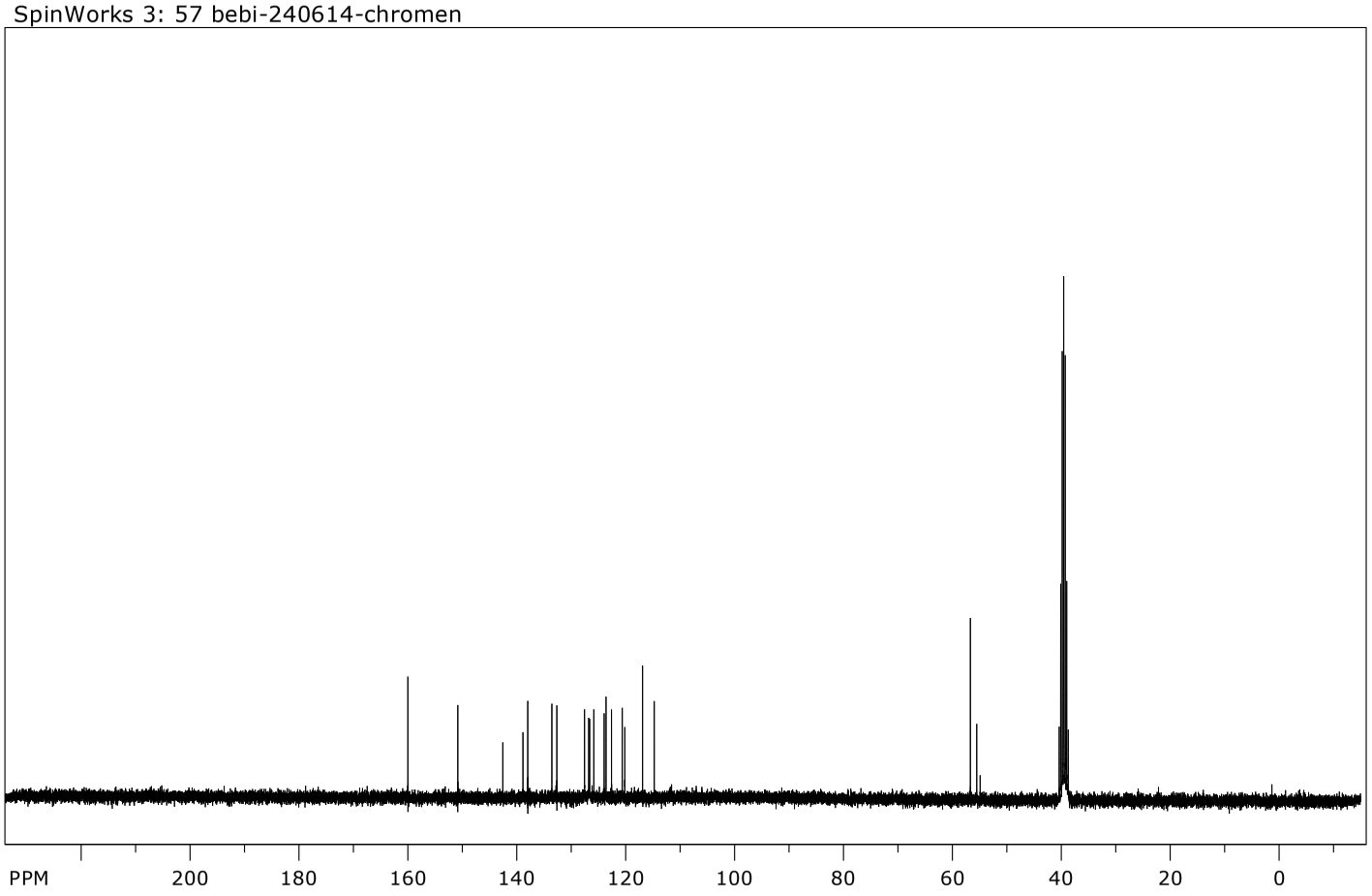

file: ...104\Desktop\NMR.Bcr\0614bb19\2\fid expt: <zgpg30>
transmitter freq.: 75.476050 MHz
time domain size: 32768 points
width: 18832.39 Hz = 249.5148 ppm = 0.574719 Hz/pt
number of scans: 6020

freq. of 0 ppm: 75.467785 MHz
processed size: 32768 complex points
LB: 0.000 GF: 0.0000
Hz/cm: 753.296 ppm/cm: 9.98059

^{1}H NMR spectrum of **2m**

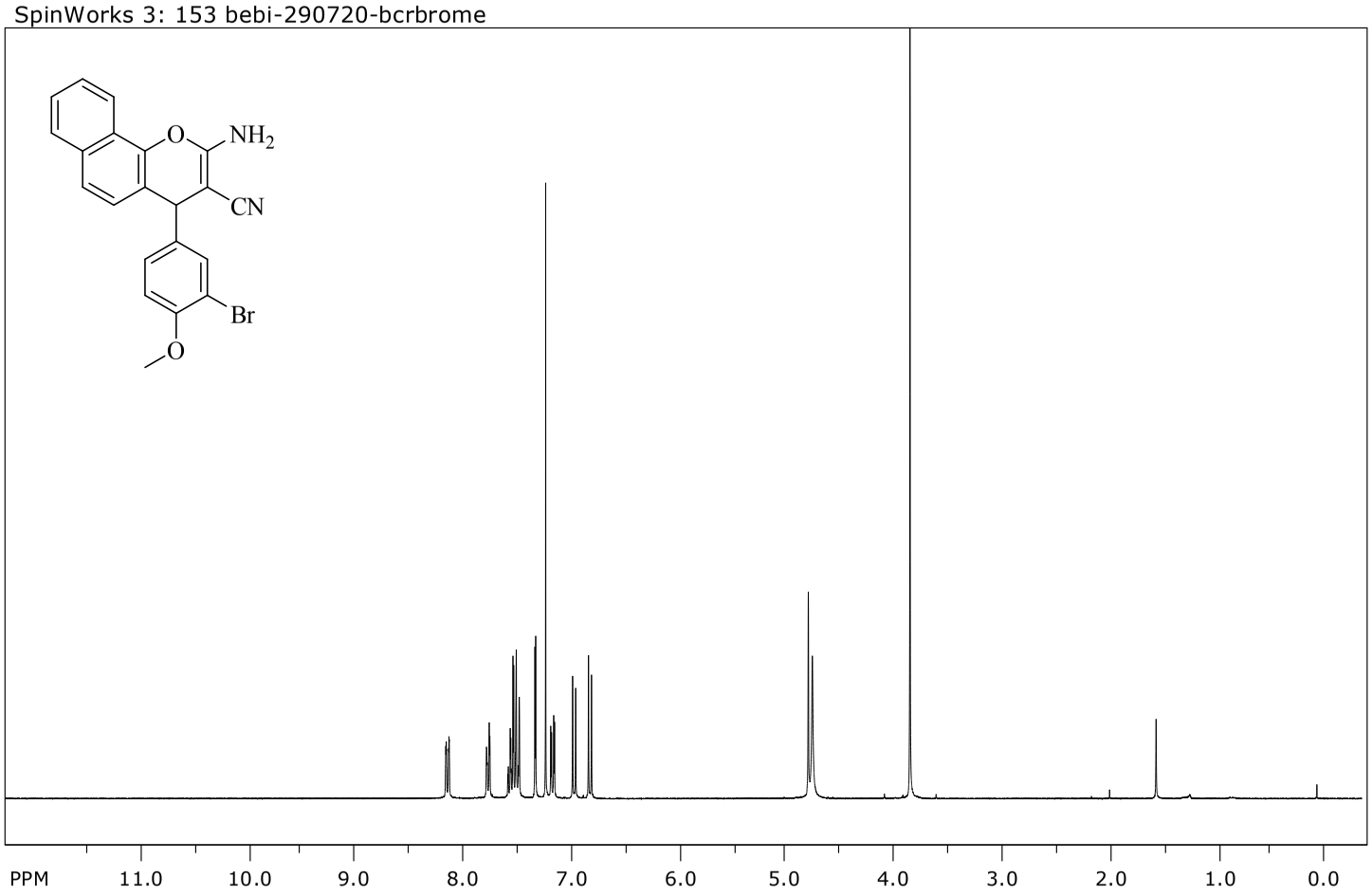

file: ...abor310104\Desktop\0720bb23\10\fid expt: <zg30>
transmitter freq.: 300.131801 MHz
time domain size: 65536 points
width: 8992.81 Hz = 29.9629 ppm = 0.137219 Hz/pt
number of scans: 40

freq. of 0 ppm: 300.130013 MHz
processed size: 65536 complex points
LB: 0.000 GF: 0.0000
Hz/cm: 151.754 ppm/cm: 0.50562

^{13}C NMR spectrum of **2m**

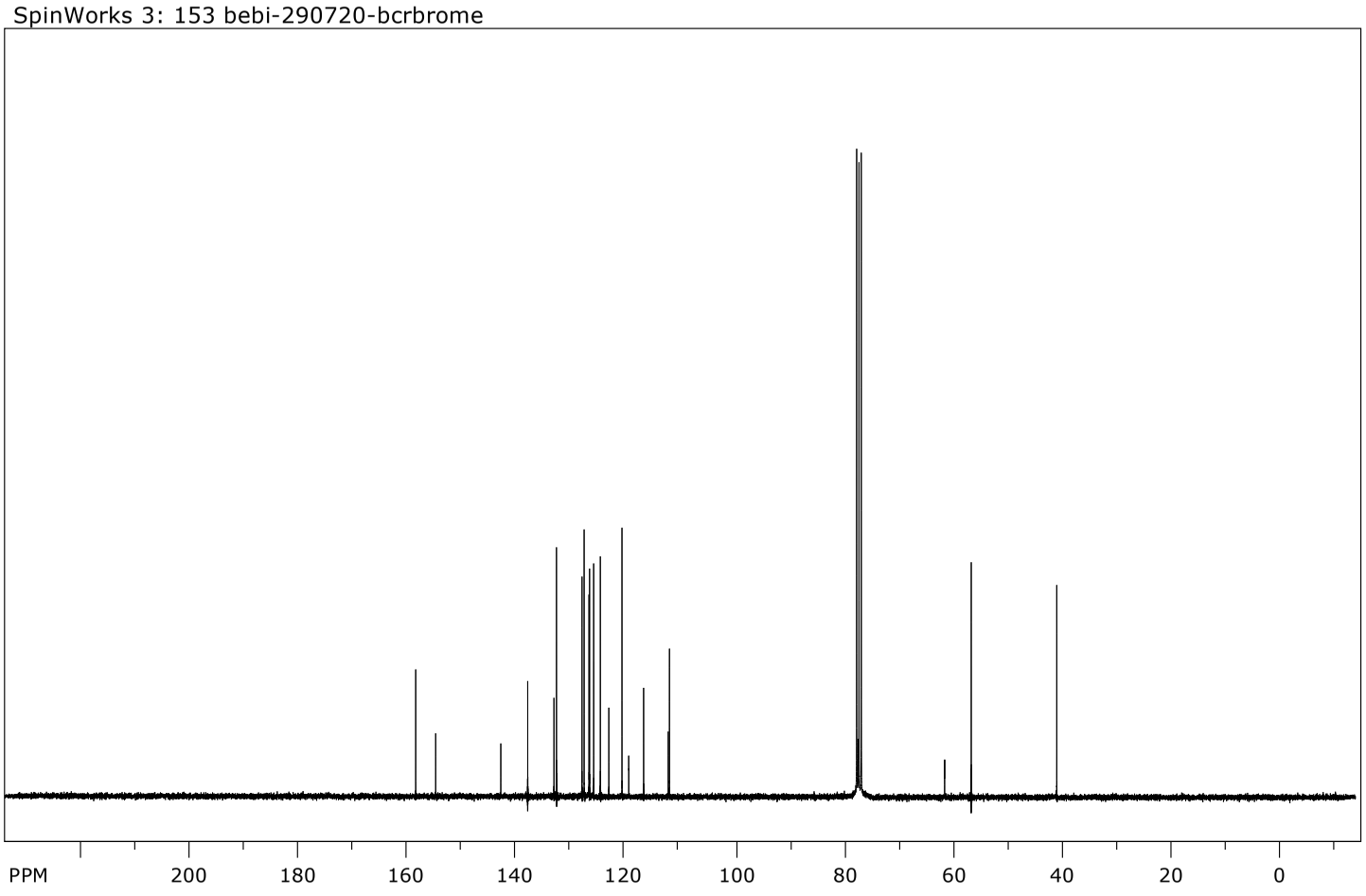

file: ...abor310104\Desktop\0720bb23\20\fid expt: <zgpg30>
transmitter freq.: 75.476050 MHz
time domain size: 32768 points
width: 18832.39 Hz = 249.5148 ppm = 0.574719 Hz/pt
number of scans: 47616

freq. of 0 ppm: 75.467750 MHz
processed size: 32768 complex points
LB: 0.000 GF: 0.0000
Hz/cm: 753.296 ppm/cm: 9.98059

120

^{1}H NMR spectrum of **2o**

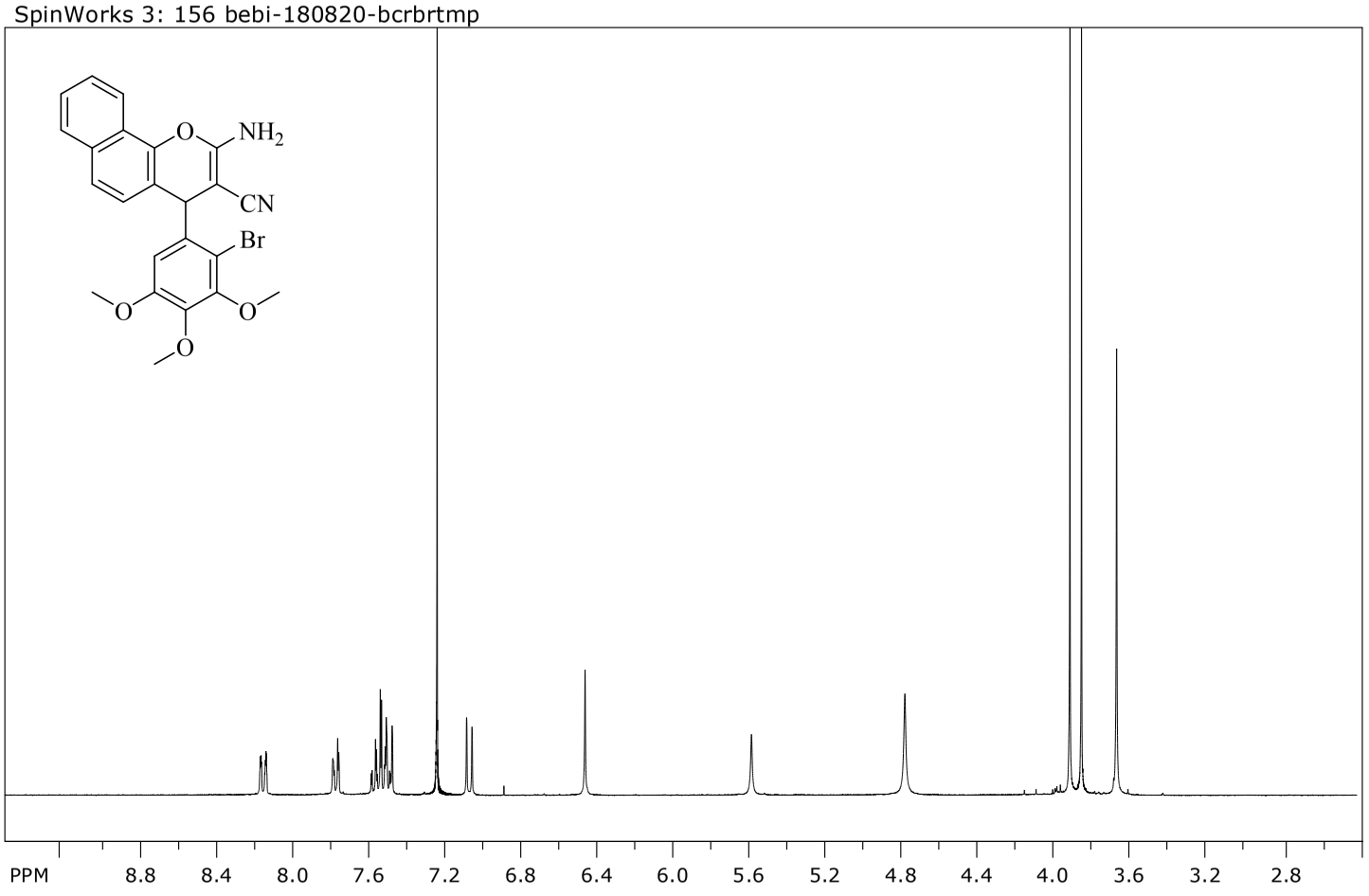

file: ...Labor310104\Desktop\0820bb22\1\fid expt: <zg30>
transmitter freq.: 300.131801 MHz
time domain size: 65536 points
width: 8992.81 Hz = 29.9629 ppm = 0.137219 Hz/pt
number of scans: 200

freq. of 0 ppm: 300.130013 MHz
processed size: 65536 complex points
LB: 0.000 GF: 0.0000
Hz/cm: 85.361 ppm/cm: 0.28441

^{13}C NMR spectrum of **2o**

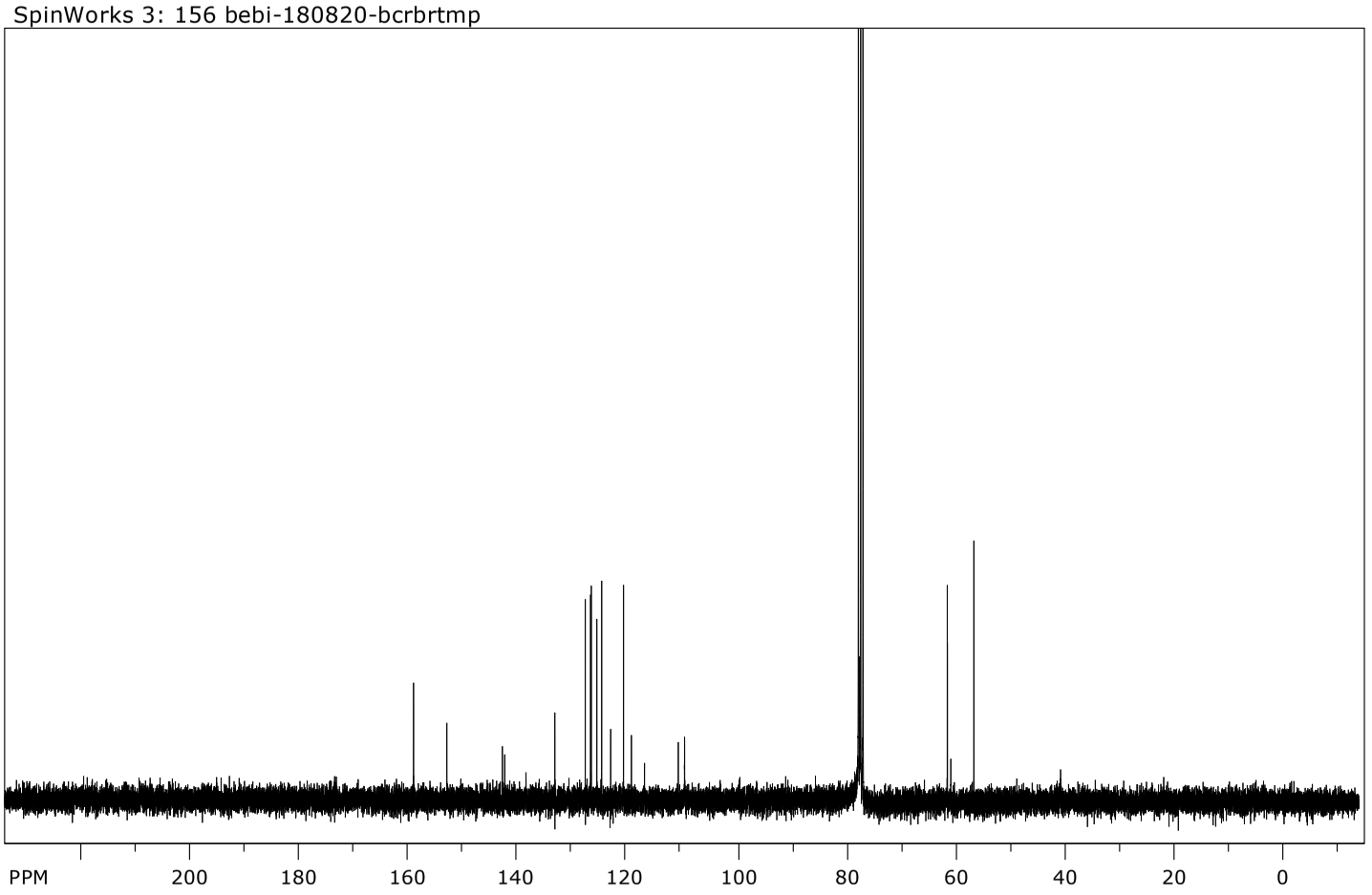

file: ...Labor310104\Desktop\0820bb22\2\fid expt: <zgpg30>
transmitter freq.: 75.476050 MHz
time domain size: 32768 points
width: 18832.39 Hz = 249.5148 ppm = 0.574719 Hz/pt
number of scans: 10356

freq. of 0 ppm: 75.467750 MHz
processed size: 32768 complex points
LB: 0.000 GF: 0.0000
Hz/cm: 753.296 ppm/cm: 9.98059

^{1}H NMR spectrum of **2p**

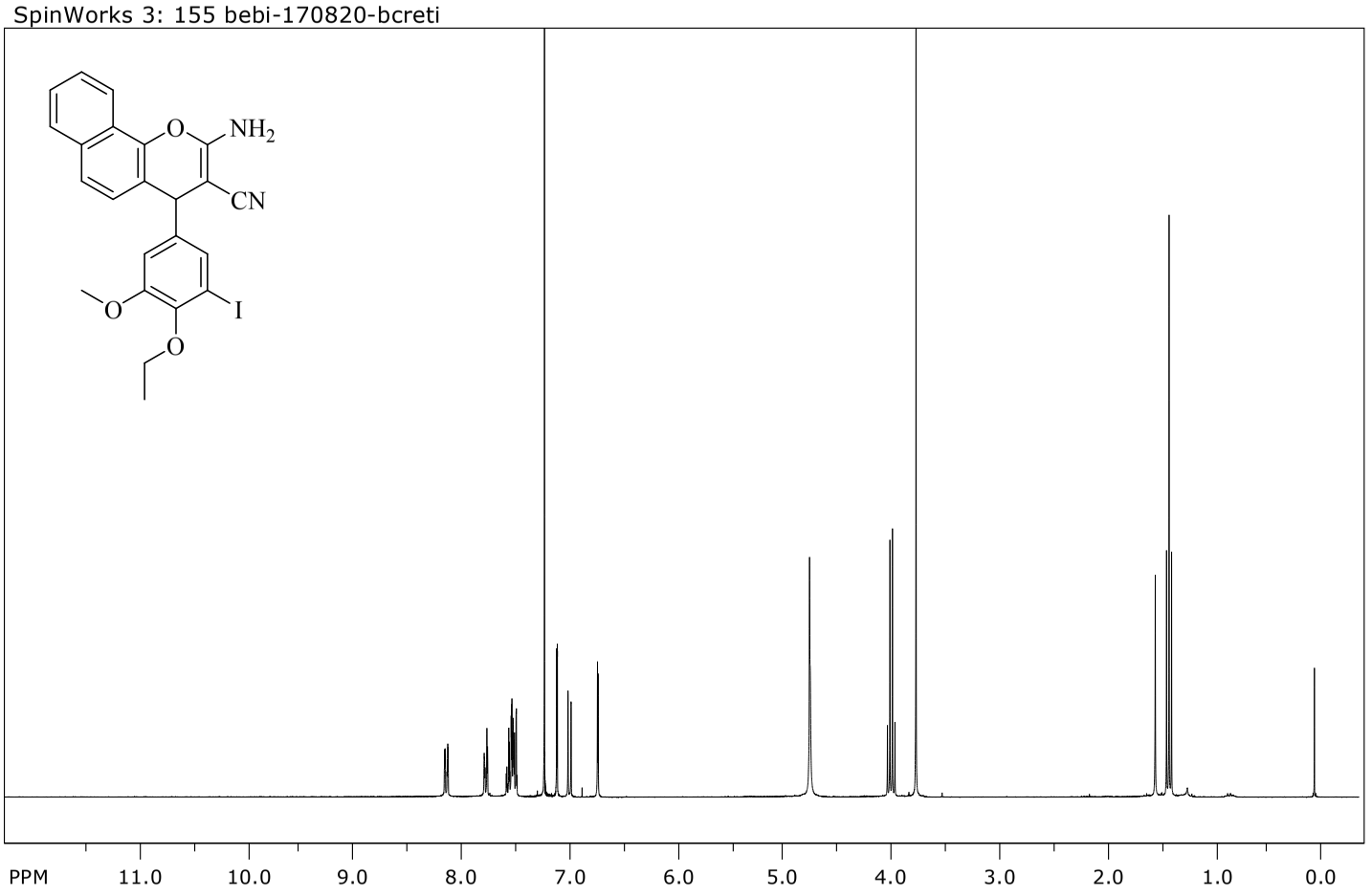

file: ...abor310104\Desktop\0820bb21\10\fid expt: <zg30>
transmitter freq.: 300.131801 MHz
time domain size: 65536 points
width: 8992.81 Hz = 29.9629 ppm = 0.137219 Hz/pt
number of scans: 200

freq. of 0 ppm: 300.130013 MHz
processed size: 65536 complex points
LB: 0.000 GF: 0.0000
Hz/cm: 151.754 ppm/cm: 0.50562

123

^{13}C NMR spectrum of **2p**

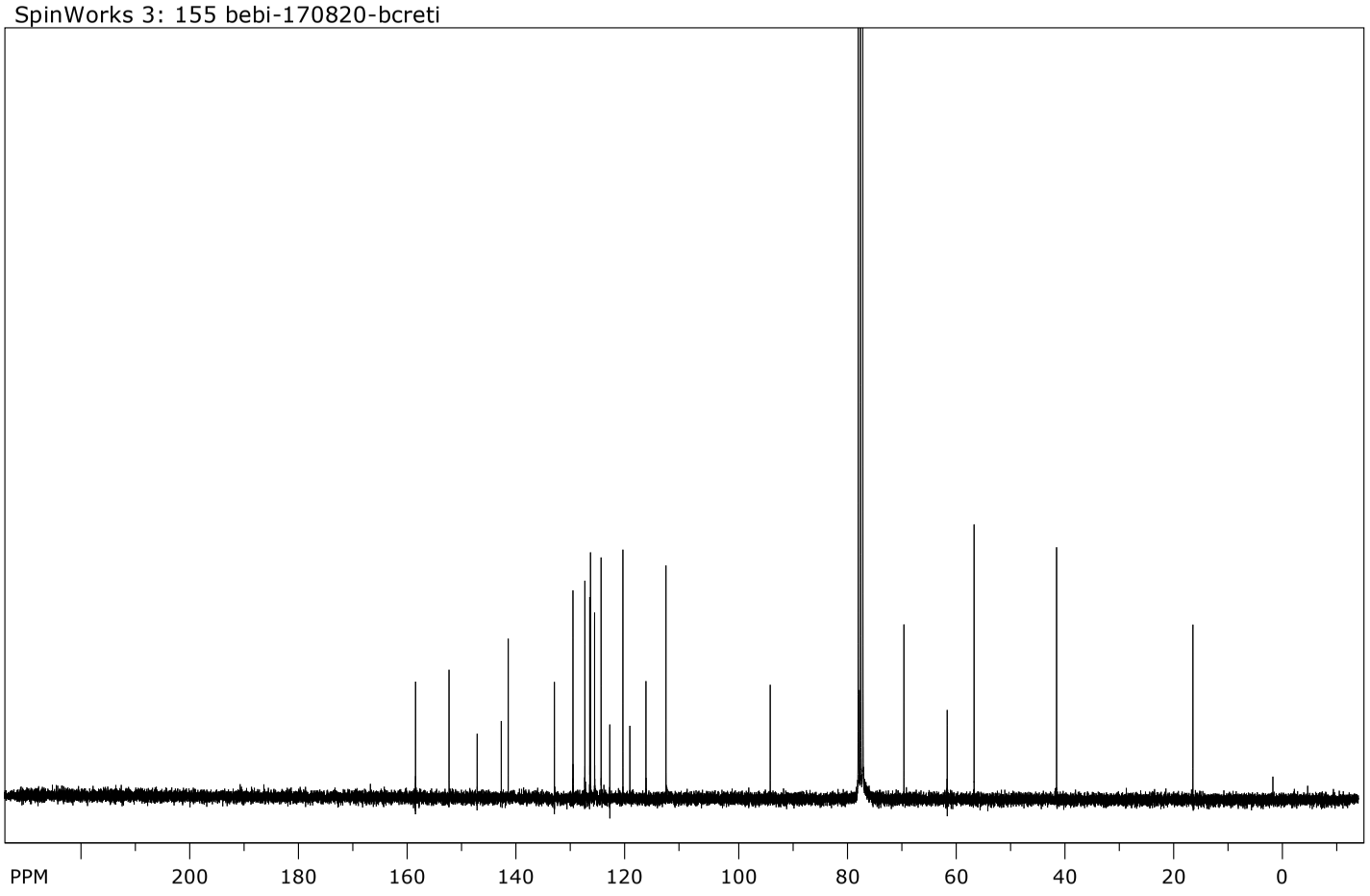

file: ...abor310104\Desktop\0820bb21\11\fid expt: <zgpg30>
transmitter freq.: 75.476050 MHz
time domain size: 32768 points
width: 18832.39 Hz = 249.5148 ppm = 0.574719 Hz/pt
number of scans: 28268

freq. of 0 ppm: 75.467749 MHz
processed size: 32768 complex points
LB: 0.000 GF: 0.0000
Hz/cm: 753.296 ppm/cm: 9.98059

124

^{1}H NMR spectrum of **2q**

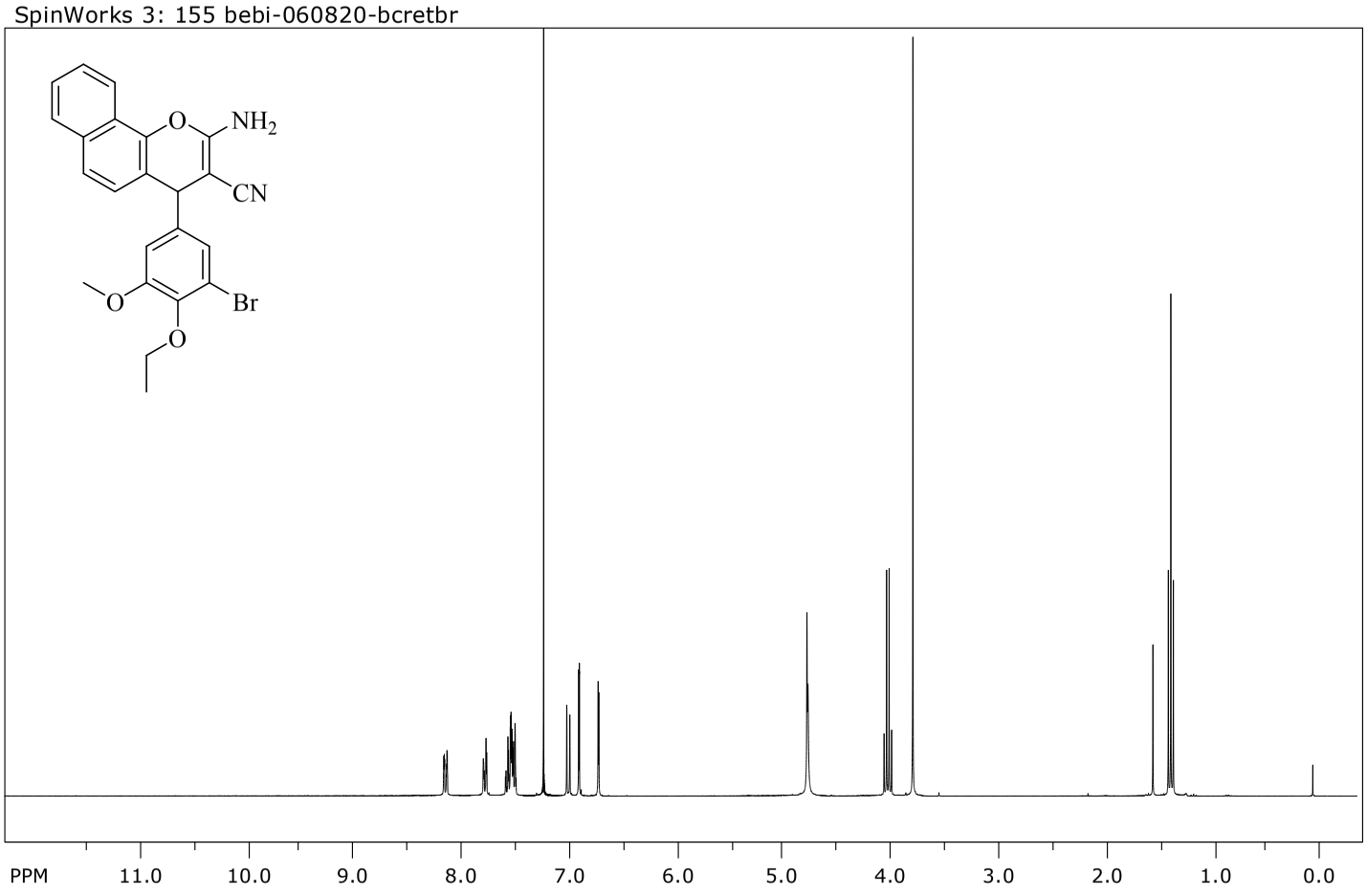

file: ...abor310104\Desktop\0820bb11\10\fid expt: <zg30>
transmitter freq.: 300.131801 MHz
time domain size: 65536 points
width: 8992.81 Hz = 29.9629 ppm = 0.137219 Hz/pt
number of scans: 200

freq. of 0 ppm: 300.130013 MHz
processed size: 65536 complex points
LB: 0.000 GF: 0.0000
Hz/cm: 151.754 ppm/cm: 0.50562

^{13}C NMR spectrum of **2q**

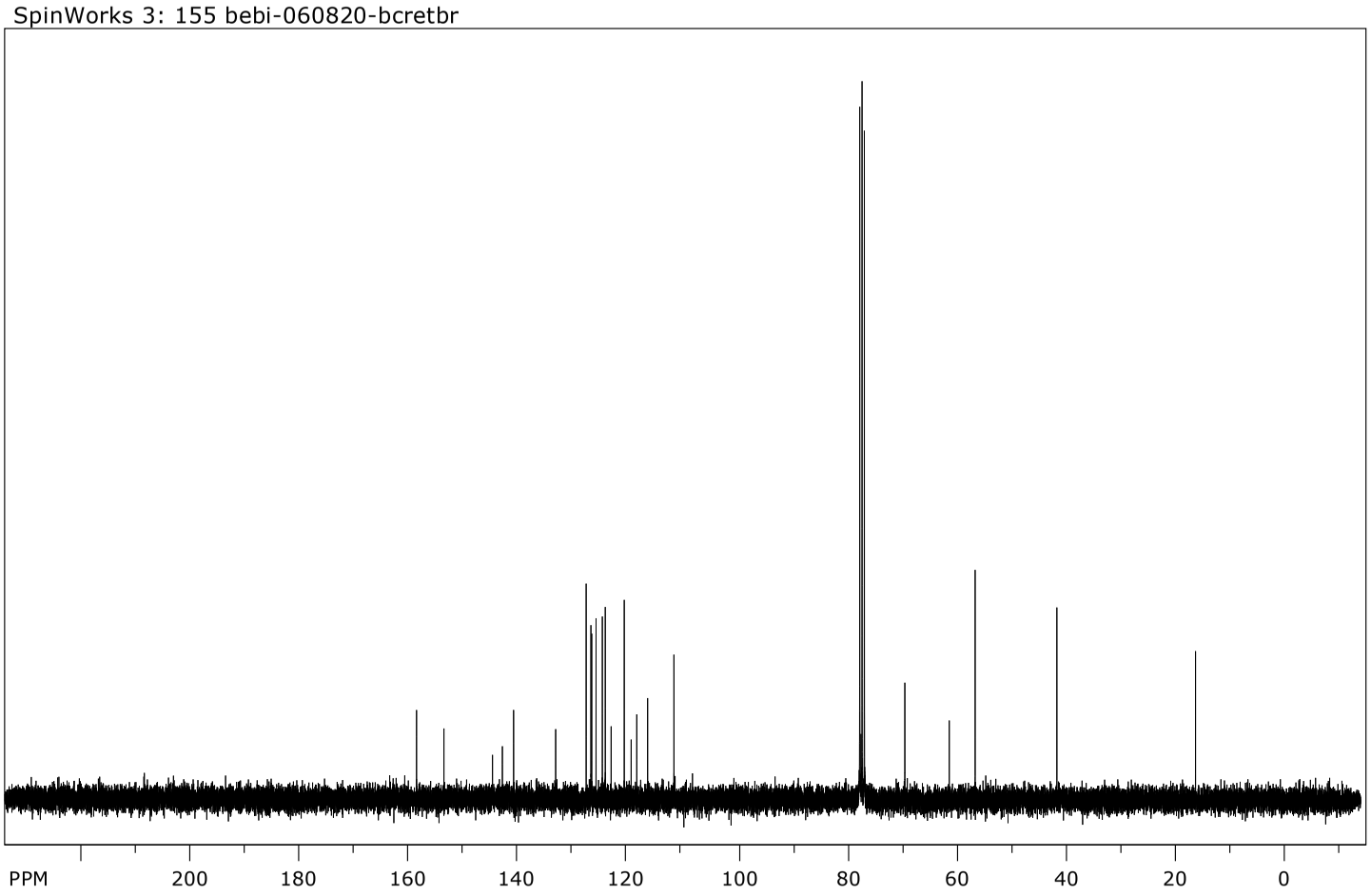

file: ...abor310104\Desktop\0820bb11\11\fid expt: <zgpg30>
transmitter freq.: 75.476050 MHz
time domain size: 32768 points
width: 18832.39 Hz = 249.5148 ppm = 0.574719 Hz/pt
number of scans: 2320

freq. of 0 ppm: 75.467750 MHz
processed size: 32768 complex points
LB: 0.000 GF: 0.0000
Hz/cm: 753.296 ppm/cm: 9.98059

^{1}H NMR spectrum of **3a**

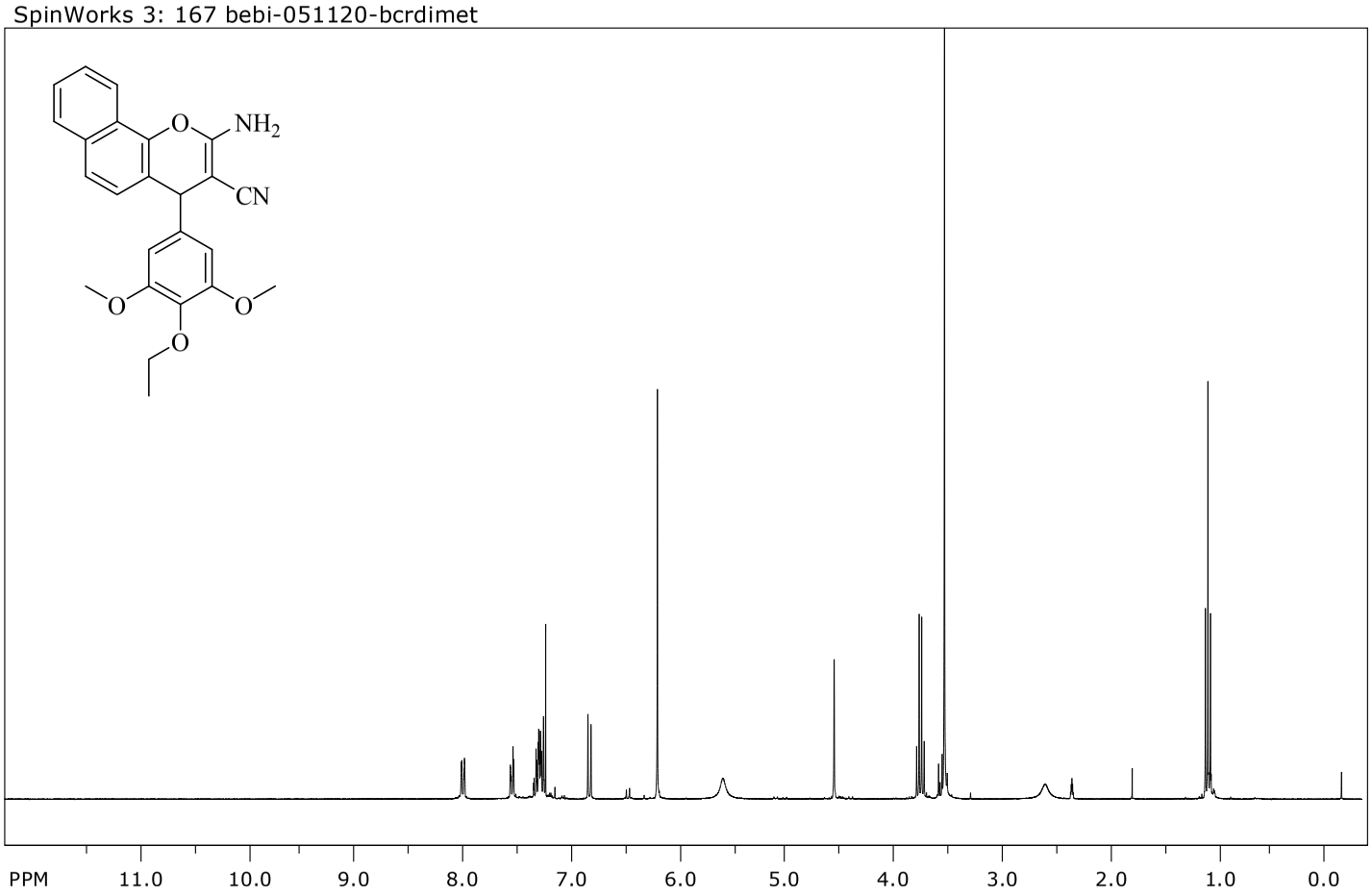

file: ...04\Desktop\NMR.Bcr\1120bb12\10\fid expt: <zg30>
transmitter freq.: 300.131801 MHz
time domain size: 65536 points
width: 8992.81 Hz = 29.9629 ppm = 0.137219 Hz/pt
number of scans: 32

freq. of 0 ppm: 300.130013 MHz
processed size: 65536 complex points
LB: 0.000 GF: 0.0000
Hz/cm: 151.754 ppm/cm: 0.50562

127

^{13}C NMR spectrum of **3a**

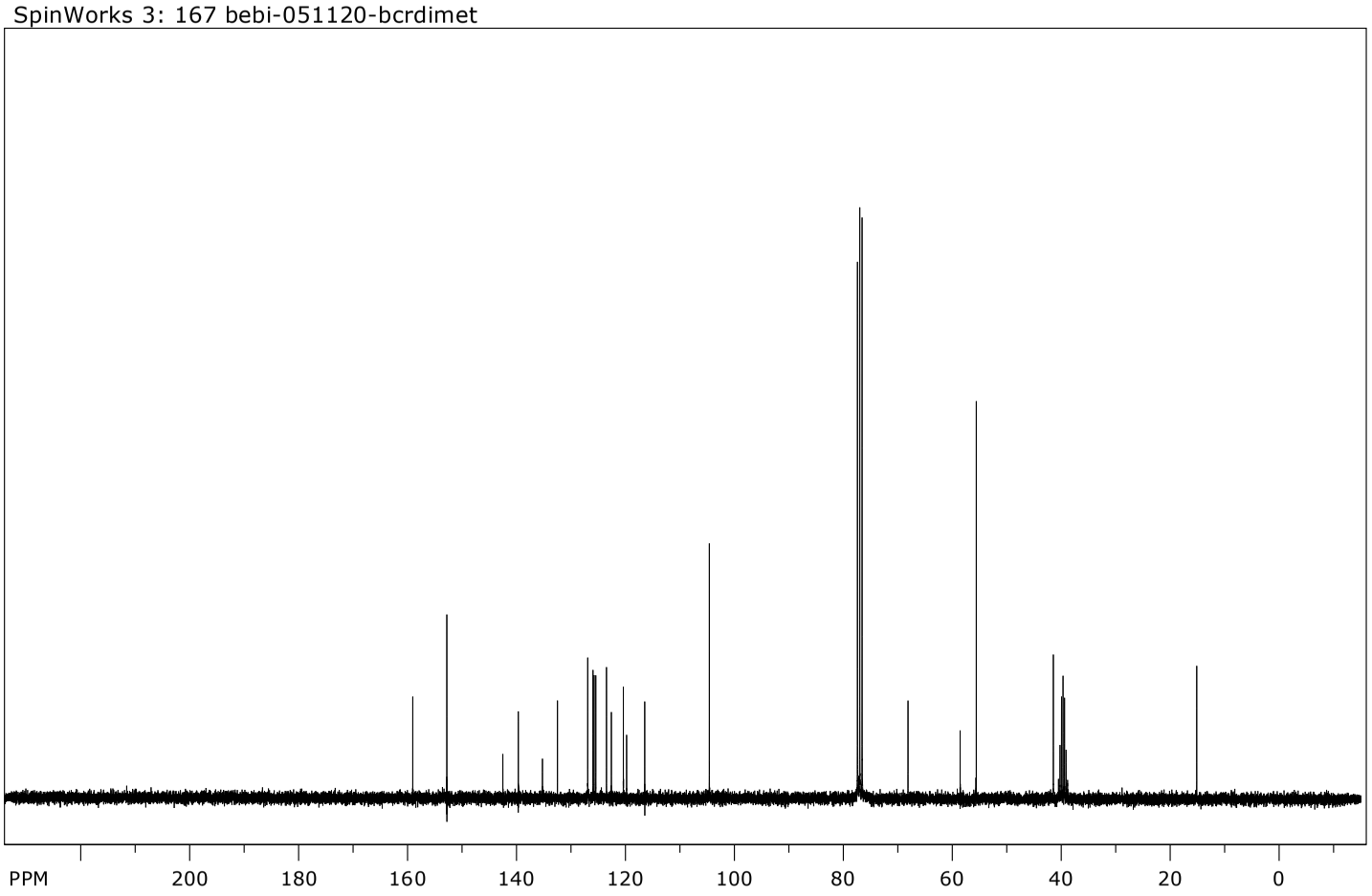

file: ...04\Desktop\NMR.Bcr\1120bb12\20\fid expt: <zgpg30>
transmitter freq.: 75.476050 MHz
time domain size: 32768 points
width: 18832.39 Hz = 249.5148 ppm = 0.574719 Hz/pt
number of scans: 6144

freq. of 0 ppm: 75.467780 MHz
processed size: 32768 complex points
LB: 0.000 GF: 0.0000
Hz/cm: 753.296 ppm/cm: 9.98059

128

^{1}H NMR spectrum of **3b**

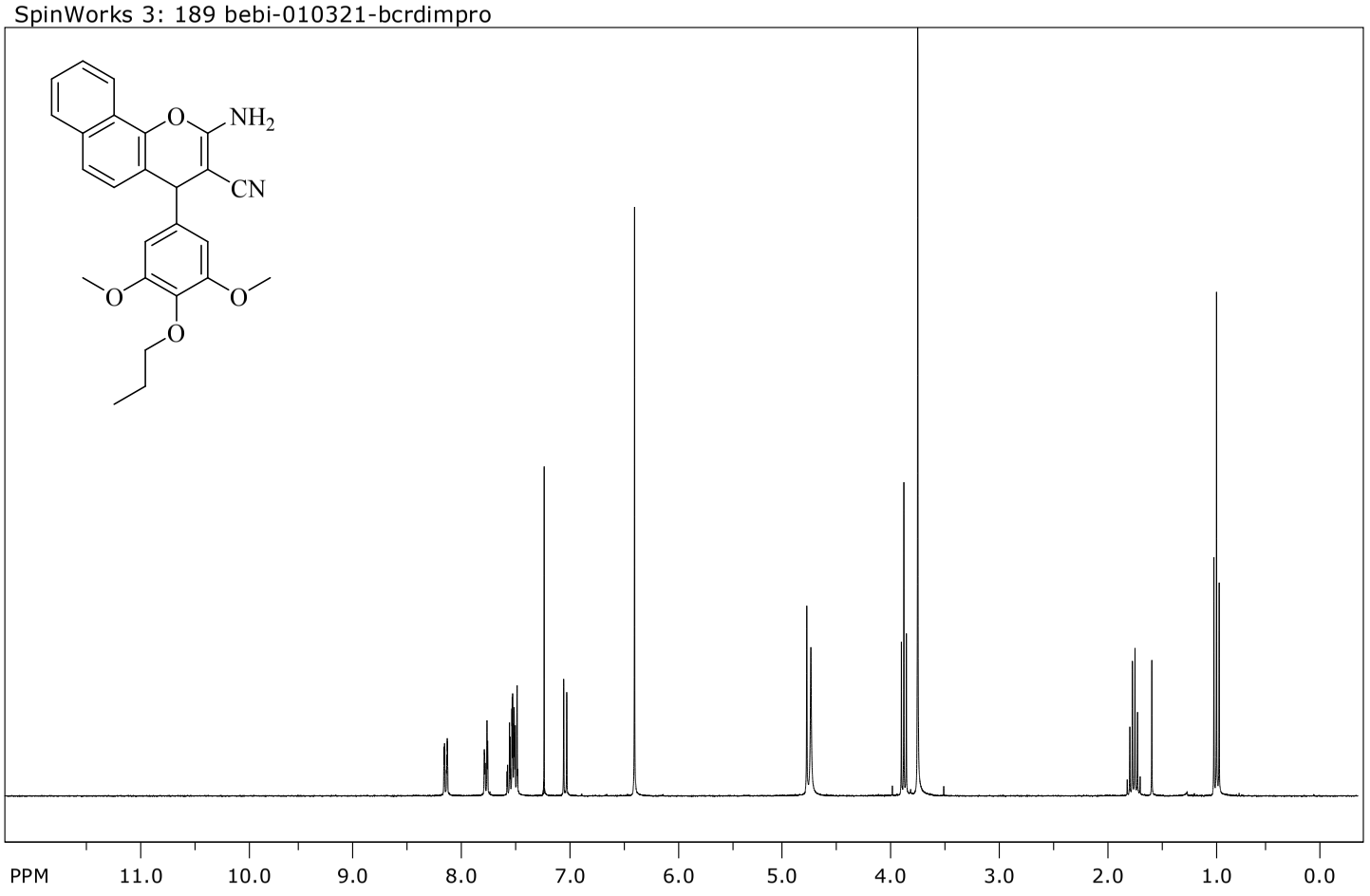

file: ...104\Desktop\NMR.Bcr\0321bb1\10\fid expt: <zg30>
transmitter freq.: 300.131801 MHz
time domain size: 65536 points
width: 8992.81 Hz = 29.9629 ppm = 0.137219 Hz/pt
number of scans: 44

freq. of 0 ppm: 300.130013 MHz
processed size: 65536 complex points
LB: 0.000 GF: 0.0000
Hz/cm: 151.754 ppm/cm: 0.50562

129

^{13}C NMR spectrum of **3b**

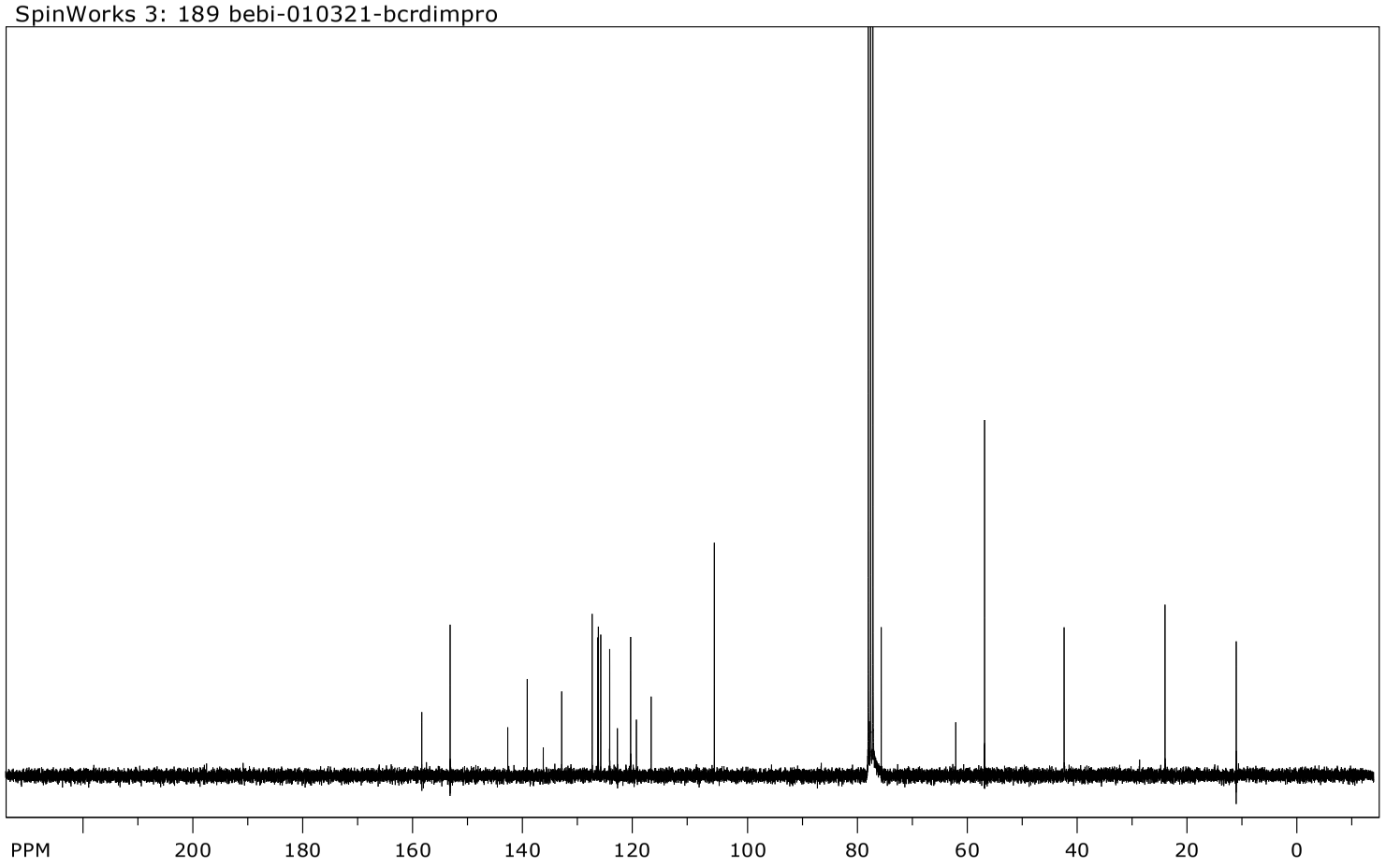

file: ...Labor310104\Desktop\0321bb1\20\fid expt: <zgpg30>
transmitter freq.: 75.476050 MHz
time domain size: 32768 points
width: 18832.39 Hz = 249.5148 ppm = 0.574719 Hz/pt
number of scans: 28268

freq. of 0 ppm: 75.467750 MHz
processed size: 32768 complex points
LB: 0.000 GF: 0.0000
Hz/cm: 753.296 ppm/cm: 9.98059

130

^{1}H NMR spectrum of **3c**

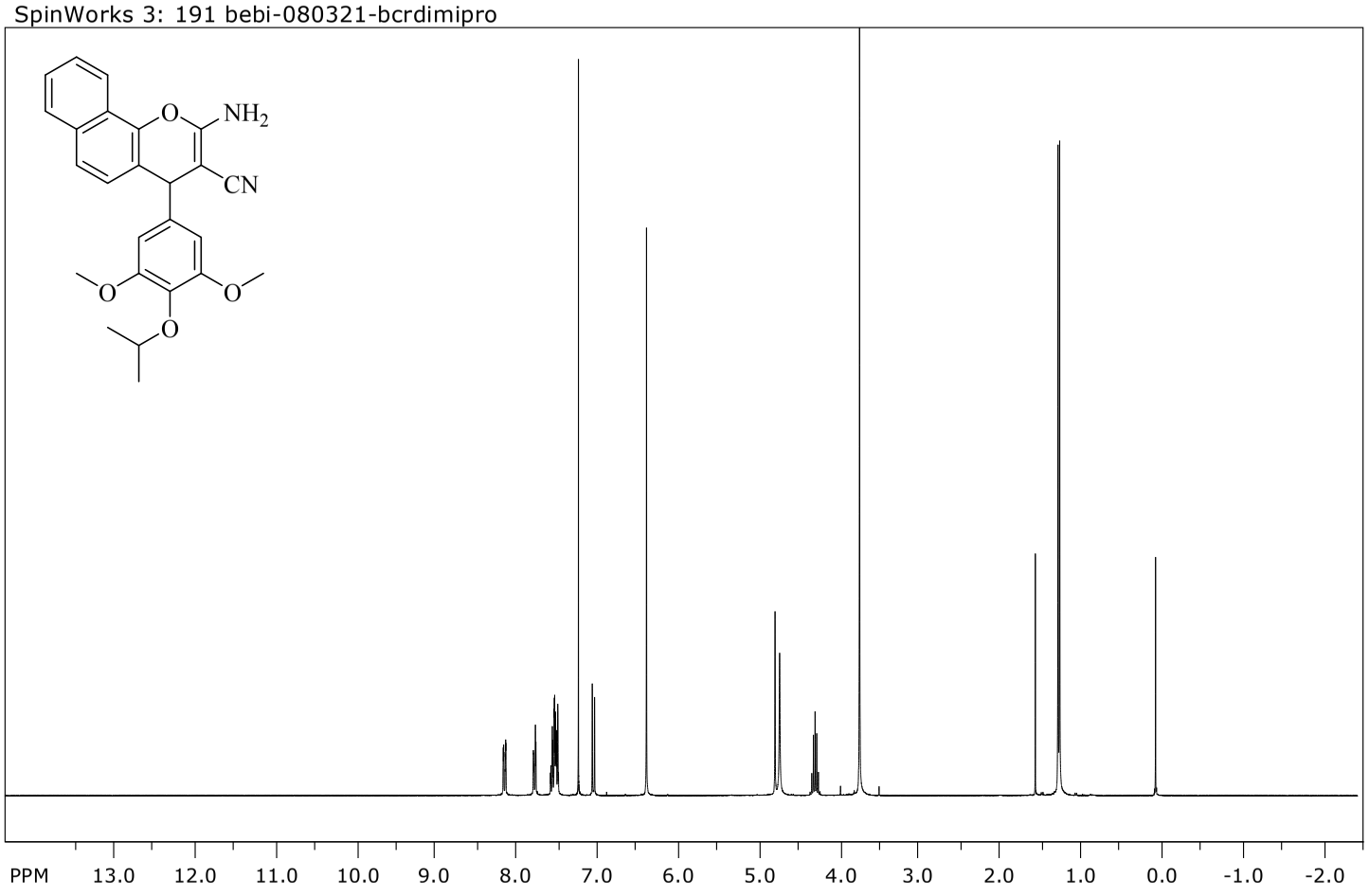

file: ...04\Desktop\NMR.Bcr\0321bb11\10\fid expt: <zg30>
transmitter freq.: 300.131801 MHz
time domain size: 65536 points
width: 8992.81 Hz = 29.9629 ppm = 0.137219 Hz/pt
number of scans: 200

freq. of 0 ppm: 300.130013 MHz
processed size: 65536 complex points
LB: 0.000 GF: 0.0000
Hz/cm: 202.338 ppm/cm: 0.67416

131

^{13}C NMR spectrum of **3c**

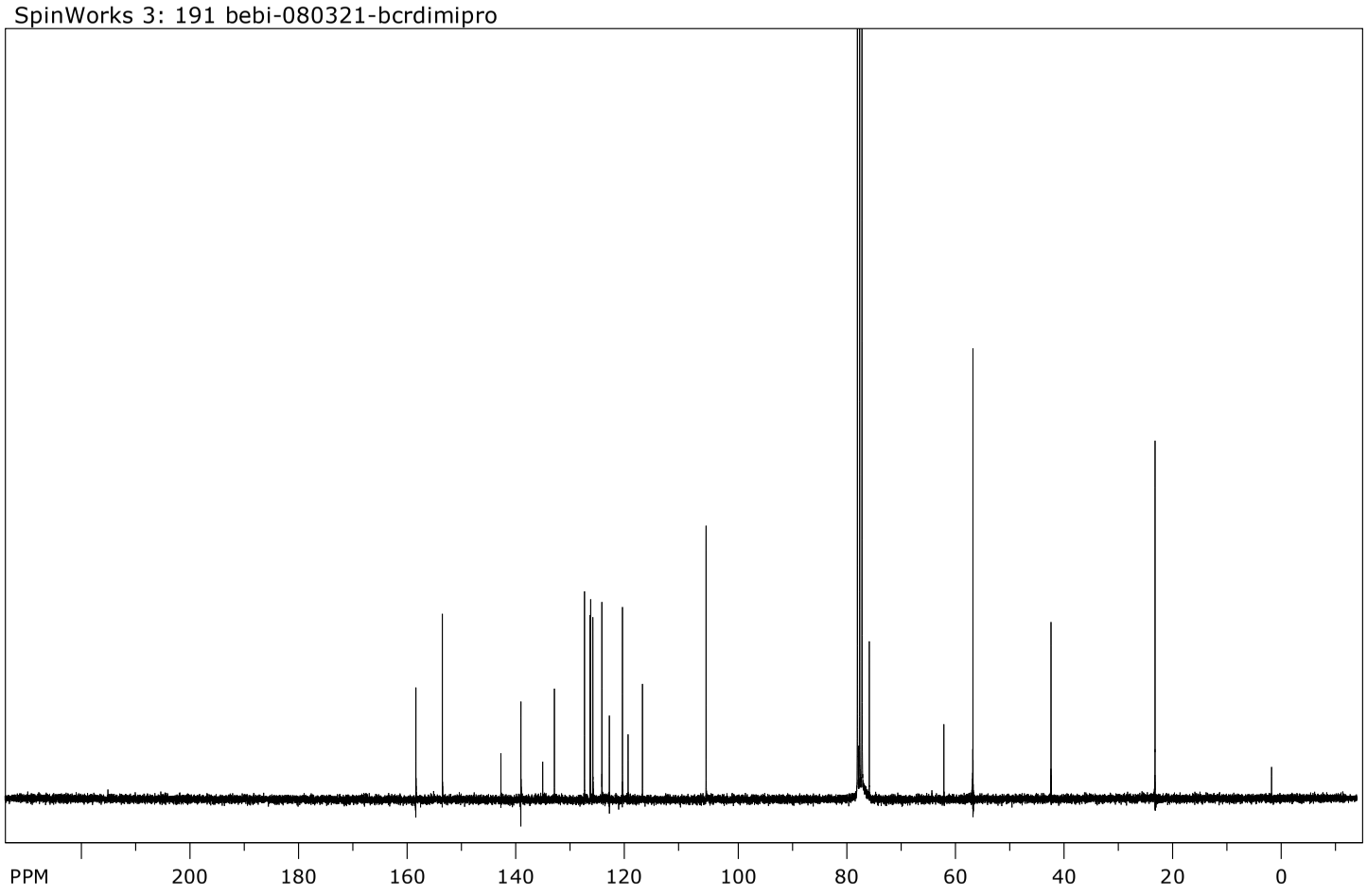

file: ...04\Desktop\NMR.Bcr\0321bb11\11\fid expt: <zgpg30>
transmitter freq.: 75.476050 MHz
time domain size: 32768 points
width: 18832.39 Hz = 249.5148 ppm = 0.574719 Hz/pt
number of scans: 48508

freq. of 0 ppm: 75.467750 MHz
processed size: 32768 complex points
LB: 0.000 GF: 0.0000
Hz/cm: 753.296 ppm/cm: 9.98059

^{1}H NMR spectrum of **3d**

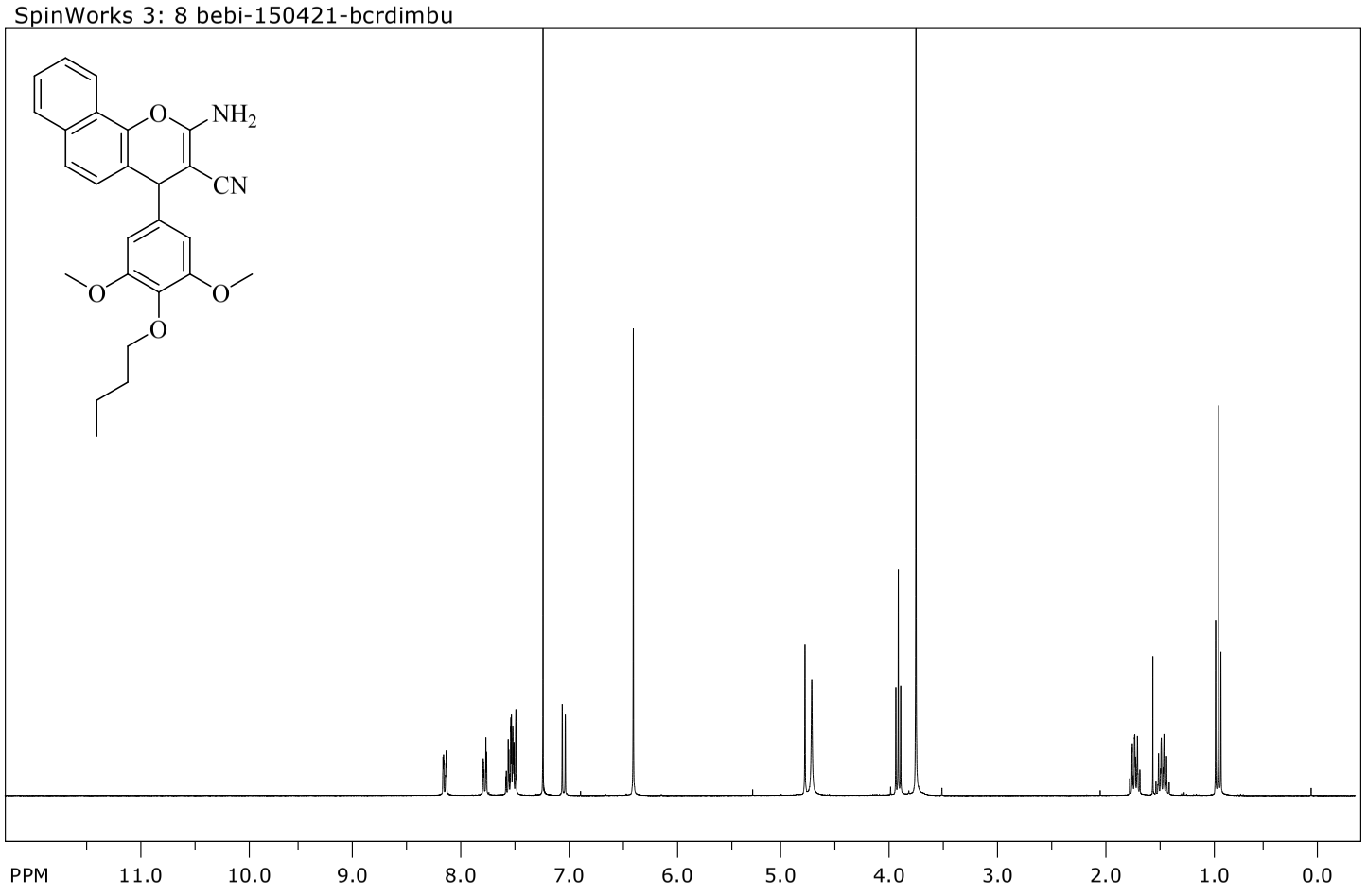

file: ...04\Desktop\NMR.Bcr\0421bb24\10\fid expt: <zg30>
transmitter freq.: 300.131801 MHz
time domain size: 65536 points
width: 8992.81 Hz = 29.9629 ppm = 0.137219 Hz/pt
number of scans: 200

freq. of 0 ppm: 300.130013 MHz
processed size: 65536 complex points
LB: 0.000 GF: 0.0000
Hz/cm: 151.754 ppm/cm: 0.50562

^{13}C NMR spectrum of **3d**

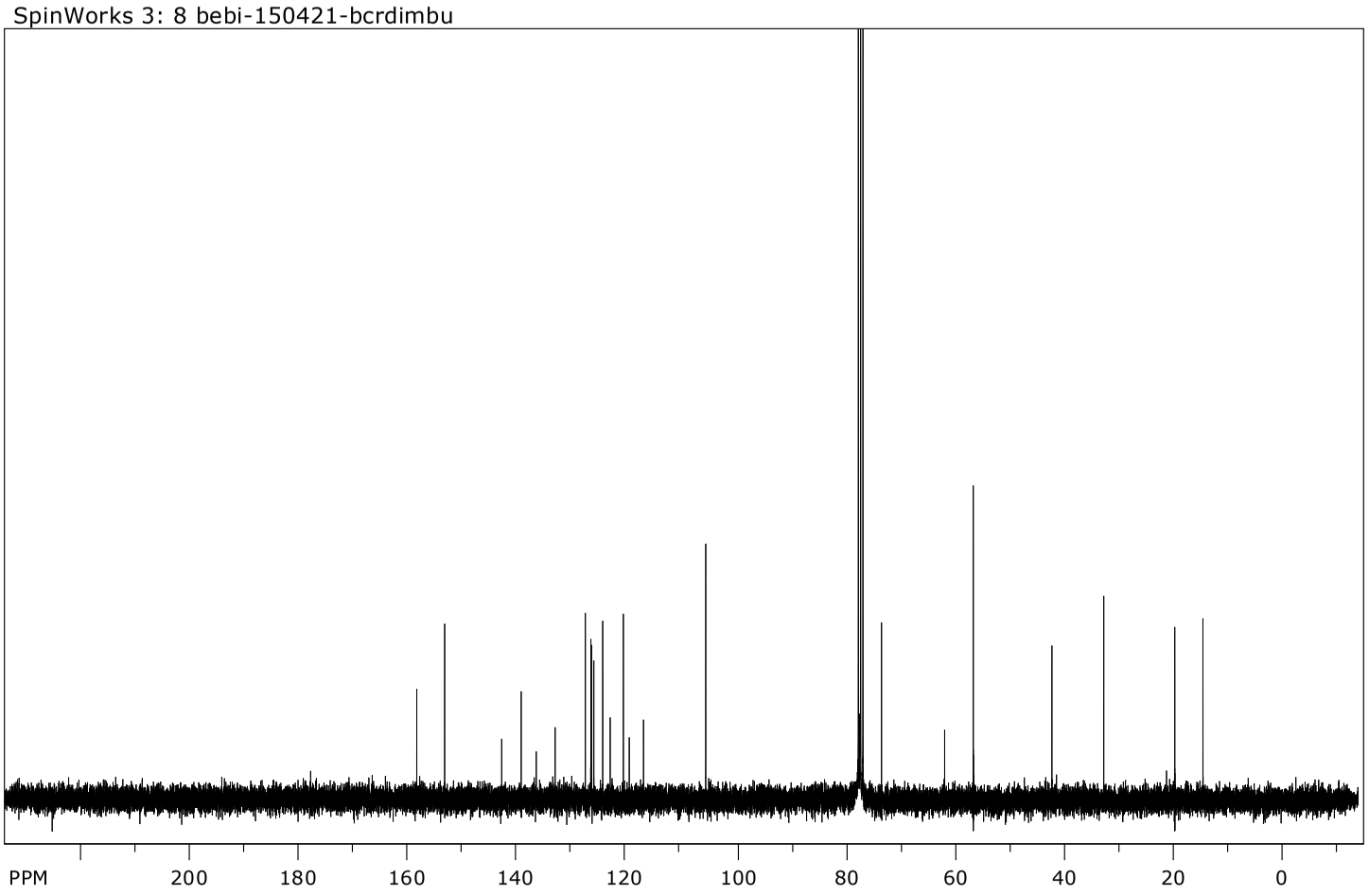

file: ...04\Desktop\NMR.Bcr\0421bb24\20\fid expt: <zgpg30>
transmitter freq.: 75.476050 MHz
time domain size: 32768 points
width: 18832.39 Hz = 249.5148 ppm = 0.574719 Hz/pt
number of scans: 4380

freq. of 0 ppm: 75.467750 MHz
processed size: 32768 complex points
LB: 0.000 GF: 0.0000
Hz/cm: 753.296 ppm/cm: 9.98059

^{1}H NMR spectrum of **3e**

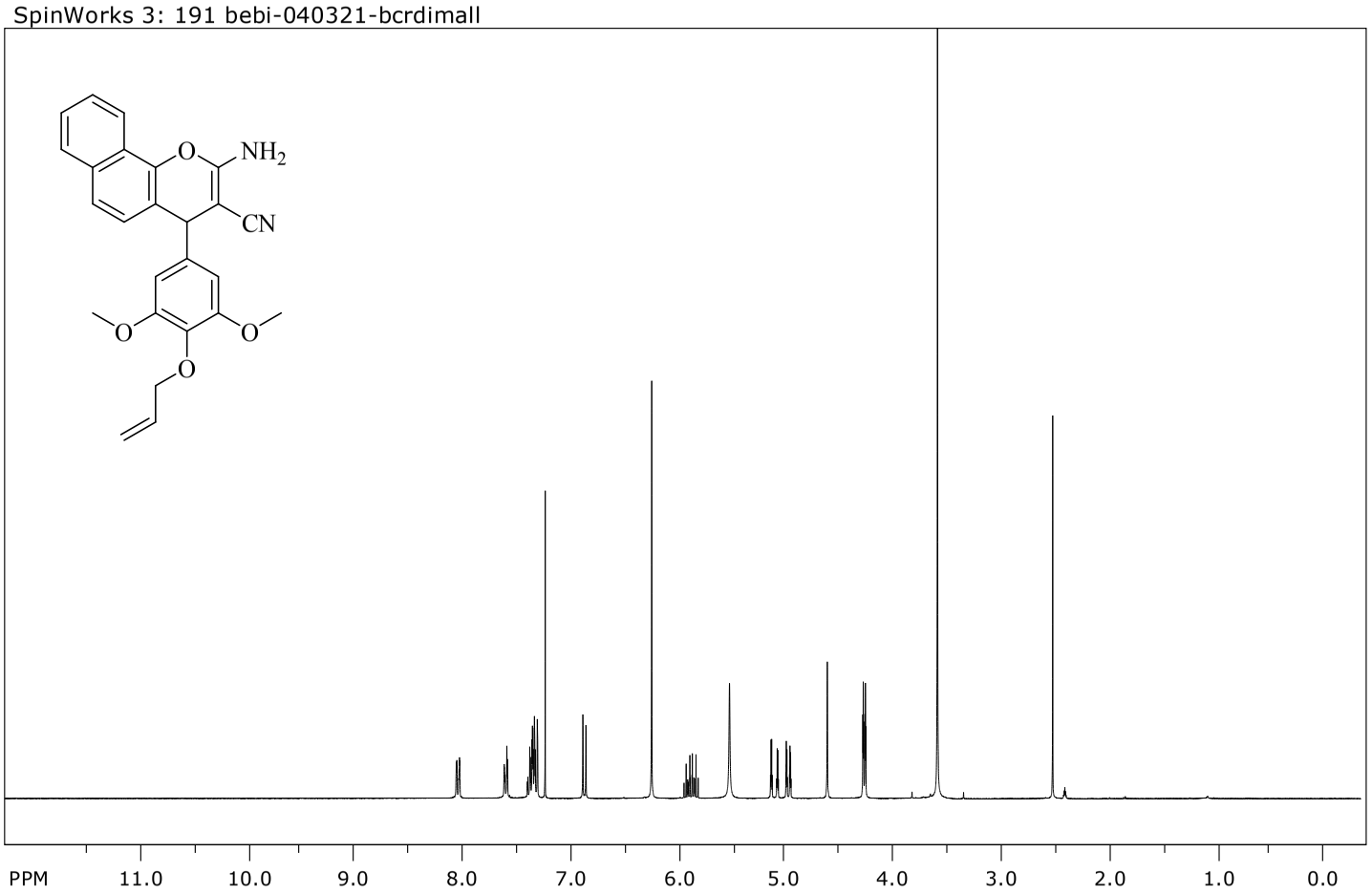

file: ...0104\Desktop\NMR.Bcr\0321bb8\1\fid expt: <zg30>
transmitter freq.: 300.131801 MHz
time domain size: 65536 points
width: 8992.81 Hz = 29.9629 ppm = 0.137219 Hz/pt
number of scans: 104

freq. of 0 ppm: 300.130013 MHz
processed size: 65536 complex points
LB: 0.000 GF: 0.0000
Hz/cm: 151.754 ppm/cm: 0.50562

^{13}C NMR spectrum of **3e**

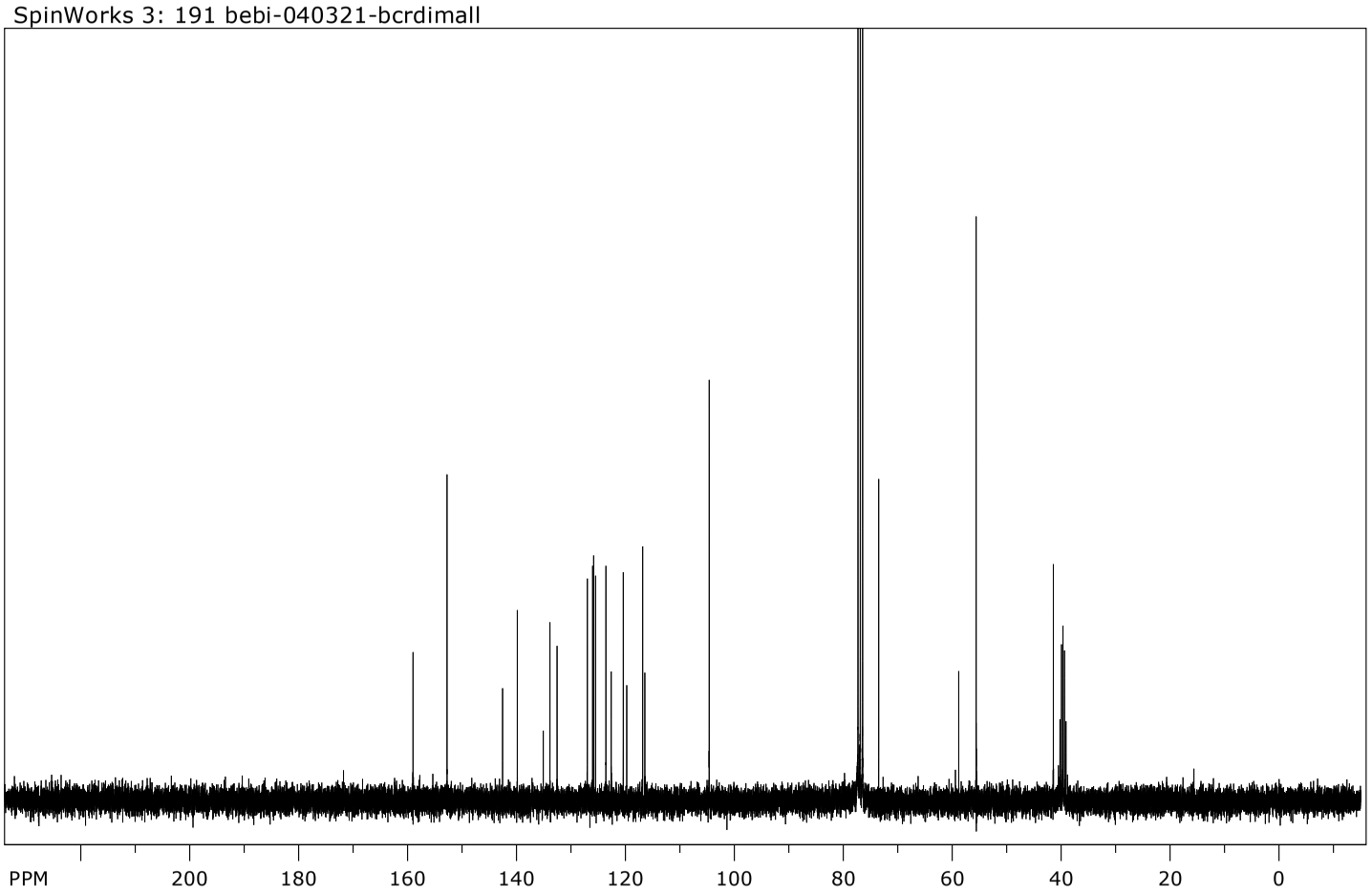

file: ...0104\Desktop\NMR.Bcr\0321bb8\2\fid expt: <zgpg30>
transmitter freq.: 75.476050 MHz
time domain size: 32768 points
width: 18832.39 Hz = 249.5148 ppm = 0.574719 Hz/pt
number of scans: 4776

freq. of 0 ppm: 75.467773 MHz
processed size: 32768 complex points
LB: 0.000 GF: 0.0000
Hz/cm: 753.296 ppm/cm: 9.98059

136

^{1}H NMR spectrum of **3f**

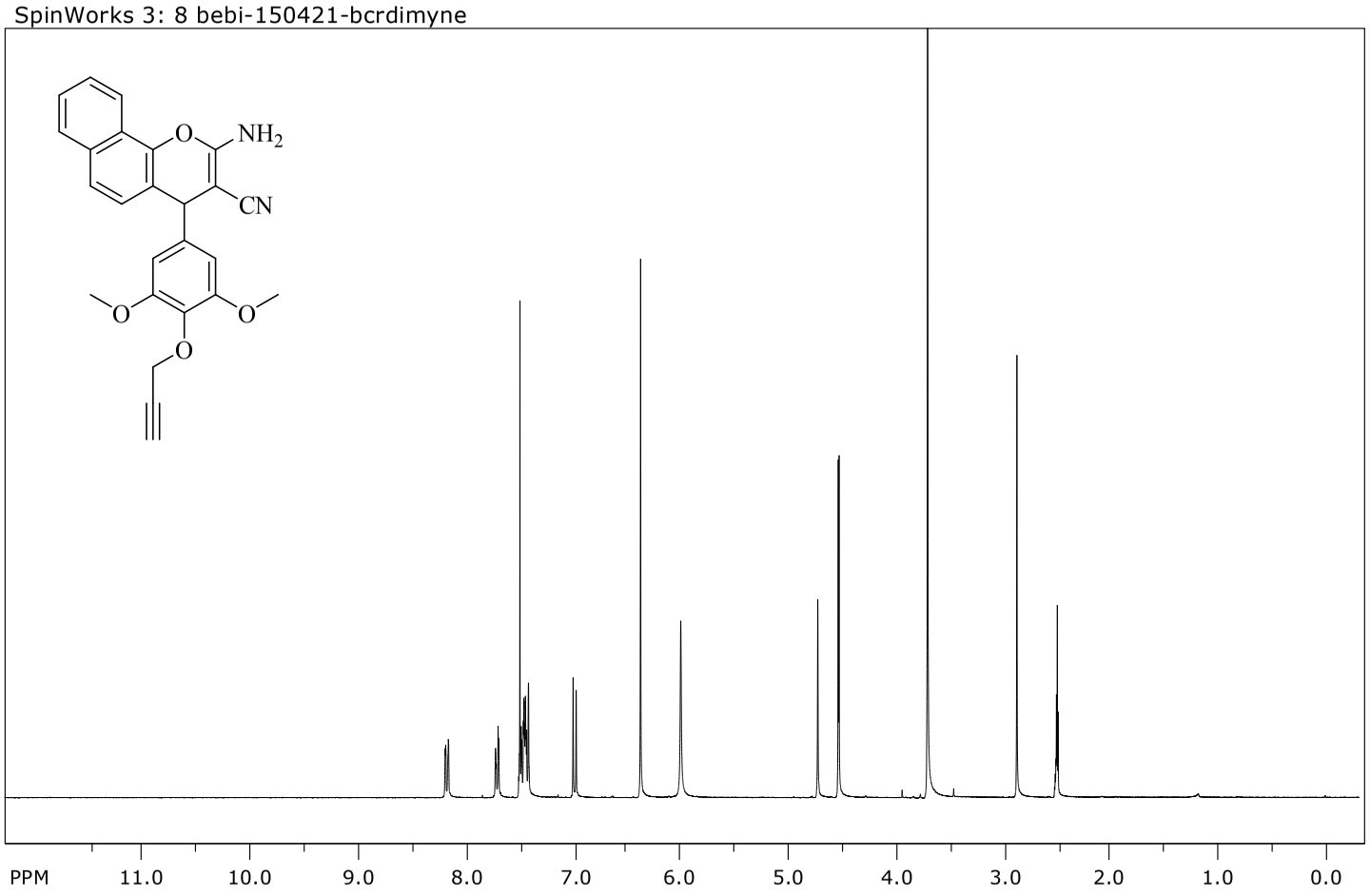

file: ...04\Desktop\NMR.Bcr\0421bb25\10\fid expt: <zg30>
transmitter freq.: 300.131801 MHz
time domain size: 65536 points
width: 8992.81 Hz = 29.9629 ppm = 0.137219 Hz/pt
number of scans: 200

freq. of 0 ppm: 300.130003 MHz
processed size: 65536 complex points
LB: 0.000 GF: 0.0000
Hz/cm: 151.754 ppm/cm: 0.50562

137

^{13}C NMR spectrum of **3f**

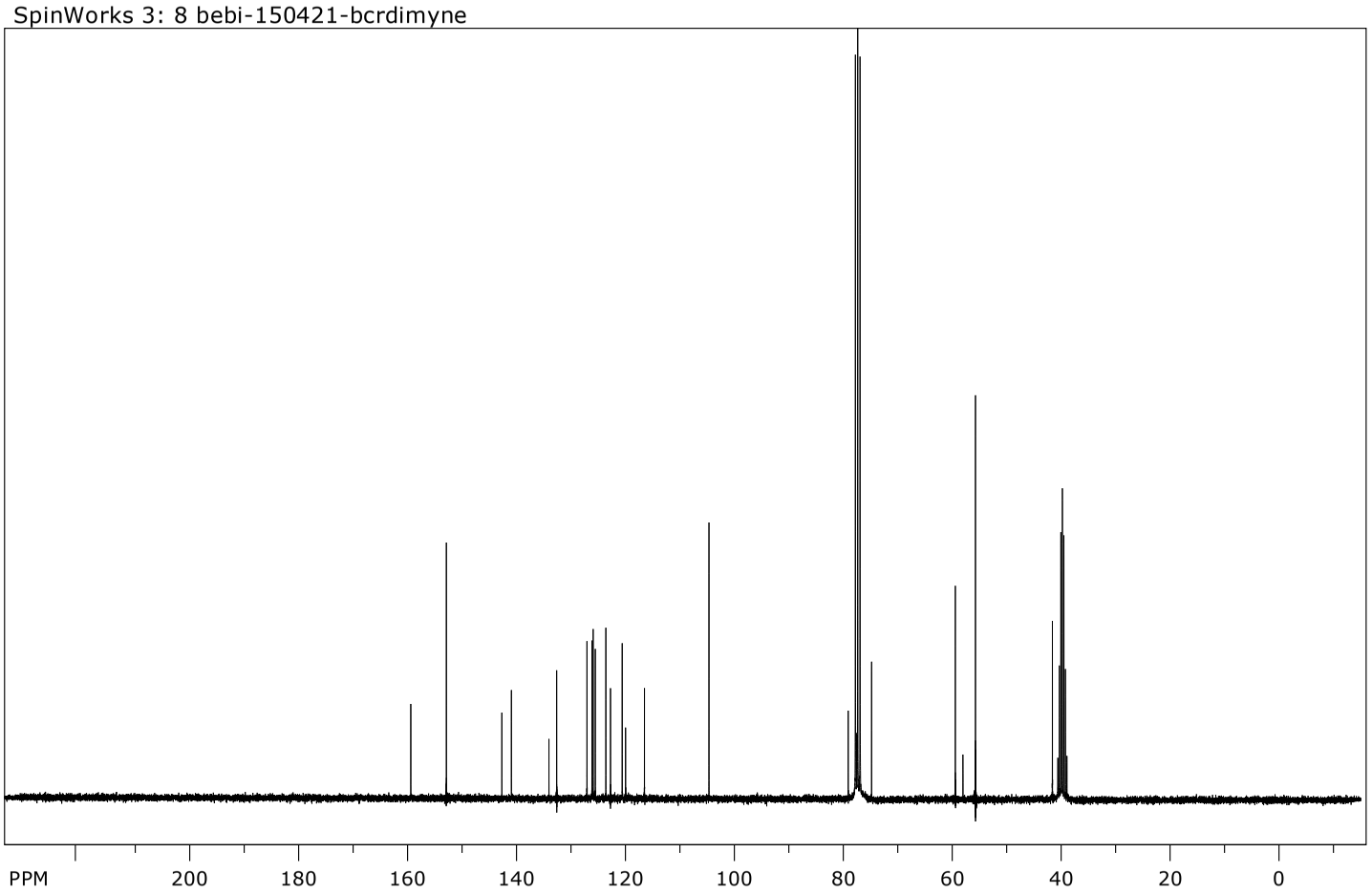

file: ...04\Desktop\NMR.Bcr\0421bb25\20\fid expt: <zgpg30>
transmitter freq.: 75.476050 MHz
time domain size: 32768 points
width: 18832.39 Hz = 249.5148 ppm = 0.574719 Hz/pt
number of scans: 67860

freq. of 0 ppm: 75.467810 MHz
processed size: 32768 complex points
LB: 0.000 GF: 0.0000
Hz/cm: 753.296 ppm/cm: 9.98059

^{1}H NMR spectrum of **3g**

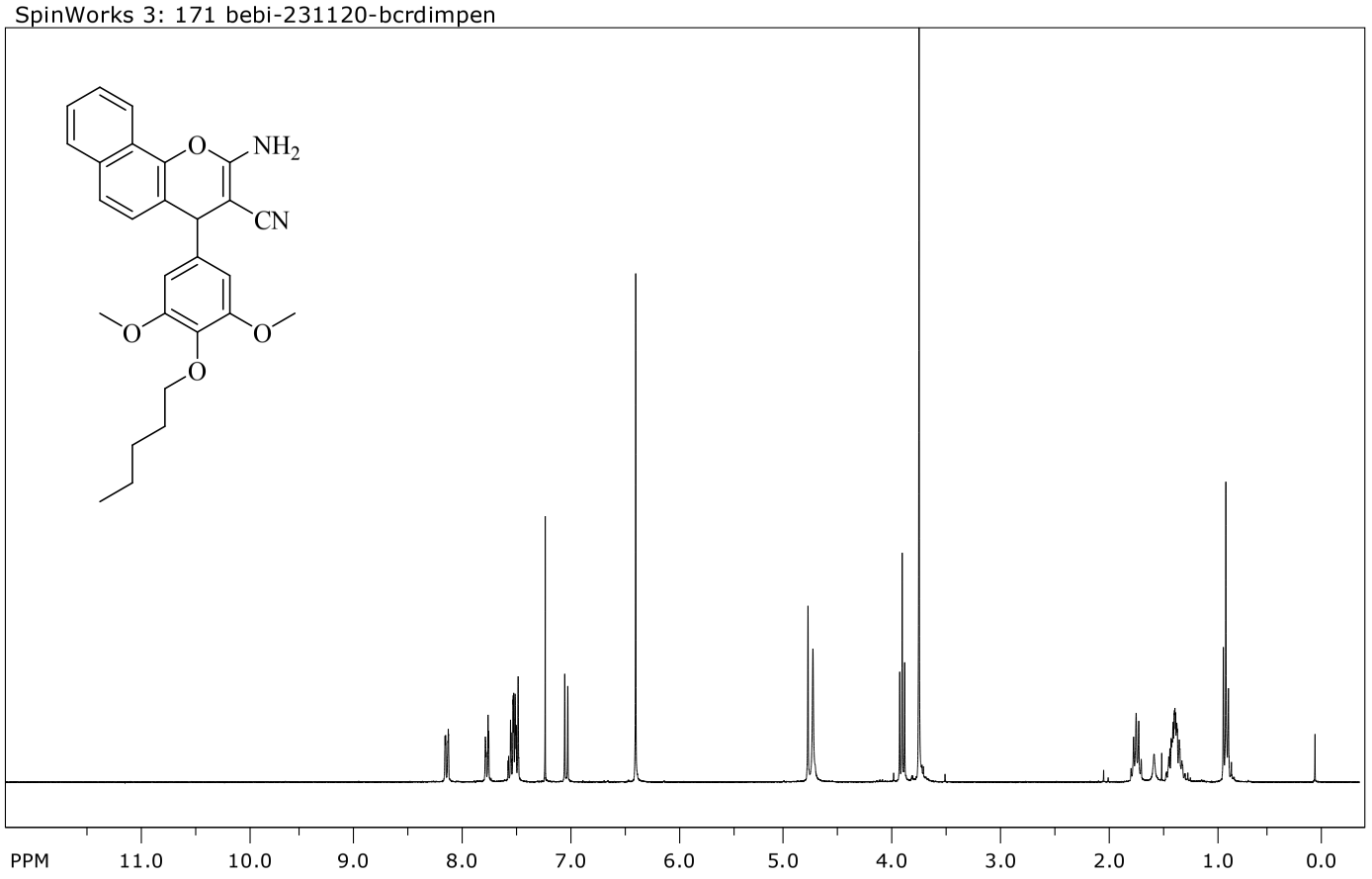

file: ...abor310104\Desktop\1120bb32\10\fid expt: <zg30>
transmitter freq.: 300.131801 MHz
time domain size: 65536 points
width: 8992.81 Hz = 29.9629 ppm = 0.137219 Hz/pt
number of scans: 56

freq. of 0 ppm: 300.130013 MHz
processed size: 65536 complex points
LB: 0.000 GF: 0.0000
Hz/cm: 151.754 ppm/cm: 0.50562

^{13}C NMR spectrum of **3g**

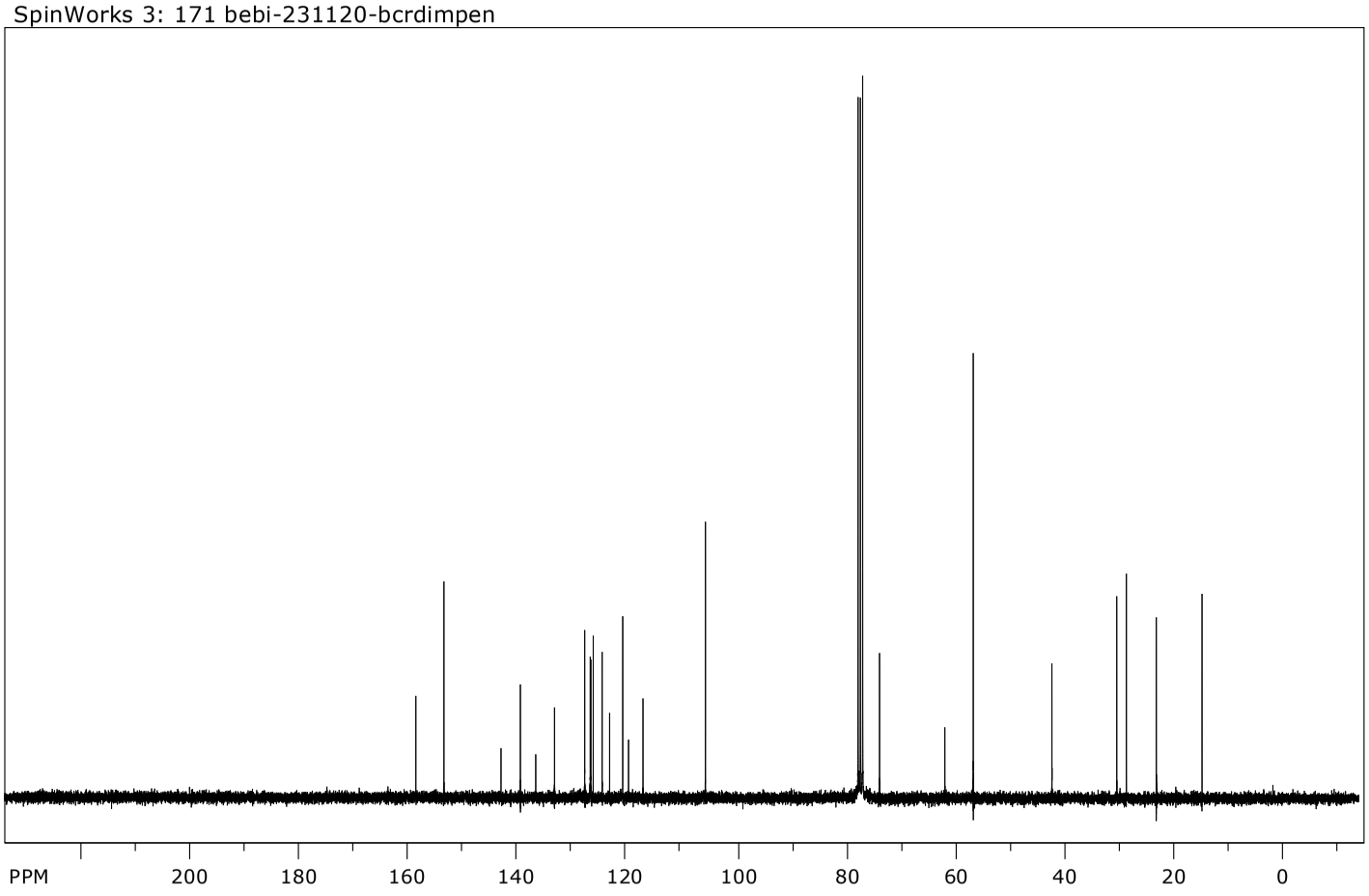

140

Vitality-decrease of HDFa and cancer cells

The selectivity towards cancer cells of substances **1b** and **3a-f** were tested on adult human dermal fibroblasts (HDFa) by MTT assay.[7] Dose response curves of all tested cancer cell lines (black) or HDFa cells (red) were calculated using GraphPad Prism 9 and depicted for each compound (Figure S1).

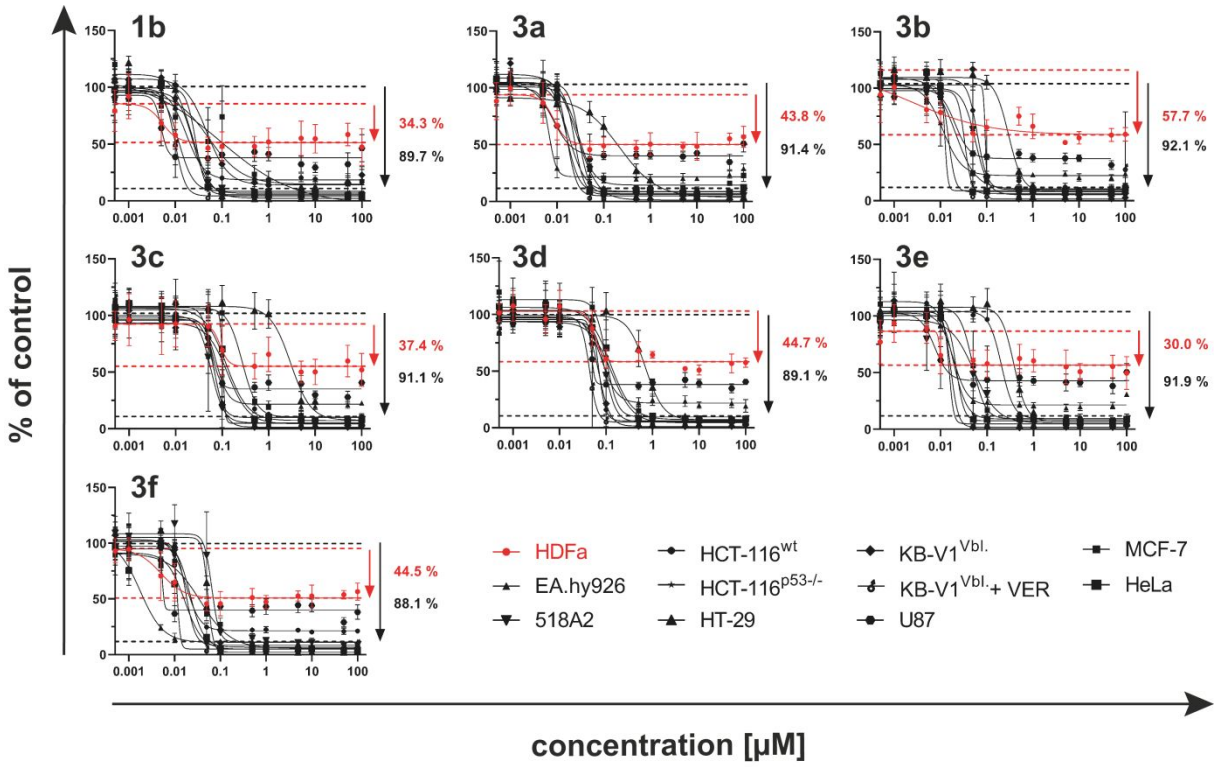

Figure S1. Dose response curves of substances **1b** and **3a-f** for the cancer cell lines (black) 518A2 (melanoma), HeLa (cervix carcinoma), KB-V1^{Vbl} (MDR cervix carcinoma), U-87 (glioblastoma), MCF-7 (breast carcinoma), HT-29 (colon carcinoma), HCT-116 (colon carcinoma) and HCT-116p53-/- (p53 knockout mutant), EA.hy926 (endothelial hybrid cells), and nonmalignant (red) HDFa (adult human dermal fibroblasts) cells. The difference between the top and bottom of the curves was determined and stated in percent (GraphPad Prism 9).

Meaningful IC_{50} values could not be determined, as the vitality of the HDFA cells did not fall below 50% (compared to solvent control).[9] Instead, the dose response curves were plotted, and the difference between the top and bottom of the curves was matched. Although it is not a common method to compare selectivity, it is possible to roughly estimate the difference between healthy and malignant cells. Figure S2 shows the vitality decrease in the dose response curves from 0.5 nM to 100 µM, which represents the entire observed concentration range. All tested compounds were less cytotoxic in healthy HDFa cells, indicating a selectivity for cancer cells.

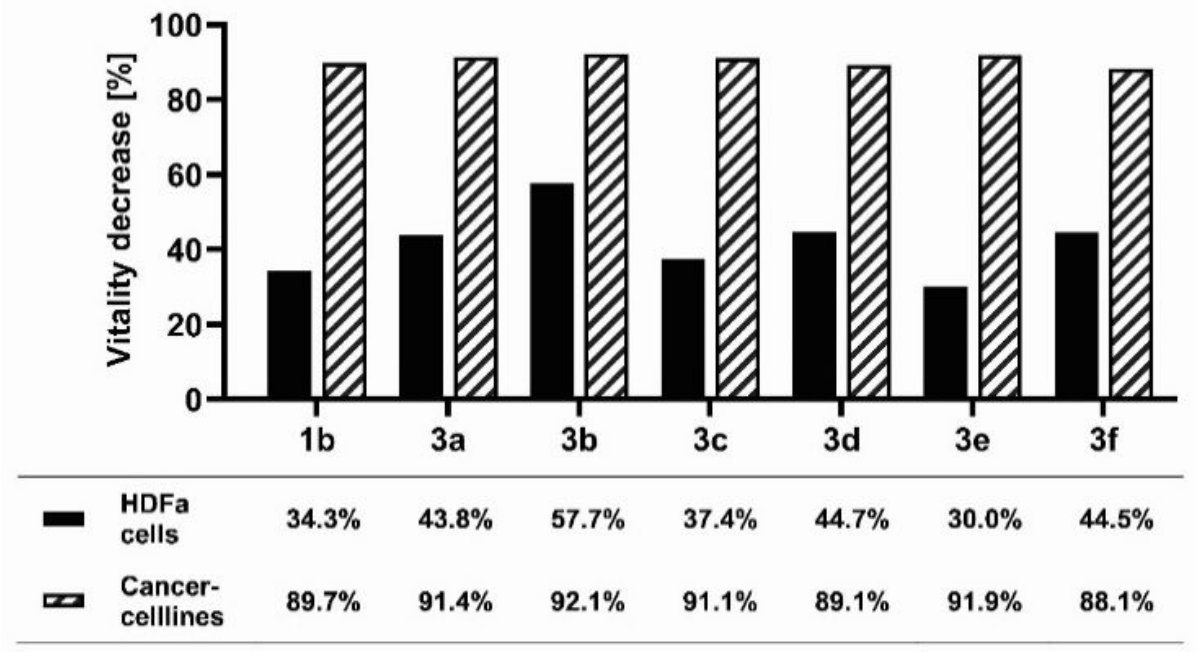

	1b	3a	3b	3c	3d	3e	3f
HDFa cells	34.3%	43.8%	57.7%	37.4%	44.7%	30.0%	44.5%
Cancer-celllines	89.7%	91.4%	92.1%	91.1%	89.1%	91.9%	88.1%

Figure S2. Concentration dependent vitality decrease of HDFa and cancer cells (mean of all tested cells) after 72 h incubation with substances **1b** and **3a-f**. Values are the difference between top and bottom values of the dose-response curves calculated with GraphPad Prism 9 (Fig. S1).

Molecular docking analysis

The docking analysis was accomplished with AutoDock 4.2.6 software (Lamarckian Genetic Algorithm and empirical free energy scoring function).[10] As target the tubulin-colchicine complex (PDB ID: 1sa0) was docked with compounds **1b** and **3f**, after health was assured by plotting Ramachandran´s plot in Discovery studio visualizer (Figure S3).

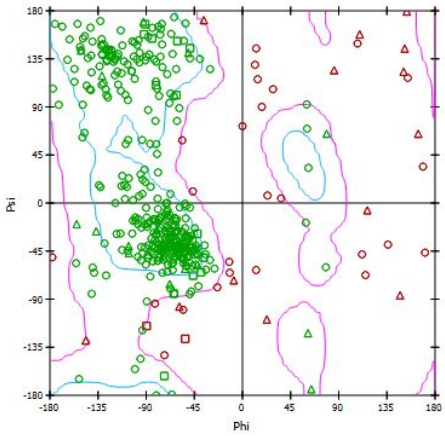

Figure S3. Ramchandran's plot for Tubulin-colchicine complex (1sa0) before molecular docking

From figure below it is clear that the protein is suitable for actual molecular docking. All the compounds were docked in the active site of target enzymes. Finally Docking results were

visualized and analyzed in Discovery studio visualizer and UCSF Chimera visualization tools and PYMOL programs (Table S1).

Table S1. Calculation of Binding Energy, Inhibition constant, H-bonds and Amino acids involved in interactions was calculated using AutoDock 4.2.6 with Lamarckian Genetic Algorithm and empirical free energy scoring function

Compound	Binding Energy (Kcal/mol)	Inhibition constant (K_i)	Number of H bonds (Drug-enzyme)	Amino acids involved in interactions
1b	-7.93	1.53 μM	1	Ala354, Val318, Ala316, Thr353, Lys352, Leu248, Cys241, Leu242, Ala250, Leu255, Lys254
3f	-8.69	0.43 μM	1	Ala354, Ala316, Met259, Lys352, Lys254, Leu248, Cys241, Ala250, Leu255, Leu242, Val318, Leu252, Asn258

Intracellular localization via copper catalyzed click-reaction

The ethynyl-substituted derivative **3f** was linked to 3-azido-7-hydroxycoumarin via copper(I)-catalysed azide-alkyne cycloaddition, producing a fluorescent triazole (red, Figure S4). The nuclei were counterstained with Nuclear Green (blue).

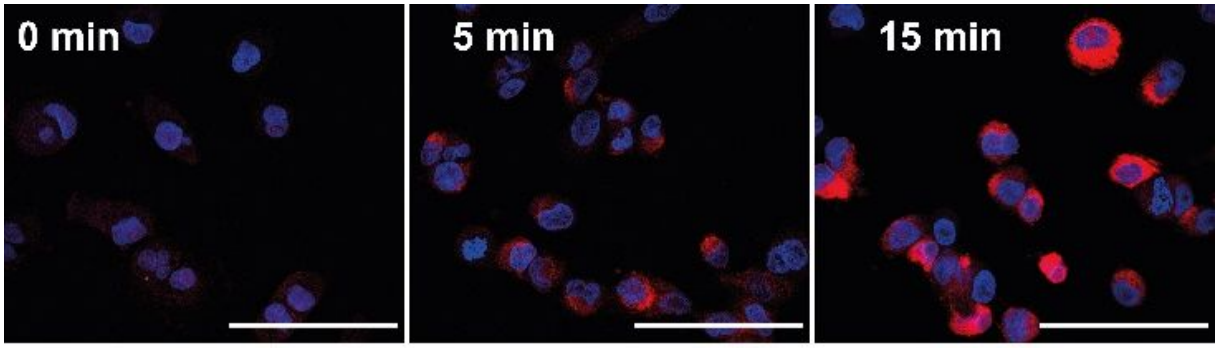

Figure S4. Intracellular localization of **3f** (25 μM) via copper(I)-catalyzed azide-alkyne cycloaddition with 3-azido-7-hydroxycoumarin (red) after 0, 5 and 15 min of treatment in 518A2 melanoma cells. Nuclei were colocalized with Nuclear Green (blue). Images are representative of at least three independent experiments. Magnification 630×, scale bars correspond to 100 μm.

Activation of executioner caspases 3 and 7 in 518A2 melanoma cells

The activity of effector caspases 3 and 7 was determined through a Cell Meter™ Caspase 3/7 Activity Apoptosis Assay Kit (ATT Bioquest®). 518A2 melanoma cells were treated with substances **1b**, **3a-f**, C-A4 (25 nM), staurosporine (1 μM) or solvent (DMSO) for 6 and 24 h (Figure S5).

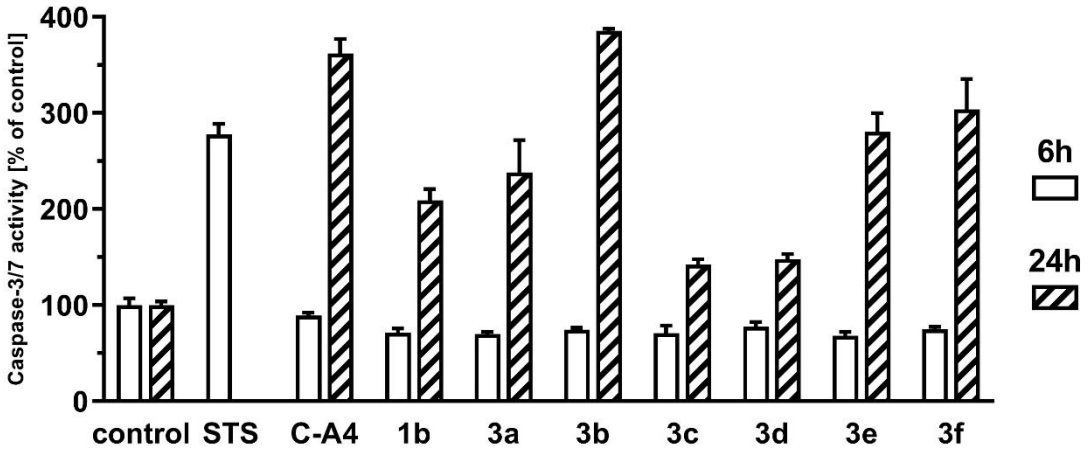

Figure S5. Measurement of caspase-3/7 activity via Cell Meter™ Caspase 3/7 Activity Apoptosis Assay Kit (ATT Bioquest®) after treatment of 518A2 melanoma cells with **1b**, **3a-f**, C-A4 (25 nM), staurosporine (1 μM) or solvent (DMSO) for 6 and 24 h. Cell vitality was reviewed via MTT assay and above 80 % for all experiments. The measurements were performed in triplicate and quoted as means ± SEM.

EA.hy926 tube-formation assay

The tube formation assay is an easy to run screening method for anti-angiogenic agents, which uses EA.hy926 endothelial hybrid cells to form 2D vessel-like structures on a basement membrane matrix (Matrigel®).[11] The effect of compounds **1b**, **3a-f** (25 nM) and C-A4 (25 nM) on the tube-formation ability of EA.hy926 cells was documented after 5 h of treatment (Figure S6, SI).

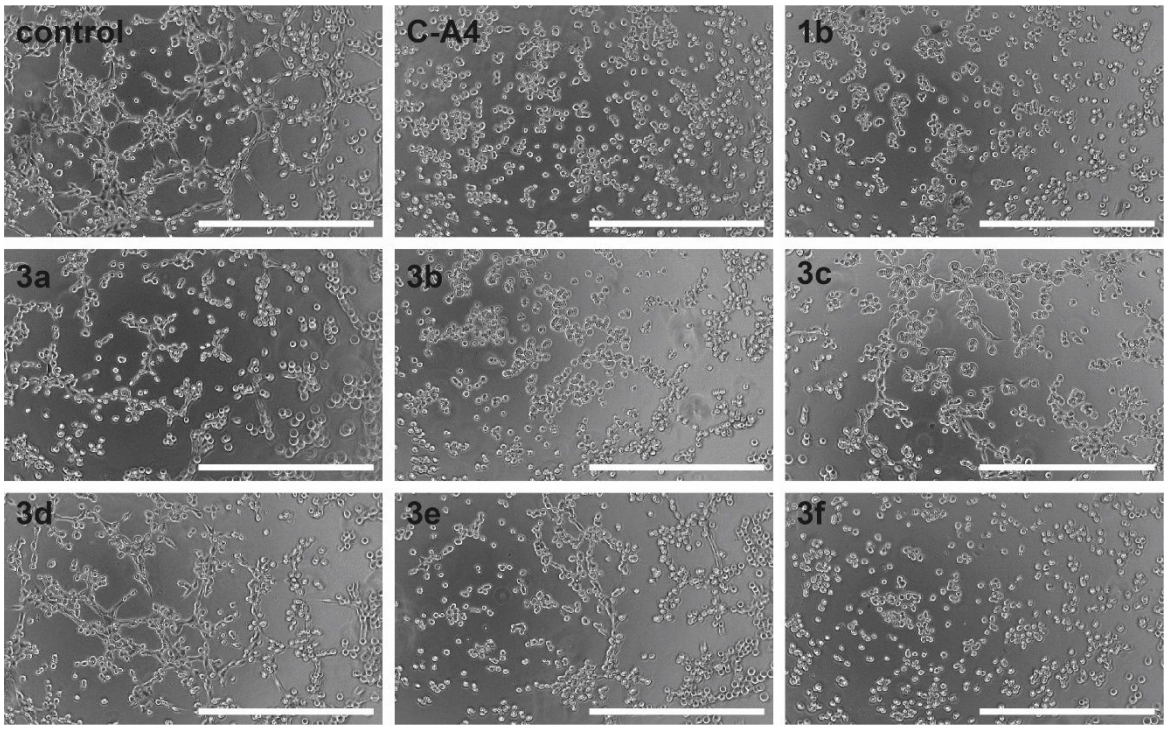

Figure S6. The ability of EA.hy926 endothelial hybrid cells to form vessel-like structures was reduced by compounds **1b** and **3a-f** (25 nM) as well as positive control C-A4 (25 nM) compared to solvent (DMSO)

treated cells. Images are representative of two independent experiments. Vitality (assessed by MTT-assay) was greater than 80 % compared to controls set to 100%. Magnification 100×. Scale bars correspond to 500 µm.

The vehicle (DMSO) treated cells developed a strongly branched mesh through cell flattening, migration, and the formation of cell-cell connections. Both C-A4 and compounds **1b** and **3a-f** showed anti-angiogenic effects, albeit to different extents. While **3d** treated cells formed few tubes, **3a**, **3c**, and **3e** led to only single sprouting cells and relatively few cell-cell contacts. Compounds **1b**, **3b** and **3f**, as well as C-A4, inhibited cell motility completely, resulting in a round cell morphology and few cell contacts. The vitality of the cells was confirmed by MTT-assays to be higher than 80%, excluding cytotoxic effects.

Hydrolytic stability via NMR

The stability of **1a**, **1b** and **3f** in aqueous solution was verified by ^{1}H NMR spectroscopy (Figure S7).

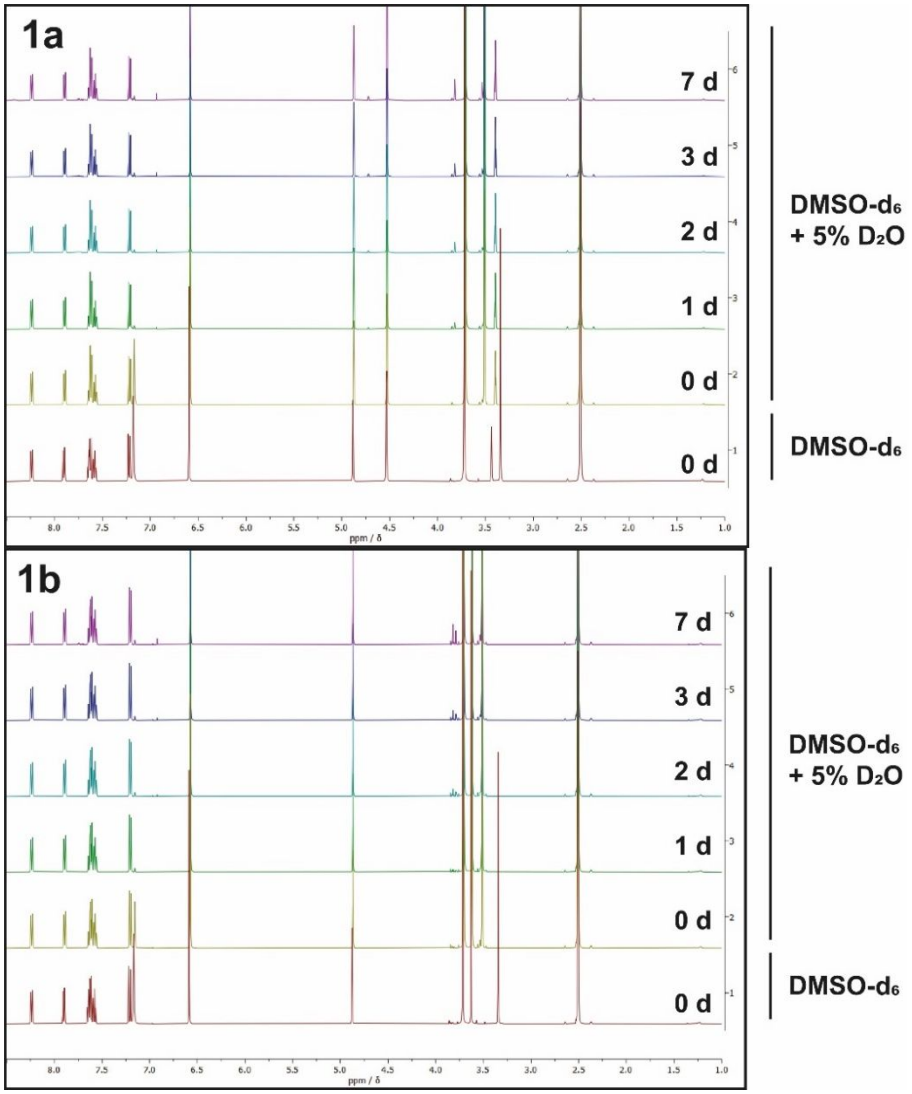

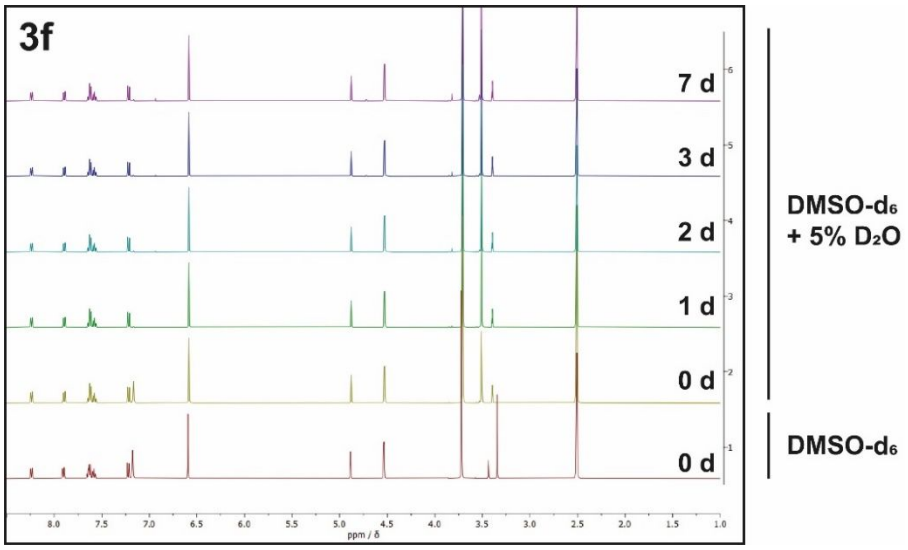

Figure S7. ^{1}H NMR spectra (500 MHz, DMSO-d_6) of substances **1a**, **1b** and **3f** before and after the addition of 5 % D_2O and incubation for 7 days.

Drug-likeness and Pharmacokinetic studies

ADME (Absorption, Distribution, Metabolism and Excretion) and pharmacokinetic properties were checked using SwissADME. The molecular weights (MW) of all the tested compounds **3a-f** range from 402.4 to 430.5 Daltons whereas hydrogen bond acceptor and donor values are 5 and 1. The predicted values of topological polar surface area (TPSA) were found at 86.73 Å^2 suggesting the high bioavailability of compounds. The calculated molar refractivity (MR) values of all the compounds ranging from 113.66 to 123.27. Lipophilicity was assessed using Consensus $LogP_{o/w}$ descriptor ranging from 3.81 to 4.51. From the predicted values of Consensus $LogP_{o/w}$, molar refractivity and the total polar surface area in synthesized compounds indicate that the test compounds have drug likeness with no violations of Lipinski's rule of five. All substances are likely to inhibit the CYP2C19, CYP2C9 and CYP3A4 enzymes of the cytochrome P450 mixed-function oxidase system, but only **3a** might be a CYP1A2 inhibitor. The drug likeness is based on Lipinski´s rule of five and the parameters are shown in Table S2. Absorption parameters like gastrointestinal absorption (GI), oral bioavailability, and distribution parameters like blood brain barrier (BBB) crossing were illustrated using the BOILED-Egg model and bioavailability radar graphs (Figure S8, A and B). The drug likeness is based on Lipinski´s rule of five and the parameters are shown in Table S2.

Table S2. Predicted physiochemical, pharmacokinetic, and drug-likeness properties of the synthesized compounds **3a-3f**.

	3a	**3b**	**3c**	**3d**	**3e**	**3f**
MW (Dalton)	402.4	416.4	430.5	430.5	414.45	412.44
TPSA (Å^2)	86.73	86.73	86.73	86.73	86.73	86.73
nHD (H-Donor)	1	1	1	1	1	1
nHA (H-Aceptor)	5	5	5	5	5	5

MR (Molar refractivity)	113.66	118.47	123.27	123.27	117.99	116.63
Log Po/w (Lipophilicity)	3,85	4,20	4,44	4,51	4,08	3,81
GI absorption	↑	↑	↑	↑	↑	↑
BBB permeance	-	-	-	-	-	-
CYP1A2 inhibitor	+	-	-	-	-	-
CYP2C19 inhibitor	+	+	+	+	+	+
CYP2C9 inhibitor	+	+	+	+	+	+
CYP2D6 inhibitor	-	-	-	-	-	-
CYP3A4 inhibitor	+	+	+	+	+	+
Lipinski	+	+	+	+	+	+

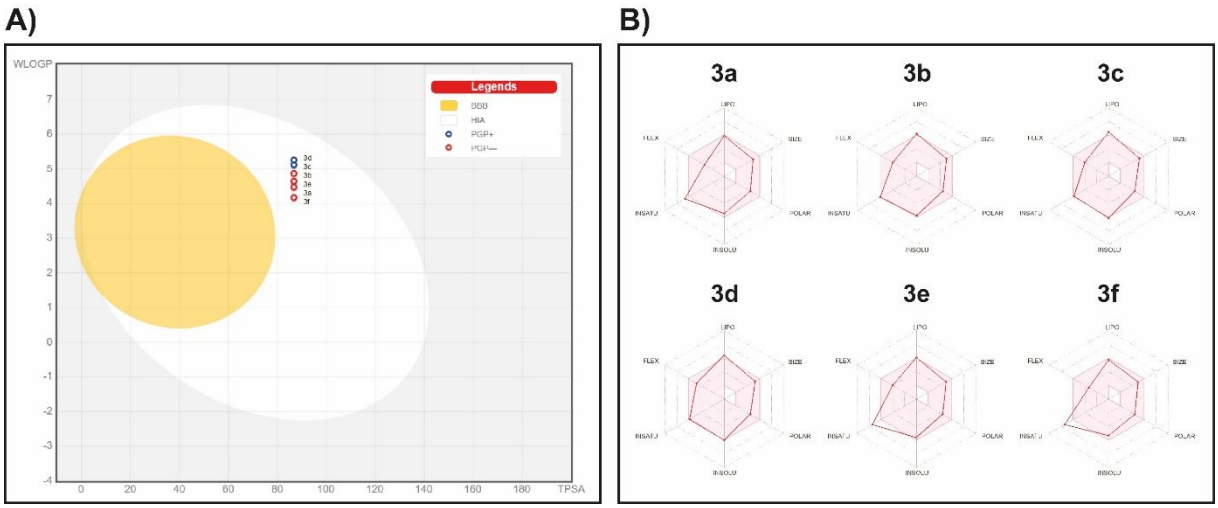

Figure S8. (A) BOILED-Egg model for predicting gastrointestinal absorption and brain access. (B) Bioavailability radar graph of synthesized compounds **3a-f**.

Metabolic stability monitored by UV-absorption

Compound **3f** was treated with 518A2 cell extract and stability was reviewed via UV-absorption (Thermo Fischer Varioskan LUX Microplate reader) after 0, 10, 30 min and 24 h (Figure S9).

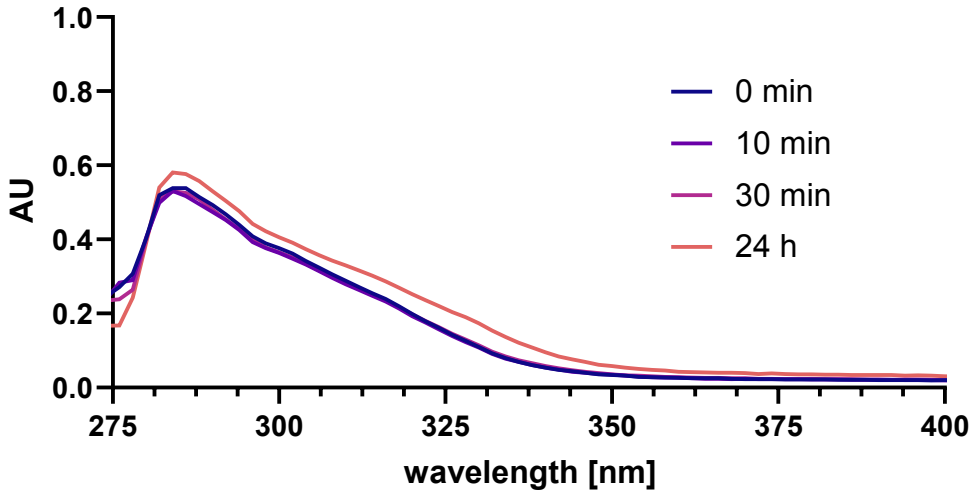

Figure S9. UV absorption spectra (275-400 nm) of cell lysate treated test compound **3f** after 0, 10, 30 min and 24 h.

RP-HPLC analysis of substance stability

Treatment of test compound **3f** with 518A2 cell lysate for 72 h showed no susceptibility to biotransformation. The area of RP-HPLC chromatograms (Waters ACQUITY UPLC H Class System) revealed an area decrease of 0.05 % after 72 h (Fig. S10).

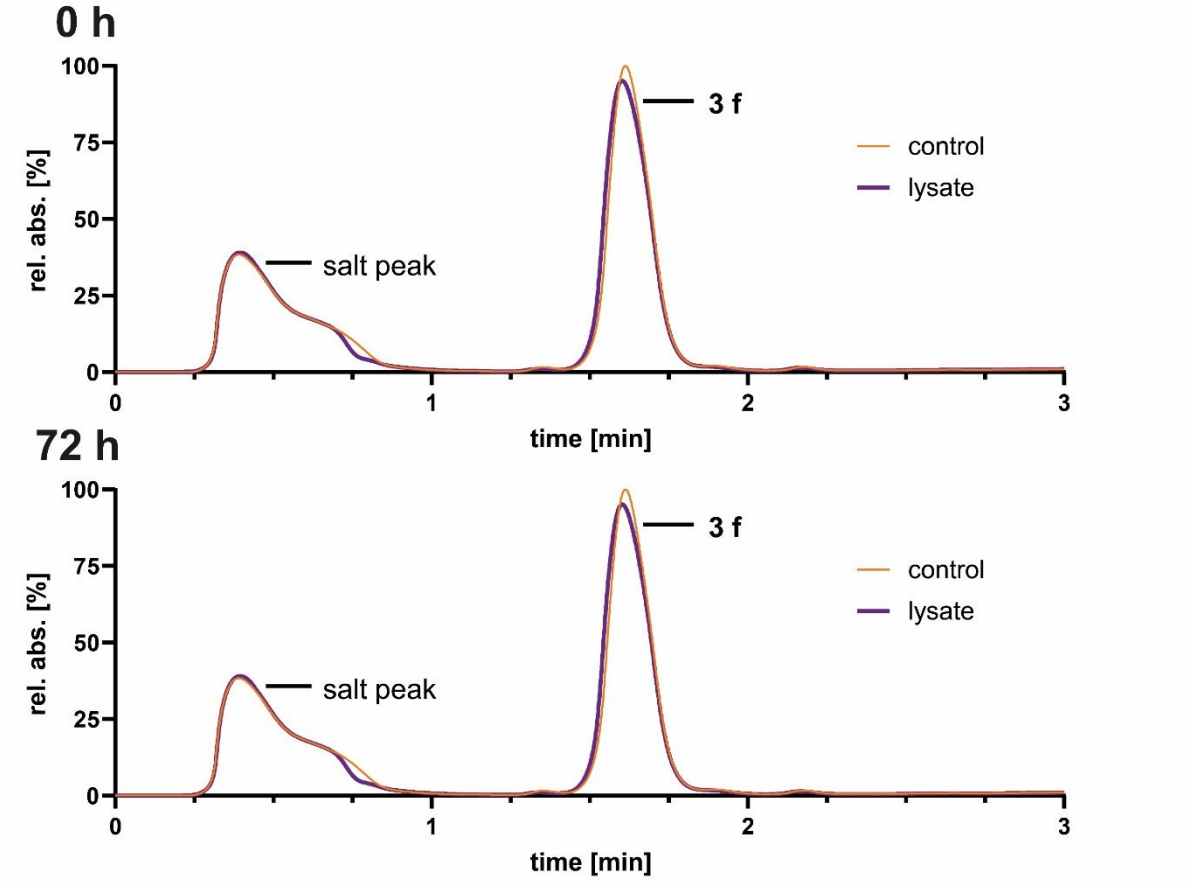

Figure S10. RP-HPLC of compound **3f**, treated with cell lysate or buffer (control) for 0 and 72 h.

Zebrafish angiogenesis assay

Representative images of substance treated zebra fish show the inhibition of SIV growth (yellow arrows), which is particularly evident for **3e**, **3f** and axitinib (Figure S11).

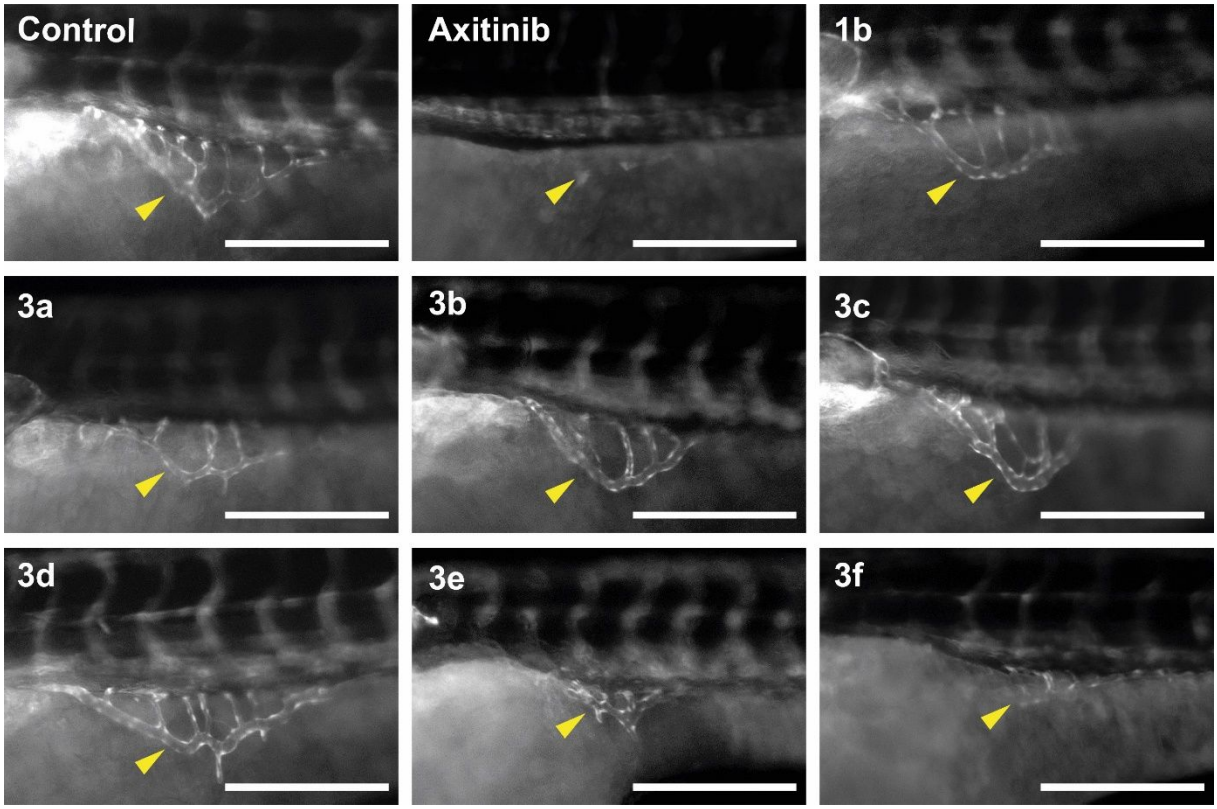

Figure S11. Antiangiogenic effects of **1b** and **3a-f** (100 nM) on the SIVs (yellow arrows) of zebrafish embryos (24 hpf) after 48 h exposure. Negative controls were treated with vehicle DMSO and positive controls with axitinib (500 nM). Magnification 630×, scale bar corresponds to 250 µm.

References

(1) Jansen, B.; Inoue, S. A.; Wadl, H.; Eichler, H.-G.; Wolff, K.; van Elsas, A.; Schrier, P. I.; Pehamberger, H. N-ras oncogene expression changes the growth characteristics of human melanoma in two independent SCID-hu mouse models. *Int. J. Cancer* **1996**, *67* (6), 821–825.
(2) Yusenko, M.; Jakobs, A.; Klempnauer, K.-H. A novel cell-based screening assay for small-molecule MYB inhibitors identifies podophyllotoxins teniposide and etoposide as inhibitors of MYB activity. *Sci. Rep.* **2018**, *8* (1), 13159.
(3) Chayka, O.; Kintscher, J.; Braas, D.; Klempnauer, K.-H. v-Myb mediates cooperation of a cell-specific enhancer with the mim-1 promoter. *Mol. Cell. Biol.* **2005**, *25* (1), 499–511.
(4) Carpentier, G.; Berndt, S.; Ferratge, S.; Rasband, W.; Cuendet, M.; Uzan, G.; Albanese, P. Angiogenesis Analyzer for ImageJ - A comparative morphometric analysis of "Endothelial Tube Formation Assay" and "Fibrin Bead Assay". *Sci. Rep.* **2020**, *10* (1), 11568.
(5) Lawson, N. D.; Weinstein, B. M. In vivo imaging of embryonic vascular development using transgenic zebrafish. *Dev. Biol.***2002**, *248* (2), 307–318.
(6) White, R. M.; Sessa, A.; Burke, C.; Bowman, T.; LeBlanc, J.; Ceol, C.; Bourque, C.; Dovey, M.; Goessling, W.; Burns, C. E.; Zon, L. I. Transparent adult zebrafish as a tool for in vivo transplantation analysis. *Cell Stem Cell* **2008**, *2* (2), 183–189.
(7) Daina, A.; Michielin, O.; Zoete, V. SwissADME: a free web tool to evaluate pharmacokinetics, drug-likeness and medicinal chemistry friendliness of small molecules. *Sci Rep* **2017**, *7* (1), 42717.
(8) Adinolfi, B.; Pellegrino, M.; Baldini, F. Human dermal fibroblasts HDFa can be used as an appropriate healthy control for PMMA nanoparticles-survivin molecular beacon cellular uptake studies. *BBiomed. Pharmacother.* **2015**, *69*, 228–232.
(9) Sebaugh, J. L. Guidelines for accurate EC50/IC50 estimation. *Pharm. Stat.* **2011**, *10* (2), 128–134.
(10) Morris, G. M.; Goodsell, D. S.; Halliday, R. S.; Huey, R.; Hart, W. E.; Belew, R. K.; Olson, A. J. Automated docking using a Lamarckian genetic algorithm and an empirical binding free energy function. *J. Comput. Chem.* **1998**, *19* (14), 1639–1662.
(11) Aranda, E.; Owen, G. I. A semi-quantitative assay to screen for angiogenic compounds and compounds with angiogenic potential using the EA.hy926 endothelial cell line. *Biol. Res.* **2009**, *42* (3), 377-389.

4.4 Publikation III

Multimodal 4-arylchromene derivatives with microtubule-destabilizing, anti-angiogenic, and MYB-inhibitory activities

Leonhard H. F. Köhler,[a] Sebastian Reich,[a] Maria Yusenko,[b] Karl-Heinz Klempnauer,[b] Gerrit Begemann,[d] Rainer Schobert,[a] und Bernhard Biersack.[a]*

[a] Organic Chemistry Laboratory University of Bayreuth, Universitätsstraße 30, 95440 Bayreuth (Germany)
[b] Institute for Biochemistry, Westfälische-Wilhelms-Universität, Wilhelm-Klemm-Strasse 2, 48149 Münster (Germany)
[d] Developmental Biology, University of Bayreuth, Universitätsstraße 30, Bayreuth 95440 (Germany)

*Corresponding author. E-Mail address: bernhard.biersack@yahoo.com

Cancer Drug Resist **2023**, *6, 59*

Köhler *et al. Cancer Drug Resist* 2023;6:59-77
DOI: 10.20517/cdr.2022.90

Cancer Drug Resistance

Original Article **Open Access**

Multimodal 4-arylchromene derivatives with microtubule-destabilizing, anti-angiogenic, and MYB-inhibitory activities

Leonhard H. F. Köhler[1], Sebastian Reich[1], Maria Yusenko[2], Karl-Heinz Klempnauer[2], Gerrit Begemann[3], Rainer Schobert[1], Bernhard Biersack[1]

[1]Organic Chemistry Laboratory, University of Bayreuth, Bayreuth 95440, Germany.
[2]Institute for Biochemistry, Westfälische-Wilhelms-Universität, Münster 48149, Germany.
[3]Developmental Biology, University of Bayreuth, Bayreuth 95440, Germany.

Correspondence to: Dr. Bernhard Biersack, Organic Chemistry Laboratory, University of Bayreuth, Universitätsstrasse 30, Bayreuth 95440, Germany. E-mail: bernhard.biersack@uni-bayreuth.de

How to cite this article: Köhler LHF, Reich S, Yusenko M, Klempnauer KH, Begemann G, Schobert R, Biersack B. Multimodal 4-arylchromene derivatives with microtubule-destabilizing, anti-angiogenic, and MYB-inhibitory activities. *Cancer Drug Resist* 2023;6:59-78. https://dx.doi.org/10.20517/cdr.2022.90

Received: 31 Jul 2022 **First Decision:** 11 Nov 2022 **Revised:** 28 Dec 2022 **Accepted:** 19 Jan 2023 **Published:** 1 Feb 2023

Academic Editors: Francesco Pezzella, Godefridus J. Peters **Copy Editor:** Ke-Cui Yang **Production Editor:** Ke-Cui Yang

Abstract

Aim: Efficient and readily available anticancer drugs are sought as treatment options. For this reason, chromene derivatives were prepared using the one-pot reaction and tested for their anticancer and anti-angiogenic properties.

Methods: 2-Amino-3-cyano-4-(aryl)-7-methoxy-4H-chromene compounds (2A-R) were repurposed or newly synthesized via a three-component reaction of 3-methoxyphenol, various aryl aldehydes, and malononitrile. We performed assays to study the inhibition of tumor cell growth [3-(4, 5-dimethylthiazol-2-yl)-2, 5-diphenyl tetrazolium bromid (MTT) assay], effects on microtubules (immunofluorescence), cell cycle (flow-activated cell sorting analysis), angiogenesis (zebrafish model), and MYB activity (luciferase reporter assay). Fluorescence microscopy was applied for localization studies via copper-catalyzed azide-alkyne click reaction of an alkyne-tagged drug derivative.

Results: Compounds 2A-C and 2F exhibited robust antiproliferative activities against several human cancer cell lines (50% inhibitory concentrations in the low nanomolar range) and showed potent MYB inhibition. The alkyne derivative 3 was localized in the cytoplasm after only 10 min of incubation. Substantial microtubule disruption and

G2/M cell-cycle arrest were observed, where compound 2F stood out as a promising microtubule-disrupting agent. The study of anti-angiogenic properties showed that 2A was the only candidate with a high potential to inhibit blood vessel formation *in vivo*.

Conclusion: The close interplay of various mechanisms, including cell-cycle arrest, MYB inhibition, and anti-angiogenic activity, led to identifying promising multimodal anticancer drug candidates.

Keywords: Chromene, pyran, anticancer drugs, microtubule, angiogenesis, MYB inhibition

INTRODUCTION

Multi-component reactions such as the Biginelli reaction, Van Leusen reaction, and the Ugi reaction, and their modifications are helpful for the design of biologically active compounds[1-4]. An efficient three-component synthesis of biologically active pyrans was reported using naphthol, phenol, and hydroxyquinoline derivatives, which led to several new anticancer compounds[5-8]. For instance, the naphthopyran LY290181 or 2-amino-4-(3-nitrophenyl)-4*H*-naphtho(1, 2-*b*)pyran-3-carbonitrile (1A) was identified as an active anticancer MDA (microtubule-binding/destabilizing agent)[9,10]. The close analog 1B was initially described as an apoptosis inducer in breast cancer and non-small-cell lung cancer cells[6]. It was also recently determined to be a highly potent inhibitor of the transcription factor MYB[11]. MYB is encoded by the proto-oncogene MYB and is involved in the development of malignancies, making it a potential therapeutic target[12]. The structurally optimized 7-methoxy-4*H*-chromene 2B is an even more potent apoptosis-inducing agent than 1B and showed high antiproliferative activities[5]. The 2-amino-4-aryl-5-oxo-4, 5-dihydropyrano[3,2-c]chromene-3-carbonitrile 1C inhibited centrosome clustering in melanoma cells, leading to the formation of multiple mitotic spindles, chromosome segregation defects, and cell death [Figure 1][13].

Based on these active anticancer pyran heterocycles, several 2-amino-3-cyano-4-aryl-7-methoxy-4*H*-chromenes were prepared for testing their antiproliferative and MYB-inhibitory activities. Experiments on cell death induction, microtubule destabilization, drug localization, and anti-angiogenic effects were performed to investigate the underlying mechanisms of action of the most active compounds.

METHODS

Chemistry

General

Starting compounds and reagents were obtained from Aldrich, TCI, and Alfa Aesar. The already published compounds 1A, 1B, 2B, 2O, and 2R were prepared as described[5,6,9,14]. For compound analysis, the following instruments were used: Gallenkamp for melting points (uncorrected); Perkin-Elmer Spectrum One FT-IR spectrophotometer (ATR) for IR spectra; BRUKER Avance 300 spectrometer for nuclear magnetic resonance spectra; chemical shifts were expressed as ppm (parts per million, δ) downfield from TMS (tetramethylsilane) as the internal standard; Varian MAT 311A (EI) and UPLC/Orbitrap (ESI-HRMS) for mass spectra; Perkin-Elmer 2400 CHN elemental analyzer for elemental analyses (microanalyses), and compounds were > 95% pure as to elemental analysis.

Synthesis

2-Amino-3-cyano-4-(3'-chloro-4', 5'-dimethoxyphenyl)-7-methoxy-4H-chromene (2A)

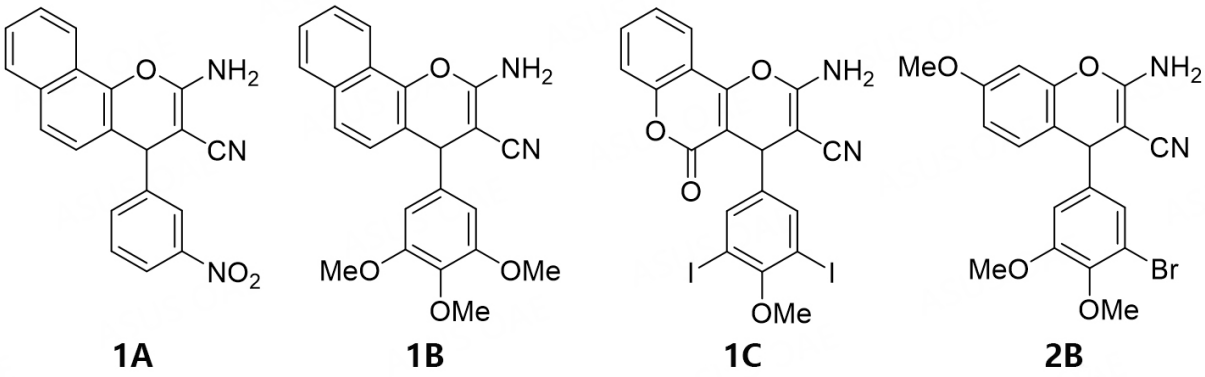

Figure 1. Structures of LY290181 (1A); MYB inhibitor Bcr-TMP (1B); chromosomal de-clustering agent 1C; and antiproliferative compound 2B.

3-Chloro-4, 5-dimethoxybenzaldehyde (200 mg, 1.0 mmol) and malononitrile (70 mg, 1.0 mmol) were dissolved in MeCN (5 mL), and three drops of Et_3N were added. The reaction mixture was stirred at room temperature for 30 min. 3-Methoxyphenol (109 µL, 1.0 mmol) was added, and the reaction mixture was heated with a heat gun and stirred at room temperature for 2 h. The precipitate was collected, washed with MeCN and *n*-hexane, and dried in a vacuum. Yield: 80 mg (0.22 mmol, 22%); colorless solid of mp = 224-225 °C; υ_{max}(ATR)/cm^{-1} 3397, 3332, 3220, 2943, 2846, 2186, 1651, 1619, 1572, 1509, 1465, 1430, 1415, 1399, 1313, 1281, 1258, 1231, 1207, 1193, 1178, 1148, 1137, 1124, 1051, 998, 928, 856, 834, 813, 801, 780, 753, 714, 690, 659; ^{1}H NMR (300 MHz, $CDCl_3$) 3.77 (3 H, s, OMe), 3.82 (6 H, s, 2 x OMe), 4.5-4.6 (3 H, m, 4-H, NH_2), 6.53 (1 H, d, J = 2.5 Hz, 8-H), 6.6-6.7 (3 H, m, 6'-H, 6-H), 6.71 (1 H, s, 2'-H), 6.85 (1 H, d, J = 8.7 Hz, 5-H); ^{13}C NMR (75.5 MHz, $CDCl_3$) 40.2 (4-C), 55.5 (OMe), 56.2 (OMe), 60.7 (OMe), 101.4 (8-C), 110.6 (6-C), 111.8 (6'-C), 113.9 (4a-C_q), 119.6 (CN), 121.2 (2'-C), 128.5 (3'-C), 130.1 (1'-C), 141.3 (4'-C), 149.1 (5'-C), 153.9 (8a-C_q), 159.1 (7-C), 159.6 (2-C); HRMS for $C_{19}H_{18}O_4N_2Cl$ [M^+ + H] calcd. 373.09496, found 373.09355.

2-Amino-3-cyano-4-(3'-iodo-4', 5'-dimethoxyphenyl)-7-methoxy-4H-chromene (2C)

Analogously to the synthesis of 2B, compound 2C (150 mg, 0.32 mmol, 32%) was obtained from 3-iodo-4, 5-dimethoxybenzaldehyde (292 mg, 1.0 mmol), malononitrile (70 mg, 1.0 mmol), three drops of Et_3N, and 3-methoxyphenol (109 µL, 1.0 mmol) in MeCN (5 mL). Colorless solid of m.p. 223-224 °C; υ_{max}(ATR)/cm^{-1} 3403, 3334, 3220, 2937, 2841, 2186, 1651, 1619, 1582, 1563, 1508, 1479, 1464, 1411, 1397, 1308, 1272, 1253, 1231, 1200, 1178, 1136, 1124, 1044, 999, 875, 855, 812, 801, 777, 750, 688, 655, 611; ^{1}H NMR (300 MHz, dimethyl sulfoxide [DMSO]-d_6) 3.67 (3 H, s, OMe), 3.74 (3 H, s, OMe), 3.78 (3 H, s, OMe), 4.68 (1 H, s, 4-H), 6.56 (1 H, d, J = 2.5 Hz, 8-H), 6.68 (1 H, dd, J = 8.7 Hz, 2.5 Hz, 6-H), 6.9-7.1 (5 H, m, 6'-H, 6-H, 5-H, NH_2); ^{13}C NMR (75.5 MHz, DMSO-d_6) 39.1 (4-C), 55.4 (OMe), 55.6 (OMe), 55.9 (OMe), 93.0 (3'-C), 100.9 (8-C), 111.4 (6-C), 112.7 (6'-C), 114.8 (4a-C_q), 120.4 (CN), 128.2 (5-C), 129.9 (2'-C), 144.4 (1'-C), 146.9 (4'-C), 148.7 (5'-C), 152.2 (8a-C_q), 159.0 (7-C), 160.3 (2-C); *m/z* (%) 464 (43) [M^+], 201 (100); Anal. calcd. for $C_{19}H_{17}IN_2O_4$ (%), C, 49.16, H, 3.69, N, 6.03; found: C, 49.24, H, 3.77, N, 5.98.

2-Amino-3-cyano-4-(3', 5'-dichloro-4'-methoxyphenyl)-7-methoxy-4H-chromene (2D)

Analogously to the synthesis of 2B, compound 2D (115 mg, 0.31 mmol, 31%) was obtained from 3,5-dichloro-4-methoxybenzaldehyde (205 mg, 1.0 mmol), malononitrile (70 mg, 1.0 mmol), three drops of Et_3 N, and 3-methoxyphenol (109 µL, 1.0 mmol) in MeCN (5 mL). Colorless solid of m.p. 229 °C;

υ_{max}(ATR)/cm^{-1} 3395, 3331, 3219, 3004, 2973, 2938, 2841, 2192, 1652, 1619, 1583, 1557, 1509, 1478, 1448, 1404, 1395, 1318, 1301, 1282, 1265, 1254, 1195, 1150, 1127, 1082, 1043, 1029, 996, 949, 914, 888, 857, 848, 807, 795, 775, 751, 741, 687, 667, 653; ^{1}H NMR (300 MHz, $CDCl_3$/DMSO-d_6) 3.62 (3 H, s, OMe), 3.70 (3 H, s, OMe), 4.44 (1 H, s, 4-H), 5.58 (2 H, s, NH_2), 6.4-6.5 (2 H, m, 6-H, 8-H), 6.6-6.7 (1 H, m, 5-H), 6.96 (2 H, s, 2'-H, 6'-H); ^{13}C NMR (75.5 MHz, $CDCl_3$/DMSO-d_6) 39.7 (4-C), 55.4 (OMe), 57.7 (3-C), 60.5 (OMe), 101.4 (8-C), 111.5 (6-C), 113.5 (4a-C_q), 120.2 (CN), 128.0 (2'-C, 6'-C), 129.3 (3'-C, 5'-C), 129.9 (5-C), 142.9 (1'-C), 149.0 (4'-C), 150.9 (8a-C_q), 159.5 (7-C), 160.0 (2-C); *m/z* (EI) 378 (16) [M$^+$], 376 (23) [M$^+$], 201 (100); Anal. calcd. for $C_{18}H_{14}Cl_2N_2O_3$ (%), C, 57.31, H, 3.74, N, 7.43; found: C, 57.40, H, 3.70, N, 7.36.

2-Amino-3-cyano-4-(3', 5'-dibromo-4'-methoxyphenyl)-7-methoxy-4H-chromene (2E)

Analogously to the synthesis of 2B, compound 2E (125 mg, 0.27 mmol, 31%) was obtained from 3, 5-dibromo-4-methoxybenzaldehyde (259 mg, 0.88 mmol), malononitrile (70 mg, 1.0 mmol), three drops of Et_3N, and 3-methoxyphenol (109 µL, 1.0 mmol) in MeCN (5 mL). Colorless solid of m.p. 247 °C; υ_{max}(ATR)/cm^{-1} 3396, 3331, 3218, 2943, 2190, 1652, 1619, 1582, 1547, 1508, 1471, 1420, 1407, 1394, 1317, 1296, 1282, 1253, 1194, 1150, 1125, 1064, 1045, 1028, 999, 990, 947, 888, 857, 847, 811, 800, 779, 750, 733, 704, 686, 663; ^{1}H NMR (300 MHz, $CDCl_3$/DMSO-d_6) 3.70 (3 H, s, OMe), 3.76 (3 H, s, OMe), 4.52 (1 H, s, 4-H), 5.90 (2 H, s, NH_2), 6.47 (1 H, d, J = 2.5 Hz, 8-H), 6.55 (1 H, dd, J = 8.6 Hz, 2.5 Hz, 6-H), 6.77 (1 H, d, J = 8.6 Hz, 5-H), 7.23 (2 H, s, 2'-H, 6'-H); ^{13}C NMR (75.5 MHz, $CDCl_3$/DMSO-d_6) 39.1 (4-C), 54.9 (OMe), 56.9 (3-C), 59.9 (OMe), 101.0 (8-H), 111.0 (6-C), 113.1 (4a-C_q), 117.6 (3'-C, 5'-C), 119.7 (CN), 129.4 (5-C), 131.3 (2'-C, 6'-C), 143.7 (1'-C), 148.6 (4'-C), 152.2 (8a-C_q), 159.0 (7-C), 159.7 (2-C); *m/z* (EI) 468 (8) [M$^+$], 466 (16) [M$^+$], 464 (8) [M$^+$], 201 (100); Anal. calcd. for $C_{18}H_{14}Br_2N_2O_3$ (%), C, 46.38, H, 3.03, N, 6.01; found: C, 46.29, H, 2.98, N, 6.06.

2-Amino-3-cyano-4-(3, 5-diiodo-4-methoxyphenyl)-7-methoxy-4H-chromene (2F)

Analogously to the synthesis of 2B, compound 2F (165 mg, 0.30 mmol, 30%) was obtained from 3, 5-diiodo-4-methoxybenzaldehyde (388 mg, 1.0 mmol), malononitrile (70 mg, 1.0 mmol), three drops of Et_3N, and 3-methoxyphenol (109 µL, 1.0 mmol) in MeCN (5 mL). Colorless solid of m.p. 228 °C; υ_{max}(ATR)/cm^{-1} 3400, 3332, 3219, 2936, 2841, 2187, 1652, 1619, 1580, 1534, 1506, 1460, 1405, 1387, 1316, 1293, 1281, 1247, 1198, 1150, 1124, 1048, 1028, 993, 945, 897, 885, 854, 808, 798, 778, 749, 737, 711, 708, 700, 685; ^{1}H NMR (300 MHz, $CDCl_3$/DMSO-d_6) 3.70 (3 H, s, OMe), 3.72 (3 H, s, OMe), 4.49 (1 H, s, 4-H), 6.07 (2 H, s, NH_2), 6.47 (1 H, d, J = 2.6 Hz, 8-H), 6.54 (1 H, dd, J = 8.6 Hz, 2.6 Hz, 6-H), 6.77 (1 H, d, J = 8.6 Hz, 5-H), 7.47 (2 H, s, 2'-H, 6'-H); ^{13}C NMR (75.5 MHz, $CDCl_3$/DMSO-d_6) 54.9 (OMe), 56.6 (3-C), 59.9 (OMe), 90.3 (2'-C, 6'-C), 100.9 (8-C), 111.0 (6-C), 113.3 (4a-C_q), 119.8 (CN), 129.4 (5-C), 138.4 (2'-C, 6'-C), 144.9 (1'-C), 148.6 (8a-C_q), 156.9 (4'-C), 158.9 (7-C), 159.7 (2-C); *m/z* (EI) 560 (52) [M$^+$], 201 (100); Anal. calcd. for $C_{18}H_{14}I_2N_2O_3$ (%), C, 38..60, H, 2.52, N, 5.00; found: C, 38.69, H, 2.45, N, 4.97.

2-Amino-3-cyano-4-(2'-fluorophenyl)-7-methoxy-4H-chromene (2G)

Analogously to the synthesis of 2B, compound 2G (73 mg, 0.25 mmol, 25%) was obtained from 2-fluorobenzaldehyde (124 mg, 1.0 mmol), malononitrile (70 mg, 1.0 mmol), three drops of Et_3N, and 3-methoxyphenol (109 µL, 1.0 mmol) in MeCN (5 mL). Yield: 73 mg (0.25 mmol, 25%); colorless solid of m.p. 198 °C; υ_{max}(ATR)/cm^{-1} 3405, 3336, 3214, 2194, 1652, 1619, 1582, 1509, 1486, 1453, 1435, 1405, 1317, 1292, 1255, 1240, 1224, 1193, 1152, 1124, 1103, 1092, 1045, 1031, 937, 871, 857, 817, 803, 787, 753, 721, 705, 679; ^{1}H NMR (300 MHz, $CDCl_3$) 3.75 (3 H, s, OMe), 4.65 (2 H, s, NH_2), 5.04 (1 H, s, 4-H), 6.51 (1 H, d, J = 2.6 Hz, 8-H), 6.59 (1 H, dd, J = 8.6 Hz, 2.6 Hz, 6-H), 6.92 (1 H, d, J = 8.6 Hz, 5-H), 7.0-7.2 (4 H, m, 3'-H, 4'-H, 5'-H,

6'-H); ^{13}C NMR (75.5 MHz, $CDCl_3$) 33.8 (4-C), 55.5 (OMe), 59.2 (3-C), 101.3 (8-C), 111.7 (6-C), 114.1 (4a-C_q), 115.8 (d, J = 22.0 Hz, 3'-C), 119.6 (CN), 124.6 (5'-C), 128.9 (d = 8.3 Hz, 4'-C), 129.7 (5-C), 131.5 (d = 12.7 Hz, 6'-C), 149.2 (8a-C_q), 159.4 (7-C), 159.8 (2-C), 160.0 (d = 195.9 Hz, 2'-C); *m/z* (EI) 296 (42) [M^+], 201 (100); Anal. calcd. for $C_{17}H_{13}FN_2O_2$ (%), C, 68.91, H, 4.42, N, 9.45; found: C, 68.99, H, 4.36, N, 9.39.

2-Amino-3-cyano-4-(2'-chlorophenyl)-7-methoxy-4H-chromene (2H)

Analogously to the synthesis of 2B, compound 2H (500 mg, 1.6 mmol, 40%) was obtained from 2-chlorobenzaldehyde (562 mg, 4.0 mmol), malononitrile (280 mg, 4.0 mmol), six drops of Et_3N, and 3-methoxyphenol (436 µL, 4.0 mmol) in MeCN (5 mL). Colorless solid of m.p. 184 °C; υ_{max}(ATR)/cm^{-1} 3435, 3343, 3216, 2937, 2840, 2186, 1639, 1618, 1580, 1506, 1466, 1441, 1402, 1311, 1291, 1278, 1253, 1198, 1154, 1123, 1033, 956, 935, 874, 854, 817, 782, 758, 724, 708, 694, 675; ^{1}H NMR (300 MHz, $CDCl_3$) 3.75 (3 H, s, OMe), 4.62 (2 H, s, NH_2), 5.31 (1 H, s, 4-H), 6.51 (1 H, d, J = 2.6 Hz, 8-H), 6.57 (1 H, dd, J = 8.6 Hz, 2.6 Hz, 6-H), 6.89 (1 H, d, J = 8.6 Hz, 5-H), 7.2-7.3 (3 H, m, 4'-H, 5'-H, 6'-H), 7.3-7.4 (1 H, m, 3'-H); ^{13}C NMR (75.5 MHz, $CDCl_3$) 36.8 (3-C), 55.5 (OMe), 59.7 (4-C), 101.3 (8-H), 111.6 (6-C), 114.2 (4a-C_q), 119.5 (CN), 127.5 (6'-C), 128.4 (5'-C), 129.7 (4'-C), 129.9 (3'-C), 130.7 (5-C), 133.0 (2'-C), 141.8 (1'-C), 149.1 (8a-C_q), 159.5 (7-C), 159.6 (2-C); *m/z* (EI) 314 (6) [M^+], 312 (24) [M^+], 201 (100); Anal. calcd. for $C_{17}H_{13}ClN_2O_2$ (%), C, 65.29, H, 4.19, N, 8.96; found: C, 65.36, H, 4.12, N, 9.02.

2-Amino-3-cyano-4-(3', 4'-difluorophenyl)-7-methoxy-4H-chromene (2I)

Analogously to the synthesis of 2B, compound 2I (98 mg, 0.31 mmol, 31%) was obtained from 3, 4-difluorobenzaldehyde (142 mg, 1.0 mmol), malononitrile (70 mg, 1.0 mmol) three drops of Et_3N, and 3-methoxyphenol (109 µL, 1.0 mmol) in MeCN (5 mL). Yield: 98 mg (0.31 mmol, 31%); colorless solid of m.p. 193 °C; υ_{max}(ATR)/cm^{-1} 3433, 3349, 3220, 2842, 2186, 1663, 1616, 1580, 1507, 1464, 1436, 1408, 1311, 1289, 1255, 1202, 1191, 1156, 1123, 1109, 1046, 959, 928, 889, 856, 828, 816, 802, 775, 746, 697, 673; ^{1}H NMR (300 MHz, $CDCl_3$) 3.77 (3 H, s, OMe), 4.61 (2 H, s, NH_2), 4.64 (1 H, s, 4-H), 6.53 (1 H, d, J = 2.6 Hz, 8-H), 6.62 (1 H, dd, J = 8.6 Hz, 2.6 Hz, 6-H), 6.81 (1 H, d, J = 8.6 Hz, 5-H), 6.9-7.0 (2 H, m, 5'-H, 6'-H), 7.0-7.1 (1 H, m, 2'-H); ^{13}C NMR (75.5 MHz, $CDCl_3$) 39.8 (4-C), 55.5 (OMe), 60.5 (3-C), 101.5 (8-C), 111.9 (6-C), 113.8 (4a-C_q), 116.7 (d, J = 17.6 Hz, 2'-C), 117.4 (d, J = 17.4 Hz, 5'-C), 119.4 (CN), 123.7 (d, J = 9.8 Hz, 6'-C), 130.1 (5-C), 141.8 (1'-C), 147.1 (d, J = 156.0 Hz), 149.1 (8a-C_q), 151.2 (d, J = 156.0 Hz, 3'-C), 159.1 (7-C), 159.7 (2-C); *m/z* (EI) 314 (33) [M^+], 201 (100); Anal. calcd. for $C_{17}H_{12}F_2N_2O_2$ (%), C, 64.97, H, 3.85, N, 8.91; found: C, 65.08, H, 3.79, N, 8.96.

2-Amino-3-cyano-4-(3'-chloro-4'-fluorophenyl)-7-methoxy-4H-chromene (2J)

Analogously to the synthesis of 2B, compound 2J (100 mg, 0.30 mmol, 30%) was obtained from 3-chloro-4-fluorobenzaldehyde (159 mg, 1.0 mmol), malononitrile (70 mg, 1.0 mmol), three drops of Et_3N, and 3-methoxyphenol (109 µL, 1.0 mmol) in MeCN (5 mL). Colorless solid of m.p. 192-193 °C. υ_{max}(ATR)/cm^{-1} 3432, 3350, 3285, 3219, 3087, 2972, 2842, 2186, 1659, 1615, 1579, 1505, 1495, 1464, 1435, 1412, 1401, 1320, 1306, 1291, 1254, 1221, 1201, 1153, 1122, 1058, 1044, 948, 897, 855, 828, 815, 801, 774, 755, 711, 702, 693; ^{1}H NMR (300 MHz, $CDCl_3$) 3.77 (3 H, s, OMe), 4.61 (2 H, s, NH_2), 4.64 (1 H, s, 4-H), 6.54 (1 H, d, J = 2.6 Hz, 8-H), 6.61 (1 H, dd, J = 8.6 Hz, 2.6 Hz, 6-H), 6.80 (1 H, d, J = 8.6 Hz, 5-H), 7.0-7.1 (2 H, m, 5'-H, 6'-H), 7.1-7.2 (1 H, m, 2'-H); ^{13}C NMR (75.5 MHz, $CDCl_3$) 39.7 (4-C), 55.6 (OMe), 60.5 (3-C), 101.5 (8-C), 112.0 (6-C), 113.8 (4a-C_q), 116.8 (d, J = 21.3 Hz, 5'-C), 119.4 (CN), 121.4 (d, J = 18.0 Hz, 3'-C), 127.6 (6'-C), 130.0 (2'-C), 131.1 (5-C), 141.9 (1'-C), 149.1 (8a-C_q), 157.3 (d, J = 248.9 Hz, 4'-C), 159.1 (7-C), 159.7 (2-C); *m/z* (%) 330 (47) [M^+], 201 (100), 186 (43), 158 (43). Anal. calcd. for $C_{17}H_{12}ClFN_2O_2$ (%), C, 61.74, H, 3.66, N, 8.47; found: C, 61.84, H, 3.71, N, 8.50.

2-Amino-3-cyano-4-(3', 4'-dichlorophenyl)-7-methoxy-4H-chromene (2K)

Analogously to the synthesis of 2B, compound 2K (105 mg, 0.30 mmol, 30%) was obtained from 3, 4-dichlorobenzaldehyde (175 mg, 1.0 mmol), malononitrile (70 mg, 1.0 mmol), three drops of Et_3N, and 3-methoxyphenol (109 µL, 1.0 mmol) in MeCN (5 mL). Colorless solid of m.p. 192 °C; υ_{max}(ATR)/cm^{-1} 3433, 3349, 3220, 2186, 1661, 1616, 1579, 1506, 1463, 1434, 1412, 1320, 1290, 1251, 1199, 1180, 1157, 1123, 1046, 1029, 948, 911, 895, 885, 856, 825, 809, 786, 753, 732, 703, 692, 665; ^{1}H NMR (300 MHz, $CDCl_3$) 3.77 (3 H, s, OMe), 4.63 (1 H, s, 4-H), 4.66 (2 H, s, NH_2), 6.53 (1 H, d, J = 2.6 Hz, 8-H), 6.61 (1 H, dd, J = 8.6 Hz, 2.6 Hz, 6-H), 6.80 (1 H, d, J = 8.6 Hz, 5-H), 7.03 (1 H, dd, J = 8.2 Hz, 2.1 Hz, 6'-H), 7.22 (1 H, d, J = 2.1 Hz, 2'-H), 7.37 (1 H, d, J = 8.2 Hz, 5'-H); ^{13}C NMR (75.5 MHz, $CDCl_3$) 39.8 (4-C), 55.5 (OMe), 60.0 (3-C), 101.5 (8-C), 111.9 (6-C), 113.5 (4a-C_q), 119.4 (CN), 127.3 (6'-C), 129.8 (2'-C), 130.1 (5-C), 130.8 (5'-C), 131.4 (4'-C), 132.9 (3'-C), 145.0 (1'-C), 149.0 (8a-C_q), 159.2 (7-C), 159.7 (2-C); *m/z* (EI) 348 (7) [M^+], 346 (13) [M^+], 201 (100); Anal. calcd. for $C_{17}H_{12}Cl_2N_2O_2$ (%), C, 58.81, H, 3.48, N, 8.07; found: C, 58.94, H, 3.55, N, 8.09.

2-Amino-3-cyano-4-(2', 4'-difluorophenyl)-7-methoxy-4H-chromene (2L)

Analogously to the synthesis of 2B, compound 2L (100 mg, 0.32 mmol, 32%) was obtained from 2, 4-difluorobenzaldehyde (142 mg, 1.0 mmol), malononitrile (70 mg, 1.0 mmol), three drops of Et_3N, and 3-methoxyphenol (109 µL, 1.0 mmol) in MeCN (5 mL). Colorless solid of m.p. 169-170 °C. υ_{max}(ATR)/cm^{-1} 3432, 3349, 3220, 3084, 3015, 2969, 2936, 2840, 2186, 1660, 1615, 1602, 1581, 1497, 1463, 1409, 1316, 1280, 1262, 1241, 1220, 1202, 1190, 1155, 1138, 1124, 1086, 1039, 960, 852, 827, 808, 781, 751, 730, 683; ^{1}H NMR (300 MHz, $CDCl_3$) 3.76 (3 H, s, OMe), 4.63 (2 H, s, NH_2), 5.01 (1 H, s, 4-H), 6.52 (1 H, d, J = 2.6 Hz, 8-H), 6.60 (1 H, dd, J = 8.6 Hz, 2.6 Hz, 6-H), 6.7-6.8 (2 H, m, 3'-H, 5'-H), 6.88 (1 H, d, J = 8.6 Hz, 5-H), 7.0-7.1 (1 H, m, 6'-H); ^{13}C NMR (75.5 MHz, $CDCl_3$) 33.5 (4-C), 55.5 (OMe), 59.2 (3-C), 101.4 (8-C), 103.8-104.5 (m, 3'-C), 111.6-112.0 (m, 5'-C, 6-C), 113.8 (4a-C_q), 119.4 (CN), 127.5 (d, J = 12.9 Hz), 129.7 (5-C), 130.5-130.7 (m, 6'-C), 139.0 (1'-C), 149.2 (8a-C_q), 159.6 (7-C), 159.8 (2-C), 160.3 (d, J = 247.5 Hz, 4'-C), 162.0 (d, J = 248.8 Hz, 2'-C); *m/z* (%) 314 (43) [M^+], 201 (100); Anal. calcd. for $C_{17}H_{12}F_2N_2O_2$ (%), C, 64.97, H, 3.85, N, 8.91; found: C, 64.90, H, 3.78, N, 8.88.

2-Amino-3-cyano-4-(2', 3'-difluorophenyl)-7-methoxy-4H-chromene (2M)

Analogously to the synthesis of 2B, compound 2M (100 mg, 0.32 mmol, 32%) was obtained from 2, 3-difluorobenzaldehyde (142 mg, 1.0 mmol), malononitrile (70 mg, 1.0 mmol), three drops of Et_3N, and 3-methoxyphenol (109 µL, 1.0 mmol) in MeCN (5 mL). Colorless solid of m.p. 183-184 °C. υ_{max}(ATR)/cm^{-1} 3429, 3331, 3213, 2975, 2935, 2840, 2193, 1652, 1627, 1614, 1576, 1508, 1478, 1416, 1310, 1287, 1266, 1249, 1231, 1190, 1150, 1123, 1043, 1030, 969, 929, 895, 857, 824, 792, 782, 758, 740, 718, 697, 683; ^{1}H NMR (300 MHz, $CDCl_3$) 3.76 (3 H, s, OMe), 4.64 (2 H, s, NH_2), 5.05 (1 H, s, 4-H), 6.52 (1 H, d, J = 2.6 Hz, 8-H), 6.60 (1 H, dd, J = 8.6 Hz, 2.6 Hz, 6-H), 6.9-7.1 (4 H, m, 5-H, 4'-H, 5'-H, 6'-H); ^{13}C NMR (75.5 MHz, $CDCl_3$) 34.1 (4-C), 55.5 (OMe), 58.9 (3-C), 101.5 (8-C), 111.8 (6-C), 113.5 (4a-C_q), 116.1 (d, J = 17.2 Hz, 4'-C), 119.3 (CN), 124.3-124.5 (m, 6'-C), 129.7 (5-C), 133.9 (d, J = 9.8 Hz, 5'-C), 148.1 (d, J = 151.0 Hz, (2'-C), 149.2 (8a-C_q), 151.4 (d, J = 156.0 Hz, 3'-C), 159.7 (7-C), 159.9 (2-C); *m/z* (%) 314 (27) [M^+], 201 (100); Anal. calcd. for $C_{17}H_{12}F_2N_2O_2$ (%), C, 64.97, H, 3.85, N, 8.91; found: C, 64.88, H, 3.80, N, 8.94.

2-Amino-3-cyano-4-(2', 5'-difluorophenyl)-7-methoxy-4H-chromene (2N)

Analogously to the synthesis of 2B, compound 2N (95 mg, 0.30 mmol, 30%) was obtained from 2, 5-difluorobenzaldehyde (142 mg, 1.0 mmol), malononitrile (70 mg, 1.0 mmol), three drops of Et_3N, and 3-methoxyphenol (109 µL, 1.0 mmol) in MeCN (5 mL). Colorless solid of m.p. 179-180°C. υ_{max}(ATR)/cm^{-1} 3629, 3458, 3408, 3333, 3213, 3080, 2983, 2938, 2843, 2192, 1651, 1618, 1579, 1508, 1490, 1452, 1436, 1404, 1317, 1290, 1252, 1240, 1190, 1176, 1150, 1122, 1082, 1044, 1028, 961, 942, 883, 855, 849, 817, 806, 794, 777, 752, 739, 731, 716, 700; ^{1}H NMR (300 MHz, $CDCl_3$) 3.76 (3 H, s, OMe), 4.67 (2 H, s, NH_2), 5.04 (1 H, s, 4-H), 6.52 (1 H, d, J = 2.6 Hz, 8-H), 6.61 (1 H, dd, J = 8.6 Hz, 2.6 Hz, 6-H), 6.8-7.0 (4 H, m, 5-H, 3'-H, 4'-H, 6'-H); ^{13}C NMR (75.5 MHz, $CDCl_3$) 33.8 (4-C), 55.5 (OMe), 58.8 (3-C), 101.5 (8-C), 111.9 (6-C), 113.4 (4a-C_q), 115.2-116.2 (m, 4'-C), 116.7-117.2 (m, 3'-C, 6'-C), 119.3 (CN), 129.7 (5-C), 133.1-133.4 (m, 1'-C), 149.2 (8a-C_q), 156.2 (d, J = 239.8 Hz, 2'-C), 159.0 (d, J = 243.3 Hz, 5'-C), 159.7 (7-C), 159.9 (2-C); *m/ z* (%) 314 (60) [M^+], 201 (100), 186 (37), 158 (33); Anal. calcd. for $C_{17}H_{12}F_2N_2O_2$ (%), C, 64.97, H, 3.85, N, 8.91; found: C, 65.04, H, 3.90, N, 8.98.

2-Amino-3-cyano-4-(3', 4', 5'-trifluorophenyl)-7-methoxy-4H-chromene (2P)

Analogously to the synthesis of 2B, compound 2P (105 mg, 0.32 mmol, 32%) was obtained from 3, 4, 5-trifluorobenzaldehyde (160 mg, 1.0 mmol), malononitrile (70 mg, 1.0 mmol) three drops of Et_3N, and 3-methoxyphenol (109 µL, 1.0 mmol) in MeCN (5 mL). Colorless solid of m.p. 237-238 °C; υ_{max}(ATR)/cm^{-1} 3428, 3346, 3221, 3053, 3014, 2945, 2848, 2187, 1662, 1616, 1579, 1524, 1506, 1465, 1446, 1409, 1342, 1310, 1292, 1232, 1203, 1182, 1156, 1131, 1116, 1035, 985, 897, 879, 855, 834, 822, 803, 785, 756, 716, 709, 688; ^{1}H NMR (300 MHz, DMSO-d_6) 3.79 (3 H, s, OMe), 4.81 (1 H, s, 4-H), 6.57 (1 H, d. J = 2.5 Hz, 8-H), 6.69 (1 H, dd, J = 8.7 Hz, 2.5 Hz, 6-H), 6.98 (1 H, d, J = 8.7 Hz, 5-H), 7.07 (2 H, s, NH_2), 7.1-7.2 (2 H, m, 2'-H, 6'-H); ^{13}C NMR (75.5 MHz, $CDCl_3$/DMSO-d_6) 54.8 (3-C), 55.4 (OMe), 101.1 (8-C), 111.5-112.0 (m, 2'-C, 6'-C, 6-C), 113.8 (4a-C_q), 120.2 (CN), 129.9 (5-C), 136.0 (1'C), 143.3 (4'-C), 148.8 (8a-C_q), 150.2 (dd, J = 248.7 Hz, 9.8 Hz, 3'-C, 5'-C), 159.2 (7-C), 160.4 (2-C); HR-MS (ESI, *m/z*) for $C_{17}H_{12}O_2N_2F_3$ [M^+ + H] calcd. 333.08454, found 333.08436.

2-Amino-3-cyano-4-(3'-pentafluorothiophenyl)-7-methoxy-4H-chromene (2Q)

Analogously to the synthesis of 2B, compound 2Q (130 mg, 0.32 mmol, 32%) was obtained from 3-pentafluorothiobenzaldehyde (232 mg, 1.0 mmol), malononitrile (70 mg, 1.0 mmol) three drops of Et_3N, and 3-methoxyphenol (109 µL, 1.0 mmol) in MeCN (5 mL). Colorless solid of m.p. 226-227 °C; υ_{max}(ATR)/cm^{-1} 3472, 3321, 3281, 3233, 3205, 3071, 2936, 2841, 2192, 1652, 1626, 1612, 1577, 1508, 1464, 1434, 1402, 1293, 1252, 1191, 1155, 1125, 1111, 1097, 1036, 938, 911, 884, 833, 810, 794, 780, 747, 717, 697, 688; ^{1}H NMR (300 MHz, $CDCl_3$) 3.77 (3 H, s, OMe), 4.64 (2 H, s, NH_2), 4.75 (1 H, s, 4-H), 6.55 (1 H, d, J = 2.6 Hz, 8-H), 6.62 (1 H, dd, J = 8.6 Hz, 2.6 Hz, 6-H), 6.80 (1 H, d, J = 8.6 Hz, 5-H), 7.3-7.4 (2 H, m, 5'-H, 6'-H), 7.53 (1 H, s, 2'-H), 7.6-7.7 (1 H, m, 4'-H); ^{13}C NMR (75.5 MHz, $CDCl_3$) 40.5 (4-C), 55.5 (OMe), 60.2 (3-C), 101.6 (8-C), 112.0 (6-C), 113.5 (4a-C_q), 119.3 (CN), 124.9 (2'-C), 125.3 (4'-C), 129.3 (5'-C), 130.1 (5-C), 131.1 (6'-C), 145.9 (1'-C), 149.2 (8a-C_q), 154.3-155.0 (m, 3'-C), 159.3 (7-C), 159.8 (2-C); *m/z* (%) 404 (31) [M^+], 201 (100), 186 (38), 158 (33); Anal. calcd. for $C_{17}H_{12}F_5N_2O_2S$ (%), C, 50.50, H, 3.24, N, 6.93; found: C, 50.59, H, 3.20, N, 6.88.

2-Amino-3-cyano-4-(3'-bromo-4', 5'-dimethoxyphenyl)-7-propargyloxy-4H-chromene (3)

A mixture of malononitrile (70 mg, 1.0 mmol) and 3-bromo-4, 5-dimethoxybenzaldehyde (245 mg, 1.0 mmol) in ethanol (EtOH) (5 mL) was treated with three drops of piperidine, and the reaction mixture was stirred for 30 min at room temperature. 3-Propargyloxyphenol (148 mg, 1.0 mmol) was added, and the

reaction mixture was stirred under reflux for 4 h. The solvent was evaporated, and the residue was taken up in ethyl acetate, washed with water, and dried over Na_2SO_4. The solvent was evaporated, and the residue was purified by column chromatography (silica gel 60). Yield: 50 mg (0.11 mmol, 11%); off-white solid of m.p. 206-207 °C; R_f = 0.47 (ethyl acetate / *n*-hexane, 1:1); υ_{max}(ATR)/cm^{-1} 3442, 3331, 3294, 3240, 3202, 3009, 2971, 2939, 2834, 2192, 1651, 1629, 1608, 1570, 1508, 1488, 1459, 1431, 1401, 1312, 1284, 1230, 1183, 1157, 1124, 1044, 1028, 995, 880, 850, 840, 823, 801, 780, 762, 684, 654; ^{1}H NMR (300 MHz, DMSO-d_6) 3.59 (1 H, s, CCH), 3.70 (3 H, s, OMe), 3.81 (3 H, s, OMe), 4.72 (1 H, s, 4-H), 4.80 (2 H, s, CH_2), 6.65 (1 H, d, J = 2.6 Hz, 8-H), 6.73 (1 H, dd, J = 8.6 Hz, 2.6 Hz, 6-H), 6.88 (1 H, s, 6'-H), 7.0-7.1 (4 H, m, 5-H, 2'-H, NH_2); ^{13}C NMR (75.5 MHz, DMSO-d_6) 55.4 (CH_2), 55.7 (3-C), 56.1 (OMe), 60.0 (OMe), 78.6 (C*CH*), 78.9 (*C*CH), 102.5 (8-C), 111.8 (6-C), 112.3 (4a-C_q), 115.4 (6'-C), 116.8 (3'-C), 120.4 (CN), 122.5 (2'-C), 129.9 (5-C), 143.6 (1'-C), 144.4 (4'-C), 148.6 (5'-C), 153.4 (8a-C_q), 156.9 (7-C), 160.4 (2-C); HR-MS (ESI, *m/z*) for $C_{21}H_{18}O_4N_2{}^{79}Br$ [M^+ + H] calcd. 441.04445, found 441.04419.

Biological assays

Cell lines and culture conditions

The following cell lines were used: 518A2 melanoma (Department of Radiotherapy, Medical University of Vienna, Austria)[15], HeLa cervix carcinoma, KBV1^{Vbl} (ACC-149 cervix carcinoma, MCF7 [ACC-115]) breast carcinoma, U-87 glioblastoma, HT-29 (ACC-299), HCT-116 (ACC-581) and HCT-116p53-/- colon carcinoma, EA.hy926 (ATCC® CRL-2922™) endothelial hybrid cells, and HDFa (ATCC® PCS-201-012™) adult human dermal fibroblasts. The cells were maintained in Dulbecco's Modified Eagle Medium with 10% fetal bovine serum (20% for HDFa cells) and 1% ZellShield® at 37 °C, 5% CO_2, and 95% humidity. KB-V1^{Vbl} cells were treated with 340 nM vinblastine to retain vinblastine resistance. Only mycoplasma-free cultures were used.

In vitro cytotoxicity assay

An 3-(4, 5-dimethylthiazol-2-yl)-2, 5-diphenyl tetrazolium bromid (MTT) assay was used for antiproliferative studies. Cancer cells (5 × 10^4 cells/mL, 100 µL/well) were placed in 96-well plates (10 × 10^4 cells/mL for HDFA and U87 cells), and the cells were incubated for 24 h at 5% CO_2 and 95% humidity. Then, cells were treated with test compounds (at various concentrations) or solely with DMSO as a negative control for 72 h. Then, 12.5 µL of a 0.5% MTT solution in phosphate-buffered saline (PBS) was added to the cells, followed by incubation for 2 h at 37 °C. After centrifugation of the plates (300 × g, 5 min, 4 °C), the medium was discarded, and 25 µL of DMSO containing 10% SDS and 0.6% acetic acid was added, followed by incubation at 37 °C for at least 1 h. Formazan absorbance at λ = 570 nm was measured using a Tecan infinite F200 microplate reader and corrected for the background (λ = 630 nm). The 50% inhibitory concentration (IC_{50}) values were calculated from dose-response curves (means ± SD, four independent experiments) compared to DMSO-treated control cells, which were set to 100%. GraphPad Prism 9 was used for curve-fitting.

Microtubule immunofluorescence staining

518A2 melanoma cells (10 × 10^4 cells/mL, 0.5 mL/well) were placed on coverslips in 24-well plates followed by incubation at 37 °C, 5% CO_2, and 95% humidity. The cells were treated with test compounds and controls (25 and 100 nm) for 0.5, 1, 3, and 6 h and washed with cytoskeletal buffer (100 nm PIPES, 3 nm $MgCl_2$, 138 nm KCl, 2 nm EGTA, 300 nm sucrose, pH 6.8). Fixation and permeabilization were performed for 5 min with 3.7% formaldehyde and 0.2% Triton X-100 in a cytoskeletal buffer. The cells were fixed with cold EtOH for 10 s, rehydrated in PBS, and blocked with 1% bovine serum albumin in PBS for 30 min. The microtubules were stained for 1 h with primary (anti-α-tubulin, mouse monoclonal antibody) and secondary antibodies (goat anti-mouse IgG-AF-546, Invitrogen) and washed with PBS between each treatment. Nuclei were stained using DAPI (1 µg/mL in PBS) for 30 min. The coverslips were placed in

Roti®-Mount FluorCare. Microtubules (λ_{ex} = 488 nm, λ_{em} = 507 nm) and nuclei (λ_{ex} = 358 nm, λ_{em} = 461 nm) were documented by confocal microscopy (Leica TCS SP5 confocal microscope, 630 × magnification) and edited with *ImageJ*.

Intracellular localization

518A2 melanoma cells (7.5 × 10^4 cells/mL, 0.5 mL/well) were placed on coverslips in 24-well plates and cultivated for 24 h. Cells were treated with **3** (25 µm, 0.4% tween 80 in PBS) for 10 min at room temperature. After fixation in 3.7 % formaldehyde for 15 min and washing with PBS, the cells were incubated with the "click-solution" (2 mm $CuSO_4$, 5 mm sodium ascorbate, 0.1 mm 3-azido-7-hydroxycoumarin, 1% bovine serum albumin in PBS) for 30 min and washed with PBS. The nuclei were counterstained with Nuclear Green LCS1 for another 30 min, and the coverslips were mounted in Roti®-Mount FluorCare. The clicked test compound (λ_{ex} = 404 nm, λ_{em} = 477 nm) and nuclei (λ_{ex} = 488 nm, λ_{em} = 507 nm) were analyzed with a Leica TCS SP5 confocal microscope, and the obtained images were edited with *ImageJ*.

Cell-cycle analysis

518A2 melanoma cells (10 × 10^4 cells/mL, 3 mL/well) were cultivated in six-well plates for 24 h. After the treatment with test compounds (10 and 25 nm), C-A4 (10 and 25 nm), or DMSO (vehicle) for an additional 24 h, the cells were trypsinized, centrifuged (300 × *g*, 5 min, 4 °C), and fixed in 70% EtOH for min. 24 h. For FACS measurement, cells were washed in PBS and stained with propidium iodide solution (50 µg/mL PI, 50 µg/mL RNase A in 0.1% sodium citrate) for 30 min at 37 °C. The DNA content of at least 10000 single cells was determined using a Beckmann Coulter Cytomics FC500 flow cytometer (λ_{ex} = 488 nm, λ_{em} = 570 nm). CXP software (Beckman Coulter) was used to analyze the cells in the cell cycle phases (sub-G1, G1, S, G2/M).

Tube-formation assay

EA.hy926 endothelial hybrid cells were maintained for 24 h in EndoPrime low-serum endothelial medium and seeded (3 × 10^5 cells/mL, 50 µL/well) on basement membrane-like matrix Matrigel® on Ibidi µ-Slides. After treatment with test compounds for 4 h until tubular structures had formed in the control wells, results were documented using a Zeiss Axiovert 135 light microscope. Cell vitality was measured using the MTT assay and was above 75% compared to solvent-treated cells. Experiments were performed in triplicate.

Zebrafish angiogenesis assay

Transgenic zebrafish (*Tg(fli1:EGFP, casper* mutant) were bred at 28 °C.[16] After fertilization, the eggs were transferred to E3-medium (5 mm NaCl, 0.17 mm KCl, 0.33 mm CaCl, 0.33 mm $MgSO_4$, 0.01% methylene blue, pH 7.2), followed by incubation for 24 h. The chorion was manually removed, and the larvae were treated with test compounds or solvent in six-well plates (30 fish per concentration, 5 mL/well) for 48 h. The fluorescent vasculature was documented with a Leica MZ10F and Zeiss AxioCam MRrc. To quantify the angiogenesis, the sub-intestinal vein (SIV) area was measured using ImageJ and expressed as means ± SD with the control set to 100%. The significance of SIV reduction through substance treatment was assessed using one-way analysis of variance (ANOVA), *$P < 0.05$; **$P < 0.01$; ***$P < 0.001$; ****$P < 0.0001$, with Dunnett´s multiple comparison test (GraphPad Prism 9).

Luciferase-dependent MYB activity assay

Compounds were tested using the HEK-MYB-Luc reporter cell line, which allows a doxycycline-dependent induction of MYB expression and harbors an MYB-dependent luciferase reporter plasmid, as previously described[17,18]. After 16 h of substance treatment (0.0001-3 µM), luciferase activities were analyzed as described[11].

RESULTS

The test compounds 2A-R were obtained from 3-methoxyphenol, malononitrile, the corresponding aryl aldehyde, and a cat. amount of Et_3N in acetonitrile [Scheme 1]. Synthesis and analysis of the known compounds 2B, 2O, and 2R were as described[5,14]. The new compounds 2A, 2C-N, 2P, and 2Q were colorless solids. The structures of the test compounds were confirmed by NMR, IR, and MS analyses. The compounds are racemic mixtures, and no efforts to separate enantiomers were performed. The yields were generally low but acceptable considering the simple one-pot reaction and workup and the commercially available starting compounds [Table 1].

The new propargyl ether derivative 3 was prepared to conduct localization studies of this compound within cancer cells [Scheme 2]. 3-Propargyloxyphenol was obtained from the reaction of resorcinol with 1.2 equiv. propargyl bromide (80% in toluene) in DMF under basic conditions (K_2CO_3)[19]. Harsher conditions (reflux for 5 h in EtOH) were necessary to synthesize 3 by the described three-component reaction compared with the synthesis conditions of compounds 2A-R. 3 was obtained as an off-white solid in low yields only.

The antiproliferative activity of compounds 2A-R and 3 was evaluated in nine tumor and hybrid cell lines from six entities and compared with previously published data of the known compounds 1A and 1B [Table 2][13,20].

The presentation of the cytotoxicity screening results was simplified by determining the average IC_{50} values of all cell lines and sorting them based on their antiproliferative activity [Table 3]. The halogen atom did not have any major effect on the activity among the compounds with a 3-halo-4, 5-dimethoxyphenyl group (2A, 2B, and 2C). By contrast, in the group of 3, 5-dichloro- to 3, 5-diiodo-4-methoxyphenyl derivatives 2D, 2E, and 2F, a distinct increase in activity was observed from the dichloro compound 2D via the dibromo 2E to the diiodo derivative 2F. Several striking effects were observed in addition to this trend. Comparing the structure of 1C (coumarin-based) and 2F (7-methoxy-4*H*-chromene), a clear increase in antiproliferative activity based on the methoxychromene structure was observed, while the IC_{50} values of the 4*H*-naphtho(1, 2-*b*)pyran-3-carbonitriles (1A) and the 7-methoxy-4*H*-chromenes (2R) were both in the nanomolar range. Some compounds showed certain tumor cell line-specific activities, surpassing positive controls 1A and 1B. 2C was particularly active against HCT116 p53-deficient colon carcinoma cells, verapamil-treated KB-$V1^{Vbl}$ cervix carcinoma cells and MCF-7 breast cancer cells, whereas 2F and 2O were highly active against multidrug-resistant HT-29 colon carcinoma cells. The 1A-analog 2R showed slightly less overall activity but had a much stronger effect on MCF-7 breast cancer cells than 1A. The vinblastine-resistant KB-$V1^{Vbl}$ cells were treated with the P-glycoprotein (P-gp) blocker verapamil to identify synergy effects[21]. Compounds 2I, 2B, 2C, and 2E showed 12-, 14-, 20- and 320-fold lower IC_{50} values combined with verapamil (1 μM), assuming an inhibition of the efflux pumps increases the substance efficiency by blocked drug removal via the P-gp membrane transporter. A comparison of compounds 2B and 3, prepared for intracellular localization purposes, showed a substantial conformity of activity, indicating a similar mode of action and accumulation behavior in most tumor cell lines. However, compound 2B was more active against verapamil-treated KB-$V1^{Vbl}$ cells than against untreated cells and HeLa cells (which is the parent cell line of KB-3-1, from which KB-$V1^{Vbl}$ cells are derived), while 3 was more active against HeLa cells and KB-$V1^{Vbl}$ cells in the absence of verapamil than against verapamil-treated KB-$V1^{Vbl}$ cells.

The most active derivatives 2A-C and 2E-F and the positive control 1A were tested for their toxic effects on non-malignant HDFa cells [Table 3]. The selectivity index (SI) was calculated as a measure of selectivity toward cancer cells compared to non-malignant cells. 2B, 2C, and 2F displayed exceptionally high SI values, highlighting their potential as anticancer drug candidates.

Table 1. Yields of the syntheses of compounds 2A-R

Compound	Yield	Compound	Yield	Compound	Yield
2A	22%	2G	25%	2M	32%
2B	30%	2H	40%	2N	30%
2C	32%	2I	31%	2O	20%
2D	31%	2J	30%	2P	32%
2E	31%	2K	30%	2Q	32%
2F	30%	2L	32%	2R	30%

Table 2. IC_{50} values (in nM) of 2A-R and 3 in tumor cell lines.[a] 1A (LY290181) and 1B (Bcr-TMP) were used as positive controls

	EA.hy926	518A2	HCT-116	HCT-116 p53-/-	U87	HT-29	KB-V1^{Vbl}	KB-V1^{Vbl}[b]	HeLa	MCF-7	HDFa
1A[c]	30 ± 1	10 ± 1	8 ± 0.7	30 ± 3	70 ± 9	30 ± 3	20 ± 2	80 ± 2	40 ± 2	200 ± 20	40,700 ± 1500
1B[c]	20 ± 1	30 ± 0.1	20 ± 1.9	30 ± 2	5 ± 0.2	300 ± 40	30 ± 1	9 ± 1	10 ± 1	34 ± 2.5	-
1C[d]	2800 ± 70	1500 ± 100	3100 ± 100	2900 ± 60	5500 ± 300	2500 ± 200	3700 ± 60	3500 ± 80	-	3400 ± 200	-
2A	0.4 ± 0.06	4 ± 0.3	70 ± 5	70 ± 5	20 ± 3	300 ± 20	6 ± 0.5	0.9 ± 0.08	10 ± 0.4	40 ± 7	11,500 ± 1200
2B	0.8 ± 0.09	6 ± 0.2	100 ± 10	30 ± 3	80 ± 5	200 ± 20	10 ± 1	0.7 ± 0.06	2 ± 0.2	100 ± 8	> 50,000
2C	60 ± 5	20 ± 2	70 ± 1	6 ± 0.7	25 ± 2	200 ± 20	60 ± 5	3 ± 0.3	10 ± 0.9	20 ± 1	> 50,000
2D	1100 ± 70	2100 ± 200	2500 ± 200	1900 ± 200	3900 ± 400	1400 ± 100	2100 ± 100	2400 ± 100	700 ± 50	2400 ± 300	-
2E	20 ± 1	20 ± 2	20 ± 2	40 ± 3	20 ± 2	300 ± 2	3200 ± 300	10 ± 0.5	30 ± 3	80 ± 3	22,200 ± 2100
2F	20 ± 2	20 ± 0.4	30 ± 5	30 ± 1	50 ± 10	60 ± 1	70 ± 7	40 ± 2	30 ± 3	80 ± 4	> 50,000
2G	900 ± 90	700 ± 40	200 ± 20	300 ± 40	3200 ± 100	200 ± 10	700 ± 20	500 ± 20	400 ± 60	500 ± 40	-
2H	3700 ± 300	2000 ± 100	3700 ± 400	2800 ± 300	7400 ± 200	5300 ± 970	1900 ± 200	1600 ± 200	1400 ± 100	5100 ± 370	-
2I	700 ± 10	700 ± 5	800 ± 6	600 ± 6	3600 ± 500	800 ± 30	700 ± 30	60 ± 5	600 ± 30	700 ± 100	-
2J	400 ± 20	400 ± 10	300 ± 30	400 ± 40	1200 ± 70	500 ± 50	300 ± 20	210 ± 10	100 ± 6	150 ± 20	-
2K	600 ± 80	600 ± 7	300 ± 10	800 ± 20	8500 ± 300	1900 ± 100	1300 ± 100	600 ± 50	800 ± 70	1000 ± 50	-
2L	200 ± 10	500 ± 30	2500 ± 40	1600 ± 160	5100 ± 500	500 ± 50	3800 ± 400	1000 ± 100	1500 ± 70	> 50,000	-
2M	400 ± 10	300 ± 10	500 ± 50	200 ± 8	400 ± 60	200 ± 20	900 ± 90	100 ± 4	90 ± 2	200 ± 30	-
2N	4700 ± 900	90 ± 60	500 ± 50	200 ± 10	500 ± 100	400 ± 30	700 ± 70	200 ± 20	200 ± 20	300 ± 7	-
2O	40 ± 1	60 ± 6	1400 ± 50	40 ± 3	100 ± 10	70 ± 8	20 ± 2	60 ± 4	40 ± 4	400 ± 60	-
2P	400 ± 40	300 ± 30	300 ± 20	300 ± 20	1100 ± 90	200 ± 5	100 ± 5	100 ± 10	100 ± 20	400 ± 50	-
2Q	600 ± 20	300 ± 10	700 ± 40	2900 ± 10	900 ± 60	400 ± 30	1900 ± 100	2000 ± 100	400 ± 4	800 ± 30	-
2R	300 ± 9	30 ± 2	300 ± 30	200 ± 20	900 ± 50	200 ± 20	30 ± 0.4	70 ± 6	300 ± 20	10 ± 0.8	-
3	80 ± 2	60 ± 3	300 ± 10	90 ± 7	90 ± 3	2100 ± 300	80 ± 3	100 ± 3	40 ± 2	70 ± 4	-

[a]Means of min. four independent experiments (± SD); [b]plus verapamil; [c]Köhler *et al.*[20]; [d]Köhler *et al.*[13].

For a more detailed investigation of possible drug mechanisms, compounds 2A-C and 2F were tested for their influence on the cell cycle of 518A2 melanoma cells. FACS analysis at doses of 25 nM revealed a significant G2/M cell-cycle arrest for these compounds and the positive control combretastatin A4 (CA4), but to varying extents [Figure 2].

Table 3. Average IC_{50} value [nM] of the tested cancer and hybrid cell lines for compounds 1A-B, 2A-R, and 3, and SI (IC_{50} HDFa cells/ IC_{50} tumor cell average)

	2F	2C	2B	1A	2A	1B	2O	2R	3	2M	2P	2E	2J	2G, 2N, 2J, 2Q, 2K, 2D, 1C, 2H, 2L
Ø IC_{50} [nm]	43	47	49	52	53	53	203	227	321	330	330	374	396	> 500
SI	1163	1055	952	786	219	-	-	-	-	-	-	59	-	-

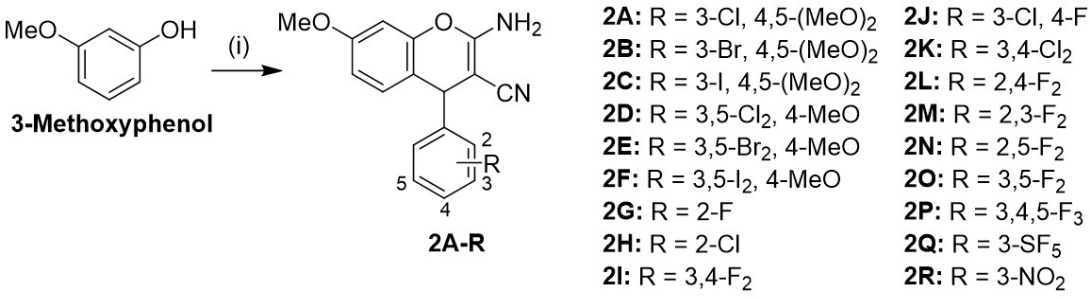

Scheme 1. Reagents and conditions: (i) Malononitrile; aryl aldehyde; cat. Et_3N; MeCN; rt; 3-16 h.

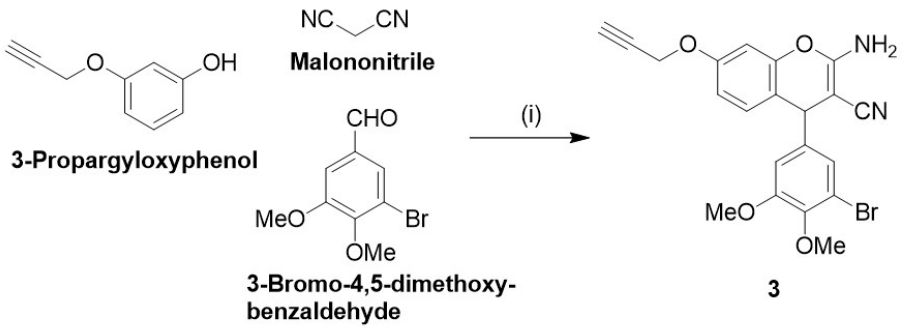

Scheme 2. Reagents and conditions: (i) cat. piperidine; EtOH; reflux; 5 h; 11%.

Among the compounds 2A-C, the 3-chloro-4, 5-dimethoxyphenyl derivative 2A showed more significant cell-cycle arrest than its 3-bromo and 3-iodo congeners 2B and 2C. However, an opposite effect was observed for the 3, 5-dihalo-4-methoxyphenyl derivatives 2D-F, where the 3, 5-diiodo-4-methoxyphenyl derivative 2F triggered by far the most significant arrest. The analogous 3, 5-dichloro (2D) and 3, 5-dibromo (2E) compounds induced only a slight increase in G2/M phase cells (data not shown). Substance 2F arrested about 74% of cells before or during mitosis and exceeded the C-A4 control. C-A4, 1A, and 1B caused G2/M arrest by microtubule depolymerization, thus preventing the formation of a functional spindle apparatus required for cell division[7,11,22].

Because of the structural similarity of the new cell cycle arresting compounds 2A-C and 2F to the known tubulin-depolymerizing agent C-A4, the effects on the microtubule cytoskeleton were investigated. Time-dependent imaging of 518A2 melanoma cells was applied to provide insights into the dynamics of the depolymerization process [Figure 3].

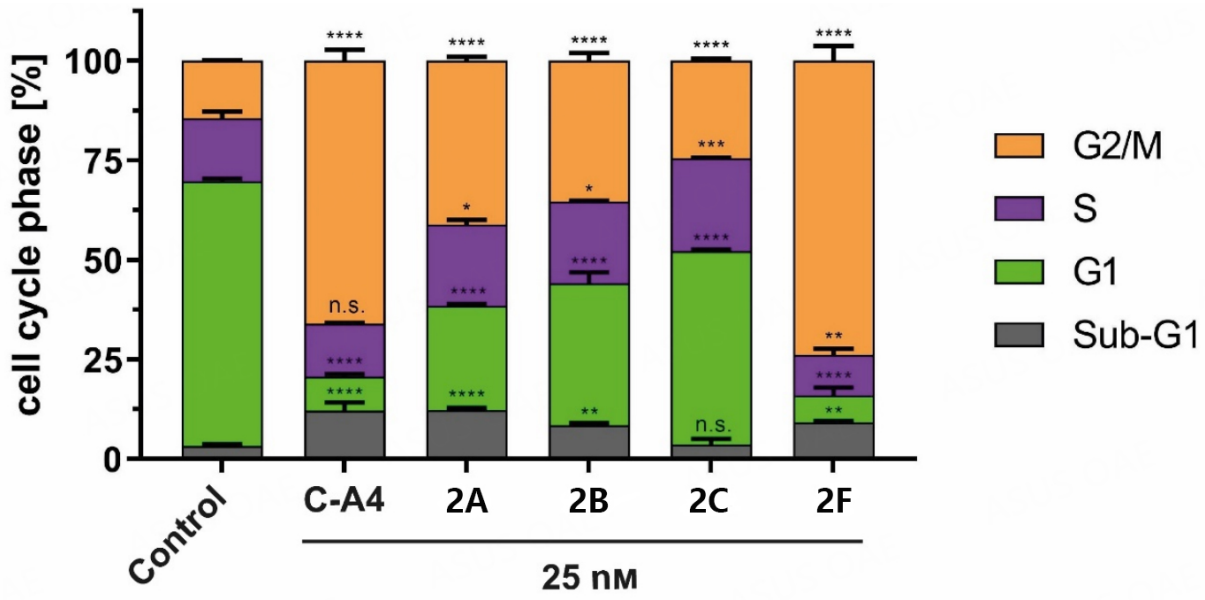

Figure 2. Cell cycle events of 518A2 melanoma cells treated with 2A-C and 2F (25 nM) for 24 h. Positive control (C-A4) and solvent (DMSO) were treated similarly to the substances. Measurements were carried out in triplicate and expressed as means ± SD with GraphPad Prism. Significance is expressed as n.s. $P > 0.05$; *$P < 0.05$; **$P < 0.01$; ***$P < 0.001$; ****$P < 0.0001$ against control (two-way ANOVA, with Dunnett's multiple comparison test).

In solvent-treated cells, the tubulin cytoskeleton consists of fine filaments extending throughout the cytoplasm. Upon treatment with test compounds 2A-C and 2F, these filaments were initially shortened and fragmented, leading to their destruction and distribution within the cytoplasm. However, the timing of this disintegration process was highly dependent on the substance used. For instance, 2A-C showed a breakdown of the cytoskeleton after 6 h, whereas 2F led to a change in the microtubule structure after 1 h. A similar effect was observed for the C-A4 control after 30 min, which can be attributed to a faster uptake or higher target affinity.

The alkynyl derivative 3 was designed to investigate compound uptake and localization within tumor cells. The propargyl group allows orthogonal fluorescence labeling with 3-azido-7-hydroxycoumarin using a copper-catalyzed click reaction. After 10 min, a distinct increase in fluorescence was observed within the treated cells, with most of the fluorescence found in the cytoplasm [Figure 4]. This finding suggests an accumulation of 3 in the cytoplasm, supporting the hypothesis that cytoplasmic tubulin is the primary target for 3 and its close analogs used in this study. The conformity of the basic structure and the antiproliferative activity of 3 with compound 2 suggests a similar mechanism.

In addition to antiproliferative and cytotoxic effects, microtubule-destabilizing agents possess additional antitumor properties[23]. In the case of C-A4, anti-angiogenic and vascular disruptive effects have been demonstrated. In this context, the tube-formation assay is a suitable method to observe the effects on the two-dimensional (2D) vessel structures by EA.hy926 cells[24]. The inhibition of cell migration and the development of cell-cell junctions (necessary for tube formation) by 2A-C and 2F were investigated [Figure 5]. At 100 nM, all four test compounds showed anti-angiogenic effects on EA.hy926 cells seeded on Matrigel®. The cells could not form a cross-linked 2D structure within 4 h, as with the negative control or at 25 nM substance concentration. Even if cell-cell junctions were formed in isolated cases, most cells agglomerated due to their spatial proximity. In addition, rounding was observed in many cells, as in C-A4 treated cells, presumably because of microtubule-destabilizing effects.

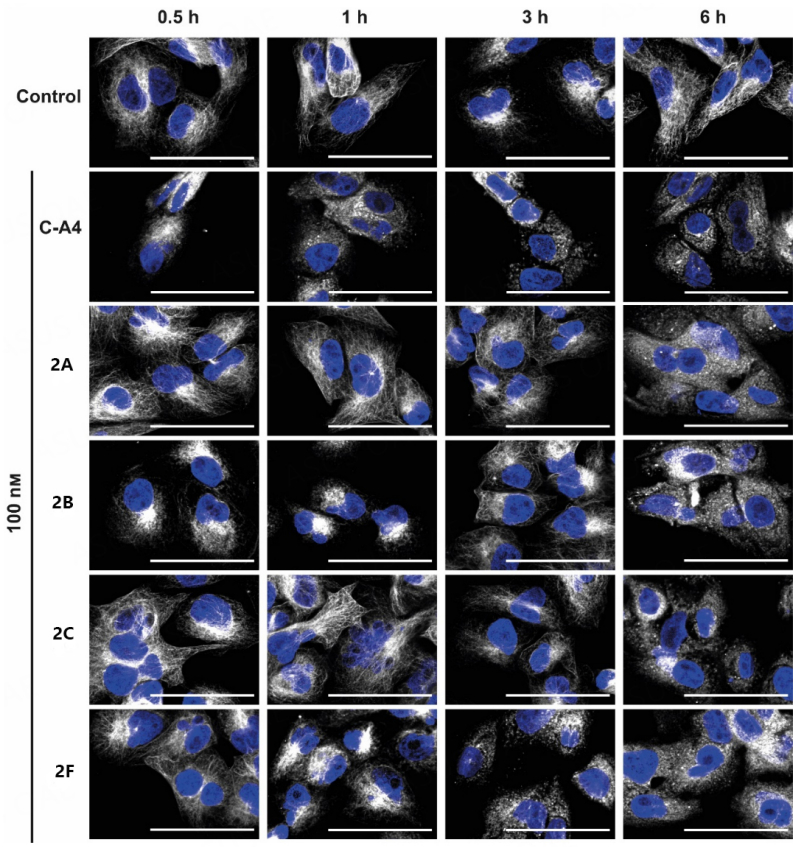

Figure 3. Immunofluorescence images of 518A2 melanoma cells treated with compounds 2A-C; 2F; and CA4 (100 nM) or vehicle (DMSO) for 0.5, 1, 3, and 6 h. Representative images (of two experiments) illustrate stained microtubules (white) and nuclei (blue). The scale bar corresponds to 100 µm, magnification of 630×.

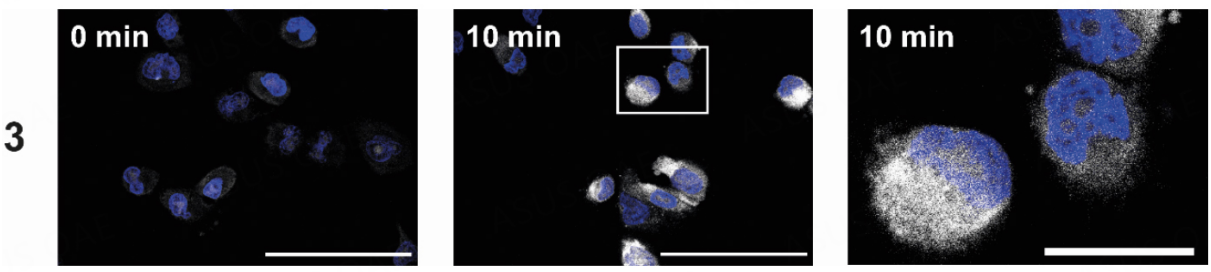

Figure 4. Intracellular localization of 3 (25 µM) using melanoma cells (518A2) after 10 min. The uptake was visualized using a Cu(I)-catalyzed reaction with 3-azido-7-hydroxycoumarin (white), and the nuclei were counterstained (Nuclear Green, blue). The right image shows the magnified section marked with a white box. The experiment was carried out in duplicate. The scale bar corresponds to 100 µm (left) or 25 µm (right), magnification of 630×.

The development of blood vessels is based on a complex mechanism with various regulators, which are essential targets for the treatment of tumor growth. Angiogenesis can be seen in the embryonal development of zebrafish larvae, where the SIV can be used to measure anti-angiogenic effects[25]. After exposure of 24-h-old zebrafish embryos to substances 2A-C and 2F or positive control axitinib for 48 h, we

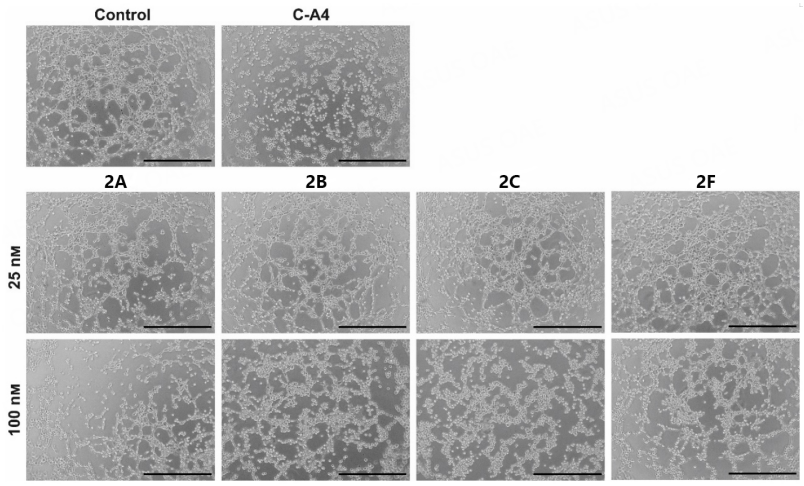

Figure 5. Images show EA.hy926 cells seeded on Matrigel® after 4 h treatment with substances 2A-C; 2F (25, 100 nM); and C-A4 (25 nM) or vehicle (DMSO). Representative images of a min. of two experiments. The scale bar corresponds to 500 µm, magnification of 100×.

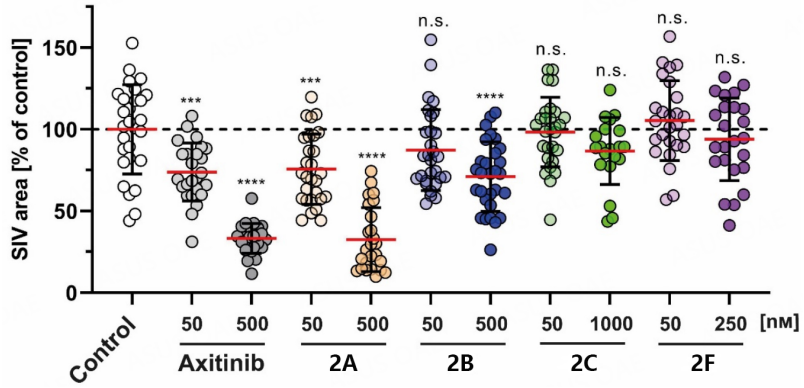

Figure 6. Effects of 2A; 2B (50, 500 nM); 2C (50, 1000 nM); and 2F (50, 250 nM) on the SIV growth of zebrafish larvae (24 hpf) after treatment (48 h). Positive controls used axitinib (50, 500 nM). Negative controls used equivalent amounts of DMSO. The SIV area was quantified using ImageJ and expressed as mean ± SD of at least 20 zebrafish. The significance is expressed as n.s. $P > 0.05$; ***$P < 0.001$; ****$P < 0.0001$ against control (one-way ANOVA, with Dunnett´s multiple comparison test).

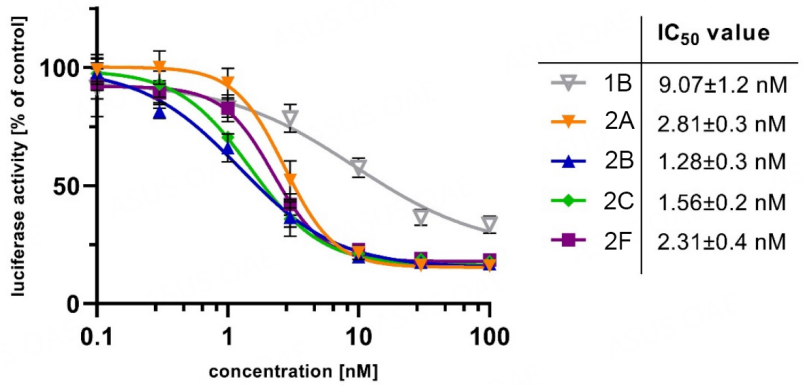

Figure 7. Inhibition of MYB activity in HEK-293 cells containing the reporter plasmid pGL4-5xMRE(GG)-Myc and the expression vector for MYB-2KR, upon treatment with compounds 1B; 2A-C; and 2F (0.1-100 nM) for 16 h. IC_{50} values were calculated with at least four independent experiments using GraphPad Prism 9.

measured the SIV area and compared it to solvent-treated fish [Figure 6]. Here, 2F showed no significant change in blood vessel growth, and 2F had a toxic effect above 250 nM. 2B and 2C showed no SIV decrease in the tolerated concentration range. However, 2A inhibited angiogenesis to an extent comparable to the known inhibitor axitinib[26]. This finding suggests a different mechanism of action for 2A, a bimodal compound with selective antiproliferative properties against cancer cells and angiogenesis-inhibiting features.

Due to their structural similarity to the potent MYB inhibitor 1B (data to be published elsewhere), compounds 2A-C and 2F were tested for their MYB-inhibitory activity [Figure 7]. Inhibition of MYB activity by 2A-C and 2F (1.28-2.81 nM) was superior to the inhibition by reference compound 1B (9.07 nM). Because the values are very close, it is challenging to identify a structure-dependent activity trend; however, the activity was in the order 2B > 2C > 2F > 2A.

DISCUSSION

This study's objective was to develop and optimize the lead structures 1A, 1B, and 1C. For this reason, we reduced the size of the benzo[*h*]chromene backbone to a 7-methoxy-4*H*-chromene structure, which led to increased activity. In addition, various phenyl substituents were tested to optimize the lead structure. Initial cytotoxicity studies against nine cancer cell lines confirmed that the C-A4-derived 3-iodo-, 3-bromo-, and 3-chloro-4, 5-dimethoxyphenyl motifs (2A-C) and the analogous 3, 5-diiodo- and 3, 5-dibromo-4-methoxyphenyl derivatives (2E-F) are excellent pharmacophores with selectivity against malignant cells. Only the 3, 5-dichloro-4-methoxyphenyl stands out with only micromolar IC_{50} values. Interestingly, differences in the specificity for HeLa cells, derived KB-V1^{Vbl} cells, and KB-V1^{Vbl} cells treated with the P-gp inhibitor verapamil were observed for the close analogs 2B and 3. 2B is more active against the parent HeLa cells than against the vinblastine-resistant KB-V1^{Vbl} cells. In contrast, the addition of verapamil strongly sensitized the KB-V1^{Vbl} cells to treatment with 2B, leading to a higher activity of 2B against verapamil-treated KB-V1^{Vbl} cells than against HeLa cells. A comparable hypersensitizing effect of verapamil was observed for KB-V1^{Vbl} cells treated with 2A, 2C, and 2I, surpassing their activity against HeLa cells, which may have explanations beyond mere P-gp inhibition by verapamil. The hypersensitivity effects of resistant P-gp-overexpressing cancer cells upon verapamil treatment were reported (e.g., based on disrupted energy homeostasis upon ATP depletion), which might lead to enhanced anticancer activity combined with other active drug candidates such as 2A-C (but not 2F) compared with their activity against related cell lines without (overexpressed) P-gp transporter[27]. For unknown reasons, compound 3 showed only slightly reduced activity against KB-V1^{Vbl} cells when combined with verapamil than against HeLa cells.

In addition, a reversal of P-gp- and BCRP-mediated resistance was documented for the 3-chloro-4-fluoroanilino-derivative gefitinib, an approved EGFR inhibitor[28,29]. However, the new 3-chloro-4-fluorophenyl derivative 2J appears to be a substrate of P-gp. Among the remaining fluorophenyl derivatives, 2, 3-difluorophenyl 2M and 2, 5-difluorophenyl 2N were identified as P-gp substrates, while 3, 5-difluorophenyl 2O and 3, 4, 5-trifluorophenyl 2P showed no dependence on P-gp, indicating a considerable influence of the fluoro-substitution pattern on the activity against P-gp-overexpressing cells (also compared with the effects of 3, 4-difluorophenyl derivative 2I mentioned above).

Because P-gp tends to have relatively hydrophobic substrates with aromatic rings, substituting methoxy groups with halogen atoms may already have an efflux-attenuating effect due to increased hydrophilicity[30]. Treatment with P-gp modulators can provide more significant cytotoxicity by reducing effective concentrations by 100-fold (paclitaxel) or 351-fold (vinblastine) in MDR colorectal cancer SW620/Ad300 cells[31,32].

The test compounds were obtained and tested as racemic mixtures. An increase in activity might be achieved by the separation of the enantiomers of the active derivatives and evaluating the separated enantiomers via MTT assay to identify any enantiomers which are more active or less active than the mixture. Instead of separating racemic mixtures, chiral synthetic procedures (e.g., using chiral organic bases instead of piperidine or triethylamine) might be applied to generate enantiopure compounds for biological testing.

The evaluation of the four most active test compounds (2A-C and 2F) revealed a correlation between the rate of microtubule destruction and the cell-cycle arrest in the G2/M phase in 518A2 melanoma cells. Compared with C-A4, 2F showed almost equal efficacy and led to early morphological changes in the microtubules (i.e., within 1 h). Localization of the structurally related alkynyl derivative 3 in the cytosol confirmed the accumulation near the cytoplasmic target. As previously demonstrated for the controls 1C and C-A4, the influence on angiogenesis (essential for tumor growth and metastases) was investigated for the test substances[13,33]. Using the 2D tube-formation assay, the concentration-dependent impairment of cell motility and intercellular junctions could be demonstrated, probably due to the damaged tubulin cytoskeleton. Nevertheless, this model can only partially simulate the complex mechanisms of blood vessel formation, which is why the substances were also tested for anti-angiogenic effects in zebrafish. This assay offers the possibility of estimating toxicity in a vertebrate and investigating the direct influence on the angiogenesis of the so-called SIVs. Surprisingly, only 2A showed a significant decrease in SIV growth, which occurred independently of its antiproliferative and microtubule-associated effects. As a third potential target, the inhibitory effect on the transcription factor MYB was tested and revealed the enhancement by three- to seven-fold compared to the previously discovered inhibitor 1B[11]. Overexpression of MYB in leukemias and various solid cancers such as colon and ER-positive breast cancers contributes to their development and thus represents a valuable target[34-39]. The rapid development of resistance to selective chemotherapeutics (e.g., kinase inhibitors, including RAF inhibitors) is a problem that can be overcome by addressing various targets by drugs with dual or multimodal mechanisms of action such as dual BRAF/HDAC inhibitors[40,41]. In this context, compound 2A represents a promising scaffold that can be used for further optimization and advanced stages of preclinical anticancer testing.

DECLARATIONS

Authors' contributions

The manuscript was written through the contributions of all authors.
Conceptualization: Köhler LHF, Klempnauer KH, Schobert R, Biersack B
Methodology: Köhler LHF, Reich S, Yusenko M, Biersack B
Formal analysis: Köhler LHF, Yusenko M, Biersack B
Resources: Klempnauer KH, Begemann G, Schobert R
Data curation: Köhler LHF, Yusenko M, Biersack B
Writing - original draft preparation: Köhler LHF, Biersack B
Writing - review and editing: Klempnauer KH, Begemann G, Schobert R
Supervision: Klempnauer KH, Schobert R, Biersack B
Funding acquisition: Klempnauer KH
All authors have read and agreed to the published version of the manuscript.

Availability of data and materials

Data supporting the findings of this study are available from the authors upon request.

Financial support and sponsorship
Yusenko M and Klempnauer KH were supported by the Wilhelm-Sander-Stiftung (grant 2020.071.1).

Conflicts of interest
All authors declared that there are no conflicts of interest.

Ethical approval and consent to participate
Not applicable.

Consent for publication
Not applicable.

REFERENCES

1. Fouad MA, Abdel-Hamid H, Ayoup MS. Two decades of recent advances of Ugi reactions: synthetic and pharmaceutical applications. *RSC Adv* 2020;10:42644-81. DOI PubMed PMC
2. Nagarajaiah H, Mukhopadhyay A, Moorthy JN. Biginelli reaction: an overview. *Tetrahedron Lett* 2016;57:5135-49. DOI
3. Zheng X, Liu W, Zhang D. Recent advances in the synthesis of oxazole-based molecules via van leusen oxazole synthesis. *Molecules* 2020;25:1594. DOI PubMed PMC
4. Wang L, Woods KW, Li Q, et al. Potent, orally active heterocycle-based combretastatin A-4 analogues: synthesis, structure-activity relationship, pharmacokinetics, and in vivo antitumor activity evaluation. *J Med Chem* 2002;45:1697-711. DOI PubMed
5. Kemnitzer W, Kasibhatla S, Jiang S, et al. Discovery of 4-aryl-4H-chromenes as a new series of apoptosis inducers using a cell- and caspase-based high-throughput screening assay. 2. Structure-activity relationships of the 7- and 5-, 6-, 8-positions. *Bioorg Med Chem Lett* 2005;15:4745-51. DOI
6. Kemnitzer W, Drewe J, Jiang S, et al. Discovery of 4-aryl-4H-chromenes as a new series of apoptosis inducers using a cell- and caspase-based high-throughput screening assay. 3. Structure-activity relationships of fused rings at the 7,8-positions. *J Med Chem* 2007;50:2858-64. DOI
7. Schmitt F, Gold M, Rothemund M, et al. New naphthopyran analogues of LY290181 as potential tumor vascular-disrupting agents. *Eur J Med Chem* 2019;163:160-8. DOI PubMed
8. Schmitt F, Schobert R, Biersack B. New pyranoquinoline derivatives as vascular-disrupting anticancer agents. *Med Chem Res* 2019;28:1694-703. DOI
9. Dell CP, Singh JP, Smith CW. Pharmaceutical Compounds. Pat. No. US005284868 A (1994).
10. Wood DL, Panda D, Wiernicki TR, Wilson L, Jordan MA, Singh JP. Inhibition of mitosis and microtubule function through direct tubulin binding by a novel antiproliferative naphthopyran LY290181. *Mol Pharmacol* 1997;52:437-44. DOI PubMed
11. Yusenko MV, Biyanee A, Frank D, et al. Bcr-TMP, a novel nanomolar-active compound that exhibits both MYB- and microtubule-inhibitory activity. *Cancers (Basel)* 2021;14:43. DOI PubMed PMC
12. Cicirò Y, Sala A. MYB oncoproteins: emerging players and potential therapeutic targets in human cancer. *Oncogenesis* 2021;10:19. DOI PubMed PMC
13. Köhler LHF, Reich S, Begemann G, Schobert R, Biersack B. 2-Amino-4-aryl-5-oxo-4,5-dihydropyrano[3,2-c]chromene-3-carbonitriles with microtubule-disruptive, centrosome-declustering, and antiangiogenic effects *in vitro* and *in vitro*. *ChemMedChem* 2022;17:e202200064. DOI PubMed PMC
14. Cai SX, Zhang H, Jiang S, Storer R. Preparation of substituted 4H-chromenes and analogs as activators of caspases and inducers of apoptosis and their uses against cancer and other disorders. Pat. No. WO2002092594 (2002).
15. Grossman D, Altieri DC. Drug resistance in melanoma: mechanisms, apoptosis, and new potential therapeutic targets. *Cancer Metast Rev* 2001;20:3-11. DOI PubMed
16. Lawson ND, Weinstein BM. In vivo imaging of embryonic vascular development using transgenic zebrafish. *Dev Biol* 2002;248:307-18. DOI PubMed
17. Chayka O, Kintscher J, Braas D, Klempnauer KH. v-Myb mediates cooperation of a cell-specific enhancer with the mim-1 promoter. *Mol Cell Biol* 2005;25:499-511. DOI PubMed PMC
18. Yusenko M, Jakobs A, Klempnauer KH. A novel cell-based screening assay for small-molecule MYB inhibitors identifies podophyllotoxins teniposide and etoposide as inhibitors of MYB activity. *Sci Rep* 2018;8:13159. DOI PubMed PMC
19. Lau VM, Pfalzgraff WC, Markland TE, Kanan MW. Electrostatic control of regioselectivity in Au(I)-catalyzed hydroarylation. *J Am Chem Soc* 2017;139:4035-41. DOI PubMed
20. Köhler LHF, Reich S, Yusenko M, et al. A new naphthopyran derivative combines c-myb inhibition, microtubule-targeting effects, and

antiangiogenic properties. *ACS Med Chem Lett* 2022;13:1783-90. DOI PubMed PMC

21. Verschraagen M, Koks CH, Schellens JH, Beijnen JH. P-glycoprotein system as a determinant of drug interactions: the case of digoxin-verapamil. *Pharmacol Res* 1999;40:301-6. DOI PubMed
22. Biersack B, Muthukumar Y, Schobert R, Sasse F. Cytotoxic and antivascular 1-methyl-4-(3-fluoro-4-methoxyphenyl)-5-(halophenyl)-imidazoles. *Bioorg Med Chem Lett* 2011;21:6270-3. DOI PubMed
23. Schwartz EL. Antivascular actions of microtubule-binding drugs. *Clin Cancer Res* 2009;15:2594-601. DOI PubMed PMC
24. Arnaoutova I, Kleinman HK. In vitro angiogenesis: endothelial cell tube formation on gelled basement membrane extract. *Nat Protoc* 2010;5:628-35. DOI PubMed
25. Cross LM, Cook MA, Lin S, Chen J, Rubinstein AL. Rapid analysis of angiogenesis drugs in a live fluorescent zebrafish assay. *Arterioscler Thromb Vasc Biol* 2003;23:911-2. DOI PubMed
26. Choueiri TK. Axitinib, a novel anti-angiogenic drug with promising activity in various solid tumors. *Curr Opin Pharmacol* 2008;9:658-71. PubMed
27. Gao X, Aguanno D, Board M, Callaghan R. Exploiting the metabolic energy demands of drug efflux pumps provides a strategy to overcome multidrug resistance in cancer. *Biochim Biophys Acta Gen Subj* 2021;1865:129915. DOI PubMed
28. Yanase K, Tsukahara S, Asada S, Ishikawa E, Imai Y, Sugimoto Y. Gefitinib reverses breast cancer resistance protein-mediated drug resistance. *Mol Cancer Ther* 2004;3:1119-25. PubMed
29. Leggas M, Panetta JC, Zhuang Y, et al. Gefitinib modulates the function of multiple ATP-binding cassette transporters *in vivo*. *Cancer Res* 2006;66:4802-7. DOI PubMed
30. Sharom FJ. The P-glycoprotein multidrug transporter. *Essays Biochem* 2011;50:161-78. DOI PubMed
31. Scala S, Akhmed N, Rao US, et al. P-glycoprotein substrates and antagonists cluster into two distinct groups. *Mol Pharmacol* 1997;51:1024-33. DOI PubMed
32. Lei ZN, Teng QX, Wu ZX, et al. Overcoming multidrug resistance by knockout of ABCB1 gene using CRISPR/Cas9 system in SW620/Ad300 colorectal cancer cells. *MedComm* 2021;2:765-77. DOI PubMed PMC
33. Su M, Huang J, Liu S, et al. The anti-angiogenic effect and novel mechanisms of action of Combretastatin A-4. *Sci Rep* 2016;6:28139. DOI PubMed PMC
34. Anfossi G, Gewirtz AM, Calabretta B. An oligomer complementary to c-myb-encoded mRNA inhibits proliferation of human myeloid leukemia cell lines. *Proc Natl Acad Sci USA* 1989;86:3379-83. DOI PubMed PMC
35. Calabretta B, Sims RB, Valtieri M, et al. Normal and leukemic hematopoietic cells manifest differential sensitivity to inhibitory effects of c-myb antisense oligodeoxynucleotides: an *in vitro* study relevant to bone marrow purging. *Proc Natl Acad Sci USA* 1991;88:2351-5. DOI PubMed PMC
36. Guérin M, Zheng ZM, Andrieu N, Riou G. Strong association between c-myb and oestrogen-receptor expression in human breast cancer. *Oncogene* 1990;5:131-5. PubMed
37. Drabsch Y, Hugo H, Zhang R, et al. Mechanism of and requirement for estrogen-regulated MYB expression in estrogen-receptor-positive breast cancer cells. *Proc Natl Acad Sci USA* 2007;104:13762-7. DOI PubMed PMC
38. Biroccio A, Benassi B, D'agnano I, et al. c-Myb and Bcl-x overexpression predicts poor prognosis in colorectal cancer. *Am J Pathol* 2001;158:1289-99. DOI PubMed PMC
39. Hugo H, Cures A, Suraweera N, et al. Mutations in the MYB intron I regulatory sequence increase transcription in colon cancers. *Gene Chromosome Canc* 2006;45:1143-54. DOI PubMed
40. Degirmenci U, Yap J, Sim YRM, Qin S, Hu J. Drug resistance in targeted cancer therapies with RAF inhibitors. *Cancer Drug Resist* 2021;4:665-83. DOI PubMed PMC
41. Li Y, Huang Y, Cheng H, et al. Discovery of BRAF/HDAC dual inhibitors suppressing proliferation of human colorectal cancer cells. *Front Chem* 2022;10:910353. DOI PubMed PMC

5. Auflistung weiterer Publikationen

1) **Guided Antitumoural Drugs: (Imidazol-2-ylidene)(L)gold(I) Complexes Seeking Cellular Targets Controlled by the Nature of Ligand L**

   Sofia I. Bär, Madeleine Gold, Sebastian W. Schleser, Dr. Tobias Rehm, Alexander Bär, Leonhard Köhler, Lucas R. Carnell, Dr. Bernhard Biersack, Prof. Dr. Rainer Schobert

   Chemistry **2021**, *27*, 5003.

2) **A New Pentafluorothio-Substituted Curcuminoid with Superior Antitumor Activity**

   Benedikt Linder, Leonhard H. F. Köhler, Lisa Reisbeck, Dominic Menger, Dharmalingam Subramaniam, Christel Herold-Mende, Shrikant Anant, Rainer Schobert, Bernhard Biersack, Donat Kögel

   Biomolecules **2021**, *11*(7), 947.

3) **Bcr-TMP, a Novel Nanomolar-Active Compound That Exhibits Both MYB- and Microtubule-Inhibitory Activity**

   Maria V. Yusenko, Abhiruchi Biyanee, Daria Frank, Leonhard H. F. Köhler, Mattias K. Andersson Cyrus Khandanpour, Rainer Schobert 3, Göran Stenman, Bernhard Biersack, Karl-Heinz Klempnauer

   Cancers **2022**, *14*(1), 43.

4) **Antitumor Effects of a New Retinoate of the Fungal Cytotoxin Illudin M in Brain Tumor Models**

   Benedikt Linder, Miroslava Zoldakova, Zsuzsanna Kornyei, Leonhard H. F. Köhler, Sebastian Seibt, Dominic Menger, André Wetzel, Emília Madarász, Rainer Schobert, Donat Kögel and Bernhard Biersack

   Int. J. Mol. Sci. **2022**, *23*(16), 9056

5) **Anti-Tumoural [NHC(thiolato)] Gold(I) Complexes Derived from HIF-1α Inhibitor AC1-004 target the Mitochondrial Redox System and Show Antiangiogenic Effects in vivo**

   Sebastian W. Schleser, Leonhard H. F. Köhler, Florian Riethmüller, Sebastian Reich, Robin Fertig, Luca Schlotte, Johnathan Seib, Alexander Goller, Gerrit Begemann, Rhett Kempe, Rainer Schobert

   ChemPlusChem **2023**, 88(5), e202300167

Danksagung

An dieser Stelle bedanke ich mich bei Allen, die mich während meiner Zeit in Bayreuth und auf dem Weg zur Promotion begleitet haben. Besonderer Dank gilt hier Prof. Dr. Rainer Schobert, der mir schon während der Masterarbeit nicht nur viel Vertrauen und Freiraum gewährt, sondern auch eine lehrreiche und angenehme Zeit am Lehrstuhl OC I ermöglicht hat. Meiner Mentorin Madeleine Gold danke ich herzlich für die umfangreiche Betreuung und die geteilten Erfahrungen die das Doktorandendasein mit sich bringt. Ich konnte so viel von dir lernen und ich bin dir sehr dankbar, dass du mich mit tollen Ideen und Ratschlägen motiviert und gefördert hast. Ein großer Dank gilt Herrn Bernhard Biersack der mich sowohl mit Testsubstanzen versorgt als auch bei allen wissenschaftlichen Veröffentlichungen maßgeblich unterstütz hat. Für die permanente Unterstützung am Lehrstuhl und den unkomplizierten bürokratischen sowie persönlichen Beistand seitens Silvia Kastner und Thomas Schmalz möchte ich mich bei euch auch sehr bedanken. Bei Sebastian Schleser möchte ich mich für eine super Zusammenarbeit und eine großartige Tetrahedron-Konferenz in Lissabon bedanken. Unter all meinen fleißigen Praktikanten möchte ich mich besonders bei Sebastian Reich für die tatkräftige Unterstützung meiner Arbeit und die sympathische und harmonische gemeinsame Zeit im Labor bedanken. Vielen Dank auch an alle Kooperationspartner und Kollegen die mir mit Ihrem Wissen, Gerätschaften oder Räumlichkeiten sehr weitergeholfen haben. Darunter die Mitarbeiter des Lehrstuhls Entwicklungsbiologie von Herrn Prof. Dr. Gerrit Begemann, die Arbeitsgruppe um Herrn Prof. Dr. Karl-Heinz Klempnauer aus Münster, Herr Prof. Dr. Khursheed Ahmed und Amin H. Shaikh aus Pune, die Mitarbeiter von Herrn Prof. Dr. Hahn sowie Prof. Dr. Olaf Stemmann und Thomas Hermann vom Lehrstuhl Genetik. Ein besonderer Dank gilt hier unseren Lehrstuhlnachbarn vom Lehrstuhl Bioorganische Chemie unter der Leitung von Herrn Prof. Dr. Unverzagt die mit großer Hilfsbereitschaft meine Arbeit unterstützt haben.

Vielen Dank an Ole Bundgaard und Andreas Dürrmann die nicht nur in fachlichen Diskursen zu dieser Dissertation beigetragen haben, sondern auch außerhalb der Universität an einer besonderen Doktorandenzeit beteiligt waren. Ebenso möchte ich mich bei allen Freunden und meiner Familie für die bedingungslose Unterstützung in allen Belangen ganz herzlich bedanken.

Eidesstattliche Versicherungen und Erklärungen des Verfassers

(§ 8 Satz 2 Nr. 3 PromO Fakultät)

Hiermit versichere ich eidesstattlich, dass ich die Arbeit selbstständig verfasst und keine anderen als die von mir angegebenen Quellen und Hilfsmittel benutzt habe (vgl. Art. 64 Abs. 1 Satz 6 BayHSchG).

(§ 8 Satz 2 Nr. 3 PromO Fakultät)

Hiermit erkläre ich, dass ich die Dissertation nicht bereits zur Erlangung eines akademischen Grades eingereicht habe und dass ich nicht bereits diese oder eine gleichartige Doktorprüfung endgültig nicht bestanden habe.

(§ 8 Satz 2 Nr. 4 PromO Fakultät)

Hiermit erkläre ich, dass ich Hilfe von gewerblichen Promotionsberatern bzw. –vermittlern oder ähnlichen Dienstleistern weder bisher in Anspruch genommen habe noch künftig in Anspruch nehmen werde.

(§ 8 Satz 2 Nr. 7 PromO Fakultät)

Hiermit erkläre ich mein Einverständnis, dass die elektronische Fassung der Dissertation unter Wahrung meiner Urheberrechte und des Datenschutzes einer gesonderten Überprüfung unterzogen werden kann.

(§ 8 Satz 2 Nr. 8 PromO Fakultät)

Hiermit erkläre ich mein Einverständnis, dass bei Verdacht wissenschaftlichen Fehlverhaltens Ermittlungen durch universitätsinterne Organe der wissenschaftlichen Selbstkontrolle stattfinden können.

…….

Ort, Datum, Unterschrift